Comparison of Test Methods for Erodibility of Bank Materials on the Lower American and Sacramento Rivers, adjacent to the City of Sacramento, California

4/1/2021

USDA, ARS, National Sedimentation Laboratory

598 McElroy Drive
Oxford, MS 38655

Research Report No. 81

Comparison of Test Methods for Erodibility of Bank Materials on the Lower American and Sacramento Rivers, adjacent to the City of Sacramento, California

Prepared by:

Michael E. Ursic and Eddy J. Langendoen

Watershed Physical Processes Research Unit
USDA, ARS, National Sedimentation Laboratory
Oxford, MS 38655

EXECUTIVE SUMMARY

The Water Resources Development Act (WRDA) of 2016 provides for engineering and design activities associated with implementing projects to reduce the flood risk on the Lower American River and the Sacramento River near Sacramento, California. The integrity of levees that protect Sacramento could be adversely affected by bank erosion. The rate of bank erosion depends, among others, on the resistance-to-erosion properties of the bank soils. The U.S. Army Corps of Engineers (USACE) Sacramento District requested both the U.S. Department of Agriculture (USDA), Agricultural Research Service, National Sedimentation Laboratory, U.S. Geological Survey (USGS) California Water Science Center, and Texas A&M University (TAMU) to use a variety of field and laboratory resistance-to-erosion measurement techniques (REMTs) to characterize the erodibility of soils in the study area. Methods used include the Jet Erosion Test (JET, NSL), Erosion Function Apparatus (EFA, TAMU) and the Borehole Erosion Test (BET, USGS & TAMU). The tests were performed during the period 2018-2020. The collected data were supplemented with JETs and EFAs conducted by USACE Engineer and Research Development Center, Vicksburg, MS, from samples collected in 2011. The purpose of this report is to compare the soil erosion-resistance parameters derived by the JET, EFA, and BET REMTs and grouped by Unified Soil Classification System (USCS) soil types.

Erosion-resistance in this study is represented by two parameters: critical shear stress (τ_c) and erodibility coefficient (k_d). The critical shear stress of a soil is the threshold shear stress flowing water has to exceed to commence erosion of the soil. The erodibility coefficient represents the rate at which the soil erodes once the critical shear stress has been exceeded. Critical shear stress and erodibility coefficient can be calculated from the erosion function, which is the relation between soil erosion rate (E, dependent variable) and applied shear stress (τ, independent variable). The critical shear stress is the shear stress where the erosion function first exceeds zero erosion-rate (i.e. $E = 0$ if $\tau \leq \tau_c$ and $E > 0$ if $\tau > \tau_c$). The erodibility coefficient is the slope of the erosion function. In this study the erosion function is approximated by a linear excess shear stress equation: $E = k_d(\tau - \tau_c)$.

The REMTs use different hydraulic principles to erode the soil surface, measure soil erosion rate, and estimate shear stress applied by the flow on the soil surface. As a result, erosion functions and erosion-resistance parameters will not only vary by soil but could also vary by REMT for similar soils. The following procedure was used to progressively improve compatibility between soil erosion-resistance parameters derived by the three REMTs:

1. Using linear regression fit a linear trendline representing the linear excess shear stress equation through the 'as-is' erosion function measured (or output) by the BET, EFA, and JET methods. Calculate the erosion-resistance parameters critical shear stress and erodibility coefficient from the trendline.
2. Same as Step 1 but limit the erosion function to the portion representing the mass soil erosion regime.
3. Same as Step 2 but base the erosion function on the shear stress acting at grain or (small) soil particle roughness length scales.
4. Same as Step 3 but account for uncertainty in measured erosion rate and estimated applied shear stress.

Step 1 includes all measured data (i.e. entire erosion function) produced by a test. However, the measured erosion function by BET, EFA, and JET methods typically includes two erosion regimes: (1) particle-by-particle erosion regime at small excess shear stresses ($\tau - \tau_c$) and (2) mass erosion regime during which aggregates and clods are detached from the soil surface at larger excess shear stresses. A measured erosion function may cover both erosion regimes or only regime (1) or (2). Erosion-resistance parameters from erosion regime (2) are typically used by computer models, simulating bank erosion processes, as the magnitude of erosion can be orders of magnitude greater for this erosion regime. Therefore, Step 2 ensures that the derived erosion-resistance parameters represent an identical erosion regime. The erosion function output by the JET is based on applied shear stresses acting at the grain roughness scale. These shear stresses are commonly associated with erosion and sediment transport. The erosion functions of BET and EFA methods are based on total shear stress that includes both skin friction (grain-scale roughness) and form drag (topographic features much greater than sediment grains or soil particles) components. Erosion-resistance parameters derived in Step 3 are therefore based on erosion functions that are associated with similarly scaled applied shear stresses. The uncertainty in measured erosion rate and estimated applied shear stress can be significant and varies by REMT. Accounting for this uncertainty as part of the linear regression allows for both an improved estimate of erosion-resistance parameters themselves and quantification of their uncertainty (Step 4).

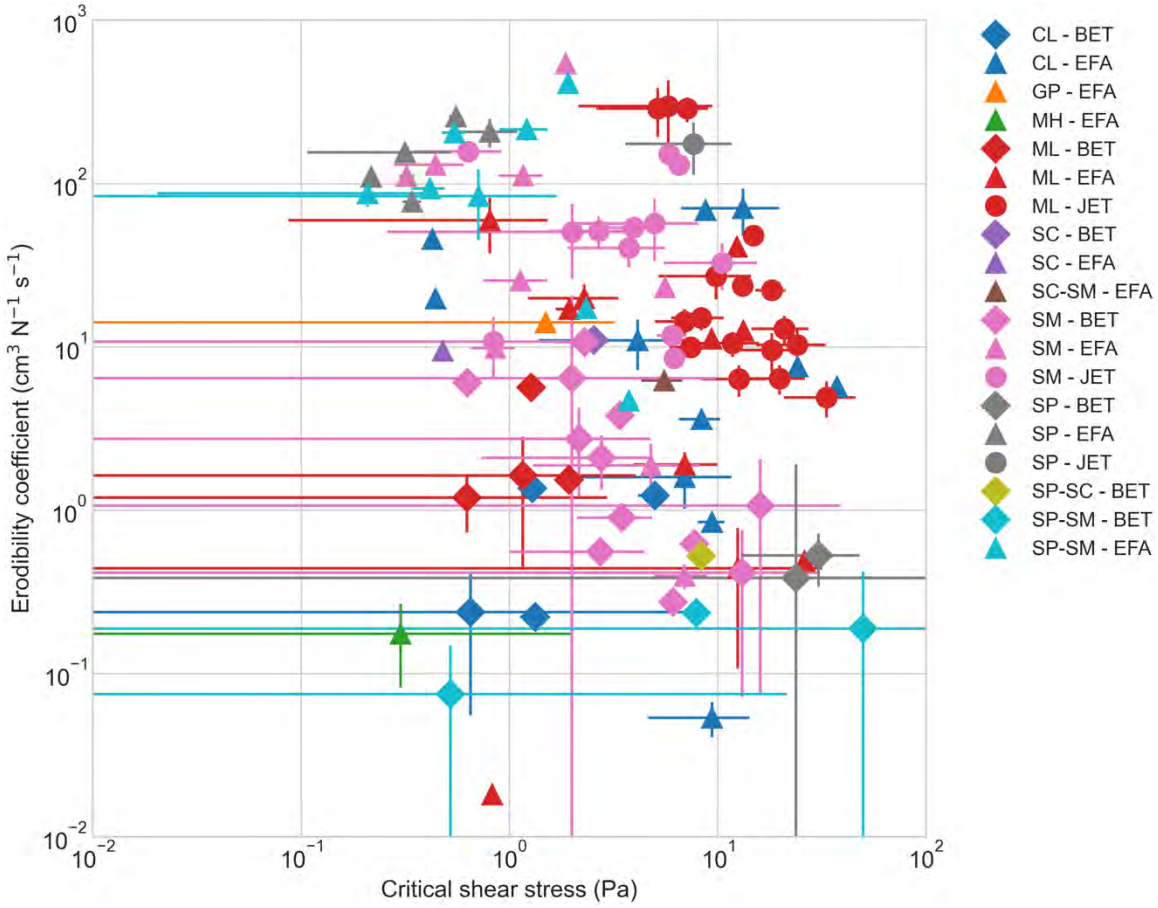

FIGURE I – ERODIBILITY COEFFICIENT PLOTTED AGAINST CRITICAL SHEAR STRESS FOR ALL MEASUREMENT TECHNIQUES (BET, EFA, AND JET). EROSION-RESISTANCE PARAMETERS WERE DERIVED FROM EROSION FUNCTIONS THAT INCLUDE UNCERTAINTY IN SHEAR STRESS AND EROSION RATE, REPRESENT THE MASS EROSION REGIME, AND ARE BASED ON GRAIN SHEAR STRESS (STEP 4 OF THE ANALYSIS PROCEDURE). THE LENGTH OF THE HORIZONTAL AND VERTICAL LINES INDICATE THE STANDARD DEVIATION OF THE UNCERTAINTY IN CRITICAL SHEAR STRESS AND ERODIBILITY COEFFICIENT, RESPECTIVELY.

Soils were either collected for laboratory testing (EFA and JET) or tested in situ (BET and JET) at 18 combined sites on the Lower American River and Sacramento River. REMT results were grouped by USCS soil type covering: CL, clay of low plasticity, GP, poorly graded gravel; MH, silt of high plasticity; ML, silt; SC, clayey sand; SC-SM, clayey and silty sand; SM, silty sand; SP-SM, poorly graded sand and silty sand; SP, poorly graded sand; and SP-SC, poorly graded sand with clay.

Figure I plots the erosion-resistance parameters derived under Step 4 of the followed procedure. Trendlines of erosion functions that would have resulted in negative critical shear stresses were omitted. Figure I shows that BET-derived critical shear stresses have similar magnitude as those derived by the EFA and JET methods. However, the erodibility coefficient provided by the BET method is one to two orders of magnitude smaller than those provided by the EFA and JET methods. The uncertainties in erosion rate and applied shear stress for the BET have similar magnitudes as the measured erosion rate and estimated shear stress themselves. Better techniques have to be developed to measure the erosion extent of the borehole wall and calculate the shear stresses acting on the borehole wall to derive erosion-resistance parameters that can be used in engineering and design methods to determine or prevent bank erosion.

Figures II and III compare the erosion-resistance parameters derived under Steps 1 and 4 for EFA and JET methods. The soils shown in Figures II and III are ordered from more cohesive to less cohesive (left to right). On average, critical shear stress reduces the less cohesive the soil, whereas erodibility coefficient increases the less cohesive the soil. Further, the EFA- and JET-derived erosion-resistance parameters are more similar for Step 4 than Step 1. JETs were limited to silt (ML) and sandy silt (SM) soil types. Table I lists the results of two-sample Kolmogorov-Smirnov (KS) tests conducted to compare the critical shear

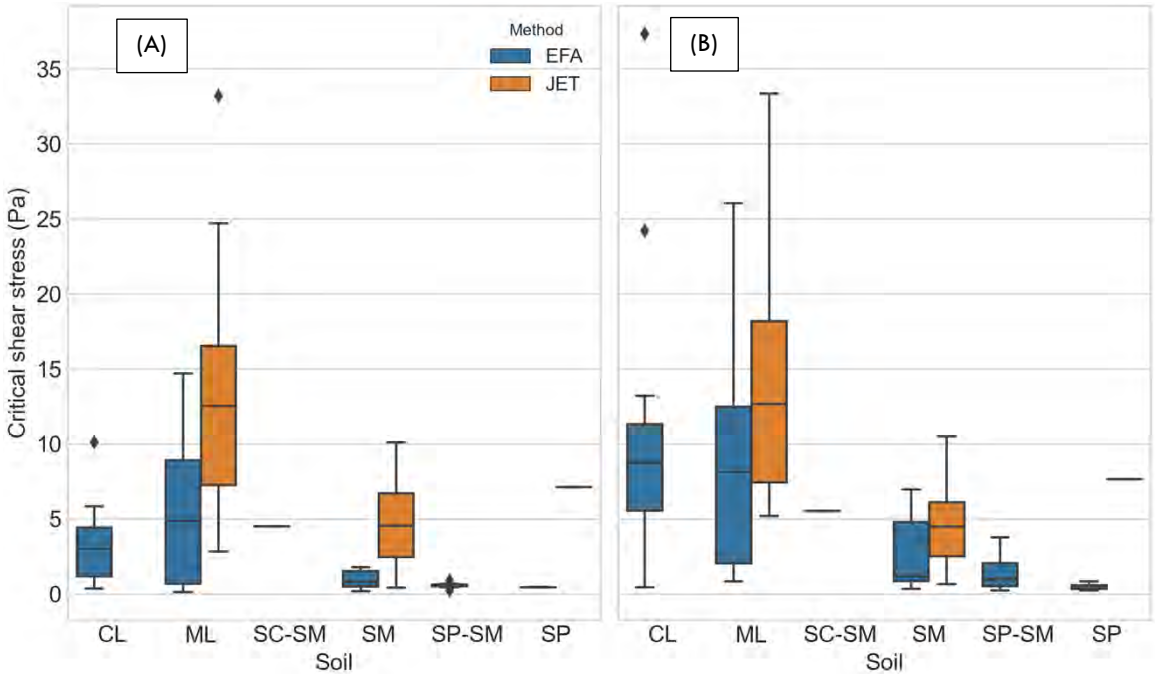

FIGURE II – COMPARISON OF (A) CRITICAL SHEAR STRESS DERIVED USING STANDARD EFA AND JET POST-PROCESSING TECHNIQUES (STEP I OF FOLLOWED PROCEDURE) AND (B) CRITICAL SHEAR STRESS ASSOCIATED WITH EROSION FUNCTIONS BASED ON GRAIN SHEAR STRESS, MASS SURFACE EROSION REGIME, AND INCLUDE UNCERTAINTY IN ESTIMATED SHEAR STRESS AND MEASURED EROSION RATE (STEP 4 OF FOLLOWED PROCEDURE).

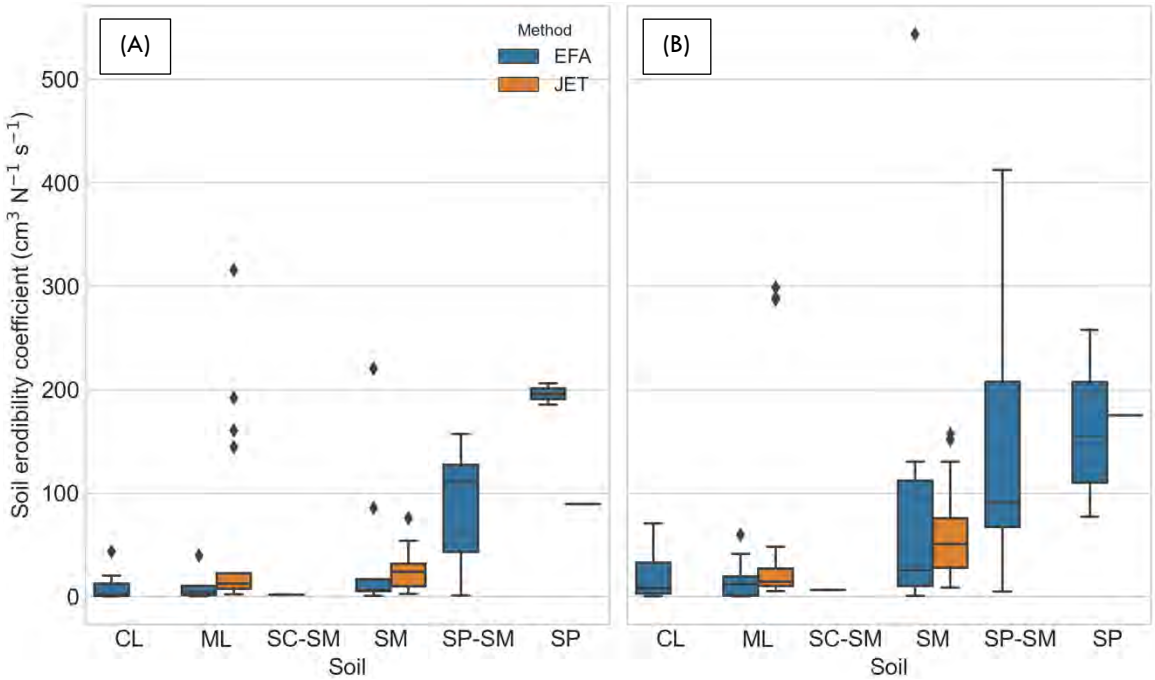

FIGURE III – COMPARISON OF (A) ERODIBILITY COEFFICIENT DERIVED USING STANDARD EFA AND JET POST-PROCESSING TECHNIQUES (STEP 1 OF FOLLOWED PROCEDURE) AND (B) ERODIBILITY COEFFICIENT ASSOCIATED WITH EROSION FUNCTIONS BASED ON GRAIN SHEAR STRESS, MASS SURFACE EROSION REGIME, AND INCLUDE UNCERTAINTY IN ESTIMATED SHEAR STRESS AND MEASURED EROSION RATE (STEP 4 OF FOLLOWED PROCEDURE).

TABLE I – OUTPUT PARAMETERS α AND p FROM KOLMOGOROV-SMIRNOV (KS) TESTS INDICATING IF DISTRIBUTIONS OF CRITICAL SHEAR STRESSES AND ERODIBILITY COEFFICIENTS DERIVED BY EFA AND JET METHODS FOR SILT AND SILTY SAND SOIL TYPES ARE THE SAME. TESTS WERE CONDUCTED FOR EROSION-RESISTANCE PARAMETERS DETERMINED FOR STEPS 1 AND 4 OF THE PRESENTED ANALYSIS PROCEDURE. THE PARAMETER α IS THE KS STATISTIC AND p IS THE TWO-TAILED p VALUE.

	Silt				Silty sand			
	Step 1		Step 4		Step 1		Step 4	
Parameter	α	p	α	p	α	p	α	p
Critical shear stress	0.500	0.088	0.400	0.201	0.833	$4.4\ 10^{-4}$	0.500	0.114
Erodibility coefficient	0.556	0.041	0.400	0.201	0.500	0.114	0.306	0.638

stress and erodibility coefficient distributions for silts and silty sands derived using the EFA and JET methods. When the KS statistic α is small or the p-value of the test is large the tested distributions are the same (i.e. we cannot reject the null hypothesis that the two distributions are the same). Generally, the α values are fairly large but improved (i.e. became smaller) for Step 4 compared to Step 1. Also, the p values improved for Step 4 relative to Step 1. Therefore, the distributions of erosion-resistance parameters compare better for Step 4 than they do for Step 1, which is shown in Figures II and III. The KS tests indicate that the EFA- and JET-derived critical shear stress distributions for silty sand soils are different for Step 1 (small p values) but compare reasonably well for Step 4 ($p_{SM} > 0.11$ and $p_{ML} > 0.201$). The erodibility coefficients determined by EFA and JET methods are different for Step 1, but compare reasonably well for silts and quite well silty sand soils..

The main findings of comparing soil erosion-resistance characterized by BET, EFA, and JET methods for various soils along the Lower American River and Sacramento River are:

1. The BET method provides a similar range in critical shear stress as the EFA and JET methods, but the corresponding erodibility coefficients are typically two orders of magnitude smaller than those provided by the EFA and JET methods (Figure I). This is likely caused by errors/uncertainty in measuring the erosion rate of the borehole wall and estimating the applied shear stresses acting on the borehole wall.
2. The erosion-resistance parameters determined by the EFA and JET methods have similar magnitude and cluster by soil type when plotted on an erodibility coefficient versus critical shear stress chart (Figure I). Both measurement techniques show the more cohesive the soil, the more erosion-resistant it is (Figures II and III); that is greater critical shear stress and lower erodibility coefficient.
3. The distribution of erodibility coefficients determined by the EFA and JET methods compare well for silts and silty sands (Table I). The distributions of critical shear stress determined by the EFA and JET methods compare reasonably well for silts and silty sands. The critical shear stresses determined by the EFA method are about half those determined by the JET method (Figure II).

Comparison of the measured erosion-resistance parameters against those calibrated using the BSTEM bank erosion model against observed bank erosion along the Lower American River shows:

1. Erosion-resistance parameters for silts only need little calibration when used in bank erosion modeling.
2. Erosion-resistance parameters for less cohesive and cohesionless soils, such as silty sands and sands, need careful calibration when used in bank erosion modeling, because the simulated rate of erosion is sensitive to the model's bank shear stress approximation and transport-capacity limitation effects on entrainment.

Table of Contents

List of Figures

List of Tables

List of Abbreviations and Units

ARS	Agricultural Research Service
BET	Borehole Erosion Test
BSTEM	Bank Stability and Toe Erosion Model
C_d	diffusion coefficient; dimensionless
C_f	friction coefficient; dimensionless
CONCEPTS	CONservational Channel Evolution and Transport System
d	nozzle diameter; m
D_h	hydraulic diameter; m
D_{50}	median grain size; mm
E	erosion rate; m s^{-1}
EFA	Erosion Function Apparatus
ERDC	Engineer Research and Design Center
f	Darcy-Weisbach friction factor; dimensionless
$f_{annulus}$	Darcy-Weisbach friction factor for an annular cross section; dimensionless
f_{pipe}	Darcy-Weisbach friction factor of a pipe, equivalent to f; dimensionless
GPS	Global Positioning System
GSL	Geotechnical Structures Laboratory
g	acceleration due to gravity; 9.81 m s^{-2}
h	scour hole depth; m
H	pressure head at nozzle; m
HEC-RAS	Hydrologic Engineering Center River Analysis System
i	time increment
JET	Jet Erosion Test
k_d	soil detachment coefficient; m s^{-1} Pa^{-1}
L	height of jet-test device nozzle above soil surface or erosion distance; m
L_0	initial height of jet-test device nozzle above soil surface; m
LAR	Lower American River
NAVD88	North American Vertical Datum of 1988
NGS	National Geodetic Survey
NSL	National Sedimentation Laboratory
ODR	Orthogonal Distance Regression
p	two-tailed p value
Q	discharge; m^3 s^{-1}
$r_{borehole}$	local borehole radius; m
$r_{outside\_rod}$	outside radius of the drilling rod; m
REMT	Resistance-to-Erosion Measurement Technique
Re	Reynolds number
SAC	Sacramento River
SPK	U.S. Army Corps of Engineers, Sacramento District
SRH-2D	Sedimentation and River Hydraulics Two-Dimensional model
t	time; s
U_0	jet centerline velocity at the nozzle; m s^{-1}
USACE	U.S. Army Corps of Engineers
USCS	Unified Soil Classification System
USDA	U.S. Department of Agriculture
USGS	U.S. Geological Survey
V	mean flow velocity; m s^{-1}
WRDA	Water Resources Development Act
α	Kolmogorov-Smirnov statistic

δ	combined error
ϵ	mean depth of surface asperities; m
ϵ_g	roughness height of sediment grains; m
μ	mean of a normally distributed random continuous variable
ρ	density of water; kg m^{-3}
σ	standard deviation of a normally distributed random continuous variable
τ	boundary (bed or bank) shear stress; Pa.
τ_c	soil critical shear stress; Pa
τ'	grain shear stress; Pa
τ''	form drag component of boundary shear stress; Pa
χ	ratio of modeled applied shear stress to actual applied shear stress; dimensionless

Conversion Factors

Multiply	*By*	*To obtain*
	Length	
millimeter (mm)	0.03937	inch (in)
meter (m)	3.281	foot (ft)
kilometer (km)	0.6214	mile (mi)
	Area	
square meter (m^2)	10.764	square foot (ft^2)
square kilometer (km^2)	0.3861	square mile (mi^2)
	Volume	
cubic meter (m^3)	35.31	cubic foot (ft^3)
	Flow	
meter per second ($m\ s^{-1}$)	3.281	foot per second ($ft\ s^{-1}$)
cubic meter per second ($m^3\ s^{-1}$)	35.31	cubic foot per second ($ft^3\ s^{-1}$)
	Erosion rate	
meter per second ($m\ s^{-1}$)	11,811	foot per hour ($ft\ hr^{-1}$)
millimeter per minute ($mm\ min^{-1}$)	0.1969	foot per hour ($ft\ hr^{-1}$)
	Mass	
gram (g)	0.03527	ounce (oz)
kilogram (kg)	2.205	pound (lb)
tonne, metric	1.102	ton (short)
metric tonne per square kilometer per year ($ton\ km^{-1} yr^{-1}$)	2.855	ton (short) per square mile per year ($ton\ mi^{-2}\ yr^{-1}$)
	Force per unit length	
kilonewton per meter ($kN\ m^{-1}$)	5.710	pound-force per inch ($lbf\ in^{-1}$)
kilonewton per meter ($kN\ m^{-1}$)	68.52	pound-force per foot ($lbf\ ft^{-1}$)
	Stress	
pascal (Pa)	0.02089	pound-force per square foot ($lbf\ ft^{-2}$)
(= newton per square meter, $N\ m^{-2}$)		
kilopascal (kPa)	0.145	pound-force per square inch ($lbf\ in^{-2}$)
kilopascal (kPa)	20.89	pound-force per square foot ($lbf\ ft^{-2}$)
	Density	
gram per cubic centimeter ($g\ cm^{-3}$)	62.43	pound per cubic foot ($lb\ ft^{-3}$)
	Unit weight	
kilonewton per cubic meter ($kN\ m^{-3}$)	6.366	pound-force per cubic foot ($lbf\ ft^{-3}$)
	Erodibility	
cubic centimeter per newton second ($cm^3\ N^{-1}\ s^{-1}$)	0.5655	cubic foot per pound-force hour ($ft^3\ lbf^{-1}\ hr^{-1}$)
centimeter per pascal hour ($cm\ Pa^{-1}\ hr^{-1}$)	1.571	cubic foot per pound-force hour ($ft^3\ lbf^{-1}\ hr^{-1}$)
meter per pascal second ($m\ Pa^{-1}\ s^{-1}$)	157.1	cubic foot per pound-force second ($ft^3\ lbf^{-1}\ s^{-1}$)

INTRODUCTION

Problem statement

The Lower American River (LAR) below Folsom Dam consists of approximately 30 miles of alluvial channel that meanders through Sacramento and other communities in northern California. Bank erosion has been a documented concern through 11 miles of this reach due to the proximity of the fluvial system to the engineered levees and the high population densities that live on the landside of the levees. There are also about 25 miles of levees (river left) along the Sacramento River (SAC) that protect Sacramento that could be adversely affected by bank erosion. The Water Resources Development Act (WRDA) of 2016 provides for engineering and design activities associates with implementing projects to reduce the flood risk on the LAR and the SAC (USACE, 2016). Being able to quantify the extent of bank erosion on the LAR and SAC is an important task, both to ensure that the designed bank protection is adequate and for prioritizing the bank protection work, ensuring that areas of higher risk for bank erosion are addressed first.

Bank erosion occurs as a result of the interaction of two processes: hydraulic and geotechnical (Langendoen & Simon, 2008). The hydraulic process involves the ability of the applied erosive forces from the water to erode the bank material, which is typically termed fluvial erosion. This requires knowing hydraulic properties representing the erosive force, such as water depth and energy slope, and bank material properties representing erosion resistance, such as soil composition (layers and type) and corresponding critical shear stress and erodibility coefficient. The geotechnical process requires insight into the strength of the soil to resist mass instabilities, or mass wasting. This requires knowing hydrologic and bank material parameters, such as soil gradations, bulk density, effective cohesion, friction angle, pore water pressure, and water content. Of these parameters, knowledge of the soil composition (layers and type) and its fluvial erosion resistance properties (critical shear stress and erodibility coefficient) have been determined to be the most important parameters in estimating long term bank erosion risk on the LAR and SAC.

The United States Army Corps of Engineers (USACE) has requested the United States Department of Agriculture (USDA), Agricultural Research Service (ARS), National Sedimentation Laboratory (NSL), Oxford, Mississippi, U.S. Geological Survey (USGS), California Water Science Center, Sacramento, California, and Texas A&M University (TAMU), Texas Transportation Institute (TTI), College Station, Texas, to characterize the resistance-to-fluvial-erosion (hereafter simplified to erosion resistance) properties of LAR and SAC bank soils to better evaluate the range of these parameters and the associated uncertainty in their measurements. Each organization used different tests to measure soil erosion-resistance: ARS used Jet Erosion Test (JET) methodology (Langendoen & Ursic, 2020); USGS used Borehole Erosion Test (BET) methodology (Work & Livsey, 2020); and TAMU used BET, Erosion Function Apparatus (EFA), and Pocket Erodometer Test (PET) methodologies (Briaud et al., 2020). These data are used to derive probability density functions of bank-soil erosion-resistance properties for input into the Bank Stability and Toe Erosion Model (BSTEM) Dynamic v3 bank erosion model, which is used by USACE to calculate the risk of levee failure caused by bank erosion.

Objective

The objectives of the presented work are:

1- Compare the erosion resistance parameters derived using BET, EFA, and JET measurement technologies by soil type; and
2- Investigate the epistemic uncertainty associated with limitations in the testing methods.
3- Provide recommendations on the use and application of the erosion-resistance parameters pertinent to the evaluation of bank erosion on the Lower American River using the USDA-ARS Bank Stability and Toe Erosion Model (BSTEM).

Study area

The geographic scope of the reported work is a 10-mi long reach on the American River and a 15-mi long reach on the Sacramento River adjacent to the City of Sacramento, California (Figure 1). The U.S. Army Corps of Engineers, Sacramento District (SPK), selected 10 study sites on the Lower American River (LAR1, LAR2, LAR3, LAR4, LAR5, LAR6, LAR7, LAR8, LAR9, LAR10, and LAR12) and 6 study sites on the Sacramento River (SAC1, SAC3, SAC5, SAC7, SAC8, and SAC9) for which soil erosion-resistance tests were conducted in 2018-2019. These data were complemented with available data from 15 sites on the Lower American River (2F-11-124, 2F-11-125, 2F-11-126A, 2F-11-126B, 2F-11-128A, 2F-11-128B, 2F-11-129B,

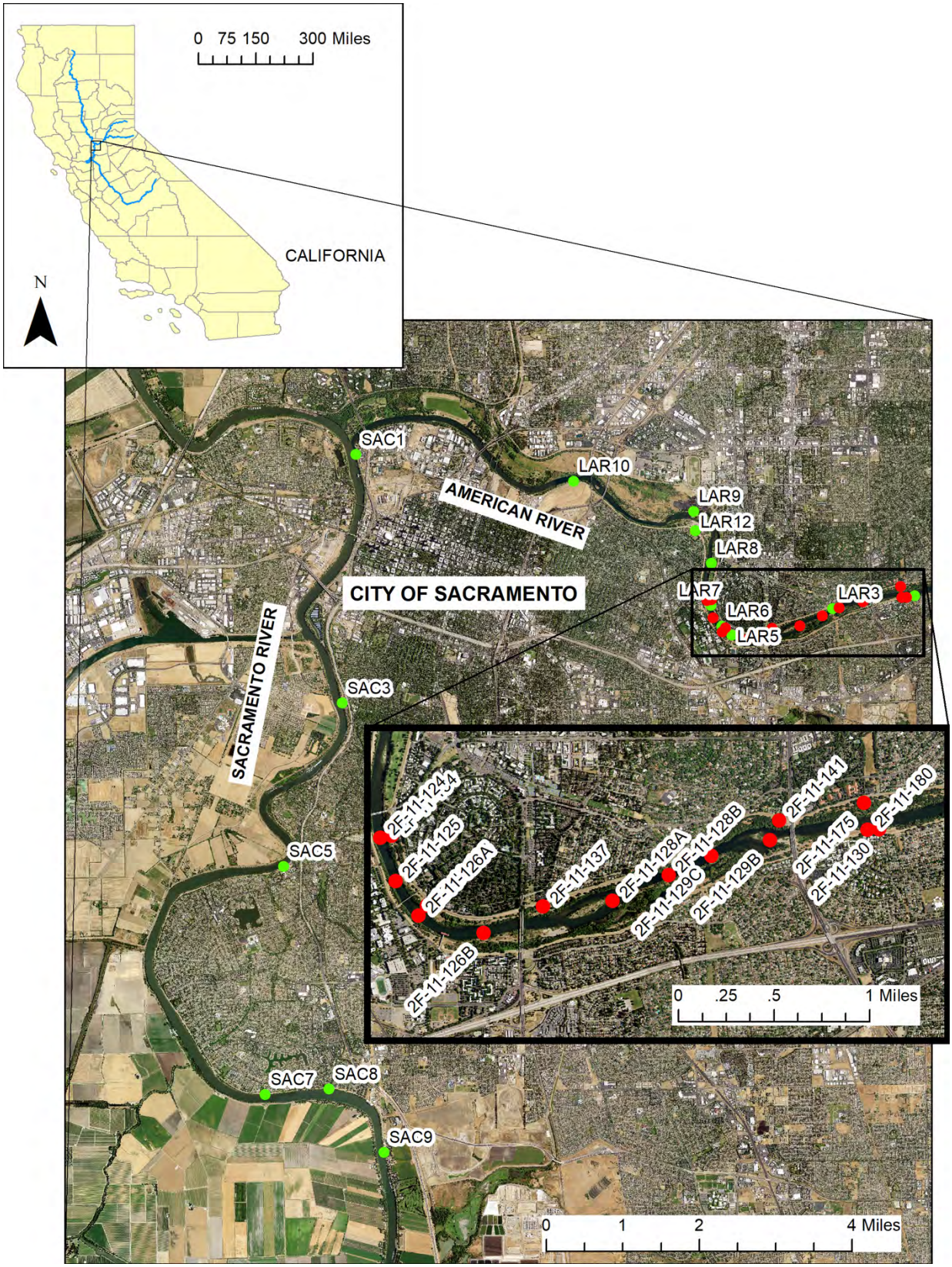

FIGURE 1 – STUDY SITES ON THE AMERICAN AND SACRAMENTO RIVERS, CALIFORNIA. GREEN CIRCLES INDICATE 2018-2019 TEST SITES, WHEREAS RED DOTS INDICATE 2011 TEST SITES.

2F-11-129C, 2F-11-130, 2F-11-134, 2F-11-135, 2F-11-137, 2F-11-141, 2F-11-175, and 2F-11-180). The soil types tested at these sites, following the Universal Soil Classification System (USCS), are: CL, clay of low plasticity, GP, poorly graded gravel; MH, silt of high plasticity; ML, silt; SC, clayey sand; SC-SM, clayey and silty sand; SM, silty sand; SP, poorly graded sand; SP-SC, poorly graded sand with clay; and SP-SM, poorly graded sand with silt.

METHODS

Overview

Erosion of fine-grained (cohesive) bank materials is a combination of scour by the flowing water and bank collapse. Fluvial erosion of fine-grained materials is controlled by the hydraulic shear acting on the bank soils and the erosion resistance of these soils. The soil erosion-resistance itself depends on various soil chemical, hydrologic, and physical properties, which are typically parameterized into few parameters that can greatly vary by and within soil types. Various testing methods exist to derive the erosion-resistance parameters, and each test method typically uses different hydraulic conditions. The natural variability in soil erodibility, its parameterization and different measurement techniques introduce both differences in magnitude and uncertainty in erosion-resistance parameters. The following sections describe the assessed resistance-to-erosion measurement techniques (REMTs) and the analysis of the soil erosion-resistance parameters derived by these measurement techniques.

Soil erodibility

The detachment of particles (that is, grains and aggregates of different sizes) from fine-grained bank materials is extremely complex because of electro-chemical bonds between such particles. Ariathurai & Arulanandan (1978) showed that the rate of erosion, E, of cohesive materials can be represented by an excess shear stress equation:

$$E = \begin{cases} k_d(\tau - \tau_c) & \tau > \tau_c \\ 0 & \tau \leq \tau_c \end{cases} \quad (1)$$

where E is erosion rate (m s^{-1} or ft hr^{-1}), τ is boundary shear stress exerted by flowing water on the soil surface (Pa or lbf ft^{-2}), τ_c is soil critical shear stress (Pa or lbf ft^{-2}), and k_d is soil detachment (or erodibility) coefficient (m s^{-1} Pa^{-1} or ft^3 lbf^{-1} hr^{-1}) representing the volume of material eroded per unit force and per unit time. Eq. (1) is an approximation of the relationship between erosion rate and shear stress deemed the 'erosion function' by Briaud et al. (2001).

The bank erosion modules of the ARS CONservational Channel Evolution and Pollutant Transport System (CONCEPTS; Langendoen & Alonso, 2008; Langendoen & Simon, 2008) and Bank Stability and Toe Erosion Model (BSTEM; Simon et al., 2011) use Eq. (1) to calculate the rate of fluvial erosion. These modules are also used by river morphologic computer models such as RVR Meander (Motta et al., 2012), HEC-RAS v5 (Brunner, 2016), and SRH-2D (Lai et al., 2015).

Data sets and test methods

To compare erosion-resistance parameters for USCS soil types obtained from different measurement methods, data sets were collected by ARS, TAMU, and USGS in 2018 and 2019. These data were complemented with results from tests conducted by USACE previously. Table 1 summarizes the data sets and instrumentation used by our analysis. Note, the BET data were collected by USGS, however the results of the analysis of the BET data conducted by TAMU were used because they related erosion rate to shear stress instead of velocity. The below paragraphs present brief overviews of the various test methods.

ARS mini-jet erosion test (mini-JET)

The ARS JETs were performed in-situ using a mini jet-test device (Figure 2). The mini-jet apparatus consists of an electric submersible 1050 GPH pump powered by a portable A/C generator that provides a head of water (H) measured by a pressure gage, a scaled-down 0.10 m-diameter submergence tank with an integrated, rotatable 3.18 mm-diameter nozzle and depth gauge, and delivery hoses. A sample is centered under the nozzle, where the jet originates, and submerged within the cylindrical tank. The initial height of the nozzle above the sample (L_0) is noted and can be adjusted prior to initiating a test. Changes in maximum scour are measured using a point gauge at specific time increments i, and regression analysis is conducted to best fit Eq. (1) to the erosion function. The head provided by the pump and the initial height of the nozzle above the sample determine the range of applied shear stress during the test.

The device and procedure have been developed based on knowledge of the hydraulic characteristics of a submerged jet and the corresponding scour produced by the jet. The maximum shear stress acting on the sample surface for a given distance to the nozzle (L) is:

$$\tau = \rho C_f \left(\frac{C_d U_0 d}{L}\right)^2 \quad (2)$$

where ρ is fluid density (kg m^{-3}), C_f is friction coefficient, C_d is diffusion coefficient, U_0 is jet centerline velocity at the nozzle (m s^{-1}), and d is nozzle diameter (m). The coefficients $C_f = 0.00416$ and $C_d = 6.3$ were experimentally determined on a smooth, flat surface (Hanson et al., 1990). The velocity $U_0 = \sqrt{2gH}$, where g is gravitational acceleration (m s^{-2}) and H is pressure head (m) at the nozzle.

TABLE 1 – SUMMARY OF DATA SETS AND INSTRUMENTATION USED TO CHARACTERIZE THE EROSION RESISTANCE OF BANK SOILS ON THE LOWER AMERICAN AND SACRAMENTO RIVERS, CALIFORNIA.

Collecting agency	Date	Test	Number of tests	Description	Reference
ARS	Fall 2018	Mini-JET	27	In-situ test on bank surfaces	Langendoen & Ursic (2020)
TAMU	Fall 2019 – Winter 2020	EFA	36	Laboratory test on collected field samples	Briaud et al. (2020)
		BET	13	Data reduction of collected field data by USGS	
USACE	Fall 2011	JET	6	Laboratory test on collected field samples	Wibowo & Robbins (2012)
USACE	Fall 2011	JET	3	Laboratory test on collected field samples	Wibowo & Robbins (2017)
USACE	Fall 2011	EFA	12	Laboratory test on collected field samples	AuBuchon (2019; personal communication)
USGS	Spring – Summer 2019	BET	13	In-situ test on borehole surface	Work & Livsey (2020)

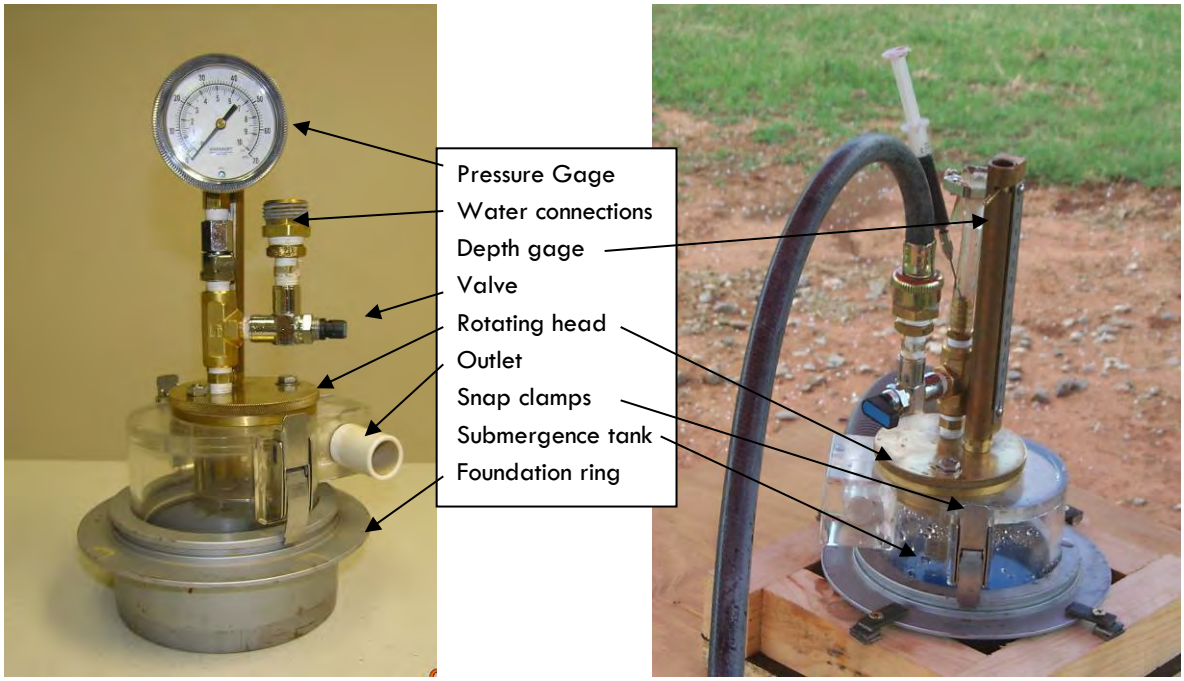

FIGURE 2 – PHOTOGRAPHS OF MINI-JET DEVICE USED TO MEASURE SOIL ERODIBILITY.

USACE jet erosion test (JET)

The USACE, Sacramento District partnered with the USACE, Engineer Research and Development Center (ERDC), Geotechnical Structures Laboratory (GSL) to perform JETs on soil samples from 4-in diameter cores taken along the American River (Wibowo & Robbins, 2012; 2017) for the American River Common Features General Reevaluation Report (USACE, 2016). The (classical) jet apparatus used by ERDC-GSL is different in scale from the aforementioned mini-jet apparatus, but the theory and analysis methods of the two devices are consistent. Eq. (2) is applicable to both jet devices; however, the nozzle diameter of the larger jet device used by ERDC-GSL is 6.35 mm as opposed to the 3.18 mm-diameter nozzle of the mini-jet apparatus. The ERDC-GSL test setup is a 12-in diameter by 12-in high Plexiglas chamber with a 4-in groove in the base center for setting 4- to 4.5-in long cut cores and an outlet hose (Figure 3). The jet apparatus consists of an inlet hose, deflector plate, nozzle, erosion reading unit or point gage, and digital pressure reading unit (Figure 4). Water is delivered to the jet nozzle by a 2-HP electric pump from a 500-gallon tank through a manifold used to control pressure. The testing sequence is identical to that of the mini-jet device. An initial point gage reading is taken to measure the distance from the nozzle to the soil surface. The chamber is then filled with water through the jet nozzle with the deflector plate in place. Once the nozzle is submerged the deflector plate is moved and the sample is jetted for a specified time increment. At the end of the time increment the point gage is lowered to measure the depth of soil below the nozzle. This process is repeated until erosion asymptotically approaches a constant value (Wibowo & Robbins, 2012; 2017). It should be noted that only 9 of the 24 tests provided by Wibowo & Robbins (2012; 2017) were considered acceptable after screening; 15 tests were removed from consideration.

Borehole erosion test (BET)

The Borehole Erosion Test (BET) is a field erosion test conducted in a borehole that is drilled by the wet rotary head method (Briaud et al., 2017). Drill bit diameters can be between 75 and 100 mm but the outside rod diameter should be 75% or less than that of the drill bit. Once the borehole is drilled, a mechanical borehole caliper is lowered to the bottom of the hole where the mechanical arms are released to press against the hole walls. During the caliper retrieval process, diameter recordings are made throughout the length of the borehole which provide initial readings for the test. In order to conduct the test, the drilling rods, without the bit, are reinserted into the hole and suspended off the bottom by 0.15 m. A sequence of flows of different discharge is then pumped (typically 10 minutes for each flow) through the drilling rods to the bottom of the borehole where it returns to the surface along the walls of the drilled hole. Discharges are selected based upon target flow velocities between 0.5 and 3 m s^{-1}. Once a given flow has been conducted, the drilling rods are removed and the calipers are lowered to the bottom of the borehole again. The calipers are then retrieved, providing diameter readings of the eroded borehole. It is suggested that 4 to 6 repetitions of flow and caliper sequences per flow be conducted (Briaud et al., 2017). The amount of erosion is associated to an average applied shear stress related to cross-sectional average velocity and friction coefficients determined by use of the Moody diagram (Moody, 1944). The local average flow velocity V within the annular cross section is:

$$V = \frac{Q}{\pi(r_{borehole}^2 - r_{outside\_rod}^2)} \tag{3}$$

where Q is discharge, $r_{borehole}$ is local radius of the borehole, and $r_{outside\_rod}$ is the outside radius of the drilling rod. Discharge values were recorded using a Tactical Flowmeter with a reported error less than 0.5% over its rated range of 200 gallons per hour (Work & Livsey, 2020). Applied shear stress values for the BET are determined by Eq. (4) (Briaud et al., 2017; Briaud et al., 2020):

$$\tau = \frac{1}{8} f \rho V^2 \tag{4}$$

where τ is the shear stress acting on the wall of the borehole, f is the friction factor of the borehole wall obtained from the Moody diagram, ρ is the mass density of water (1,000 kg m^{-3}), and V is the mean flow velocity. Determination of the friction factor (f) from the Moody diagram requires the Reynolds number and relative pipe roughness (ϵ/D_h), where D_h is the hydraulic diameter and ϵ is assumed equal to the mean depth of surface asperities evaluated at 10-cm increments (Briaud et al., 2020). While the hydraulic diameter, Reynolds number, and relative pipe roughness are evaluated at rolling 10-cm increments, shear stress and erosion rates that utilize the rolling 10-cm parameters are evaluated at approximately 6-mm increments. Additionally, due to the annular cross section, a correction factor is applied to the friction coefficient estimated from the Moody diagram as described in Eq. (**5**) (Munson, 2009).

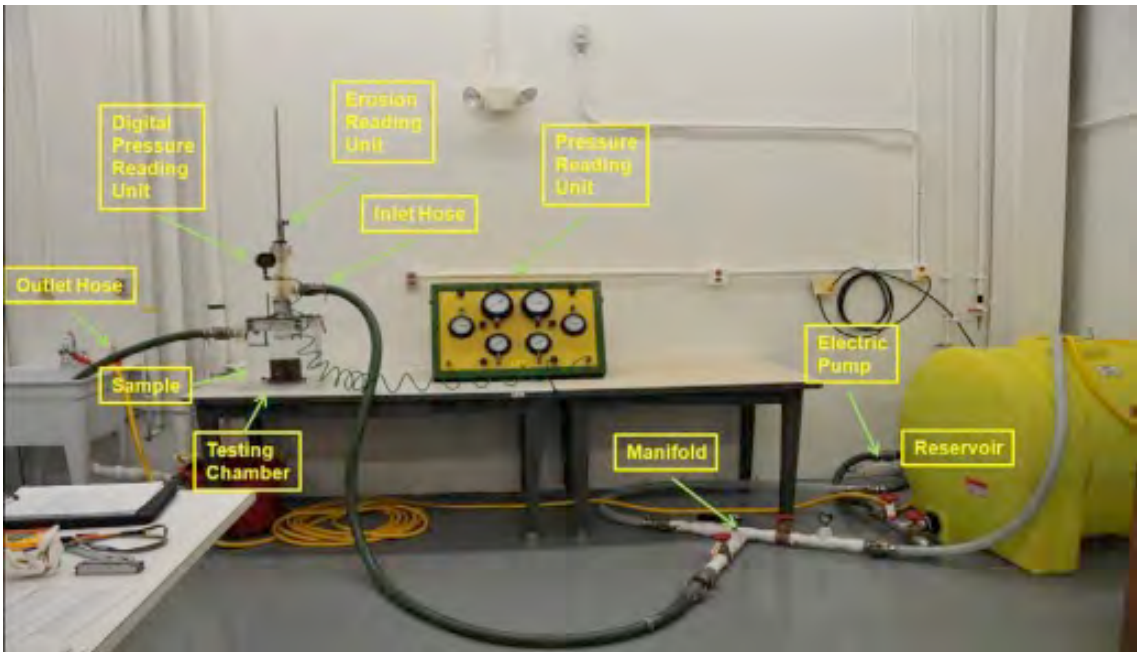

FIGURE 3 – USACE ERDC JET TESTING APPARATUS. ADAPTED FROM WIBOWO & ROBBINS (2012).

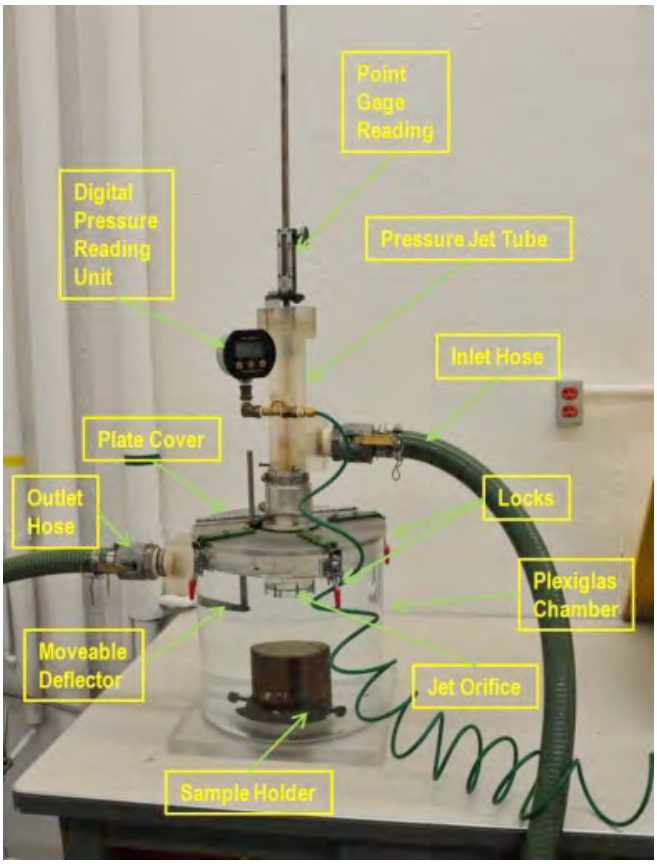

FIGURE 4 – USACE ERDC JET APPARATUS AND TESTING CHAMBER. ADAPTED FROM WIBOWO & ROBBINS (2012).

$$f_{annulus} = 1.5f \quad (5)$$

For this report, mean erosion rate and applied shear stress values are derived for each soil layer in a borehole by averaging 6-mm increment erosion rate and applied shear stress data over the length of the soil layer. Data reduction by this method limits the number of data points that are used to determine soil erodibility parameters, and therefore provides more insight in the erosion function than could be deduced by using all available data due to the large range of scatter for individual tests. Additionally, since the borehole does not erode in a uniform fashion, nor does the caliper follow the same path each time through the borehole, negative values were removed from consideration. While removal of negative values may introduce a bias to the results by providing weight to non-negative values, it is fair to assume that no accretion is occurring on the borehole sidewall.

Erosion function apparatus (EFA)

Samples from soil identification drilling efforts associated with the BET were tested for erosion resistance by Texas A&M University using an Erosion Function Apparatus (EFA). The EFA is a test that utilizes principles of flow in closed conduits to determine applied forces at the boundary where a soil sample is introduced. The conduit used in the EFA is a rectangular pipe of dimensions 101.6-mm wide by 50.8-mm high and a length of 1.22 m. Soil samples are protruded into the flow at the bottom of the conduit through a Shelby Tube (ASTM Standard D1587, 1999) using a piston that is controlled by laboratory personnel (Figure 5). Samples were provided to Texas A&M University in both Shelby Tubes (N=12) and sample bags (N=24). Samples that were provided in Shelby Tubes were tested directly without further disturbance, while the samples provided in bags required reconstitution. Reconstitution of samples required compaction by either shaker or drop hammer to obtain unit weights that corresponded to in-situ total unit weights (Briaud et al., 2020). Flow speeds in the EFA are controlled by a pump and valve system with flow rates determined by an inline flow meter. The range of mean flow velocities is between 0.1 and 6 m s^{-1} (Briaud et al., 2001). Erosion rates are determined for a range of sequential steady-state velocities over a 10-minute period or 10 mm of erosion, whichever comes first. Results of the EFA test provide an erosion function represented by applied shear stress associated with each steady-state velocity and corresponding erosion rate (Figure 5). Applied shear stress values for the EFA are determined by Eq. (4). Determination of the friction factor (f) from the Moody diagram requires the Reynolds number and relative pipe roughness (ϵ/D_h), where ϵ is assumed equal to one half the median grain size or one half of the depth of surface asperities depending on soil type (Briaud et al., 2020).

USACE erosion function apparatus (EFA)

Some samples collected for erosion testing for the American River Common Features General Reevaluation Report (USACE, 2016) were also tested in the EFA by USACE ERDC in 2011. Samples from 4" Shelby tubes were extruded and reduced in diameter for input to a 3-in tube and subsequent protrusion into the EFA. The primary difference between EFA tests conducted by TAMU (Briaud et al., 2020) and the tests conducted on the 2011 samples is the testing methodology. Tests conducted on the 2011 samples were conducted as described by (Briaud et al., 2001) where samples are protruded into the flow at 1 mm increments and erosion rates determined based on the time it takes to erode. The protrusion and erosion cycle is repeated for different velocities until the erosion function is determined. Tests conducted by TAMU (Briaud et al., 2020) were conducted by pushing the soil out of the sampling tube at a rate only equal to the rate of erosion. Additionally, samples tested by the USACE ERDC were not reconstituted. The 2011 EFA samples were also from soils dating back to the Pleistocene era, which are older and likely more consolidated than the tests run by Briaud et al. (2020), where the collected soil samples date to the Holocene era.

Data analysis and reduction

The following procedure was used to progressively improve compatibility between soil erosion-resistance parameters derived by the three REMTs:

Step 1. Calculate the erosion-resistance parameters from the 'as-is' erosion function measured (or output) by the BET, EFA, and JET methods.
Step 2. Same as Step 1 but limit the erosion function to the portion representing the mass soil erosion regime.
Step 3. Same as Step 2 but base the erosion function on the shear stress acting at grain or (small) soil particle roughness length scales.
Step 4. Same as Step 3 but account for uncertainty in measured erosion rate and estimated applied shear stress.

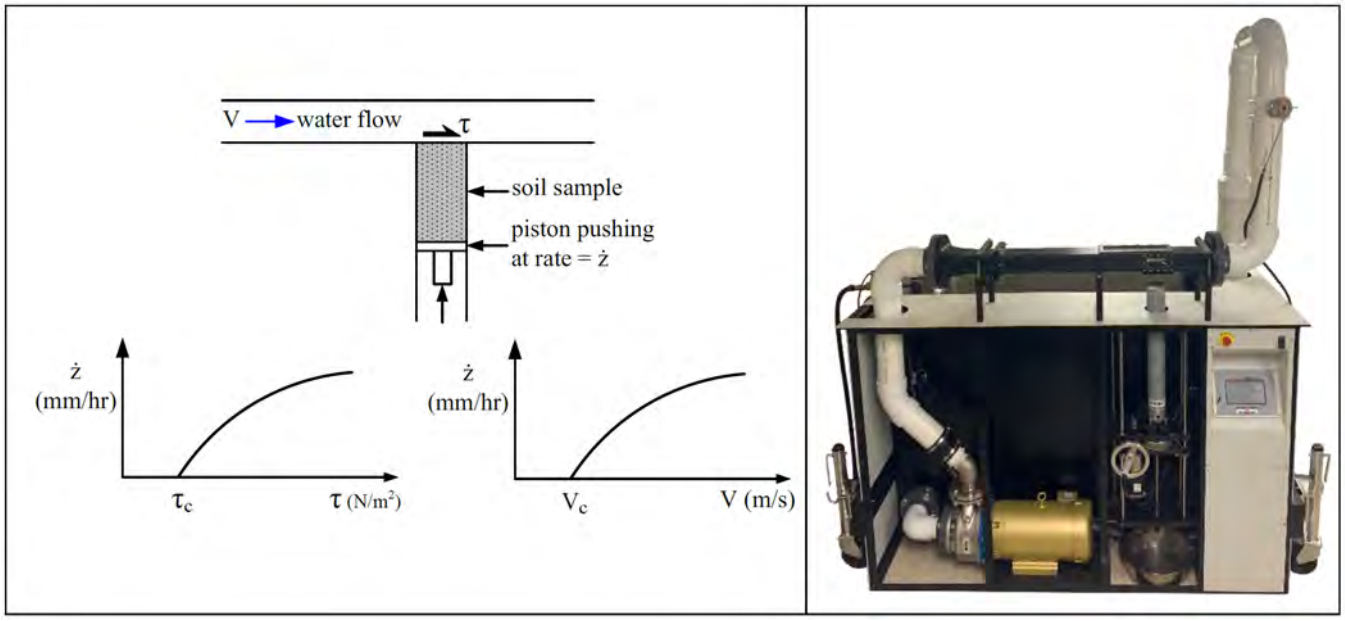

FIGURE 5 – EROSION FUNCTION APPARATUS (EFA). ADAPTED FROM BRIAUD ET AL. (2020).

Derivation of erosion-resistance parameters (Analysis Steps 1 and 2)

The resistance-to-erosion measurement techniques output two variables: erosion rate (E) and applied shear stress (τ). While each REMT may have different regressive methods to determine erodibility parameters, the use of one regressive method amongst all REMTs enables direct comparison of soil erodibility parameters. Comparisons conducted herein are based on linear regression on an arithmetic scale. The linear regression method fits a linear trendline through the measured pairs of (τ,E)-points that form the erosion function, where $E = \Delta L/\Delta t$ with ΔL the magnitude of soil surface erosion over a time increment Δt. The critical shear stress (τ_c) is determined by the intercept on the abscissa, while the erodibility coefficient (k_d) is equal to the slope of the regressed line. The resulting linear trendline is equivalent to the function provided by Eq. (1).

Erosion functions are generally non-linear as they cover different erosion regimes (Papanicolaou et al., 2017): (1) particle-by-particle erosion at low excess shear stress, (2) mass erosion when applied shear stress exceeds a critical shear stress to entrain aggregates and clods, and (3) limited detachment because of large sediment concentrations near the soil surface at very large shear stresses. A measured erosion function typically covers erosion regimes (1) and (2), only regime (1), or only regime (2). The mass-erosion regime is generally most important to erosion calculations as the erodibility coefficient for this regime is typically an order of magnitude greater than that of the particle-by-particle erosion regime and occurs at shear stresses corresponding to flood events. Our analysis presents both linear trendlines fitted through the entire erosion function (Analysis procedure Step 1) and linear trendlines fitted through the points representing the mass erosion regime only when present in the erosion function (Analysis procedure Step 2). The latter data are also referred to as 'filtered' data below.

Langendoen & Ursic (2020) derived erosion-resistance parameters for the mass-erosion regime, using the mini-JET, by linear regression, which were used as published. Figure 6 shows an example of an erosion function measured by the mini-JET. The JETs conducted by USACE (Wibowo & Robbins, 2012; 2017) were re-analyzed to obtain erosion-resistance parameters by linear regression of a linear trendline through the portion of the erosion regime representing the mass-erosion regime.

Appendix A of Briaud et al. (2020) provided individual reports for the conducted EFA tests, which included linear trendlines fit to the EFA erosion functions; an example is provided in Figure 7. The provided trendlines were used as-is to determine erodibility parameters τ_c and k_d. Additionally, linear trendlines were fitted to the EFA data points that only reflected the mass-erosion regime.

Here, for each discharge of a flow sequence, BET data were reduced to average erosion rate and applied shear stress over individual soil layers comprising a borehole at a given site (Appendix E). Data reduction by this method limits the number of points that are used to regress but provides more information than could be deduced by using all available data due to the

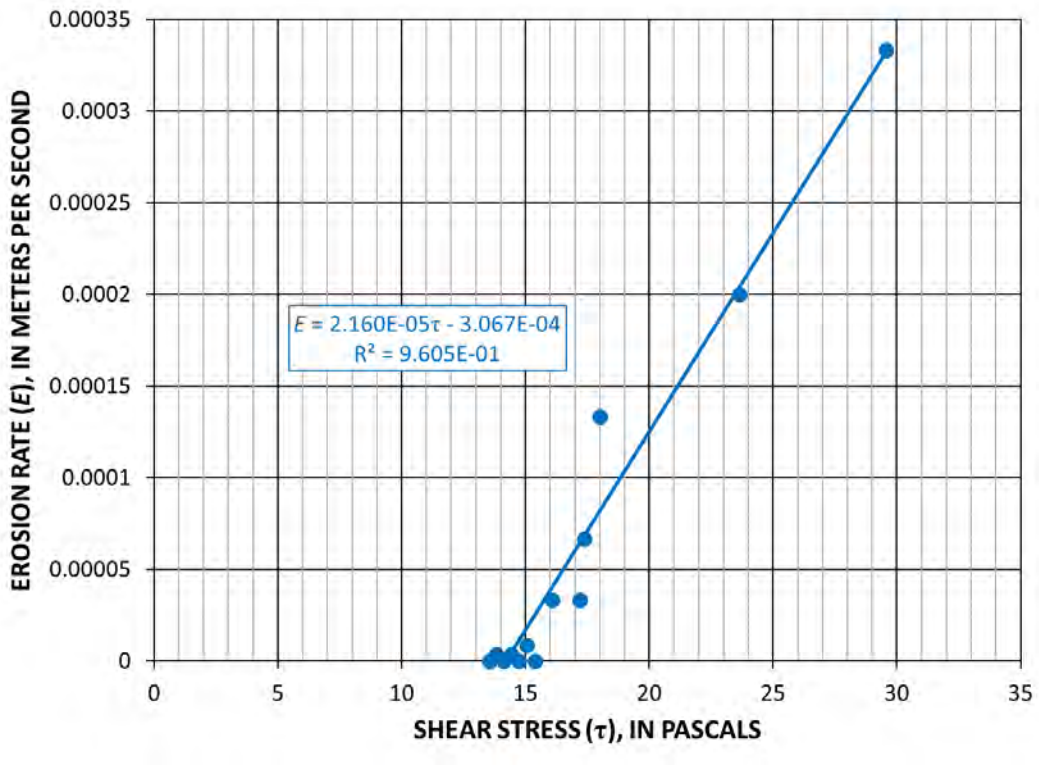

FIGURE 6 – EXAMPLE JET ANALYSIS USING THE LINEAR REGRESSION METHOD FOR STUDY SITE SAC3 (TEST 4) ON THE SACRAMENTO RIVER (LANGENDOEN & URSIC, 2020). THE REGRESSION EQUATION AND COEFFICIENT OF DETERMINATION (R^2) FOR THE LINEAR REGRESSION METHOD ARE DISPLAYED.

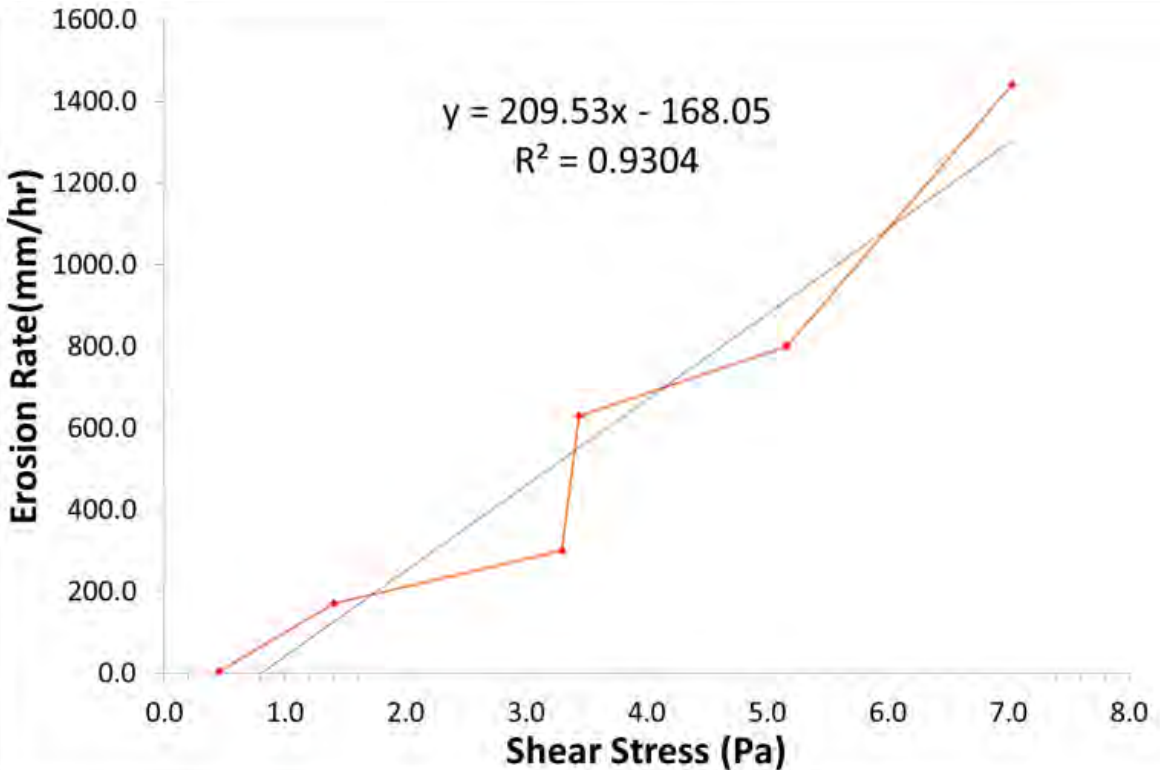

FIGURE 7 – EXAMPLE EFA ANALYSIS, TEXAS A&M UNIVERSITY (BRIAUD ET AL., 2020) – SAND SAMPLE #22 15-16.5 FT.

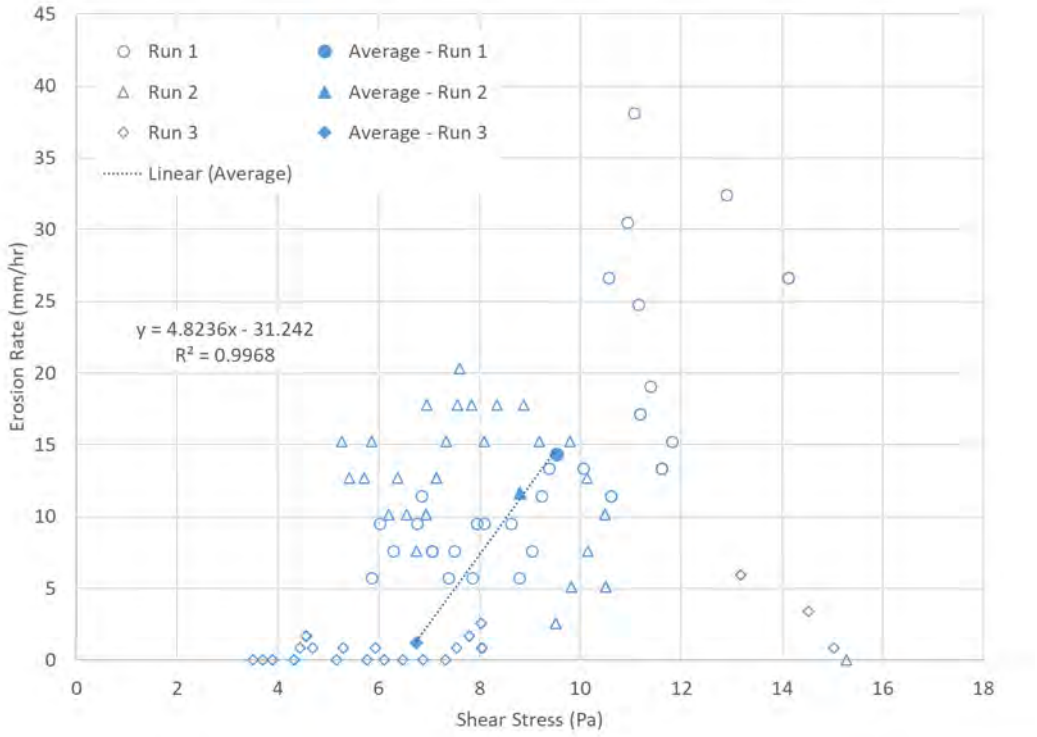

FIGURE 8 – EXAMPLE BET ANALYSIS OF SITE 'LOWER AMERICAN RIVER SITE #3 (LAR3), LEAN CLAY 1.4-1.6 M DEPTH' SHOWING DATA REDUCTION AND LINEAR REGRESSION OF REDUCED DATA. DATA IS PLOTTED WITH CORRESPONDING AVERAGE VALUES PER FLOW RUN. RAW DATA FROM BRIAUD ET AL. (2020).

large scatter in erosion rate and applied shear stress for individual tests. Additionally, values that imply accretion, or negative erosion rate values, were removed from consideration in the averaging process. Negative values are likely caused by the accuracy of the caliper, the travel path of the caliper, and uneven erosion through the borehole. It is important to note that removal of negative values may bias the resulting erodibility parameters by providing weight to non-negative values which creates slight inconsistencies with results or figures provided by Briaud et al. (2020). An example of data reduction and linear regression of reduced BET data is provided in Figure 8. Note, it is difficult to discern erosion regimes for the BETs because the derived erosion functions typically comprised three data points only.

Erosion-resistance parameters derived using applied shear acting on sediment grains or soil particles (Analysis Step 3)

The erosion functions measured by the mini-JET and JET are based on the shear stress acting on individual sediment grains and soil particles or aggregates. The contributions of surface asperities, not caused by grains and particles, to the overall shear acting on an eroding soil surface have been removed in the shear stress estimate (Eq. (2)). In contrast, the erosion functions reported by the EFA and BET method are a function of overall applied shear stress that include resistance provided by both particle-scale and larger than particle-scale roughness elements, which is reflected in the used Darcy-Weisbach friction factor f.

The reported shear stress for EFA and BET were partitioned into grain shear stress (τ') and form drag (τ'') contributions (Einstein, 1950; Vanoni & Brooks, 1957; Chow, 1959; Engelund, 1966) for direct comparison of erosion-resistance parameters between EFA, BET, mini-JET, and JET methods. The local coefficient of friction used in the JET is maintained as a constant at 0.00416 (Hanson & Cook, 2004), which relates to a Darcy-Weisbach friction factor of 0.03328. The roughness height, if taken as the median grain diameter, associated with $f = 0.03328$ is approximately equal to that of poorly graded sand (USCS classification SP) with slight variability due to hydraulics. For grain shear estimates associated with the EFA and BET, the friction factor f of 0.03328 was used as a minimum value for all tests unless the friction factor associated with half the median grain diameter (D_{50}) was larger. The use of half the median grain diameter is consistent with that suggested by Briaud et al.

(2020). Use of a minimum friction factor enables direct comparison to shear stress estimates of the JET. In order to assign a median grain size to a particular test, median grain sizes calculated from laboratory results were correlated with USCS soil types. Table 2 provides the resulting D_{50} values for each USCS soil type and Figure 9 graphically illustrates the range in data.

In order to determine the Darcy-Weisbach friction factor for half the median grain diameter in an expeditious manner, the function developed by Haaland (1983), Eq. (6), was used in lieu of the Moody diagram.

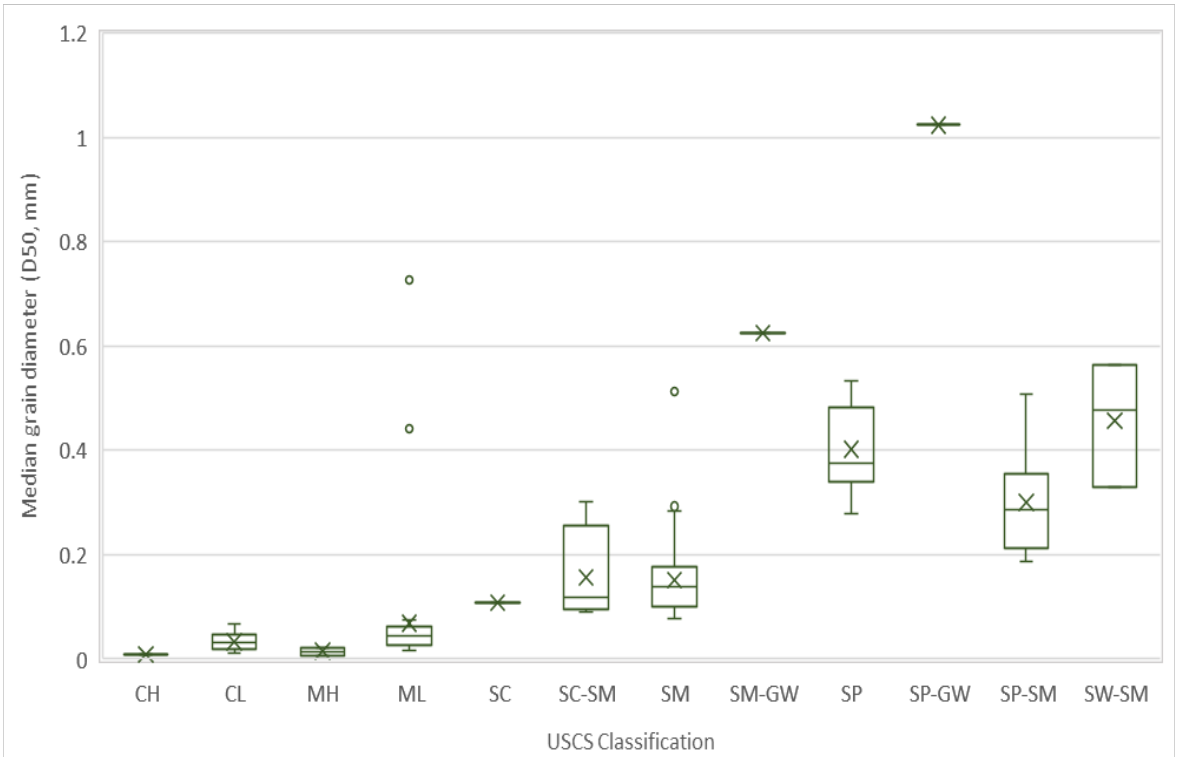

FIGURE 9 – MEDIAN GRAIN DIAMETER FOR EACH USCS SOIL TYPE – GRAIN SIZE DISTRIBUTIONS FROM BOREHOLE LABORATORY DATA.

TABLE 2 – MEDIAN GRAIN DIAMETER PER USCS CLASSIFICATION FOR ALL BOREHOLE SOILS.

USCS Classification	Average D_{50} (mm)	Standard deviation of D_{50} (mm)
CH	0.009	0.001
CL	0.033	0.018
MH	0.015	0.010
ML	0.068	0.121
SC	0.108	-
SC-SM	0.157	0.098
SM	0.151	0.080
SM-GW	0.625	-
SP	0.402	0.081
SP-GW	1.024	-
SP-SM	0.300	0.100
SW-SM	0.457	0.118

$$f = \left[\frac{1}{-1.8\log\left[\left(\frac{\epsilon_g / D_h}{3.7} \right)^{1.11} + \frac{6.9}{\mathrm{Re}} \right]} \right]^2 \quad (6)$$

where Re is the Reynolds number, ϵ_g ($= 0.5D_{50}$) is the roughness height of sediment grains or soil particles.

Effects of measurement uncertainty on erosion-resistance parameters (Analysis Step 4)

The erosion function relates a measured erosion rate (E) to an estimated shear stress (τ), both of which have associated uncertainty that could result in significant uncertainties in erosion-resistance parameters, τ_c and k_d, estimated from the erosion function. Note, that throughout this section the terms measurement uncertainty and error are used interchangeably but denote the same quantity. The uncertainty analysis used here assumes that measured erosion rate and estimated shear stress are random continuous variables, whose values are normally distributed with mean μ and standard deviation σ. The mean value represents the measured or estimated value, and the standard deviation is a measurement of the uncertainty. There exist various errors-in-variables models that account for measurement error. Here, we use Orthogonal Distance Regression (ODR), which finds the maximum likelihood estimators of parameters in measurement error models in the case of normally distributed errors (Boggs et al., 1987). The below sections describe the errors in erosion rate and shear stress for the mini-JET, JET, EFA, and BET methods.

MINI-JET AND JET METHOD

Measurement error in scour hole depth, h, is introduced by the accuracy of reading the scale of the point gage, by deposition of previously eroded soil particles or aggregates in the scour hole when flow is stopped for the scour hole depth measurement, and by asymmetric scour hole geometry. The latter two errors are negligible for small scour holes and increase with increasing scour hole depth. The point-gage scale can be read to an accuracy of $\pm$ 0.5 mm. We assume that the combined error caused by deposited particles and scour hole asymmetry is on average $\pm$ 1.0 mm over the range of tested scour hole depths. The combined error in reading the distance of the nozzle to the bottom of the scour hole is then $\delta_L = \pm\sqrt{0.5^2 + 1.0^2} = \pm 1.12$ mm. We assume (1) the error is randomly distributed with mean $\mu = 0$ mm and (2) the δ_L range includes 95% of probable error values. The standard deviation of the measurement error in distance of the nozzle to the bottom of the scour hole is then $\sigma_L = 0.56$ mm. As a result, the standard deviation of the erosion rate ($E = (L_{i+1} - L_i)/(t_{i+1} - t_i)$) error is $\sigma_E = 0.56\sqrt{2}/(t_{i+1} - t_i)$ mm s^{-1}, where i is the time increment level.

Error in estimated shear stress is a combination of the following errors: (1) approximation of values for the diffusion coefficient C_d and friction coefficient C_f; (2) measurement errors in pressure head at the nozzle (H), and therefore U_0, and scour hole depth h; and (3) the error introduced by assuming the jet is impinging on a flat plate instead of a scour hole. Error (3) is assumed to be the largest error. Unfortunately, the only available information on how the shear stress acting on the irregular bottom of a scour hole deviates from that acting on a flat plate is from numerical modeling studies (Weidner, 2012; Mercier et al., 2014). These studies found, on average, shear stress reduces in the evolving scour hole relative to that calculated using Eq. (2). The magnitude of reduction depends on the scour hole depth and aspect ratio. Note, one of the simulations conducted by Mercier et al. (2014) showed an increased shear stress. Defining the initial shear stress at the start of a JET as $\tau_0 = \rho C_d^2 C_f U_0^2/(L_0/d)^2$, one can express the shear stress at time increment i as:

$$\frac{\tau_i}{\tau_0} = \left(\frac{1}{1 + h_i / L_0} \right)^2 \quad (7)$$

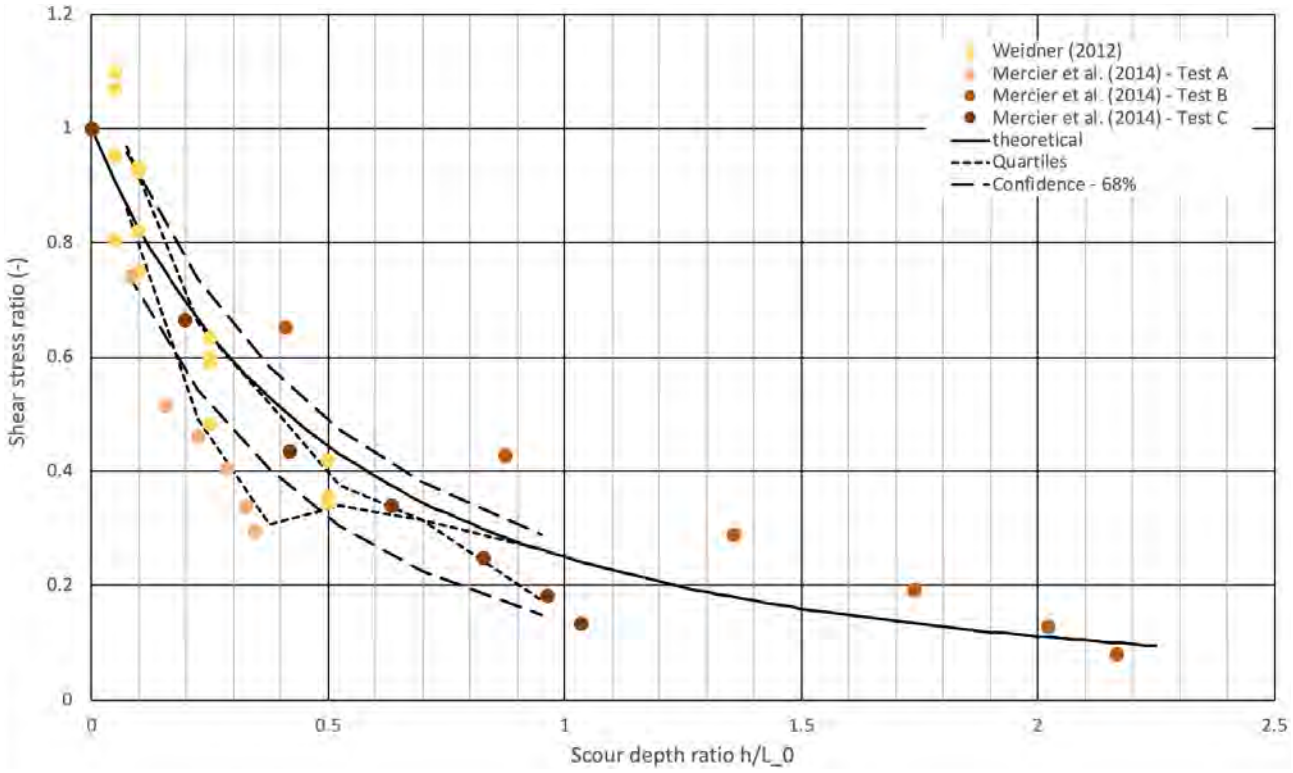

FIGURE 10 – COMPARISON OF THE SHEAR STRESS IN A SCOUR HOLE RELATIVE TO THAT ON A FLAT PLATE SURFACE. THE DOTS ARE SIMULATED DATA FROM WEIDNER (2012) AND MERCIER ET AL. (2014). THE SOLID BLACK LINE IS THE THEORETICAL CURVE ASSUMING THE SCOUR HOLE IS INFINITELY WIDE AND HAS A FLAT BOTTOM (EQ. (7)).

Which shows that the shear stress reduces quadratically with increasing scour hole depth. The simulation results from Weidner (2012) and Mercier et al. (2014) were made non-dimensional in a similar fashion and compared to Eq. (7), see Figure 10. An advantage of writing Eq. (2) as Eq. (7) is that it minimizes the inaccuracies in simulated boundary shear stress by the numerical models used by Weidner (2012) and Mercier et al. (2014) as long as the trend in boundary shear stress adjustment in an evolving scour hole is adequately captured.

The data shown in Figure 10 were used to quantify the probable error in estimated shear stress due to the flat surface assumption. It was assumed that the error was normally distributed with a mean value of $\mu_\tau = -0.179\tau\, h/L_0$ and a standard deviation $\sigma_\tau = (0.108 + 0.168\, h/L_0)\tau$. It was further assumed that shear stress error (1) is included in this error (3). Shear stress error (2) is accounted for by multiplying the above standard deviation by the factor $1 + (1/L_0(1 + h/L_0))^2$, and it is assumed that any error in U_0 is captured by shear stress error (3).

EFA METHOD

Briaud et al. (2001) estimated that the relative errors in erosion rate E and applied shear stress τ are about 10%. Note, that these errors were derived from repeated testing of near-identical manufactured samples of porcelain clay (Briaud et al., 2020), and therefore incorporate the intrinsic variability in erosion-resistance parameters for same soils and do not represent errors in shear stress estimation caused by uncertainty in velocity and friction factor (cf. Eq. (4)). When erosion-resistance parameters are derived using the grain shear stress, the friction factor f is held constant and the uncertainty in shear stress is due to measurement errors in flow velocity only. When erosion-resistance parameters are derived using the overall shear stress, both velocity errors and friction factor errors contribute to errors in estimated shear stress.

Assuming the relative error in observed erosion rate (10%) is normally distributed, with $\mu_E = 0$, and about 95% of likely E values fall within this range, the standard deviation of the error in erosion rate is $\sigma_E = 0.05E$.

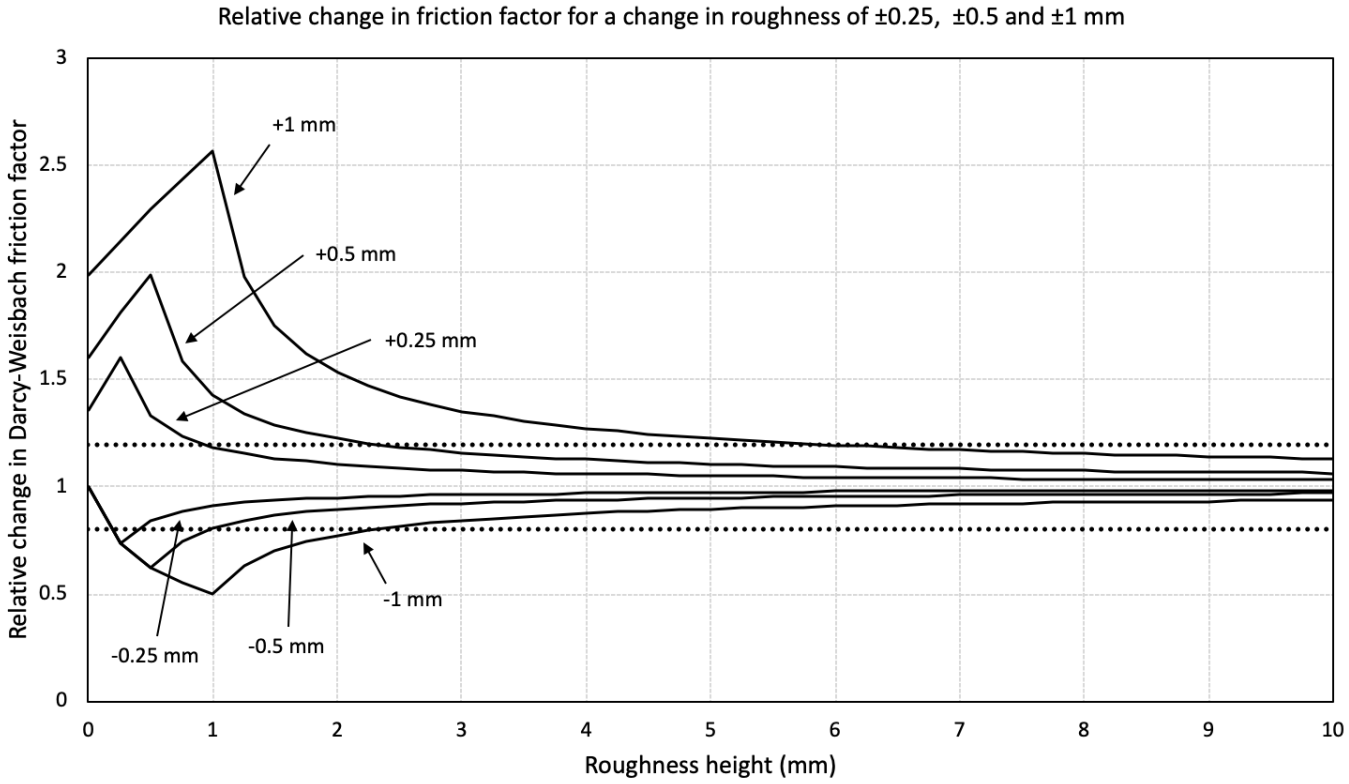

FIGURE 11 – RELATIVE CHANGE IN DARCY-WEISBACH FRICTION FACTOR FOR VARIATIONS IN ROUGHNESS HEIGHT ϵ OF ±0.25, ±0.5 AND ±1.0 MM. THE DOTTTED LINES REPRESENT A DECREASE AND INCREASE OF 20% IN DARCY-WEISBACH FRICTION FACTOR.

The typical accuracy of an electromagnetic flow meter is about 1%, which yields an uncertainty in flow velocity of $\sigma_V = 0.01V$. The uncertainty in estimated grain shear stress is then $\sigma_\tau = 0.01\sqrt{2}\tau$. The friction factor f is quite sensitive to small changes in roughness height ϵ and could vary more than 100% for small values of ϵ (< 2 mm), see Figure 11. Figure 11 further shows that equating the error in f to 20% of its value seems to be reasonable. Assuming that the friction factor error is normally distributed and about 95% of likely f values fall within this range, the standard deviation of the error in f is $\sigma_f = 0.1f$. Using principles of error propagation, the standard deviation of the error in overall shear stress is $\sigma_\tau = 0.101\tau$. We further assume $\mu_\tau = 0$ for both grain and overall shear stresses.

BET METHOD

Based on the conducted BETs, Work & Livsey (2020) concluded the measurement uncertainty in erosion rate is 1.0 in hr^{-1} (7.1 10^{-3} mm s^{-1}). However, this error does not account for asymmetric development of the borehole cross section that cannot be fully described by the three arms of the caliper, and therefore results in measurement errors of borehole diameter. By analyzing repeat caliper readings inside the same borehole, Briaud et al. (2020) found that the relative difference in measured radii varied up to 12% with a mean of 1.89% (N =109). 95% of the calculated error values were smaller than 5.08% (Table 6.3; Briaud et al., 2020). Assuming the error values in radius $r_{borehole}$ are normally distributed with zero mean, the standard deviation of the error in measured borehole radius is $\sigma_r = 0.0254r_{borehole}$. The error in erosion rate at time increment i ($E = (r_{borehole,i+1} - r_{borehole,i})/(t_{i+1} - t_i)$) is then $\sigma_E = 0.0254\sqrt{2}r_{borehole}/(t_{i+1} - t_i)$.

Figure 12 plots the estimated shear stress acting on the borehole wall during the first discharge out of a series of flows for the BET conducted at site LAR7. The shear stress is calculated using Eq. (4) with the friction coefficient f calculated using Eq. (6) with roughness ϵ_g replaced by ϵ, which is the mean depth of the asperities along the borehole wall (Briaud et al., 2020). The roughness ϵ is set equal to the standard deviation of caliper readings over 10-cm vertical segments, with each segment comprising about 17 caliper readings (~ every 6 mm). If the length of the asperities along the borehole wall is much smaller

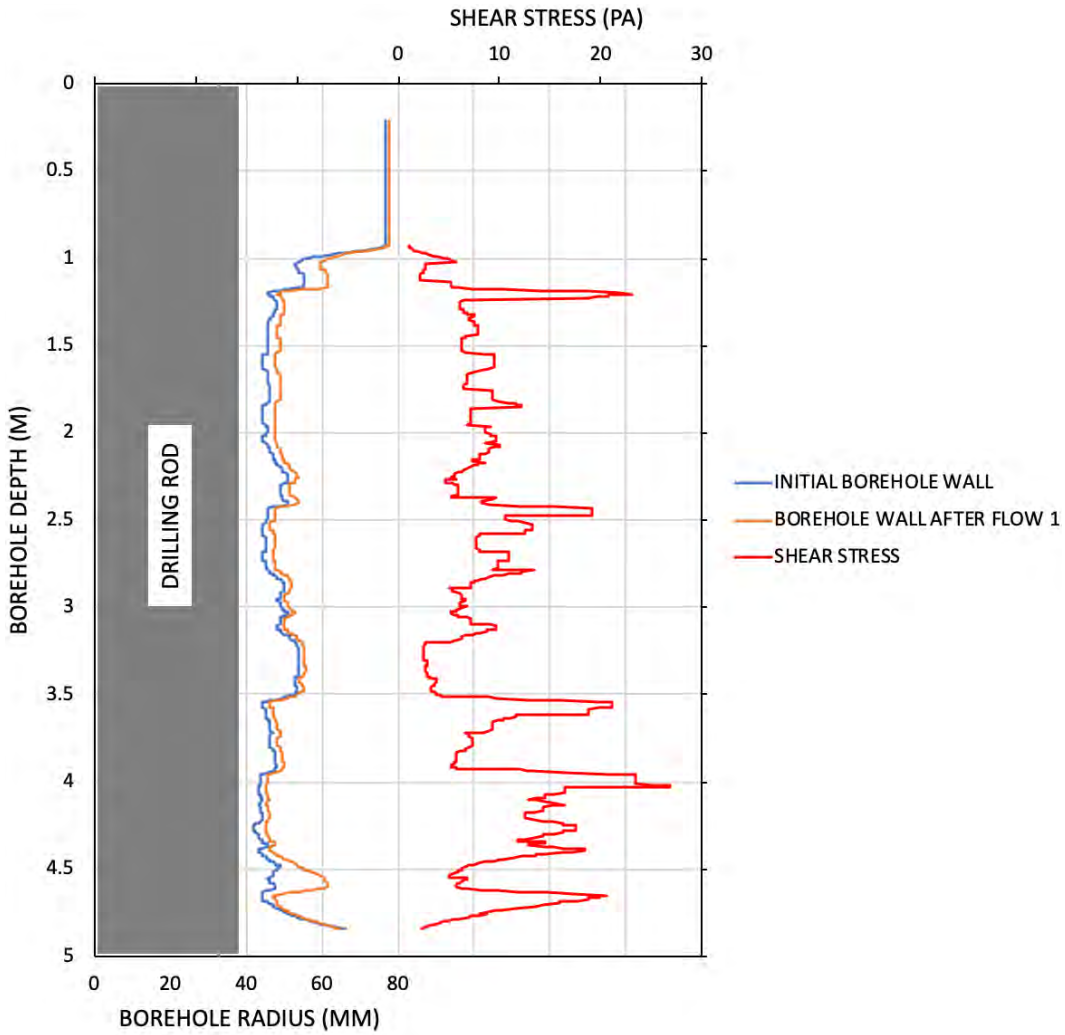

FIGURE 12 – EROSION OF BOREHOLE WALL AND ESTIMATED SHEAR STRESS (BRIAUD ET AL., 2020) DURING FLOW EVENT 1 OF THE BOREHOLE EROSION TEST CONDUCTED AT SITE LAR7.

than 10 cm and the depth of the asperities is small relative to the hydraulic diameter, the shear stress calculated using Eqs. (4) and (6) will be accurate. If the asperities are longer than 10 cm or deep relative to the hydraulic diameter, there will be zones of skimming flows and flow reversals along the borehole wall, which will primarily affect the magnitude of boundary shear stress in the more eroded areas of the borehole wall. Because of the natural variability in soil texture and physical properties, the asperities can be quite long and relatively deep, see Figure 12. Hence, there can be significant uncertainty in the estimated shear stress. Unfortunately, the uncertainty in shear stress has not been quantified yet for the BET method. As we use soil layer-averaged shear stress and erosion rate values (Figure 8), we use the standard deviation of the variation in shear stresses about the average shear stress as a measure of the uncertainty. Figure 13 shows that the standard deviation is fairly consistent between soil types and increases with increasing shear stress for both overall (or total) shear stress and grain shear stress. Hence, $\mu_\tau = 0$ for both grain and overall shear stresses, and the standard deviation of the uncertainty in overall shear stress is $\sigma_\tau = 0.822\tau + 4.48$, whereas the standard deviation of the uncertainty in grain shear stress is $\sigma_{\tau'} = 0.777\tau' + 0.908$.

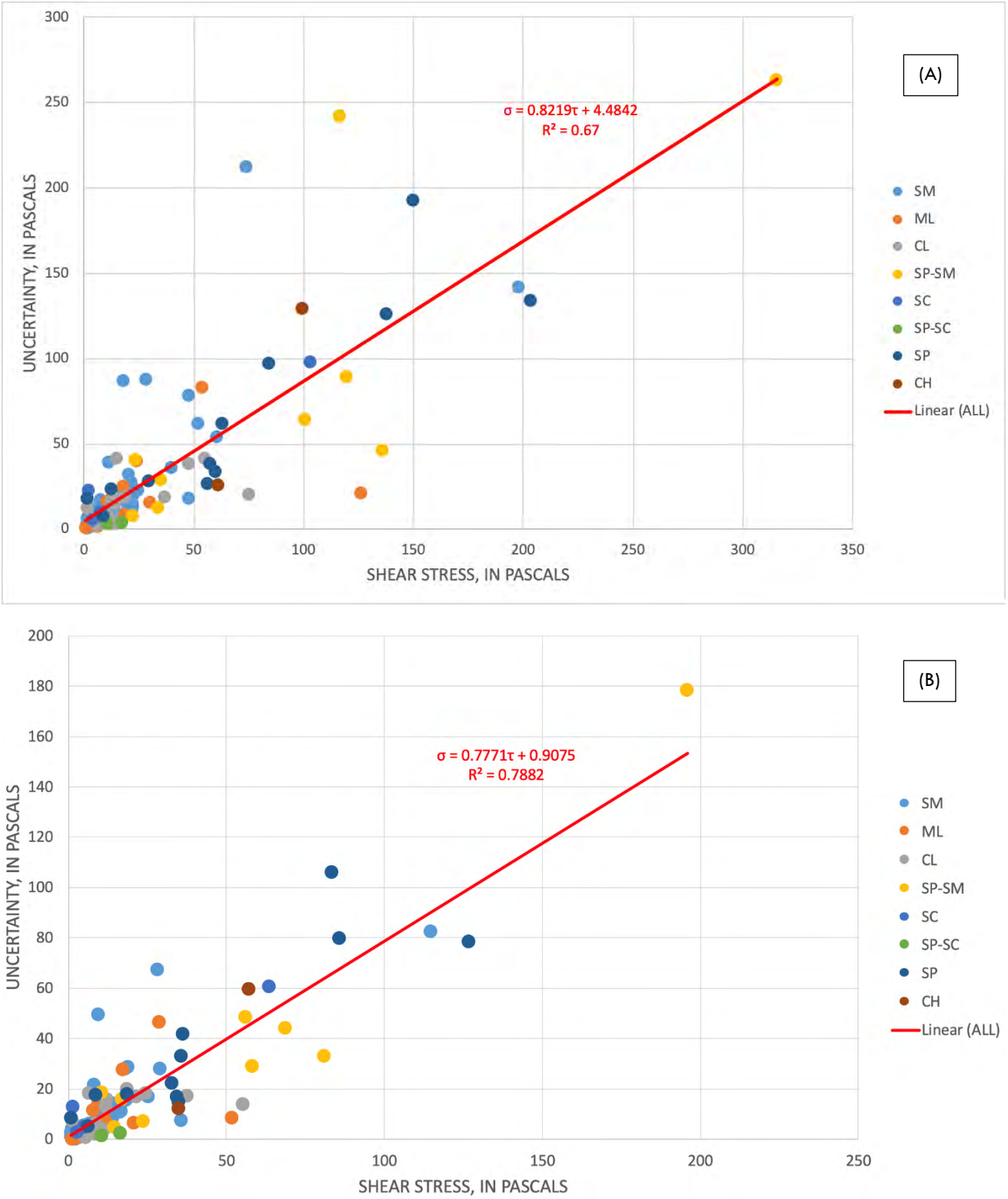

FIGURE 13 – STANDARD DEVIATION OF THE VARIATION IN SHEAR STRESSES ABOUT THE SOIL-LAYER AVERAGED SHEAR STRESS FOR THE BOREHOLE EROSION TESTS PLOTTED BY SOIL TYPE: (A) TOTAL SHEAR STRESS AND (B) GRAIN SHEAR STRESS.

RESULTS

Overview

All REMT data are presented using the logarithmic general classification plot proposed by Briaud (2008). This chart plots the logarithm of erosion rate versus the logarithm of applied shear stress. It further identifies six regions that classify the erodibility of soils as 'very high erodibility,' 'high erodibility,' 'medium erodibility,' 'low erodibility,' 'very low erodibility,' and 'non-erosive.' Comparisons are grouped by site, test type, and soil classification. Soils for EFA and BET tests were classified in both the field (ASTM D-2488) and laboratory (ASTM D-2487) using the Unified Soil Classification System (USCS) by the USGS (Work & Livsey, 2020) or USACE Prado Soils Laboratory. Laboratory results were preferred over field classifications. Soils collected for grain size distribution analysis by the NSL were also evaluated for USCS classification. However, NSL determined Atterberg Limits (ASTM D-4318) using oven-dried samples and only samples with greater than 50% fines (or 50% > 0.075 mm by weight) were tested. It should be noted that erosion rates equal to zero were changed to equal 0.1 mm hr^{-1} for plotting purposes (log-log scale) but were not altered for regression analyses. It should also be noted that BET data at LAR6 are questionable due to stratigraphy differences between the soil identification borehole (borehole A) and the BET testing borehole (borehole B). Data from the LAR6 BET were not included in any analysis except in the "C*omparison of erosion functions by test method, site and soil*" section, where, therein, it is noted that the data are questionable in the figure description. APPENDIX A tabulates all the derived erodibility parameter results.

Comparison of erosion-rate parameters provided by mini-JET, JET, EFA, and BET analysis methods

Comparison of erosion functions by test method and by soil

Figure 14 through Figure 19 present the measured pairs of (τ,E) points, or raw REMT data, for all test methods grouped by soil type and plotted on the logarithmic classification scale of Briaud (2008). It can be seen in Figure 14 that there are trends or groupings by test method, but the general erodibility classifications are somewhat consistent. It is also notable that the amount of scatter is much larger for cohesionless soils (e.g. SM, SP, SP-SM) than for the more cohesive soils (e.g. ML, CL) and that general agreement exists for the cohesive soils. The result of general agreement among cohesive soils is not surprising considering that the tests were created for these soils. Additionally, one can see that most BET data tend to be located in the high to medium erodibility classification regions regardless of soil type with lower erosion rates than the EFA or JET test data. The EFA erosion functions for cohesionless soils tend to be located in the very high to high erodibility classification regions but shift to the high to medium erodibility classification for cohesive soils, which is consistent with the JET test data.

Comparison of erodibility parameters by test method and by soil

Erodibility parameters used in the excess shear stress equation (Eq. (1)) determined by the linear regression method for all test methods as described in the section "*Data analysis and reduction*" were grouped by soil classification for statistical comparison (Figure 20 and Figure 21). Standard box and whisker plots were used for the comparison. The box represents the interquartile range, the marker 'o' are the data, the marker 'x' represents the mean of the data, and the whiskers identify the minimum and maximum of the data not considered outliers. Points outside of the whiskers are considered outliers which are identified by either the first quartile minus 1.5 times the interquartile range or the third quartile plus 1.5 times the interquartile range. Points where the box (interquartile range) and the mean are grouped together signify single data points. Mean values for the critical shear stress and erodibility coefficient by test and soil classification are provided in Table 3 and Table 4, respectively.

JET data were collected primarily on silty sand (SM) and silt (ML) USCS soil classifications. One USACE JET was conducted on poorly sorted sand (SP). Figure 20 shows that the JET method estimates higher critical shear stresses for silt (ML) than the BET and EFA methods. Critical shear stress from the BET and JET are in general agreement for silty sand (SM). The EFA test method shows high variability in the erodibility coefficient for sand classifications (SM and SP), which may be attributed to reconstitution of the tested samples (Figure 21). BET-derived erodibility coefficients are low in comparison to the other REMTs for all soil types. It should be noted that 42% of the regressed BET data resulted in negative critical shear stress values, whereas only 8% of the EFA data resulted in negative values. The JET is not insusceptible to negative critical shear stress values, but as the used JET data represent the mass-erosion regime, negative values are unlikely. Differences between the EFA and USACE EFA are considerable and are attributed to differences in measurement procedures.

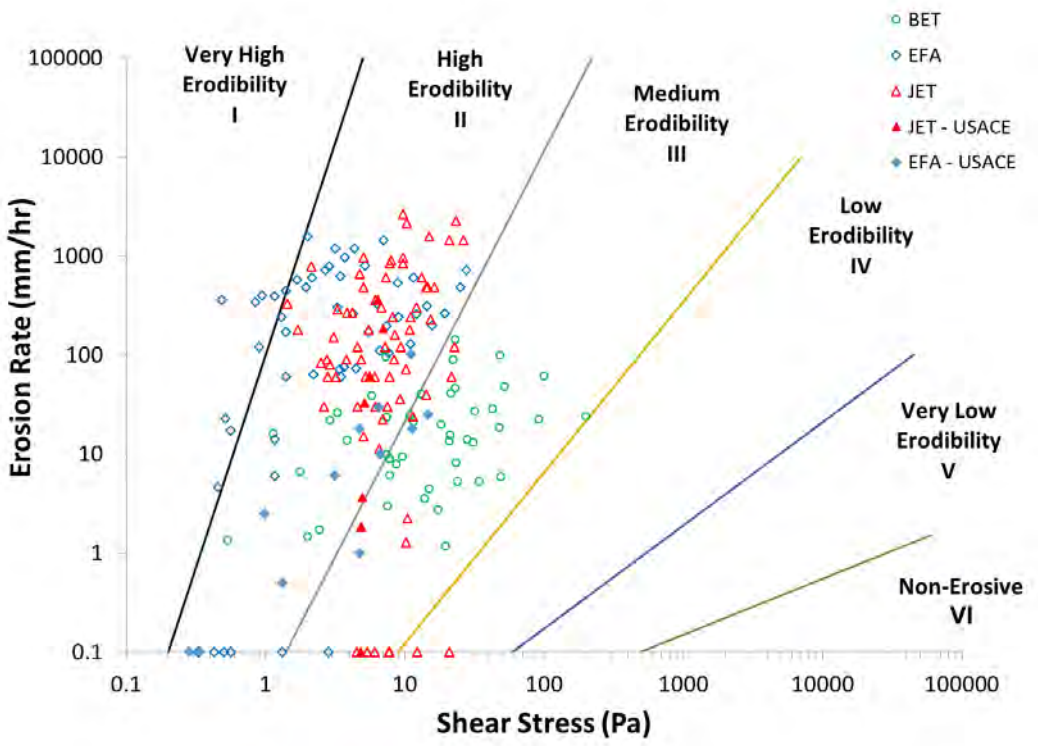

FIGURE 14 – EROSION FUNCTIONS MEASURED BY JET, EFA, AND BET METHODS FOR SILTY SAND (USCS SM).

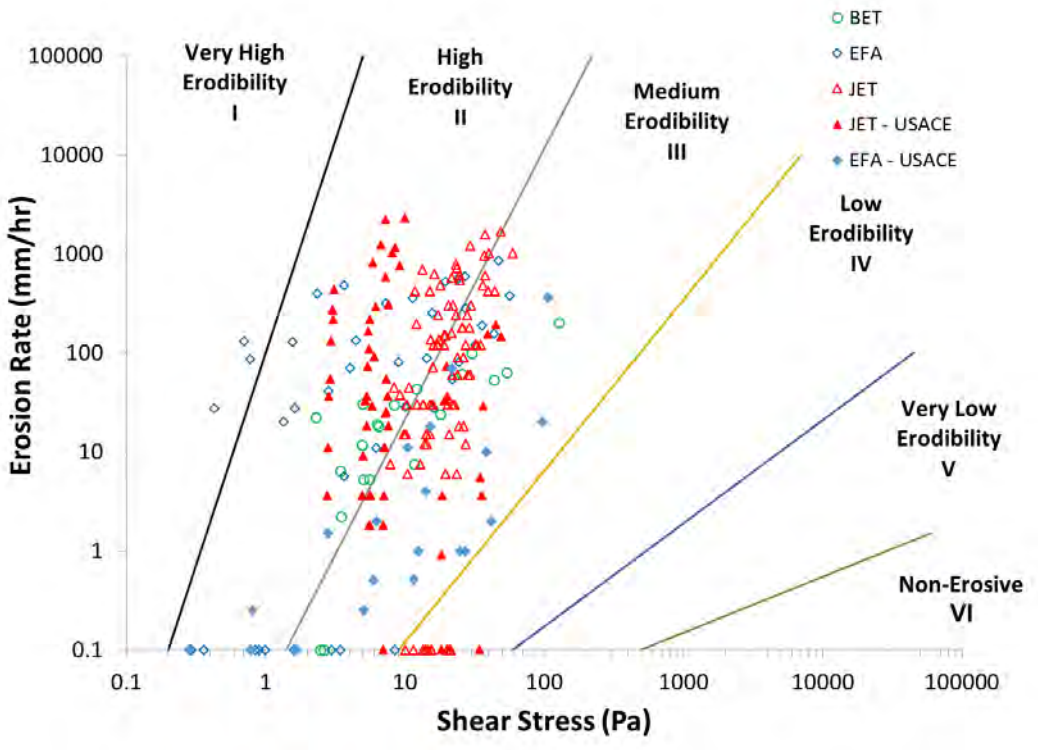

FIGURE 15 – EROSION FUNCTIONS MEASURED BY JET, EFA, AND BET METHODS FOR SILT (USCS ML).

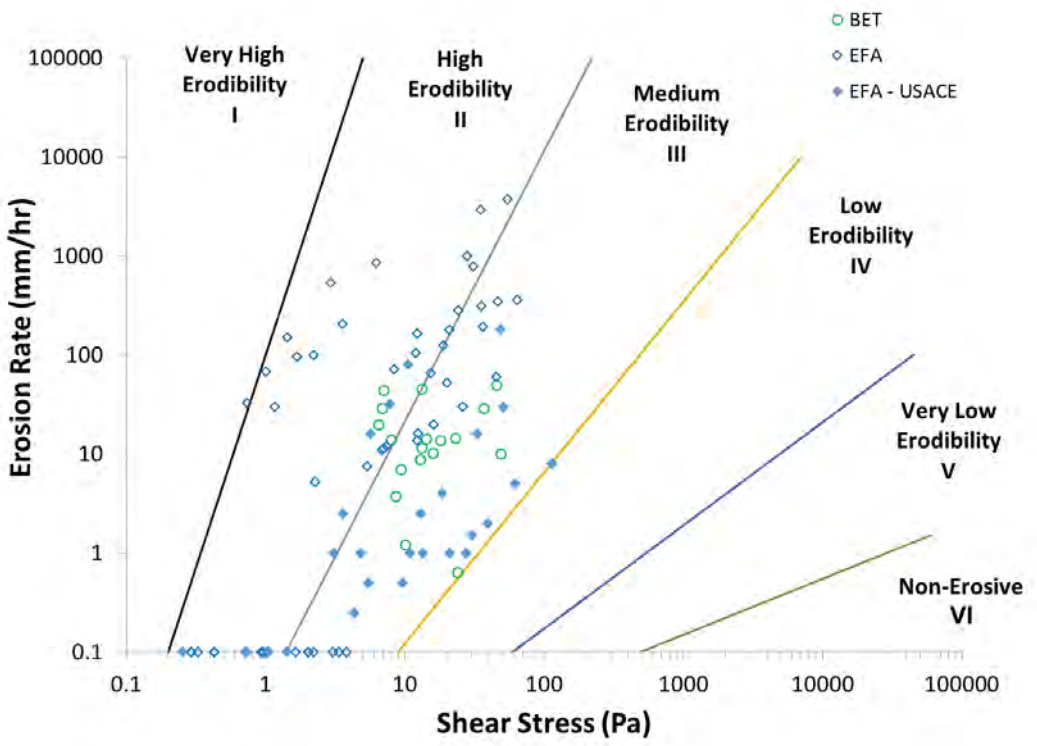

FIGURE 16 – EROSION FUNCTIONS MEASURED BY JET, EFA, AND BET METHODS FOR LEAN CLAY (USCS CL).

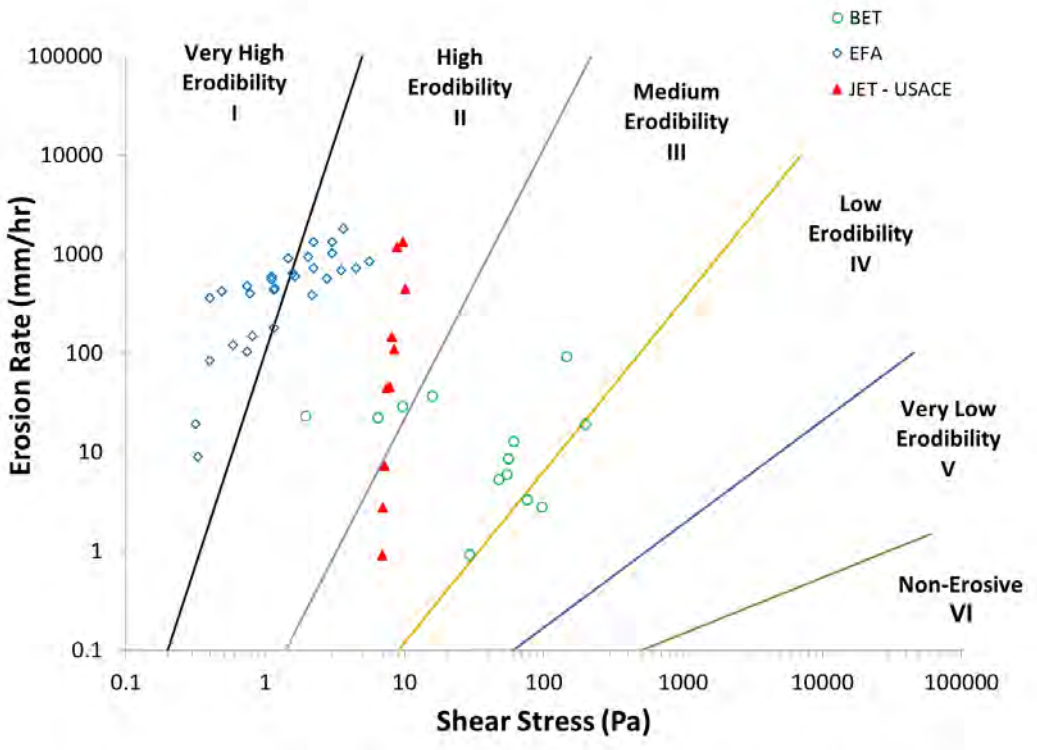

FIGURE 17 – EROSION FUNCTIONS MEASURED BY JET, EFA, AND BET METHODS FOR POORLY GRADED SAND (USCS SP).

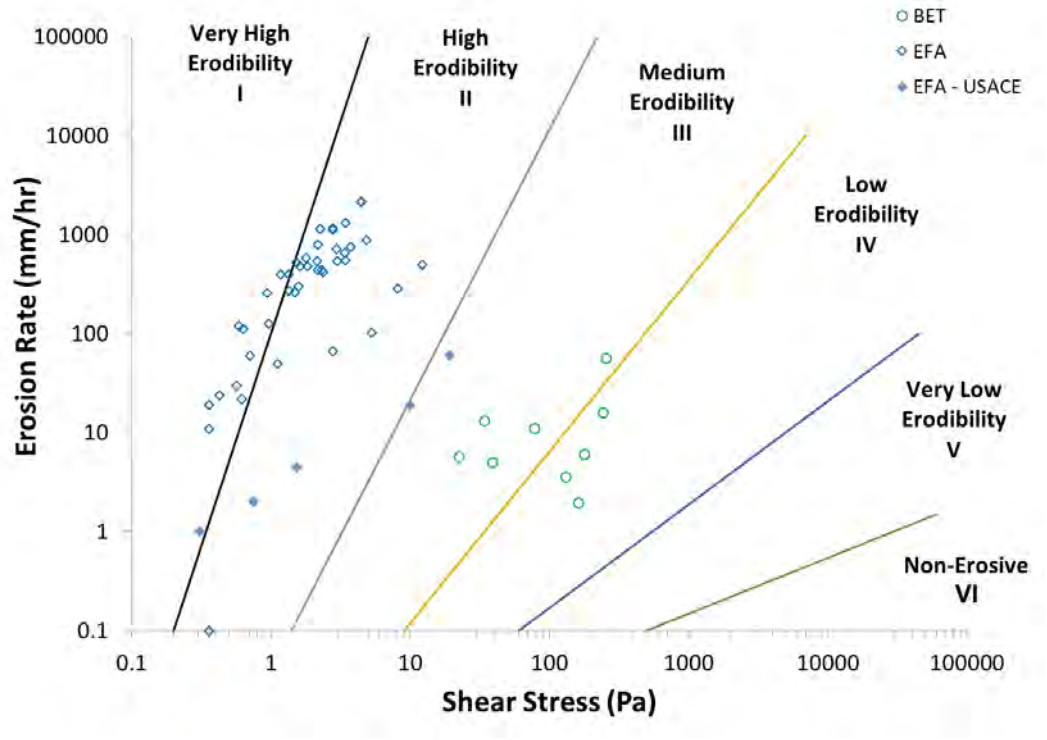

FIGURE 18 – EROSION FUNCTIONS MEASURED BY JET, EFA, AND BET METHODS FOR POORLY GRADED SAND WITH SILT (USCS SP-SM).

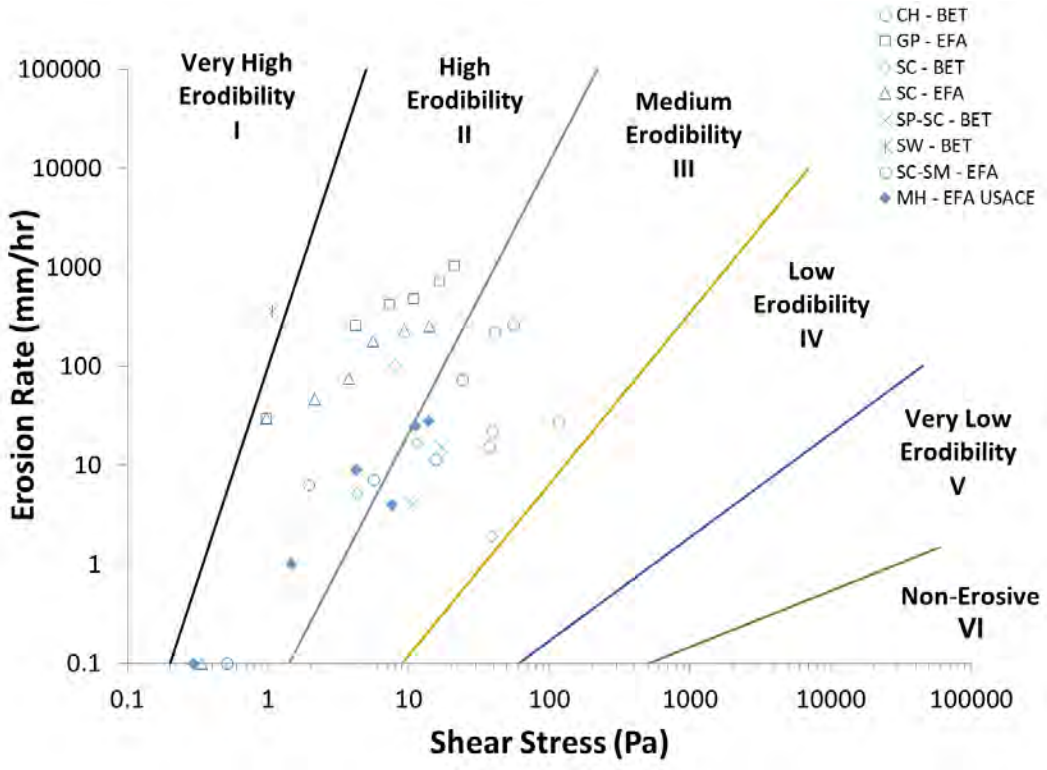

FIGURE 19 – EROSION FUNCTIONS MEASURED BY JET, EFA, AND BET METHODS USCS CLASSES CH, GP, SC, SP-SC, SW, SC-SM, SC, AND MH.

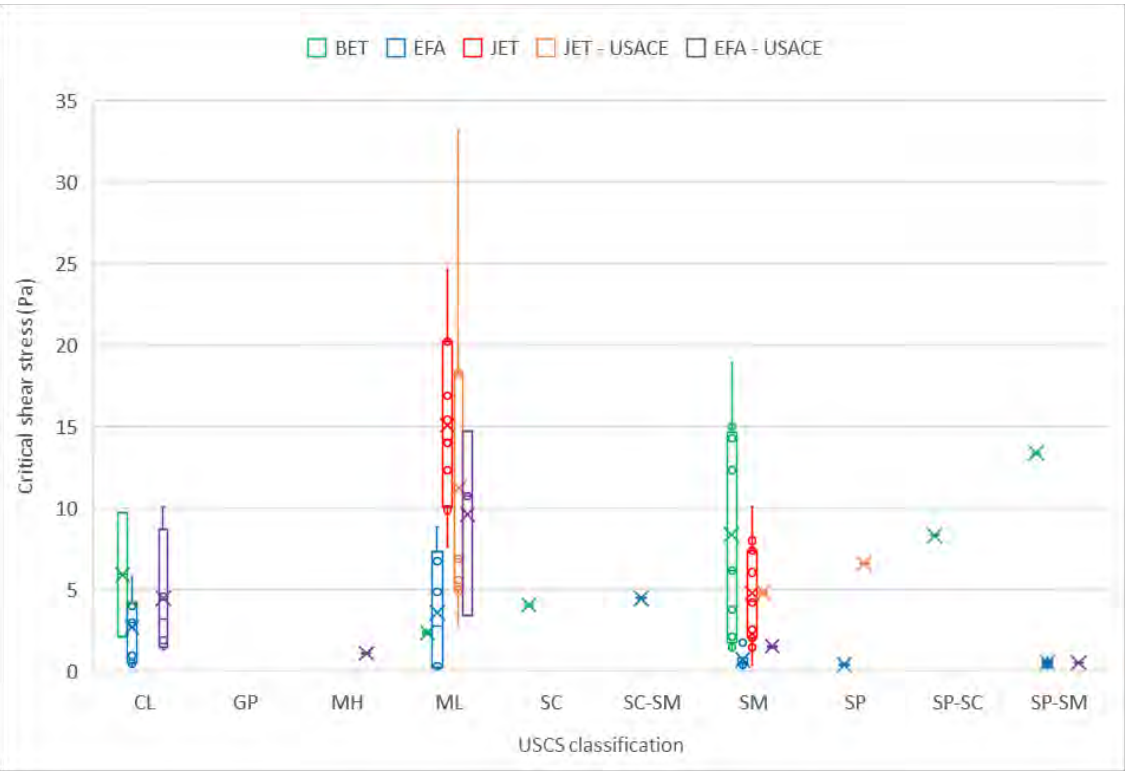

FIGURE 20 – BOX AND WHISKER PLOT OF CRITICAL SHEAR STRESS ESTIMATES BY TEST METHOD AND SOIL CLASSIFICATION.

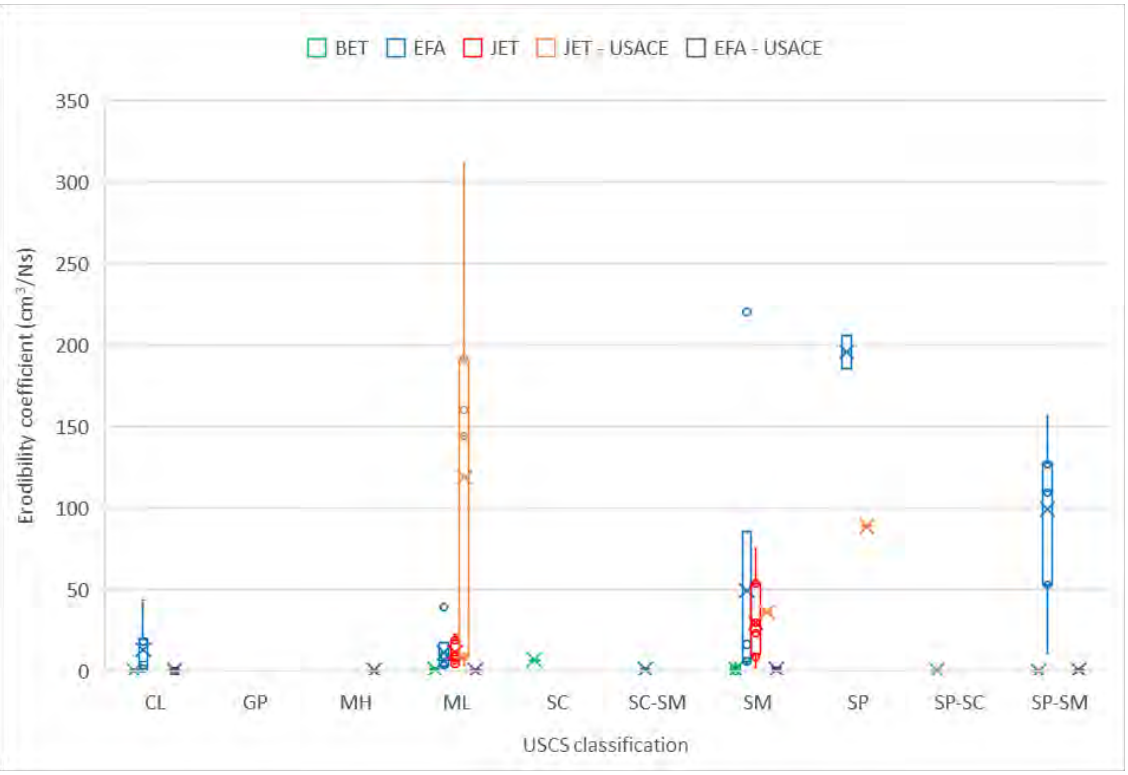

FIGURE 21 – BOX AND WHISKER PLOT OF ERODIBILITY COEFFICIENT ESTIMATES BY TEST METHOD AND SOIL CLASSIFICATION.

In addition to regressing all available data for the EFA, a second regression was conducted on filtered data. EFA data were filtered on the basis of different erosion regimes (Papanicolaou et al., 2017), where the second erosion regime associated with mass erosion was isolated. Figure 22-Figure 23 and Table 3-Table 4 provide the results with filtered EFA data and Appendix C shows which data were filtered or removed from consideration in the regression analysis. It can be seen that, in general, the filtered EFA data better approximated the JET critical shear stress than the non-filtered data. Additionally, non-filtered EFA datasets that resulted in negative erodibility parameters turned to positive values after the filter was applied (e.g. USCS Class GP, and SC).

TABLE 3 – MEAN CRITICAL SHEAR STRESS FOR EACH SOIL CLASS BY REMT.

	Mean critical shear stress value per REMT (Pa)						
USCS Class	**BET**	**EFA**	**Filtered EFA**	**EFA – USACE**	**Filtered EFA – USACE**	**JET**	**JET – USACE**
CL	5.94	2.70	12.98	4.49	14.51	-	-
GP	-	-	2.12	-	-	-	-
MH	-	-	-	1.10	1.62	-	-
ML	2.39	3.60	10.22	9.64	24.19	15.09	11.27
SC	4.08	-	0.43	-	-	-	-
SC-SM	-	4.49	12.45	-	-	-	-
SM	8.38	0.71	2.16	1.54	3.26	4.82	4.84
SP	-	0.43	0.42	-	-	-	6.63
SP-SC	8.33	-	-	-	-	-	-
SP-SM	13.39	0.55	1.34	0.54	0.54	-	-

TABLE 4 – MEAN ERODIBILITY COEFFICIENT FOR EACH SOIL CLASS BY REMT.

	Mean erodibility coefficient per REMT ($cm^3\ N^{-1}\ s^{-1}$)						
USCS Class	**BET**	**EFA**	**EFA Filtered**	**EFA – USACE**	**Filtered EFA – USACE**	**JET**	**JET-USACE**
CL	0.56	13.34	20.12	0.73	2.19	-	-
GP	-	-	14.69	-	-	-	-
MH	-	-	-	0.58	0.61	-	-
ML	1.46	11.60	15.74	0.63	0.90	11.74	119.00
SC	7.02	-	8.68	-	-	-	-
SC-SM	-	1.42	1.81	-	-	-	-
SM	1.49	49.66	154.44	1.53	2.04	30.01	36.53
SP	-	195.77	166.05	-	-	-	89.14
SP-SC	0.47	-	-	-	-	-	-
SP-SM	0.18	99.52	150.25	0.83	0.83	-	-

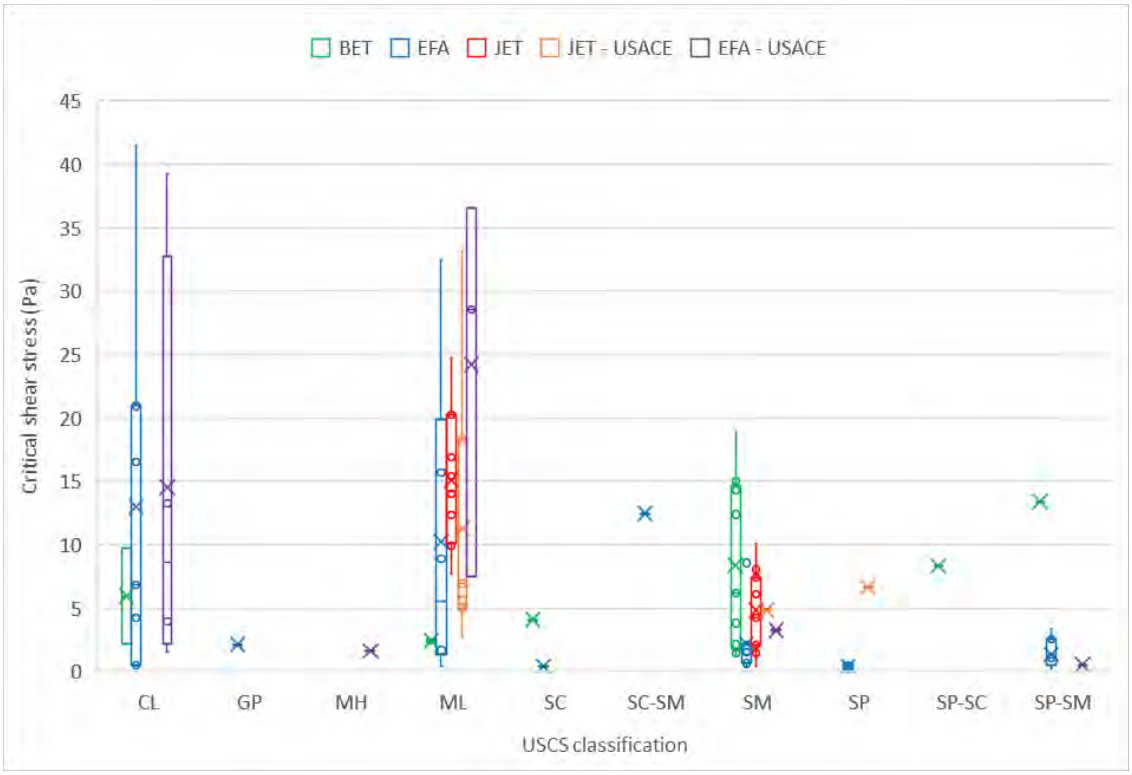

FIGURE 22 – BOX AND WHISKER PLOT OF CRITICAL SHEAR STRESS ESTIMATES BY TEST METHOD AND SOIL CLASSIFICATION – EFA FILTER APPLIED.

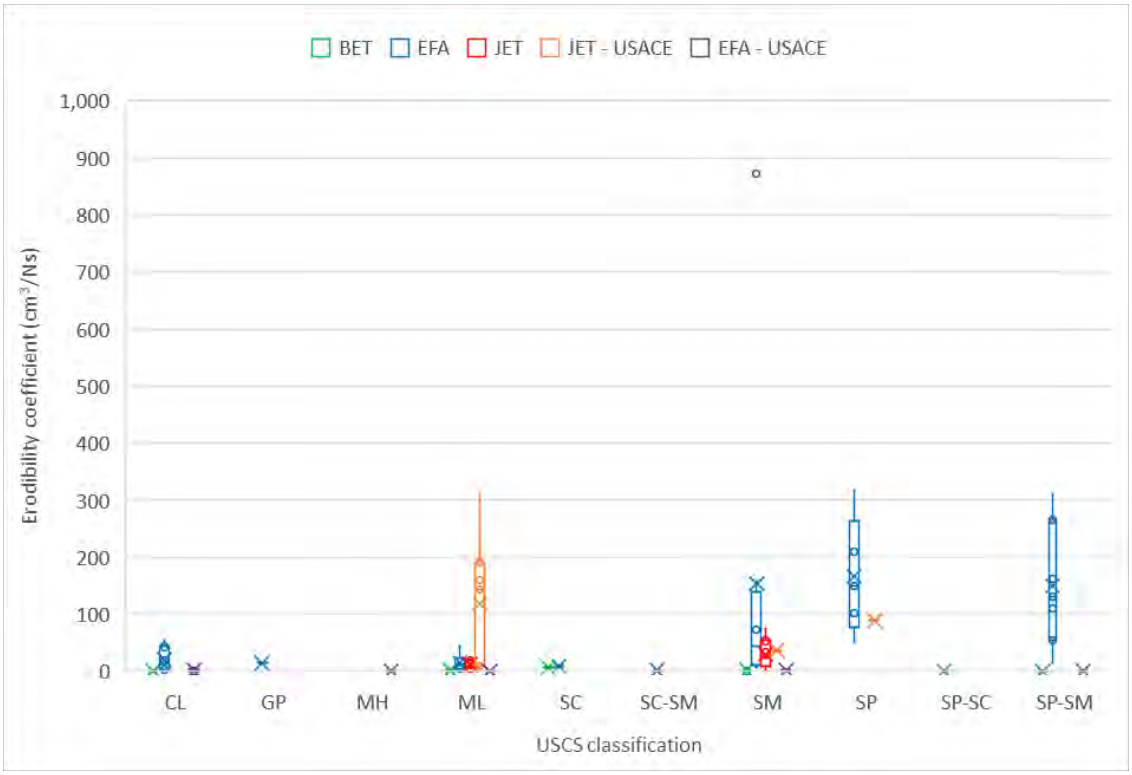

FIGURE 23 – BOX AND WHISKER PLOT OF ERODIBILITY COEFFICIENT ESTIMATES BY TEST METHOD AND SOIL CLASSIFICATION – EFA FILTER APPLIED.

Comparison of erosion functions by test method, site and soil

Figure 24 through Figure 47 plot the measured erosion functions to explore consistencies in individual tests by location. A maximum of two figures per location are presented; if a dominant soil is present at a given location then a figure was dedicated to that soil as described in the figure caption. However, if a variety of soils is present at a given location then the individual soil types are identified in the figure legend rather than the figure caption. Approximate NAVD88 elevations are provided for each test.

In general, trends identified in the section "C*omparison of erosion functions by test method and by soil*" can also be seen in the following figures. Consistency between test types typically occurs on cohesive soils, but sandy soils have significant variability. There does not appear to be significant differences for a given soil associated with a given location. EFA tests for cohesionless soils tend to plot in the very high to high erodibility classification regions but shift to the high to medium erodibility classification region for cohesive soils, which is consistent with the JET test. Also, the Sacramento River sites are generally more cohesive than those on the Lower American River.

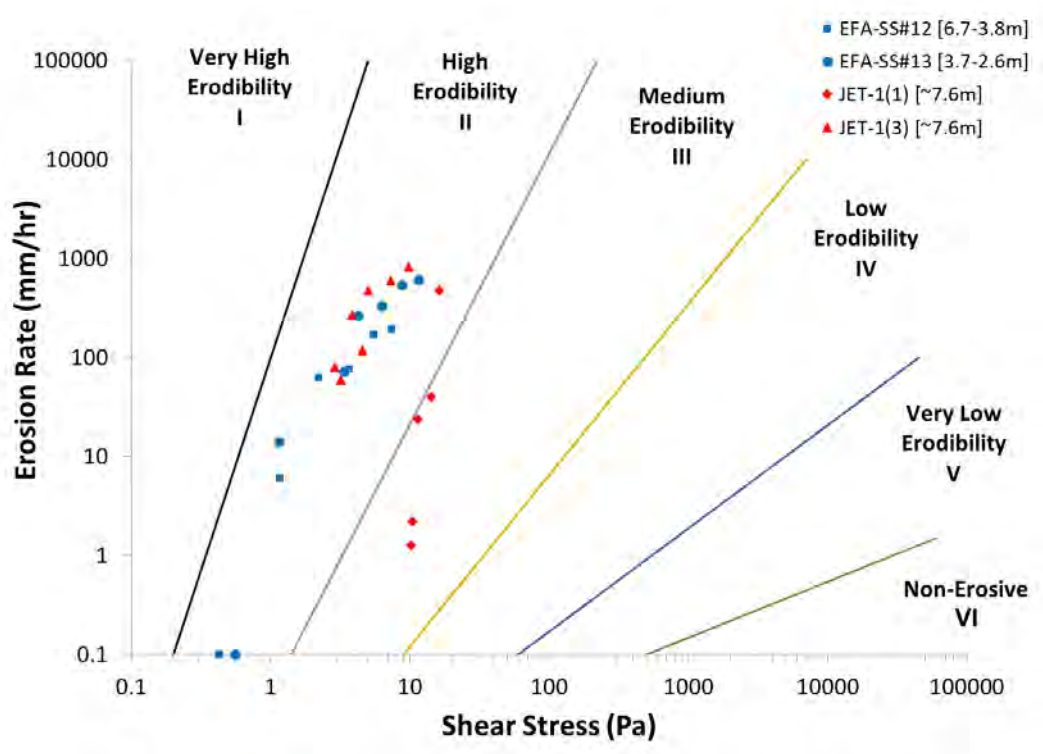

FIGURE 24 – MEASURED EROSION FUNCTIONS AT LOWER AMERICAN RIVER SITE 1 (LAR1) – SILTY SAND (USCS SM).

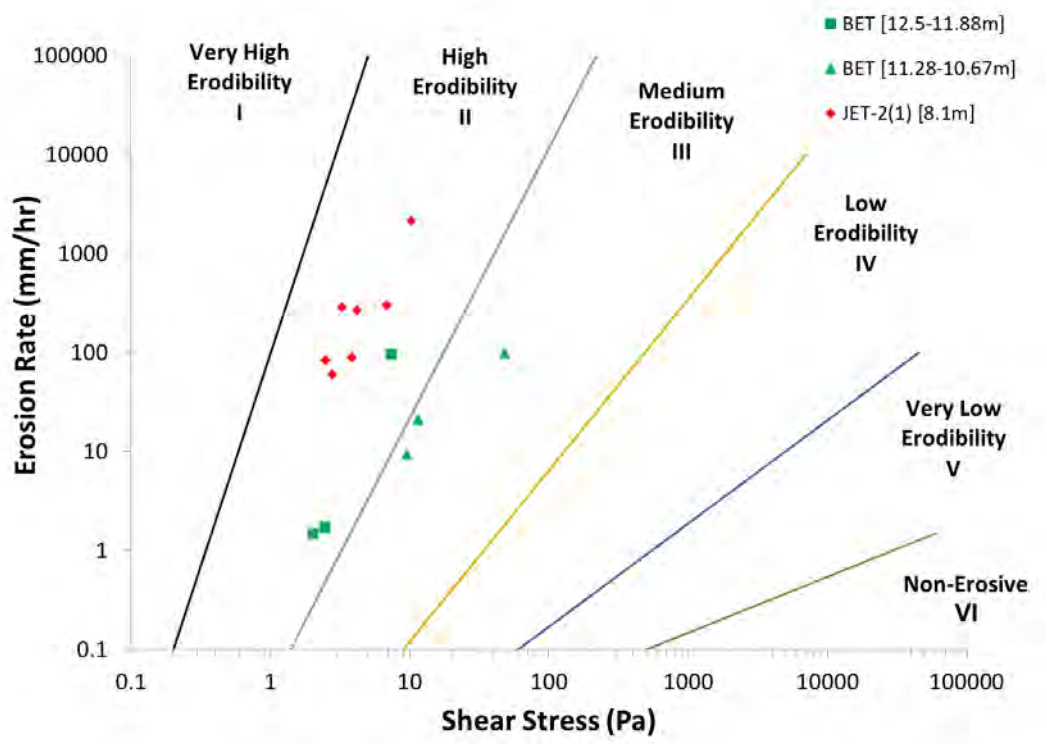

FIGURE 25 – MEASURED EROSION FUNCTIONS AT LOWER AMERICAN RIVER SITE 2 (LAR2) – SILTY SAND (USCS SM).

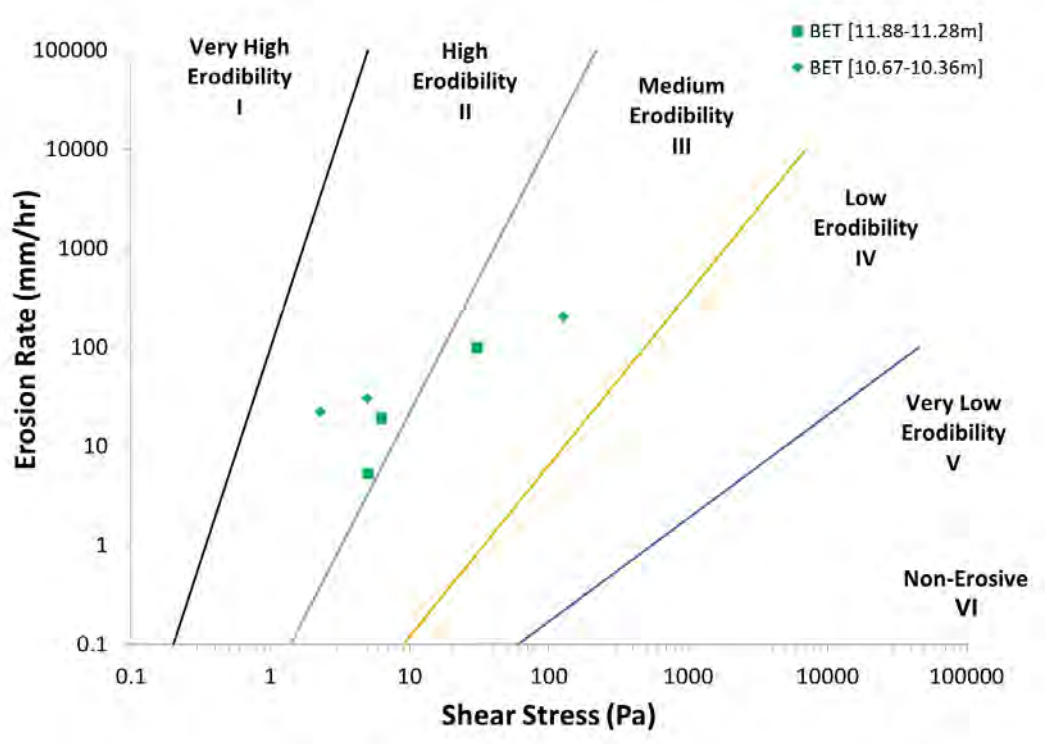

FIGURE 26 – MEASURED EROSION FUNCTIONS AT LOWER AMERICAN RIVER SITE 2 (LAR2) – SILT (USCS ML).

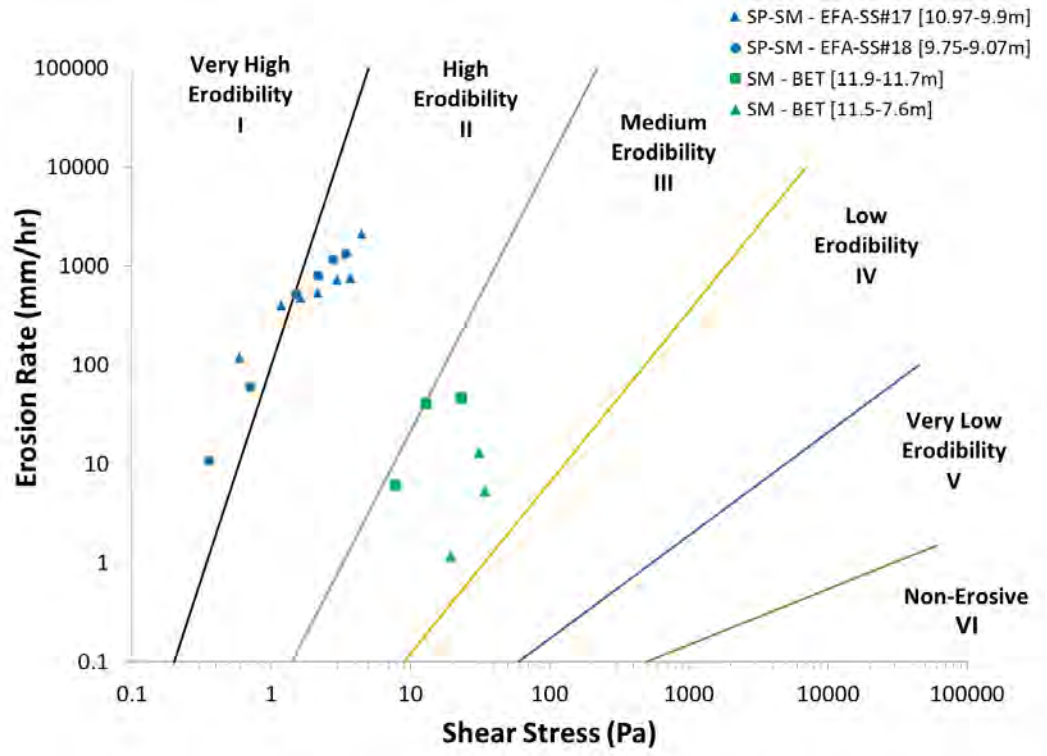

FIGURE 27 – MEASURED EROSION FUNCTIONS AT LOWER AMERICAN RIVER SITE 3 (LAR3) – (USCS SM, SP-SM).

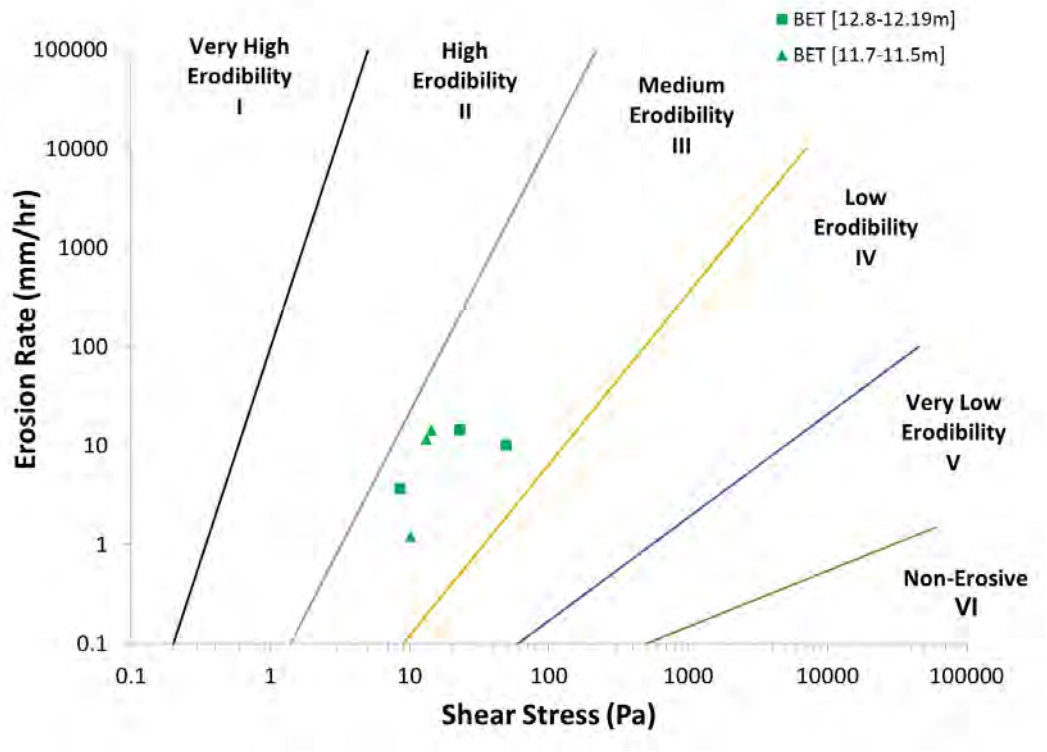

FIGURE 28 – MEASURED EROSION FUNCTIONS AT LOWER AMERICAN RIVER SITE 3 (LAR3) – LEAN CLAY (USCS CL).

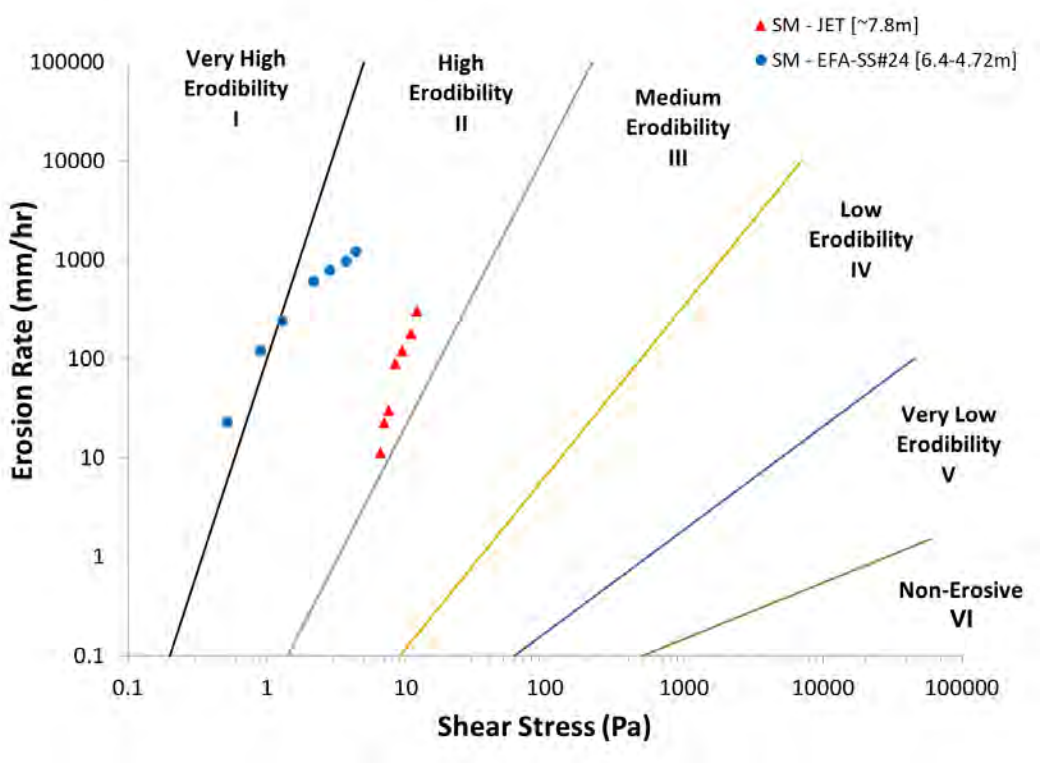

FIGURE 29 – MEASURED EROSION FUNCTIONS AT LOWER AMERICAN RIVER SITE 4 (LAR4) – OTHER USCS CLASSIFICATIONS.

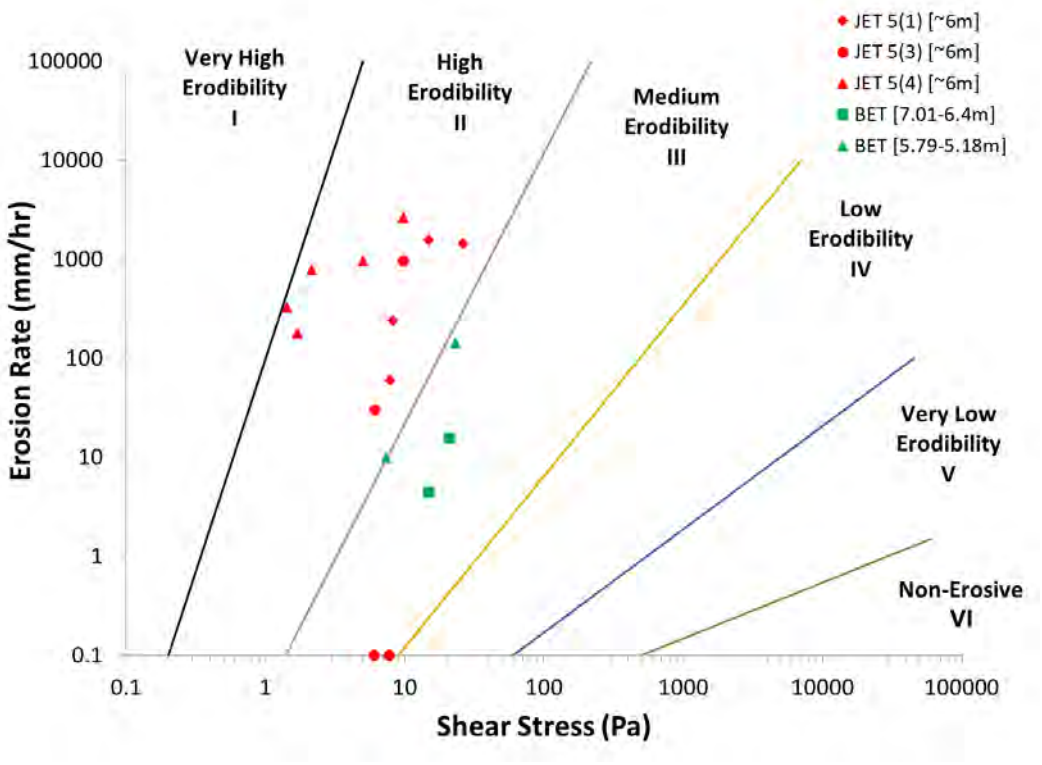

FIGURE 30 – MEASURED EROSION FUNCTIONS AT LOWER AMERICAN RIVER SITE 5 (LAR5) – SILTY SAND (USCS SM).

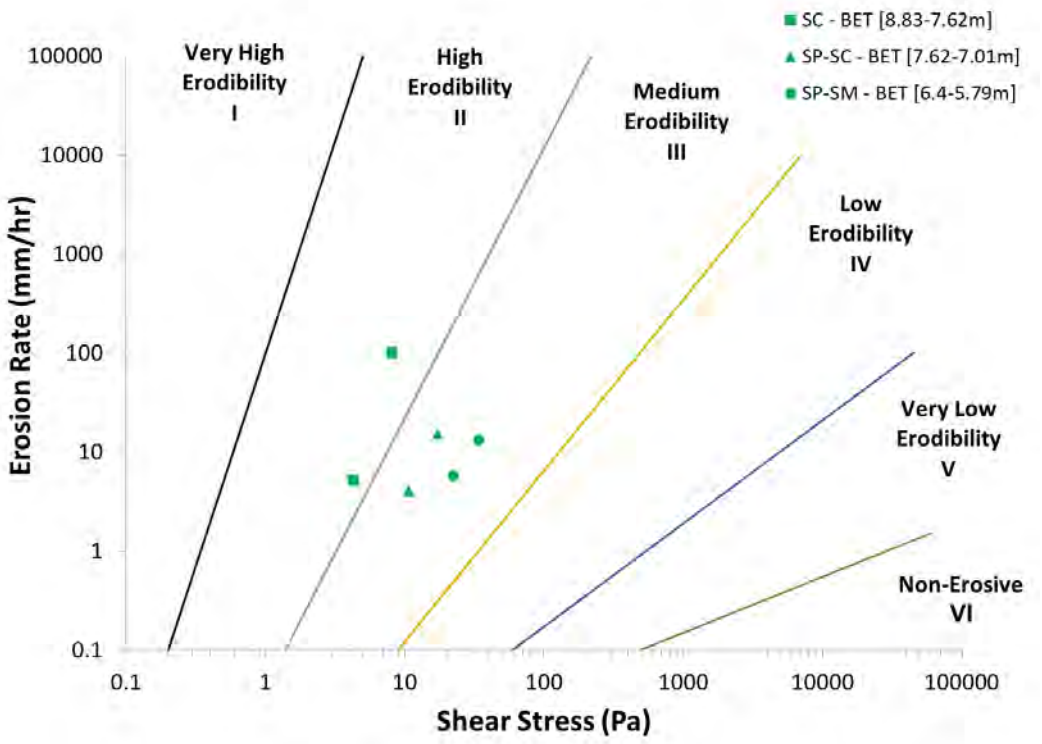

FIGURE 31 – MEASURED EROSION FUNCTIONS AT LOWER AMERICAN RIVER SITE 5 (LAR5) – OTHER USCS CLASSIFICATIONS.

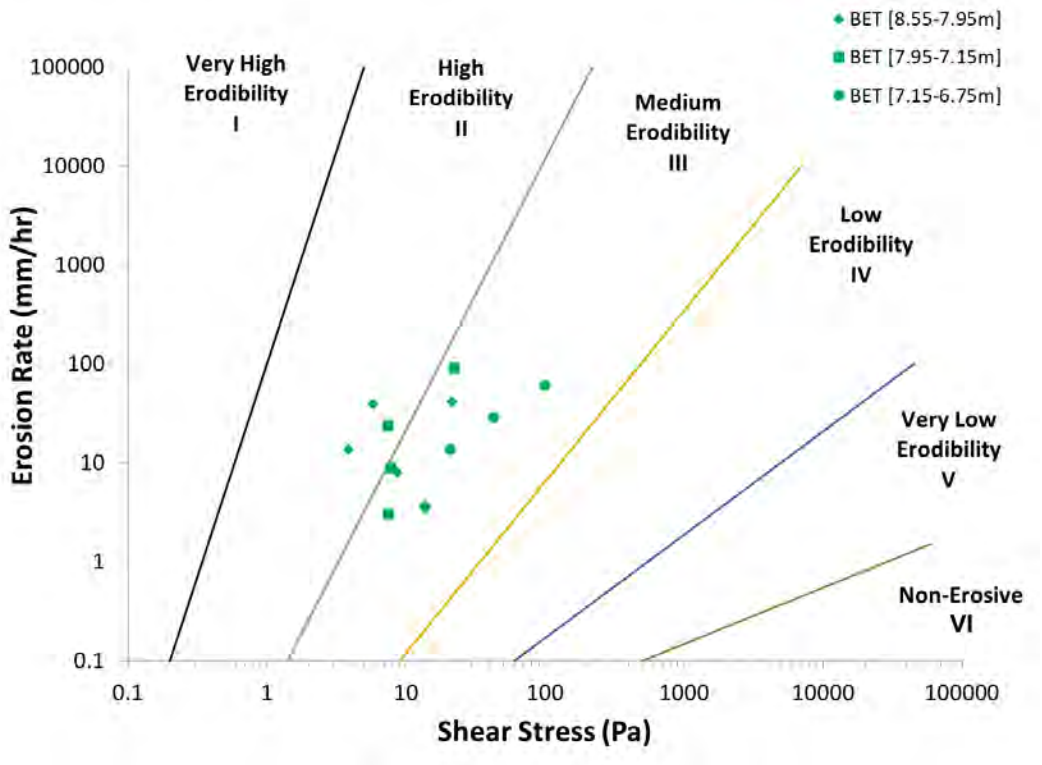

FIGURE 32 – MEASURED EROSION FUNCTIONS AT LOWER AMERICAN RIVER SITE 6 (LAR6) – SILTY SAND (USCS SM). *QUESTIONABLE BET DATA*

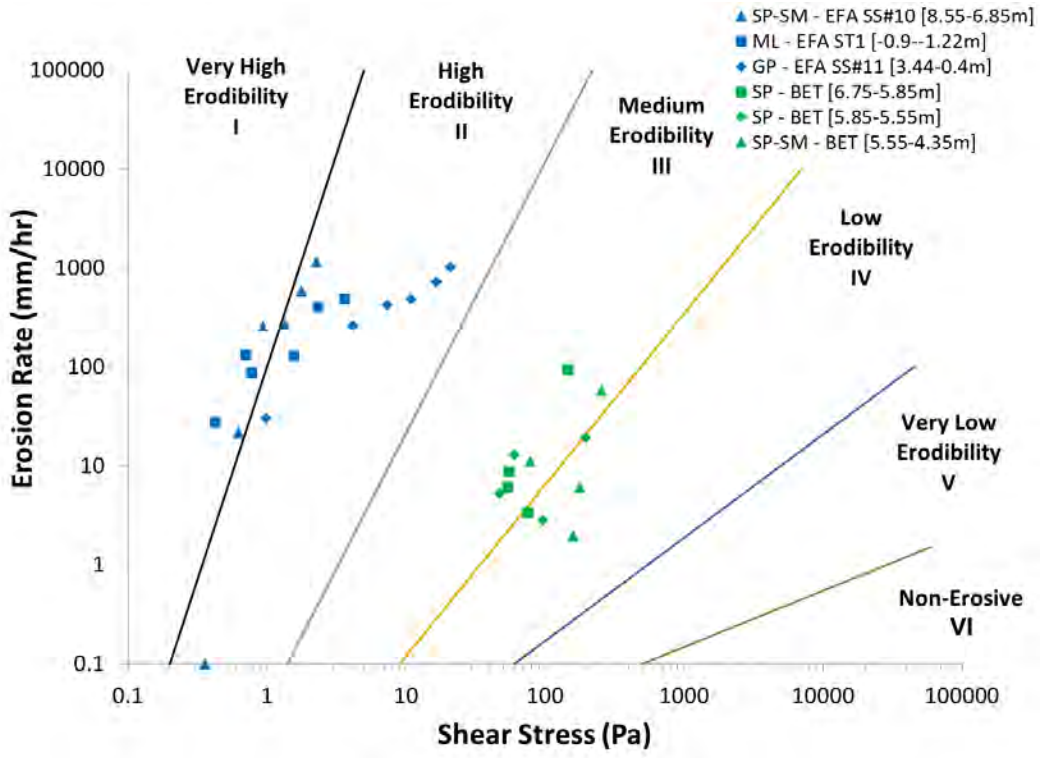

FIGURE 33 – MEASURED EROSION FUNCTIONS AT LOWER AMERICAN RIVER SITE 6 (LAR6) – OTHER USCS CLASSIFICATIONS. *QUESTIONABLE BET DATA*

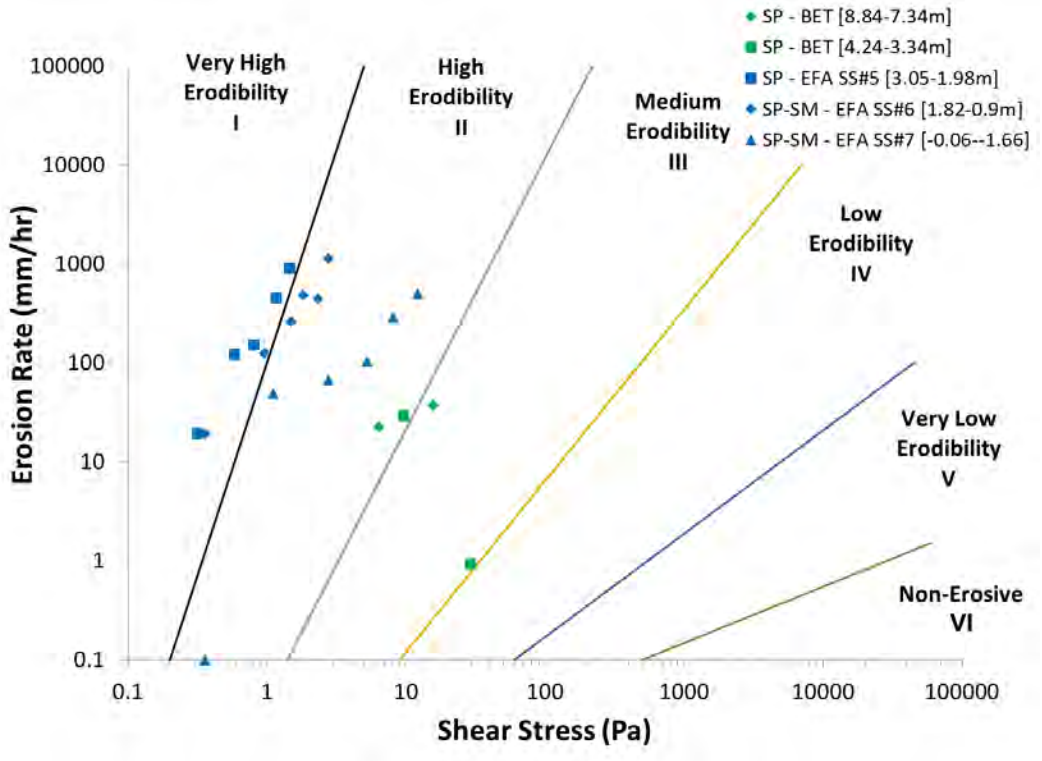

FIGURE 34 – MEASURED EROSION FUNCTIONS AT LOWER AMERICAN RIVER SITE 7 (LAR7) – (USCS SP & SP-SM).

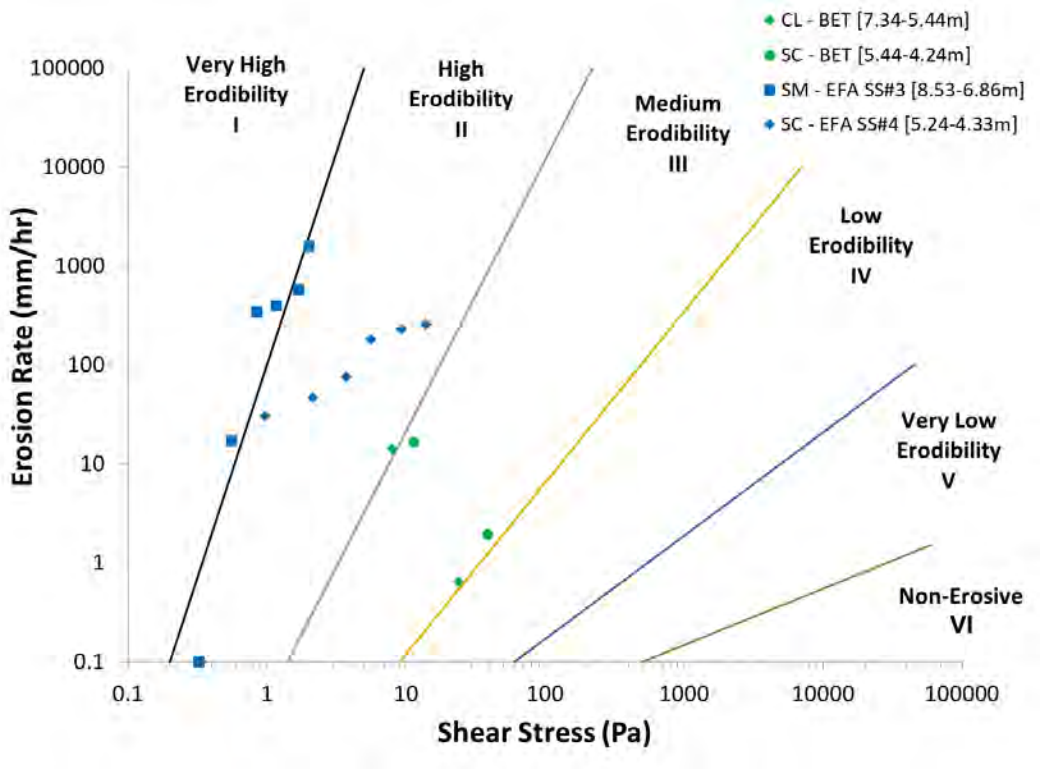

FIGURE 35 – MEASURED EROSION FUNCTIONS AT LOWER AMERICAN RIVER SITE 7 (LAR7) – OTHER USCS CLASSIFICATIONS.

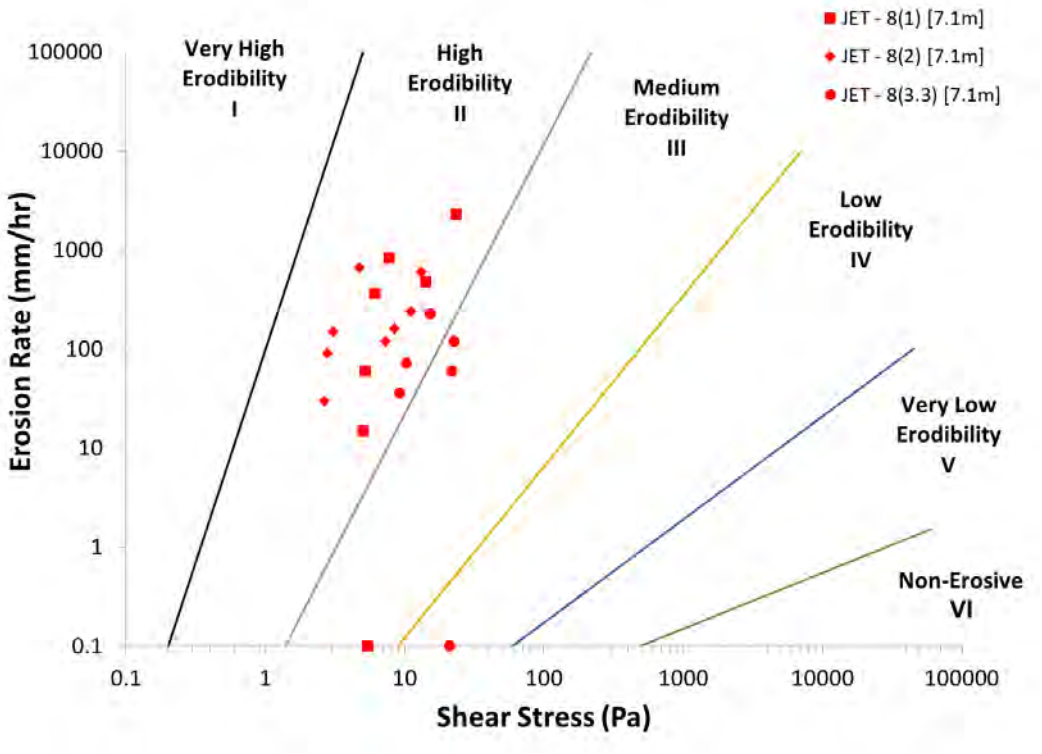

FIGURE 36 – MEASURED EROSION FUNCTIONS AT LOWER AMERICAN RIVER SITE 8 (LAR8) – SILTY SAND (USCS SM).

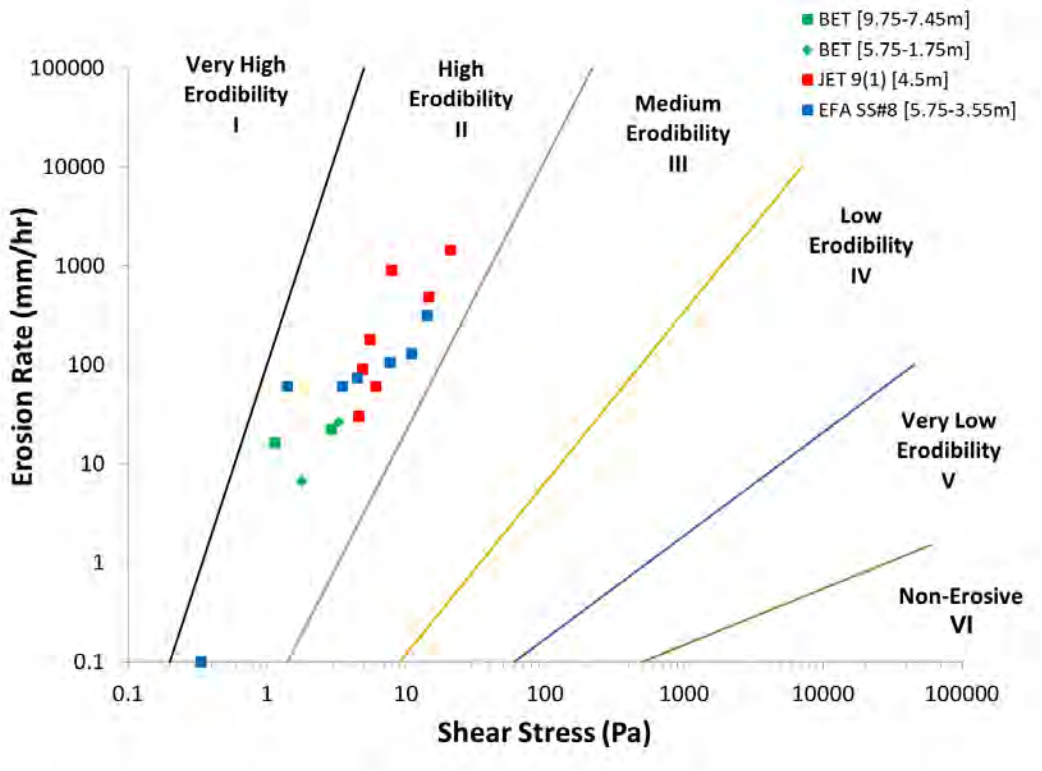

FIGURE 37 – MEASURED EROSION FUNCTIONS AT LOWER AMERICAN RIVER SITE 9 (LAR9) – SILTY SAND (USCS SM).

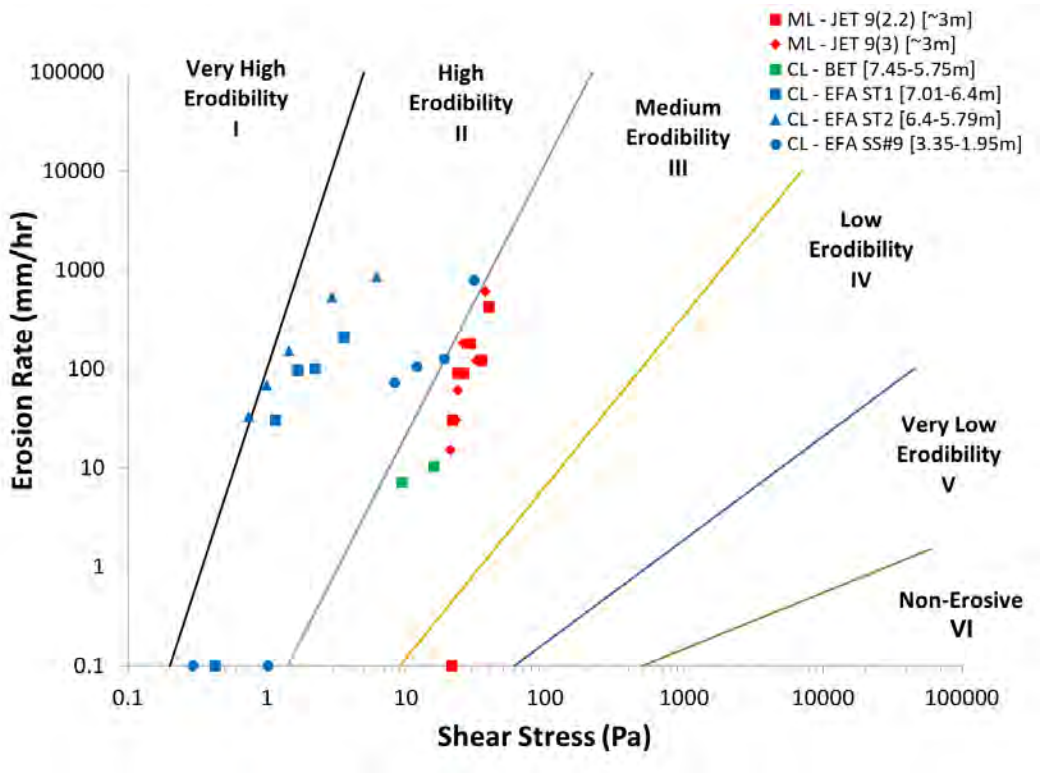

FIGURE 38 – MEASURED EROSION FUNCTIONS AT LOWER AMERICAN RIVER SITE 9 (LAR9) – (USCS ML & CL).

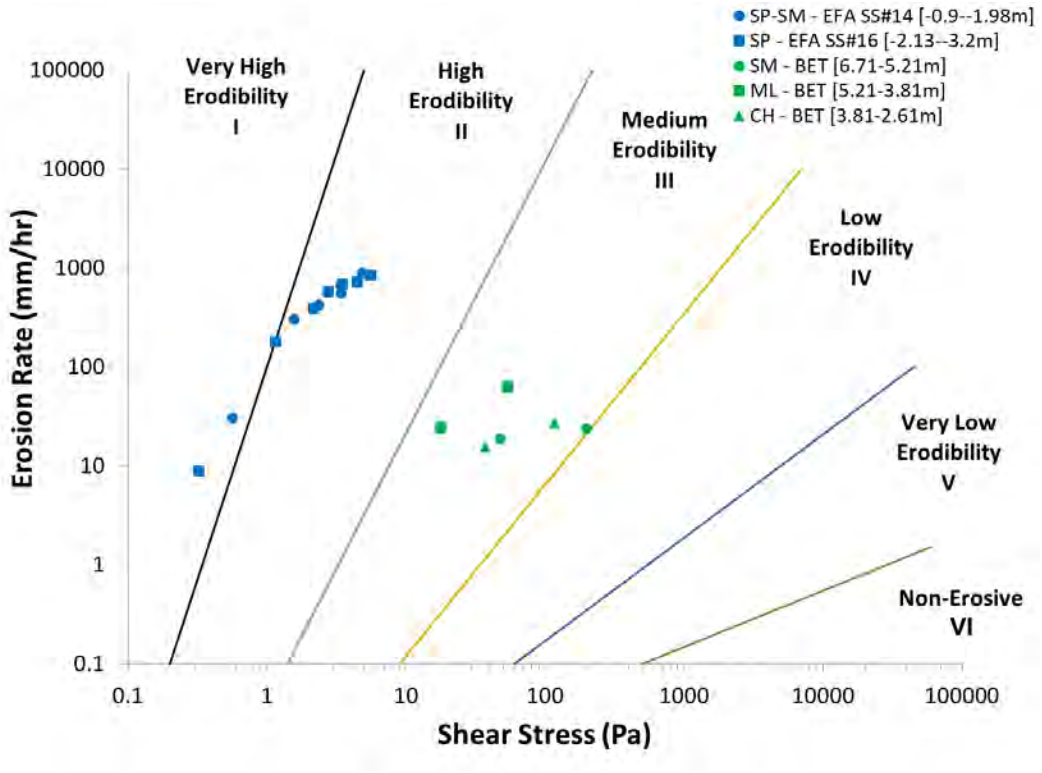

FIGURE 39 – MEASURED EROSION FUNCTIONS AT LOWER AMERICAN RIVER SITE 10 (LAR10) – OTHER USCS CLASSIFICATIONS.

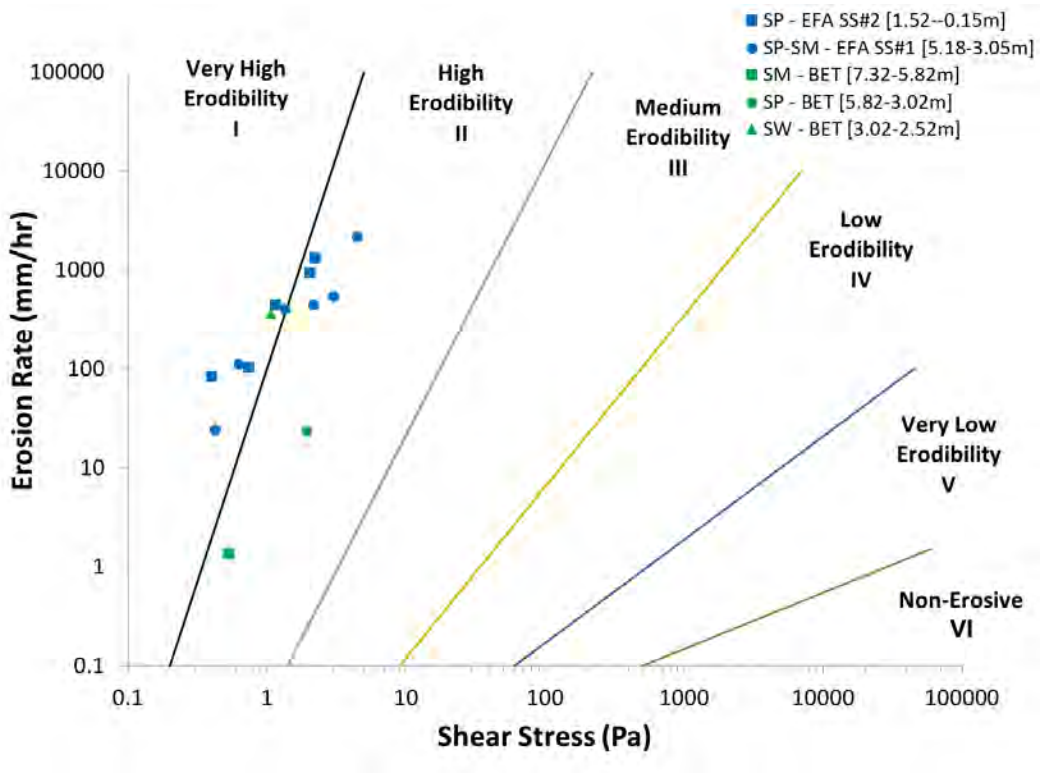

FIGURE 40 – MEASURED EROSION FUNCTIONS AT LOWER AMERICAN RIVER SITE 12 (LAR12) – OTHER USCS CLASSIFICATIONS.

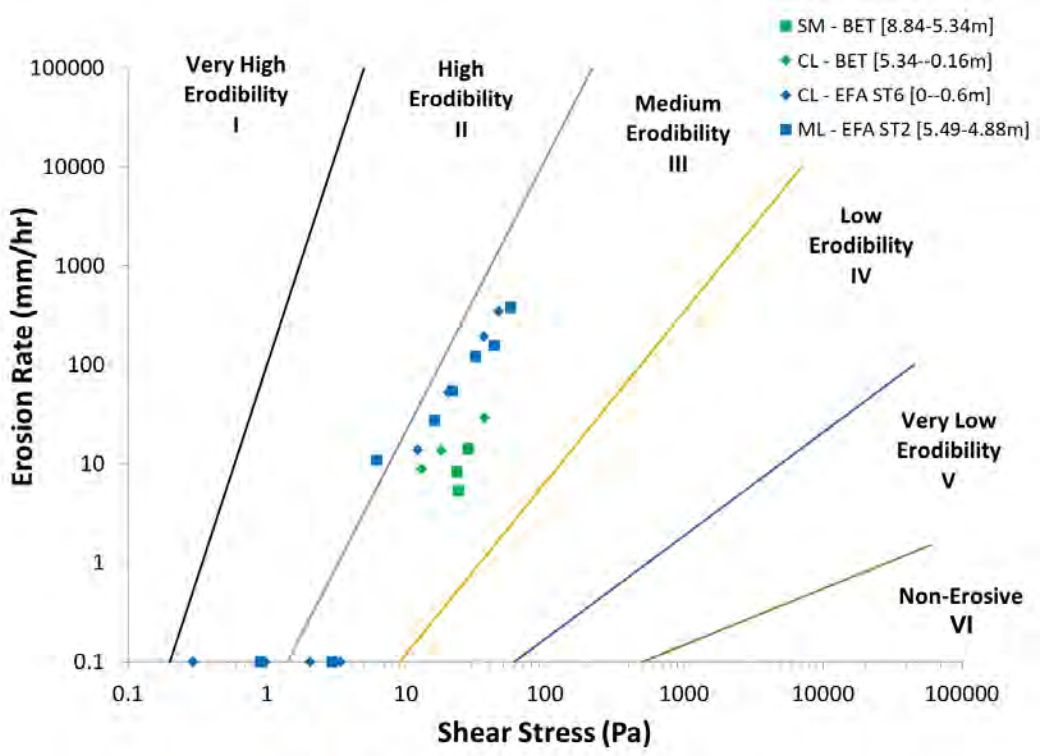

FIGURE 41 – MEASURED EROSION FUNCTIONS AT SACRAMENTO RIVER SITE 1 (SAC1) – OTHER USCS CLASSIFICATIONS.

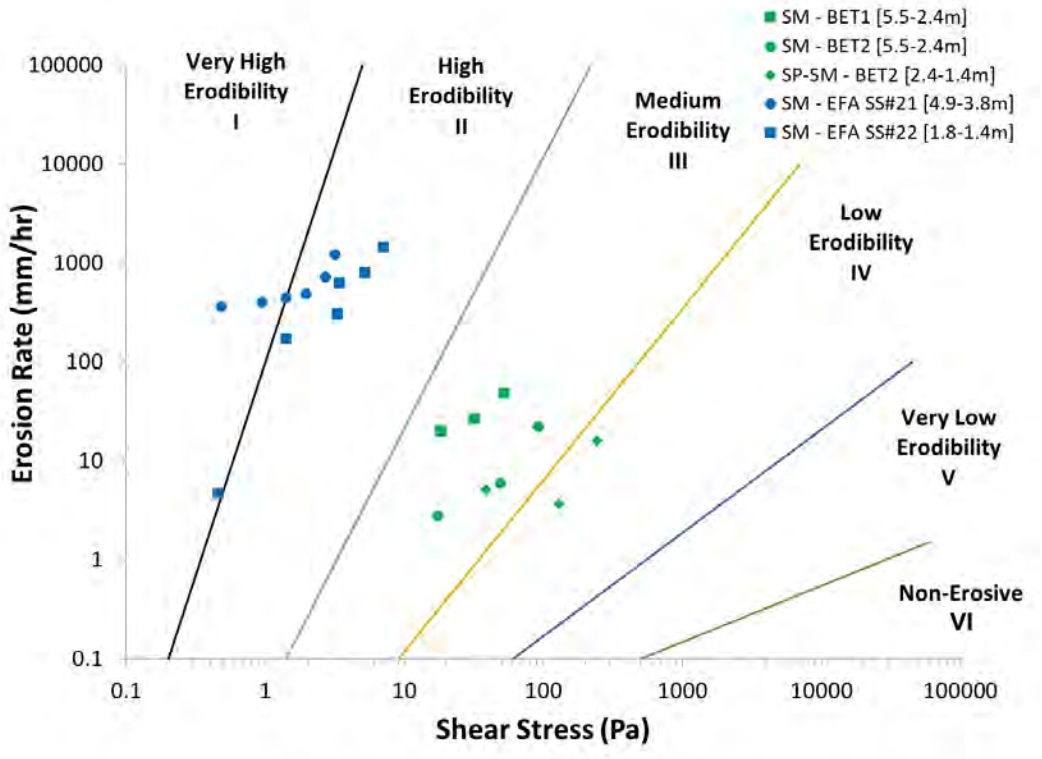

FIGURE 42 – MEASURED EROSION FUNCTIONS AT SACRAMENTO RIVER SITE 3 (SAC3) – OTHER USCS CLASSIFICATIONS.

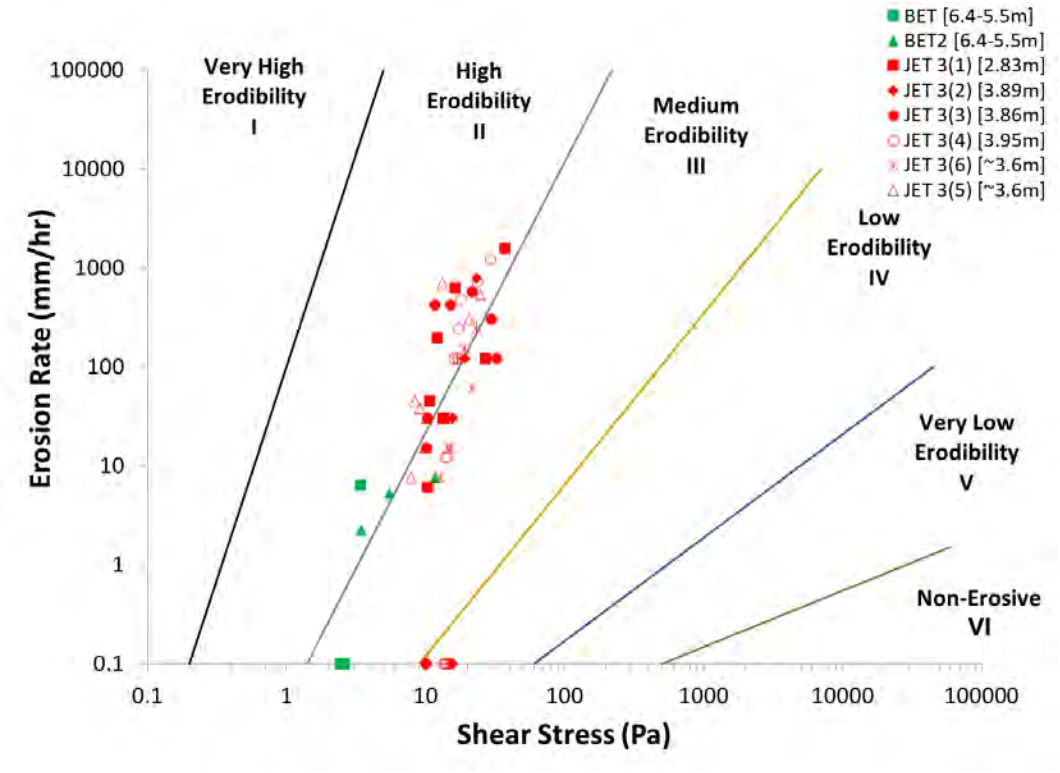

FIGURE 43 – MEASURED EROSION FUNCTIONS AT SACRAMENTO RIVER SITE 3 (SAC3) – SILT (USCS ML).

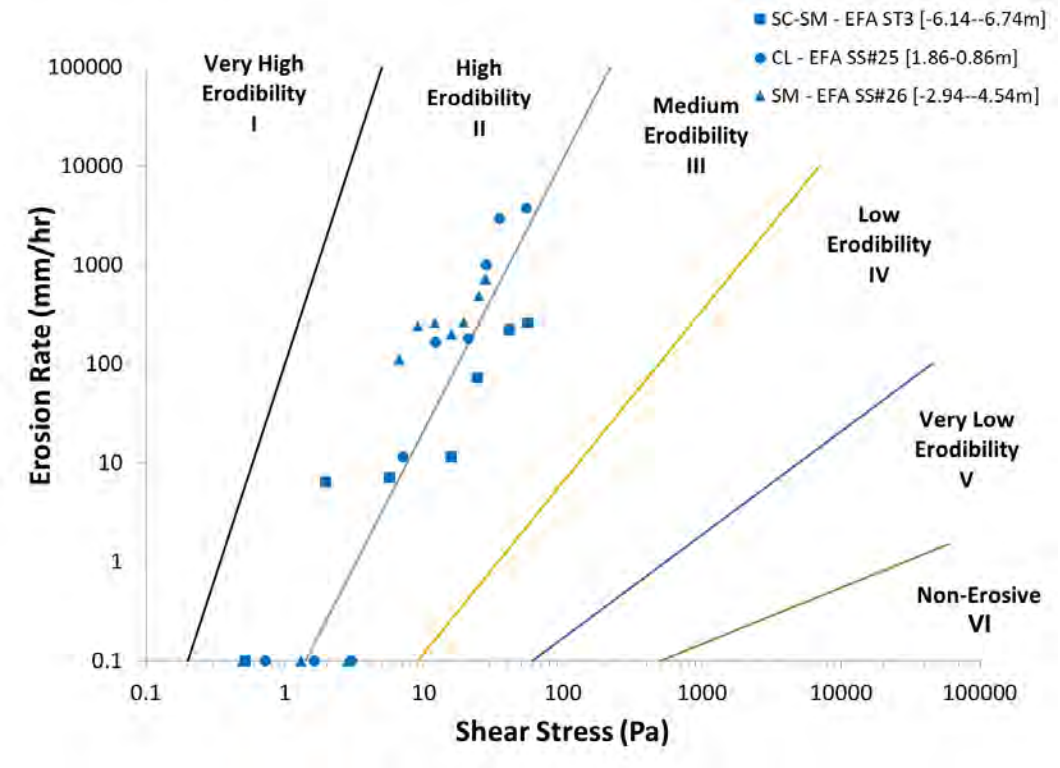

FIGURE 44 – MEASURED EROSION FUNCTIONS AT SACRAMENTO RIVER SITE 5 (SAC5) – OTHER USCS CLASSIFICATIONS.

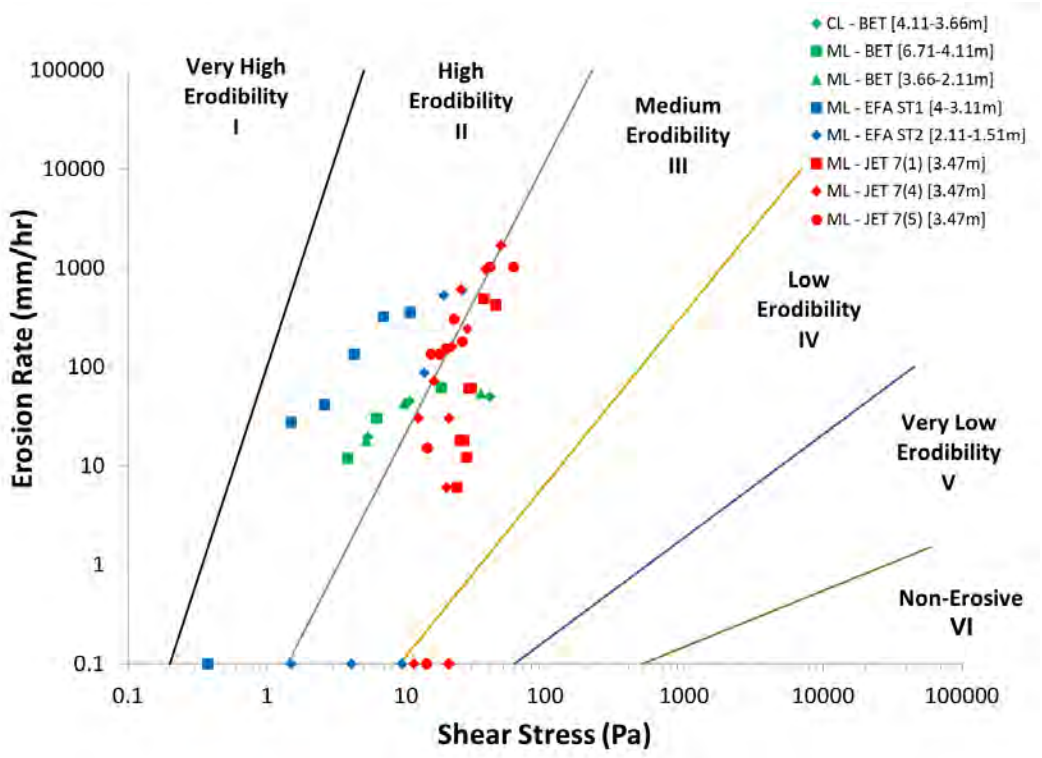

FIGURE 45 – MEASURED EROSION FUNCTIONS AT SACRAMENTO RIVER SITE 7 (SAC7) – OTHER USCS CLASSIFICATIONS.

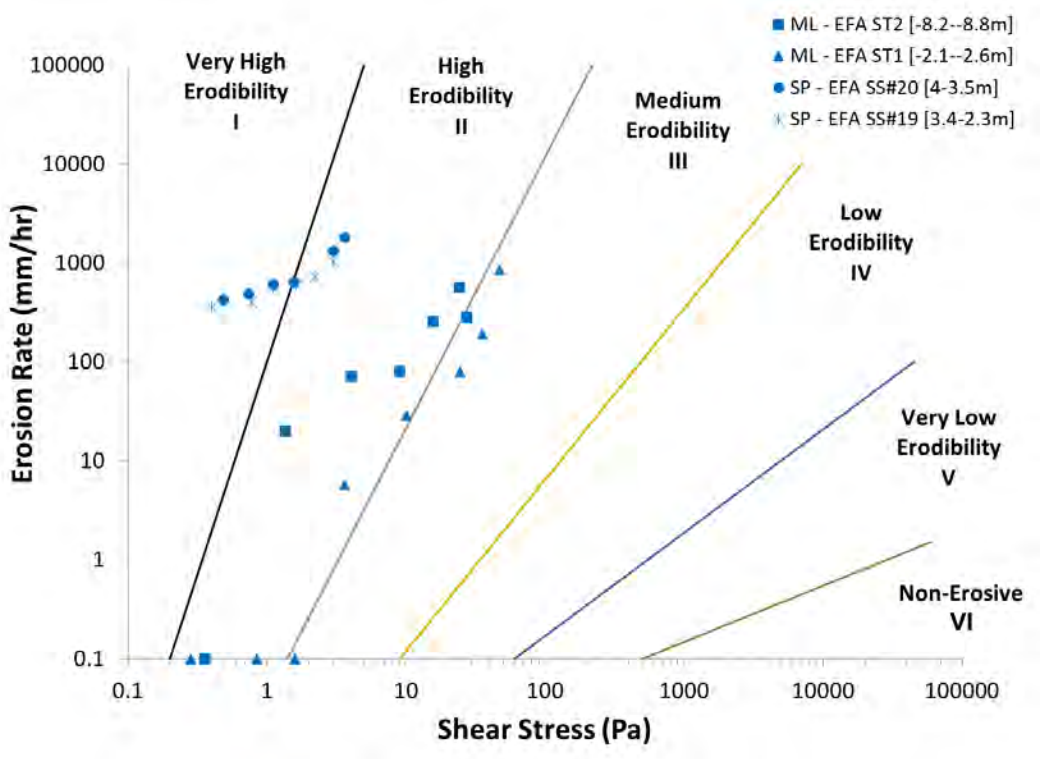

FIGURE 46 – MEASURED EROSION FUNCTIONS AT SACRAMENTO RIVER SITE 8 (SAC8) – OTHER USCS CLASSIFICATIONS.

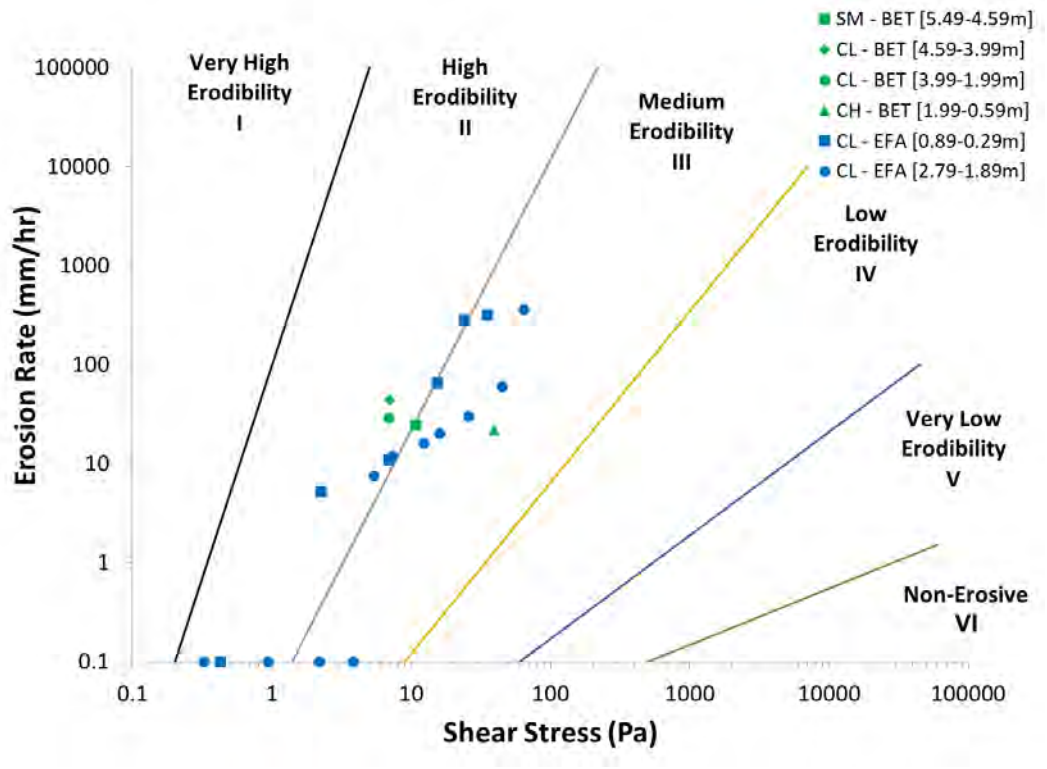

FIGURE 47 – MEASURED EROSION FUNCTIONS AT SACRAMENTO RIVER SITE 9 (SAC9) – OTHER USCS CLASSIFICATIONS.

Erosion functions and erodibility parameters based on grain resistance

Overall comparison

Results of applying the friction coefficient associated with the JET as described in "*Erosion-resistance parameters derived using applied shear acting on sediment grains or soil particles (Analysis Step 3)*" to the raw BET and filtered EFA data are illustrated in Figure 48. It can be seen that the grain shear is approximately 59% of the total shear for the EFA and 53% for the BET. Consistency between the EFA (filtered) and BET results for reduction in shear stress is not surprising since the reduction for both are a function of a constant unless grain size dictates rougher conditions than that of the constant friction factor. It is important to note that a factor of 1.5 is applied to the BET friction factor due to the annular cross section as described by Eq. (**5**) for grain shear calculations.

Regression to obtain erosion-resistance parameters was conducted on the grain shear data as described in the "*Data analysis and reduction*" section of this report. Figure 49 illustrates the change in critical shear stress when using grain shear stress for regression purposes and Figure 51 provides the erodibility coefficient of the excess shear stress equation. Results indicate that both the EFA (filtered) and BET had a considerable reduction in critical shear stress for values above 5 Pa, whereas data below 5 Pa were in general agreement (Figure 50). Figure 52 compares the erodibility coefficient for the BET derived using the overall applied shear stress and that caused by grain roughness. The BET erodibility coefficient nearly doubled as a result of the regression through the grain shear stress data, but overall remained considerably lower than other REMT datasets.

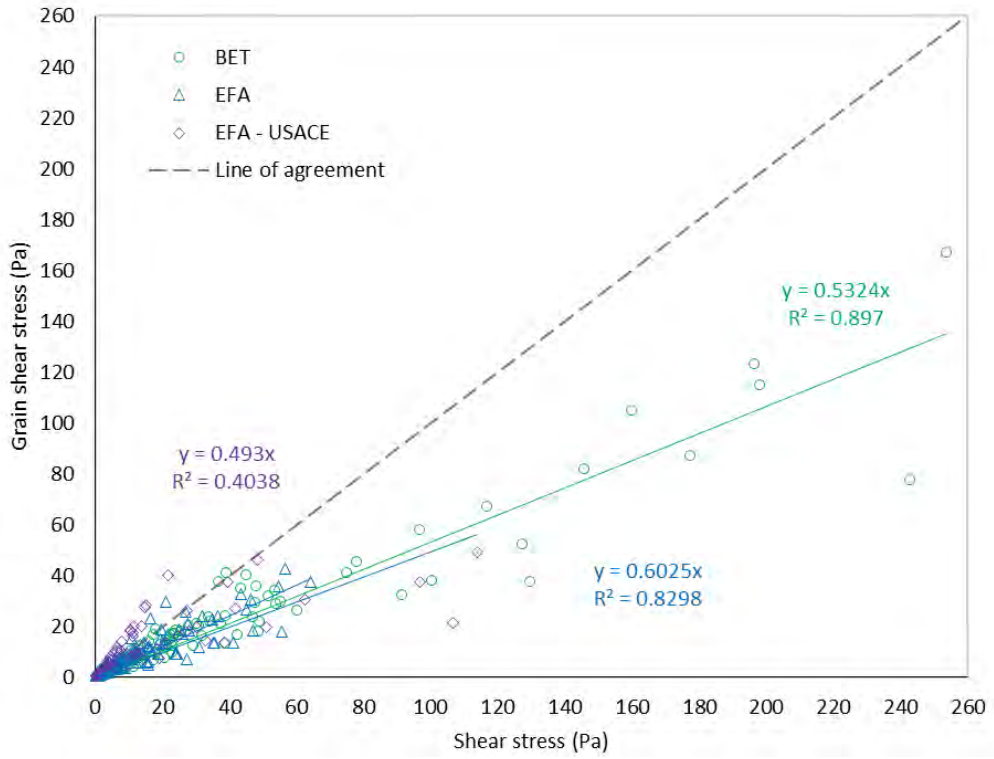

FIGURE 48 – RELATIONSHIP BETWEEN SHEAR STRESS AND GRAIN SHEAR STRESS FOR THE EFA AND BET DATA.

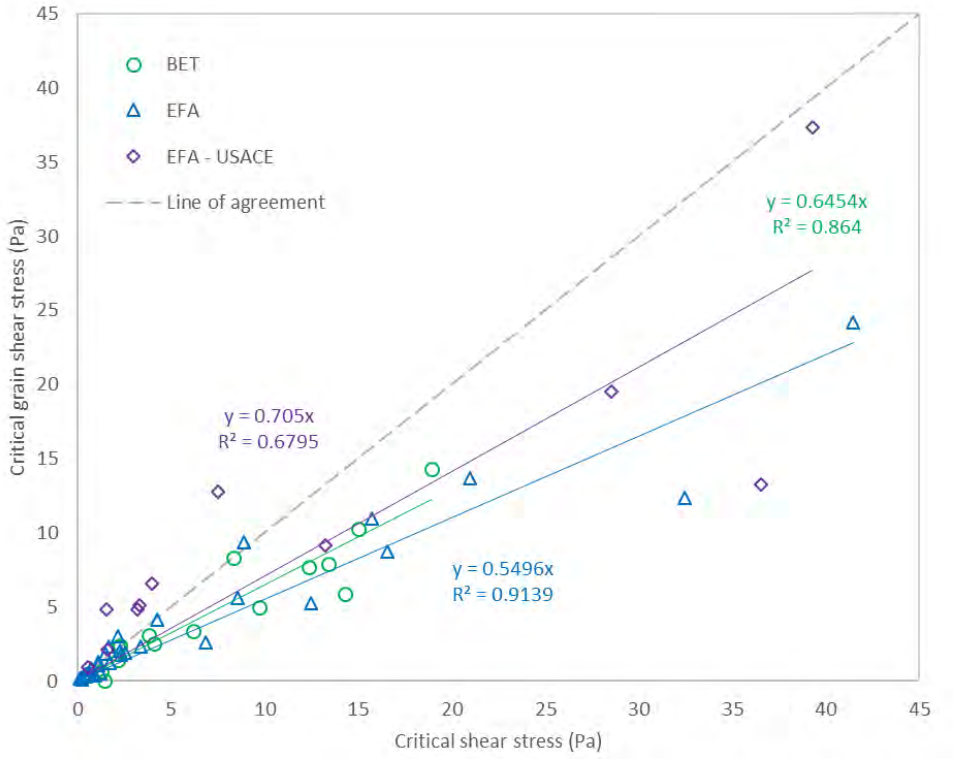

FIGURE 49 – COMPARISON OF CRITICAL SHEAR STRESS DERIVED USING TOTAL SHEAR STRESS AND GRAIN SHEAR STRESS FOR THE EFA AND BET.

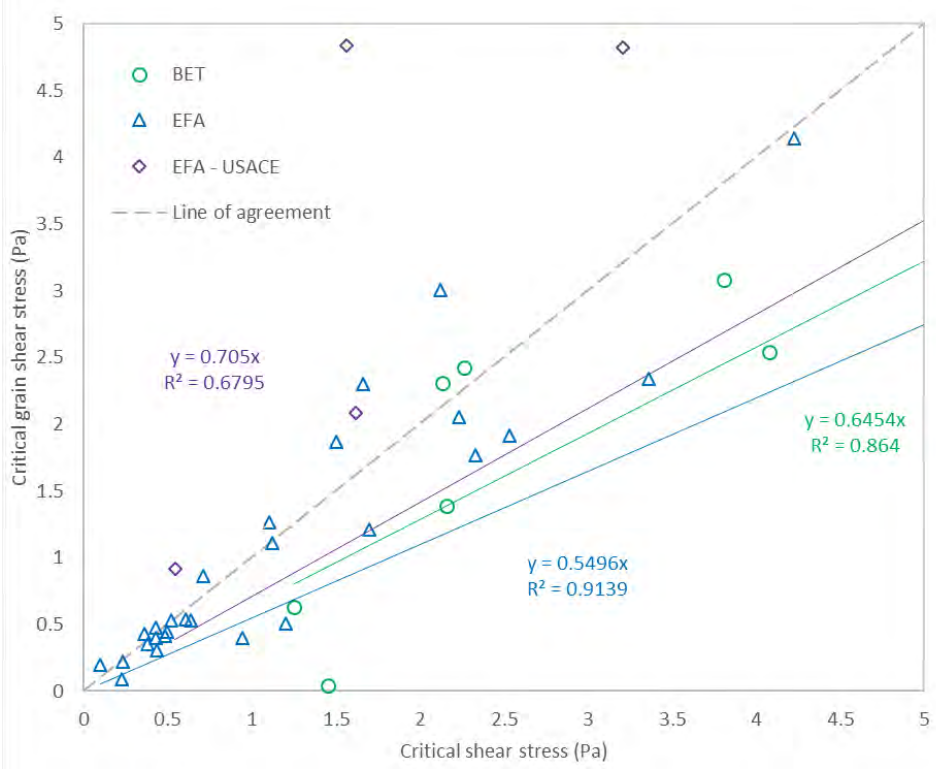

FIGURE 50 – COMPARISON OF CRITICAL SHEAR STRESS (BELOW 5 PA) DERIVED USING TOTAL SHEAR STRESS AND GRAIN SHEAR STRESS FOR THE EFA AND BET. THE PLOTTED TRENDLINES ARE THOSE BASED ON THE ENTIRE DATA SET (FIGURE 49).

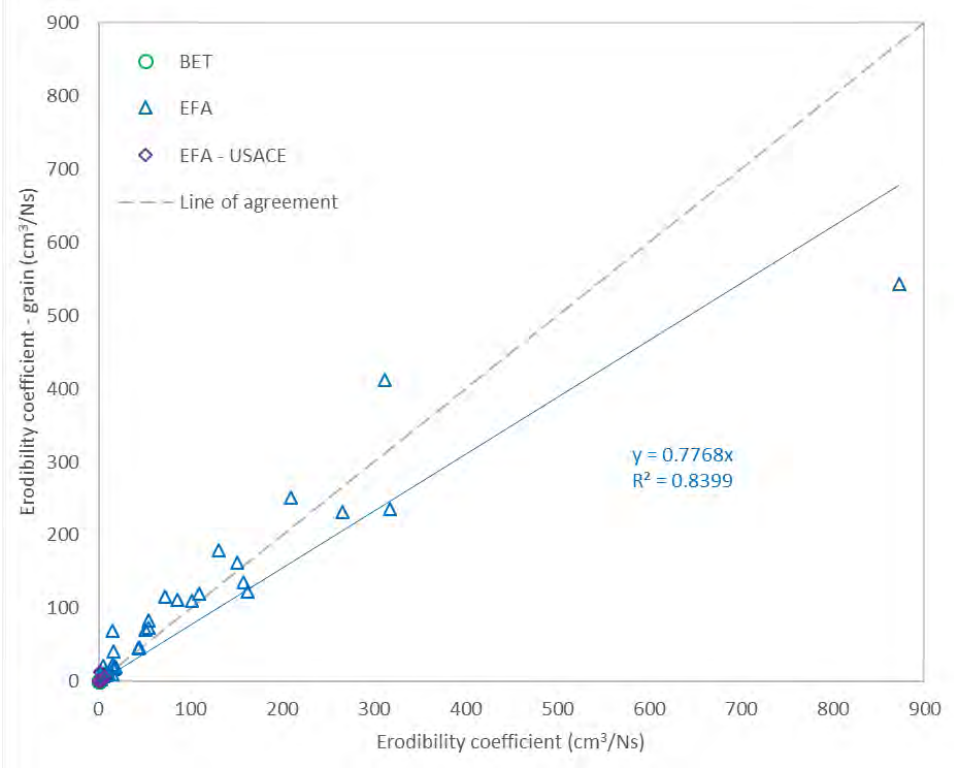

FIGURE 51 – COMPARISON OF ERODIBILITY COEFFICIENT DERIVED USING TOTAL SHEAR STRESS AND GRAIN SHEAR STRESS FOR THE EFA AND BET.

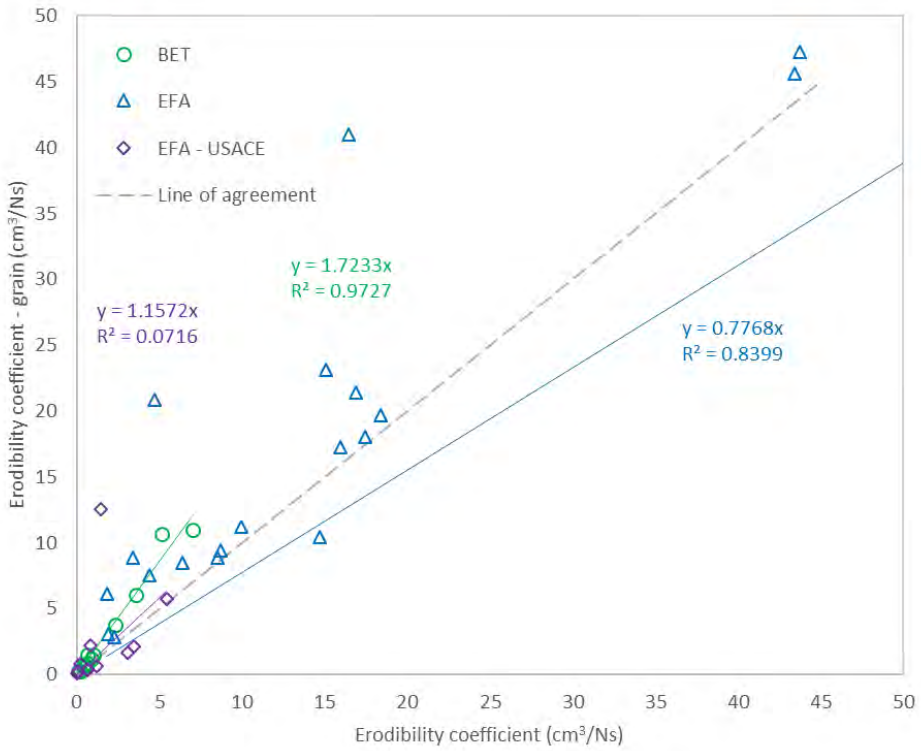

FIGURE 52 – COMPARISON OF ERODIBILITY COEFFICIENT (BELOW 50 CM^3 N^{-1} S^{-1}) DERIVED USING TOTAL SHEAR STRESS AND GRAIN SHEAR STRESS FOR THE EFA AND BETS.

Comparison of erosion functions by test method and by soil

Figure 53 through Figure 58 present the measured pairs of (τ',E) points, or raw REMT data based on grain shear stress, for all test methods grouped by soil type and plotted on the logarithmic classification scale of Briaud (2008). Trends in erosion functions using grain shear stress are similar to those based on overall shear stress in how the data are grouped. However, data for the EFA (filtered) and BET have shifted to a lower shear stress and no change is seen on the ordinate due to no change in erosion rate. The considerable scatter for cohesionless soils (e.g. SM, SP, SP-SM) remains for the grain shear-based data. The cohesive soils (e.g. ML, CL) maintain a better grouping regardless of the shift to grain shear, but, as previously stated, shift to lower shear stress values. Comparable plots to "*Comparison of erosion functions by test method, site and soil*" for grain shear estimates are provided in APPENDIX B.

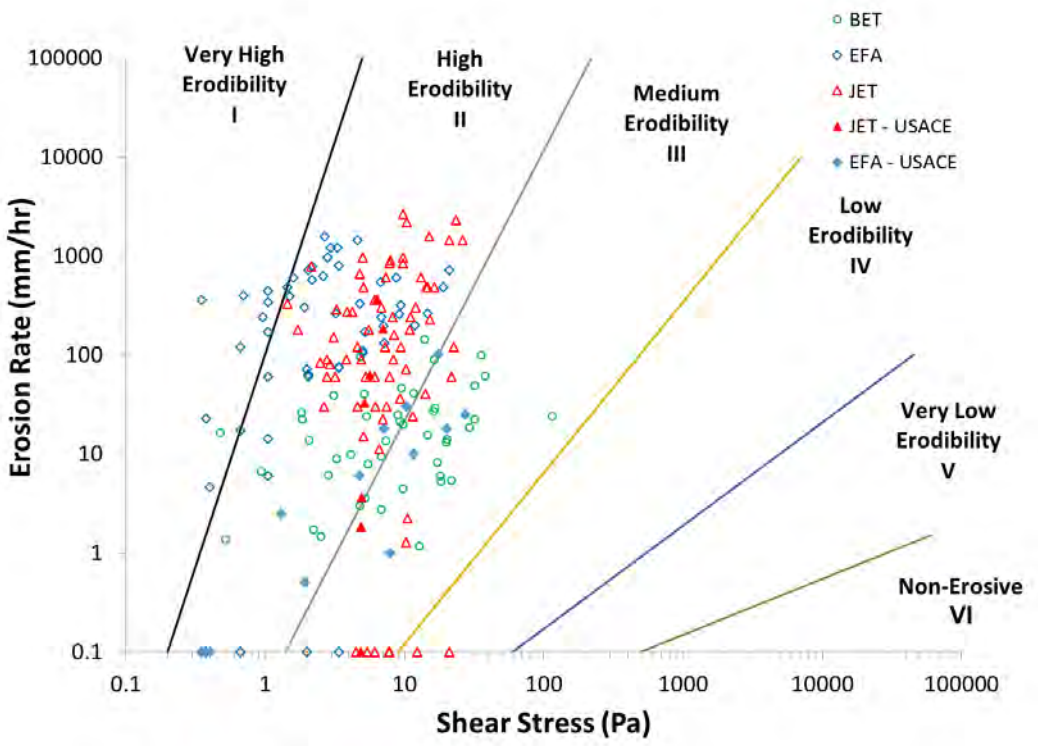

FIGURE 53 – GRAIN SHEAR-BASED EROSION FUNCTIONS MEASURED BY JET, EFA, AND BET METHODS FOR SILTY SAND (USCS SM).

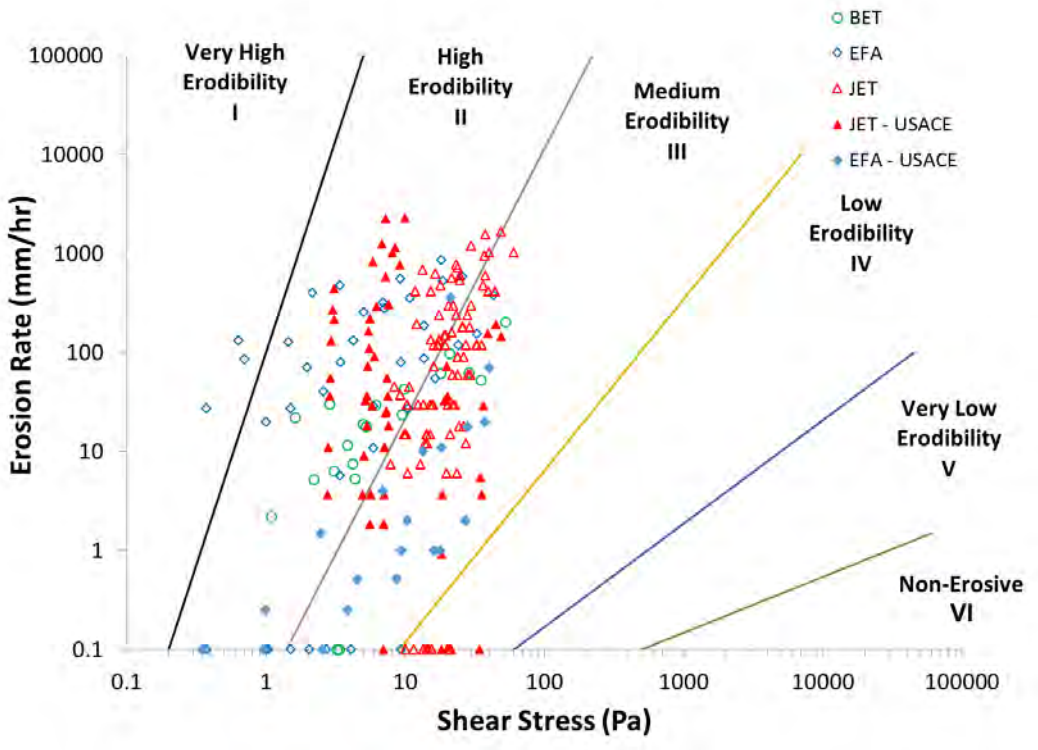

FIGURE 54 – GRAIN SHEAR-BASED EROSION FUNCTIONS MEASURED BY JET, EFA, AND BET METHODS FOR SILT (USCS ML).

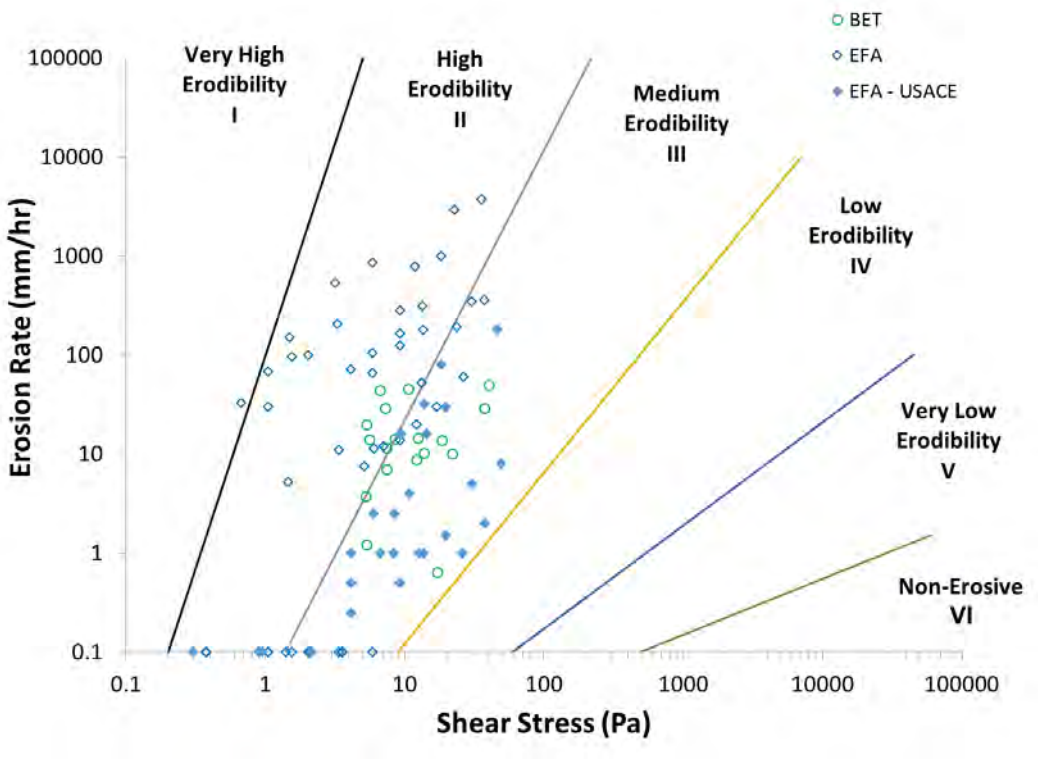

FIGURE 55 – GRAIN SHEAR-BASED EROSION FUNCTIONS MEASURED BY JET, EFA, AND BET METHODS FOR LEAN CLAY (USCS CL).

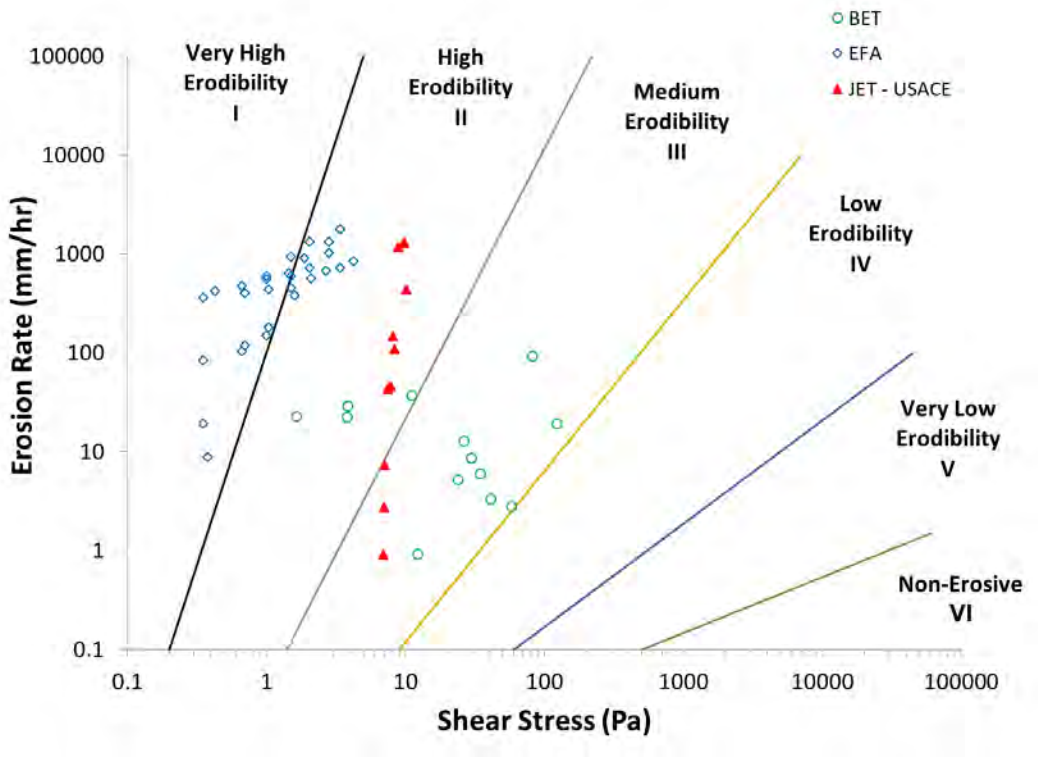

FIGURE 56 – GRAIN SHEAR-BASED EROSION FUNCTIONS MEASURED BY JET, EFA, AND BET METHODS FOR POORLY GRADED SAND (USCS SP).

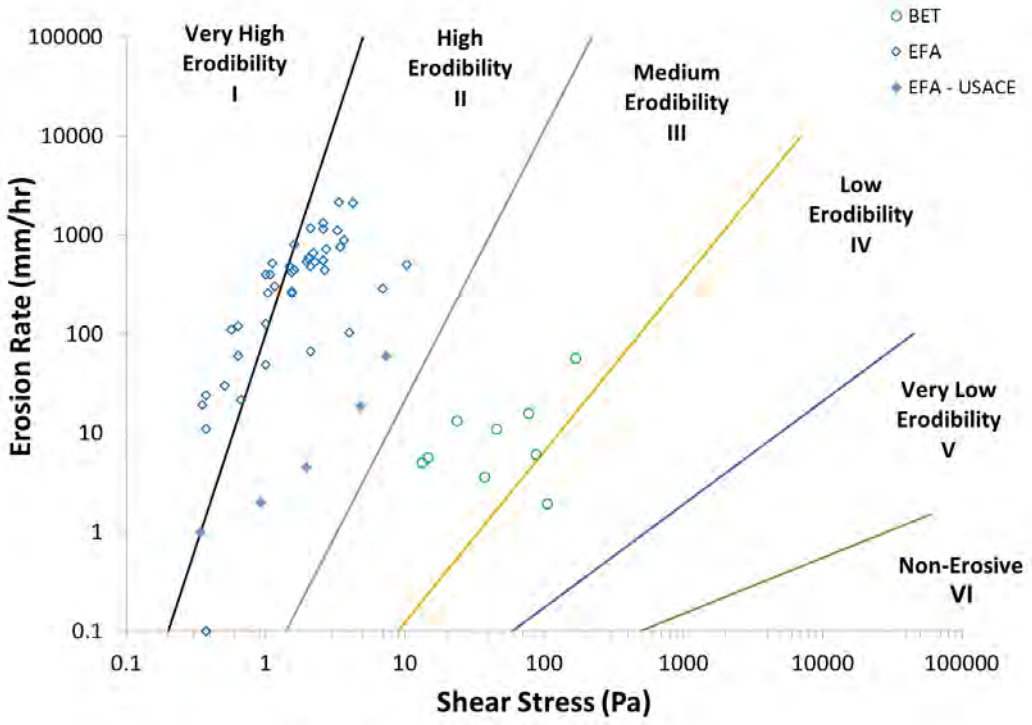

FIGURE 57 – GRAIN SHEAR-BASED EROSION FUNCTIONS MEASURED BY JET, EFA, AND BET METHODS FOR POORLY GRADED SAND WITH SILT (USCS SP-SM).

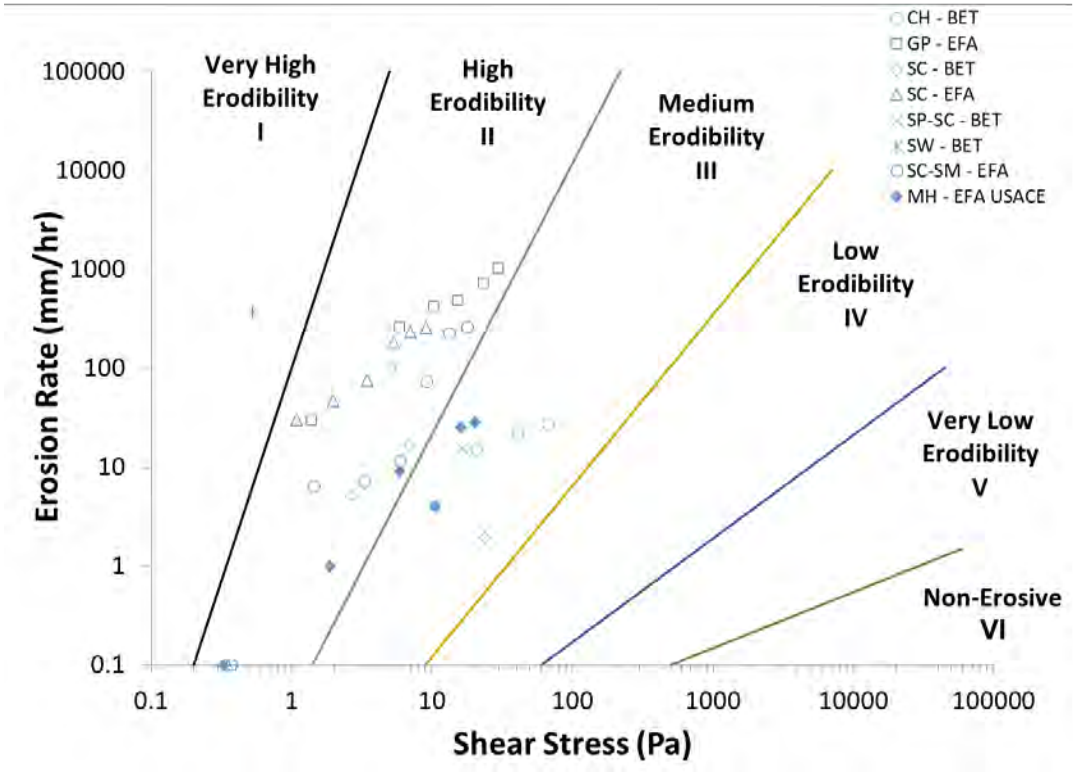

FIGURE 58 – GRAIN SHEAR-BASED EROSION FUNCTIONS MEASURED BY JET, EFA, AND BET METHODS FOR USCS CLASSES CH, SP-SC, SW, AND SC.

Comparison of erodibility parameters by test method and by soil

Erodibility parameters associated with grain resistance estimates used in the excess shear stress equation (Eq. (1)) determined by the linear regression method for all test types as described in the section "*Data analysis and reduction*" were grouped by soil classification for statistical comparison (Figure 59 and Figure 60). Mean values for the grain critical shear stress and associated erodibility coefficient by test and soil classification are provided in Table 5 and Table 6, respectively. APPENDIX A provides the erodibility parameter results for grain resistance estimates.

Table 7 presents the percent change in critical shear stress and erodibility coefficient for each USCS soil class for EFA and BET data. The changes seen in Figure 59 and Figure 60 from that of their respective counterparts, Figure 20 and Figure 21 are only in the BET and EFA data. BET erodibility coefficients, regardless of the percent increases, still remain low when compared to the other REMT types. However, it can be seen that critical shear stress estimates for the BET and JET for soil class SM are in general agreement, whereas prior to the grain shear partitioning BET had values nearly twice as large.

TABLE 5 – MEAN GRAIN SHEAR STRESS-BASED CRITICAL SHEAR STRESS FOR EACH SOIL CLASS BY REMT.

	Mean grain critical shear stress value per REMT (Pa)				
USCS Class	BET	Filtered EFA	Filtered EFA – USACE	JET	JET – USACE
CL	3.16	7.75	14.46	-	-
GP	-	3.01	-	-	-
MH	-	-	2.08	-	-
ML	2.86	6.22	15.20	15.09	11.27
SC	2.54	0.48	-	-	-
SC-SM	-	5.24	-	-	-
SM	5.29	1.52	4.95	4.82	4.84
SP	-	0.44	-	-	6.63
SP-SC	8.34	-	-	-	-
SP-SM	7.89	1.09	0.92	-	-

TABLE 6 – MEAN ERODIBILITY COEFFICIENT ASSOCIATED WITH GRAIN SHEAR ESTIMATES FOR EACH SOIL CLASS AND REMT.

	Mean grain erodibility coefficient per REMT ($cm^3\ N^{-1}\ s^{-1}$)				
USCS Class	BET	Filtered EFA	Filtered EFA – USACE	JET	JET – USACE
CL	0.71	33.85	2.06	-	-
GP	-	10.44	-	-	-
MH	-	-	0.42	-	-
ML	1.51	23.54	4.47	11.74	119.00
SC	10.98	9.42	-	-	-
SC-SM	-	6.15	-	-	-
SM	2.72	121.04	1.23	30.01	36.53
SP	-	165.98	-	-	89.14
SP-SC	0.52	-	-	-	-
SP-SM	0.23	165.23	-	-	-

TABLE 7 – AVERAGE PERCENT CHANGE IN ERODIBILITY PARAMETERS FROM ORIGINAL AND GRAIN SHEAR ESTIMATES FOR BOTH EFA AND BET DATA.

USCS Class	Percent change in τ_c	Percent change in k_d	Number of applicable data points
CL	-2.1	85.5	13
GP	41.6	-28.9	1
MH	28.7	-31.4	1
ML	-8.3	156.5	10
SC	-13.3	32.6	2
SC-SM	-57.9	240.0	1
SM	-25.2	42.4	19
SP	19.1	9.8	5
SP-SC	0.1	11.1	1
SP-SM	-9.7	31.3	9

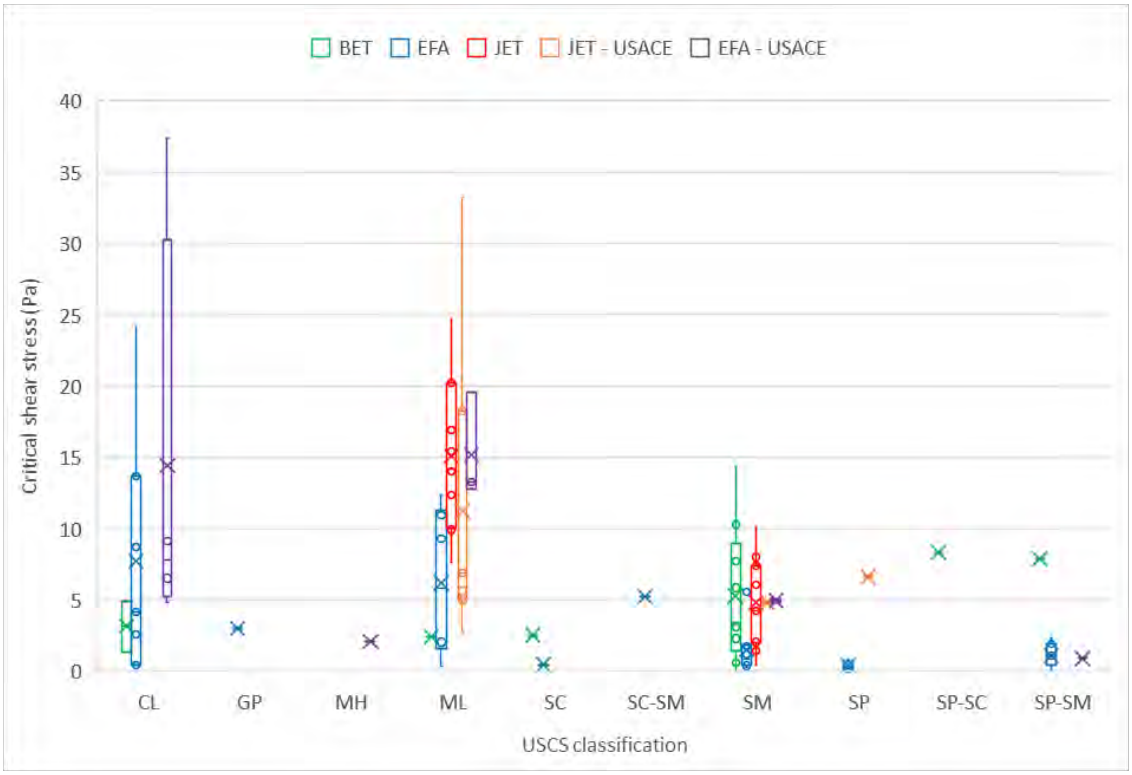

FIGURE 59 – BOX AND WHISKER PLOT OF CRITICAL SHEAR STRESS ESTIMATES ASSOCIATED WITH GRAIN SHEAR STRESS BY SOIL CLASSIFICATION.

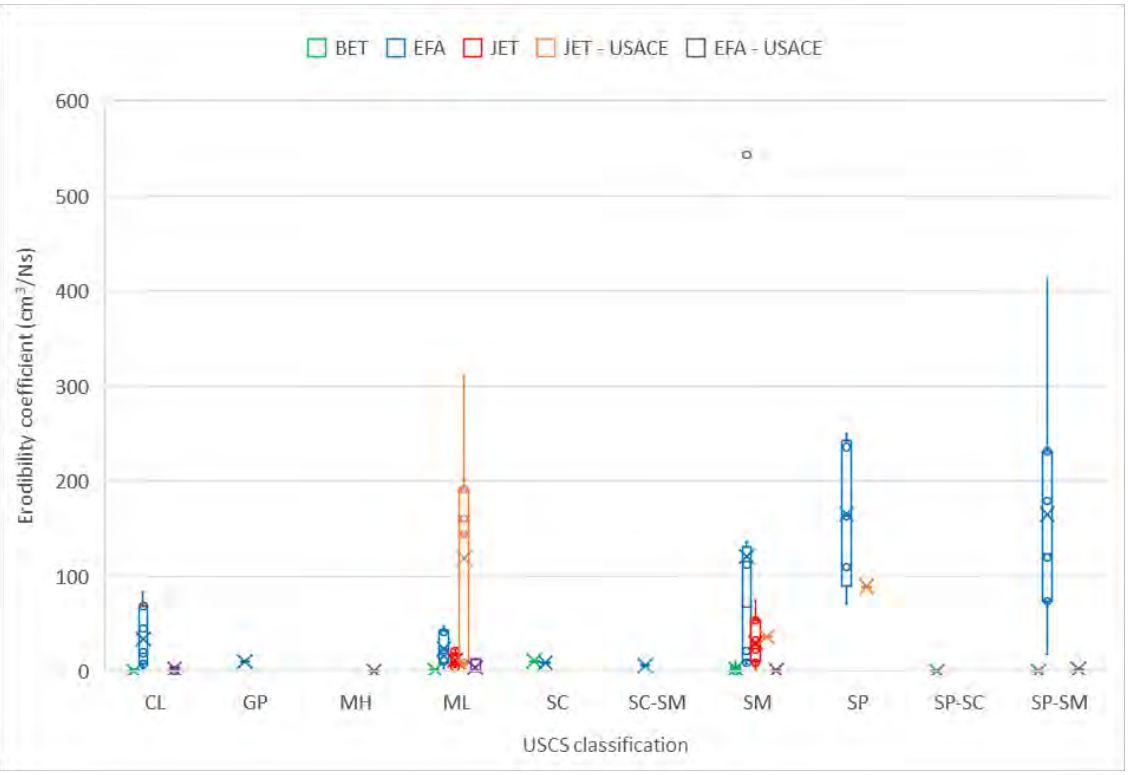

FIGURE 60 – BOX AND WHISKER PLOT OF ERODIBILITY COEFFICIENT ESTIMATES BY SOIL CLASSIFICATION – GRAIN RESISTANCE.

Effects of measurement uncertainty on soil erodibility parameters

The erosion functions presented in the above sections were augmented by including the uncertainty in shear stress estimation and erosion rate measurement (see section "*Effects of measurement uncertainty on erosion-resistance parameters*"). The linear regression of Eq. (1) through the augmented erosion functions was conducted using the ODR method. Appendix D presents plots of the erosion functions and both traditional regression (not accounting for uncertainty) and ODR regression (accounting for uncertainty) methods. The below sections present the effects of the measurement/approximation uncertainty on derived erosion-resistance parameters. The erosion functions used for the EFA method are those related to the mass-erosion regime (labeled 'filtered' in previous sections) for direct comparison with JET and BET methods.

Regression of the BET data produced many critical shear stresses and a few erodibility coefficients with negative values. For these occurrences, the critical shear stress during the regression was arbitrarily set to a small value (0.06 Pa) and only the erodibility coefficient was allowed to vary during the regression procedure.

Mini-JET and JET methods

Figure 61 through Figure 63 compare the erosion-resistance parameters derived when accounting and not accounting for uncertainty in shear stress estimates and erosion rate measurements. The critical shear stresses are generally smaller when uncertainty in shear stress and erosion rate is taken into account (Figure 61). This is due to a reduction in shear stress ($\mu_\tau < 0$) when the submerged jet impinges onto a scour hole instead of a flat surface. On the other hand, the erodibility coefficient increased when accounting for uncertainty (Figure 62). This is probably due to larger uncertainty in erosion rate for greater erosion rates and shear stresses. The reduction in critical shear stress and increase in erodibility coefficient results in a diagonal (north-west direction) shift when plotting erodibility coefficient versus critical shear stress (Figure 63).

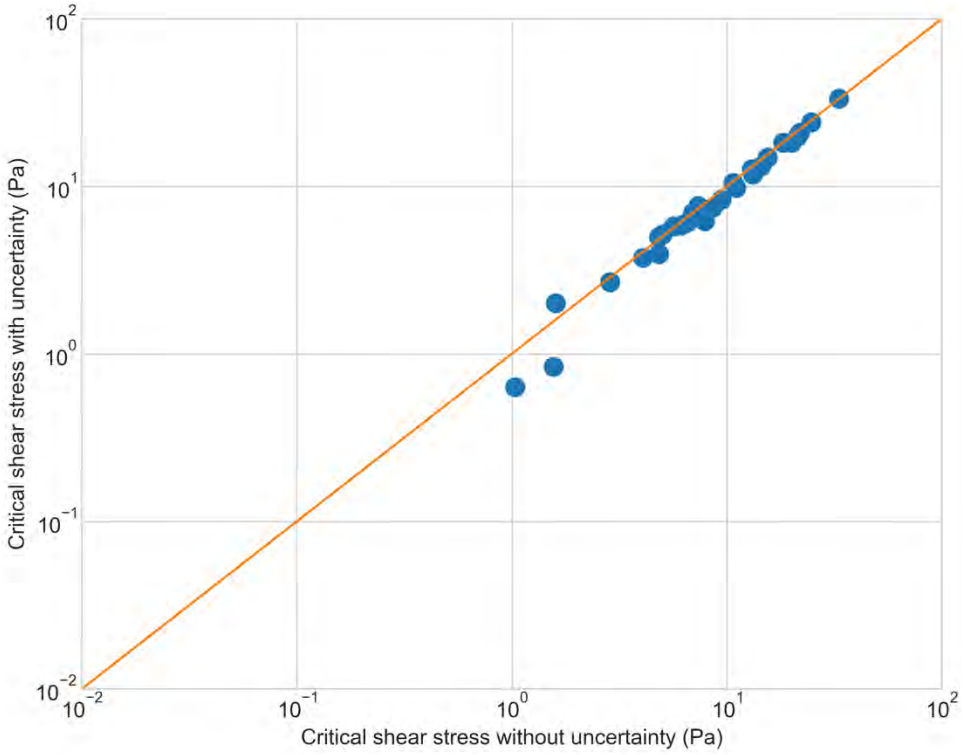

FIGURE 61 – COMPARISON OF CRITICAL SHEAR STRESS DERIVED WITHOUT AND WITH ACCOUNTING FOR UNCERTAINTY IN SHEAR STRESS AND EROSION RATE AS MEASURED BY THE JET METHOD.

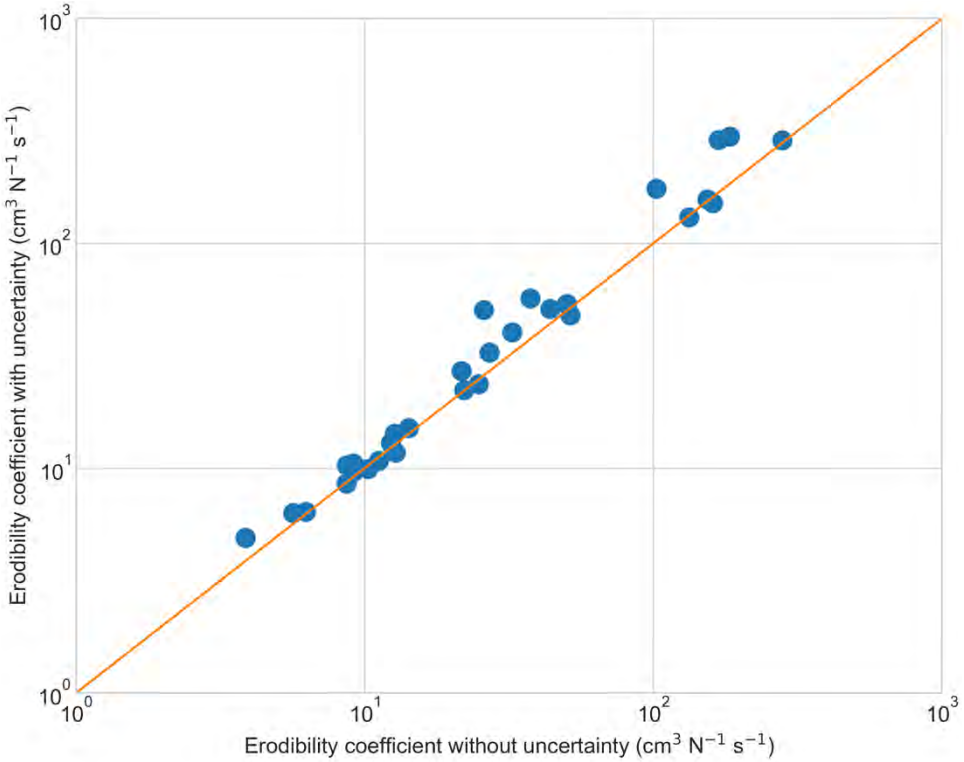

FIGURE 62 – COMPARISON OF ERODIBILITY COEFFICIENT DERIVED WITHOUT AND WITH ACCOUNTING FOR UNCERTAINTY IN SHEAR STRESS AND EROSION RATE AS MEASURED BY THE JET METHOD.

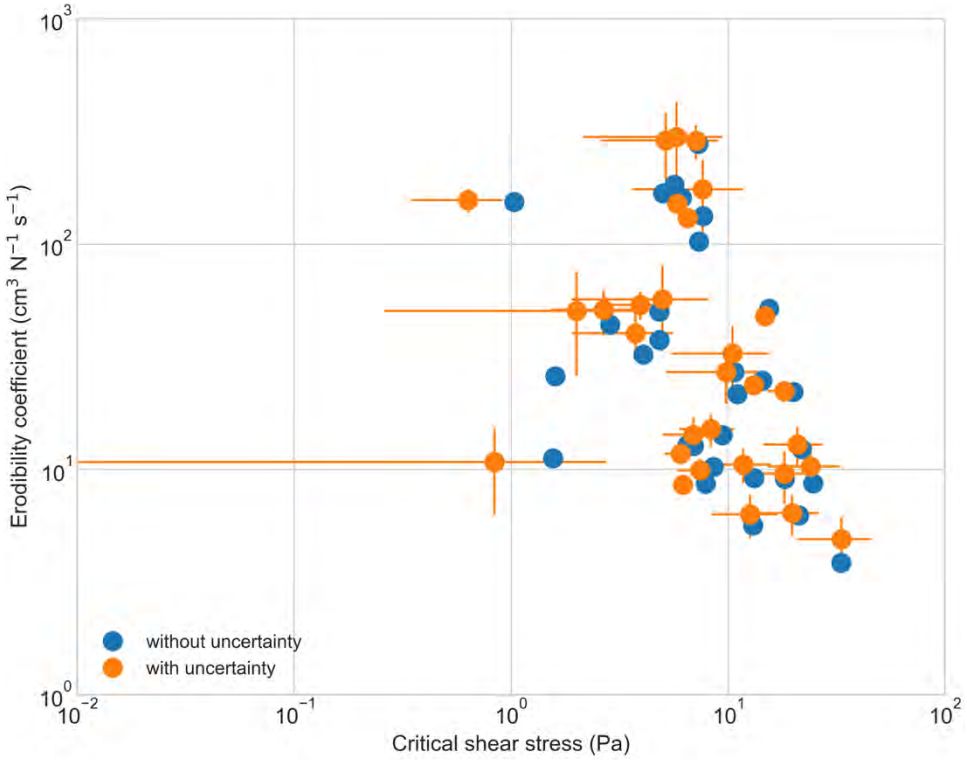

FIGURE 63 – COMPARISON OF ERODIBILITY COEFFICIENT VERSUS CRITICAL SHEAR STRESS DERIVED WITHOUT AND WITH ACCOUNTING FOR UNCERTAINTY IN SHEAR STRESS AND EROSION RATE AS MEASURED BY THE JET METHOD. THE LENGTH OF THE HORIZONTAL AND VERTICAL LINES INDICATE THE STANDARD DEVIATION OF THE UNCERTAINTY IN CRITICAL SHEAR STRESS AND ERODIBILITY COEFFICIENT, RESPECTIVELY.

EFA method

Figure 64 through Figure 69 compare the erosion-resistance parameters derived when accounting and not accounting for uncertainty in shear stress estimates and erosion rate measurements for both total shear- and grain shear-based erosion functions.

EROSION-RESISTANCE PARAMETERS DERIVED FROM TOTAL SHEAR STRESS ESTIMATES

On average, the critical shear stresses when uncertainty in shear stress and erosion rate is taken into account are similar to those without accounting for uncertainty (Figure 64). For about five EFA tests critical shear stress increased about two-fold when accounting for uncertainty, compared to one EFA test where critical shear stress reduced two-fold when accounting for uncertainty. The erodibility coefficient slightly increased on average when accounting for uncertainty (Figure 65). Plotting erodibility coefficient versus critical shear stress shows a small reduction in scatter as smaller critical shear stresses have shifted towards slightly higher critical shear stresses when accounting for measurement/approximation uncertainty (Figure 66).

EROSION-RESISTANCE PARAMETERS DERIVED FROM GRAIN SHEAR STRESS ESTIMATES

Similar to total shear stress-based critical shear stress, the grain shear stress-based critical shear stress is not much affected by accounting for measurement/approximation uncertainty (Figure 67). For small critical shear stresses (< 1 Pa) the relative changes in critical shear stress were fairly large. The erodibility coefficient slightly decreased on average when accounting for uncertainty (Figure 68). Plotting erodibility coefficient versus critical shear stress shows a small reduction in scatter as smaller critical shear stresses do not show a trend in how measurement/approximation uncertainty affects the relationship between erodibility coefficient and critical shear stress (Figure 69).

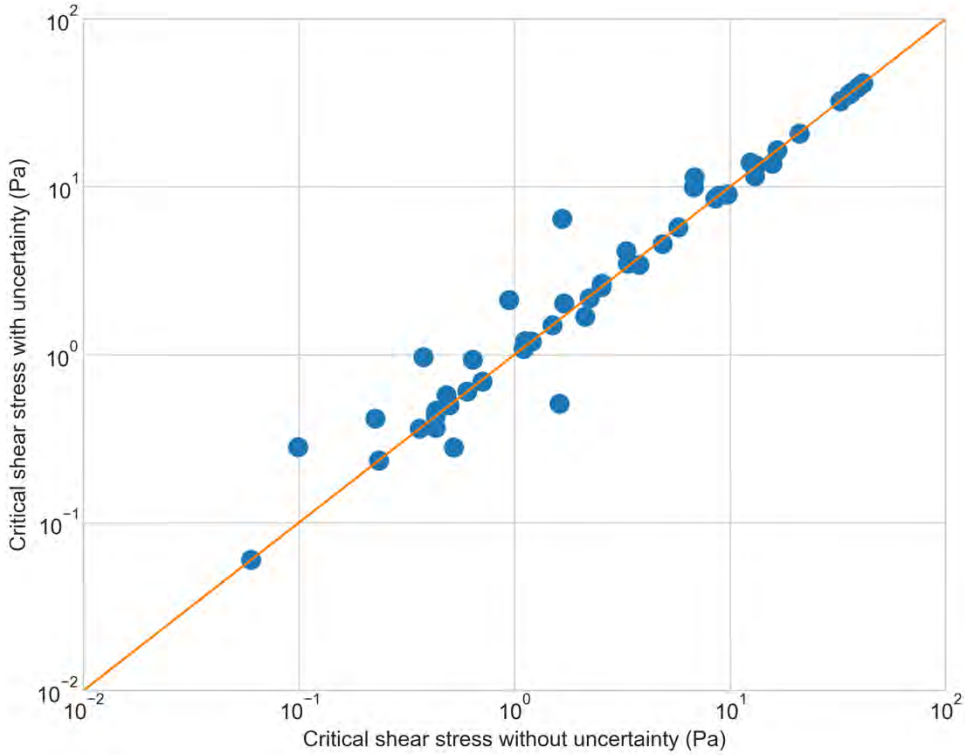

FIGURE 64 – COMPARISON OF CRITICAL SHEAR STRESS DERIVED WITHOUT AND WITH ACCOUNTING FOR UNCERTAINTY IN SHEAR STRESS AND EROSION RATE AS MEASURED BY THE EFA METHOD. THE CRITICAL SHEAR STRESS IS BASED ON TOTAL SHEAR STRESS ESTIMATES.

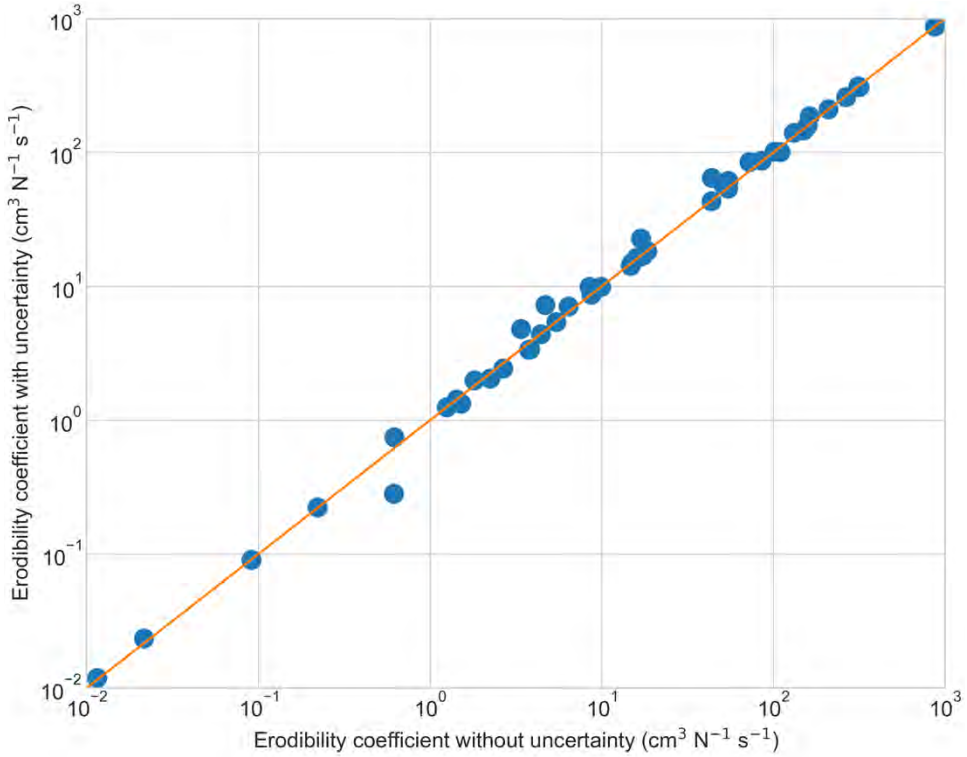

FIGURE 65 – COMPARISON OF ERODIBILITY COEFFICIENT DERIVED WITHOUT AND WITH ACCOUNTING FOR UNCERTAINTY IN SHEAR STRESS AND EROSION RATE AS MEASURED BY THE EFA METHOD. THE ERODIBILITY COEFFICIENT IS BASED ON TOTAL SHEAR STRESS ESTIMATES.

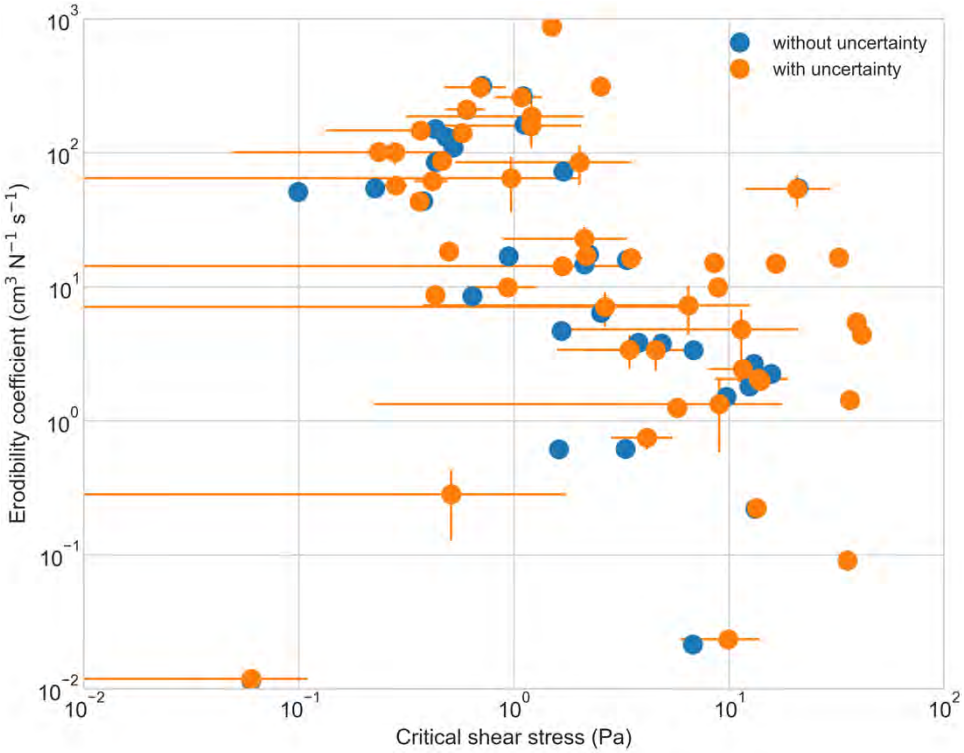

FIGURE 66 – COMPARISON OF ERODIBILITY COEFFICIENT VERSUS CRITICAL SHEAR STRESS DERIVED WITHOUT AND WITH ACCOUNTING FOR UNCERTAINTY IN SHEAR STRESS AND EROSION RATE AS MEASURED BY THE EFA METHOD. THE LENGTH OF THE HORIZONTAL AND VERTICAL LINES INDICATE THE STANDARD DEVIATION OF THE UNCERTAINTY IN CRITICAL SHEAR STRESS AND ERODIBILITY COEFFICIENT, RESPECTIVELY. EROSION-RESISTANCE PARAMETERS ARE BASED ON TOTAL SHEAR STRESS ESTIMATES.

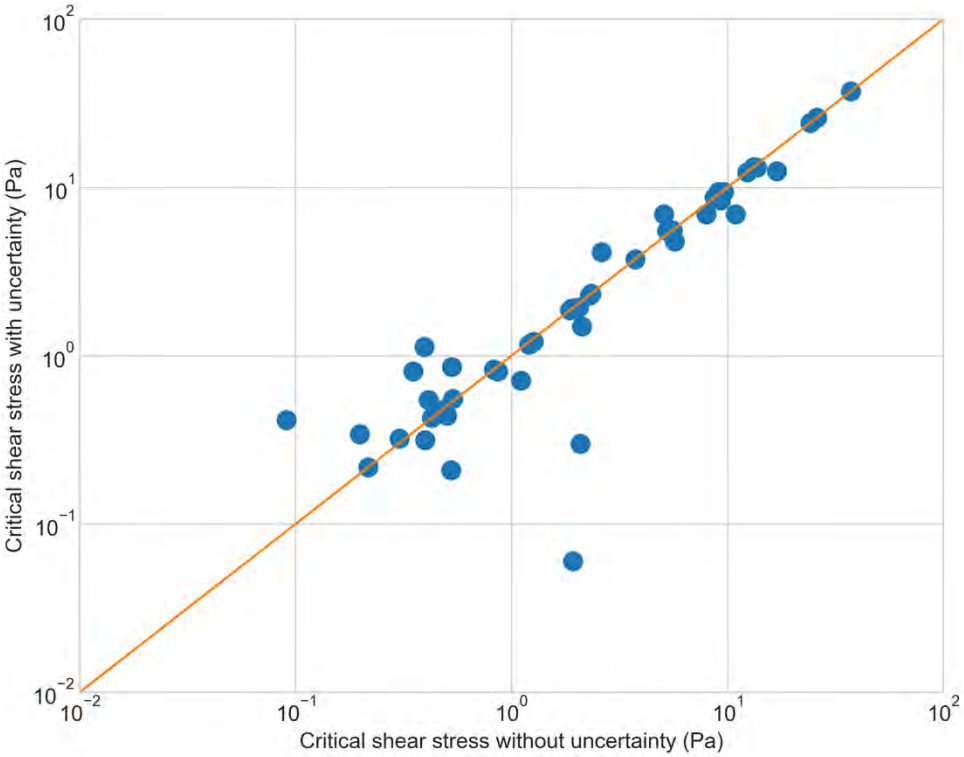

FIGURE 67 – COMPARISON OF CRITICAL SHEAR STRESS DERIVED WITHOUT AND WITH ACCOUNTING FOR UNCERTAINTY IN SHEAR STRESS AND EROSION RATE AS MEASURED BY THE EFA METHOD. THE CRITICAL SHEAR STRESS IS BASED ON GRAIN SHEAR STRESS ESTIMATES.

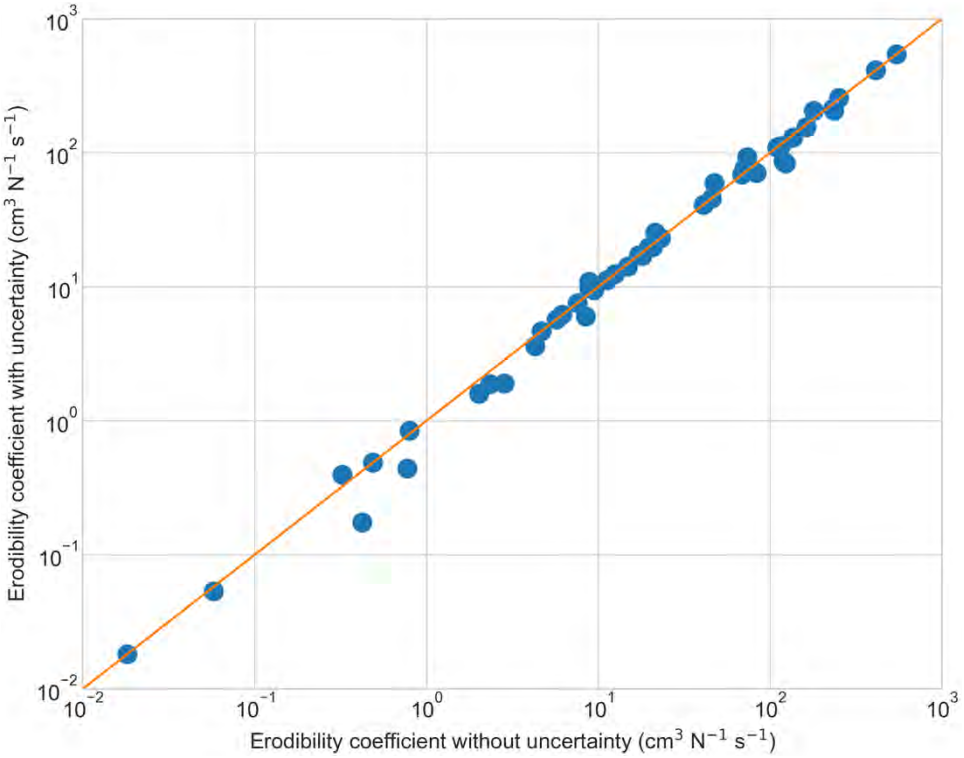

FIGURE 68 – COMPARISON OF ERODIBILITY COEFFICIENT DERIVED WITHOUT AND WITH ACCOUNTING FOR UNCERTAINTY IN SHEAR STRESS AND EROSION RATE AS MEASURED BY THE EFA METHOD. THE ERODIBILITY COEFFICIENT IS BASED ON GRAIN SHEAR STRESS ESTIMATES.

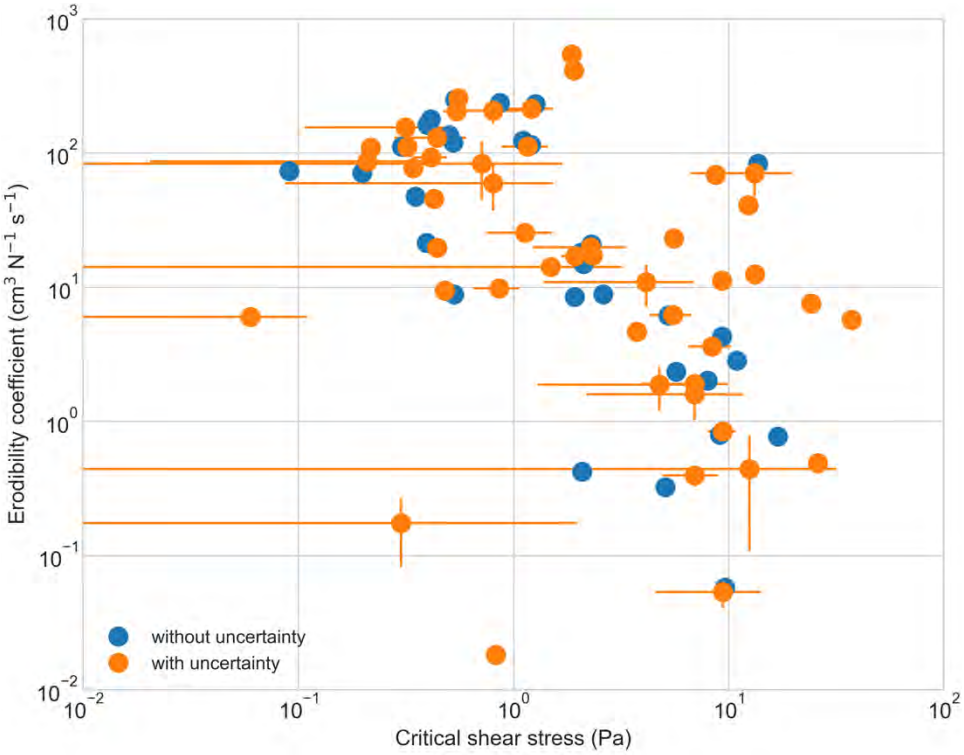

FIGURE 69 – COMPARISON OF ERODIBILITY COEFFICIENT VERSUS CRITICAL SHEAR STRESS DERIVED WITHOUT AND WITH ACCOUNTING FOR UNCERTAINTY IN SHEAR STRESS AND EROSION RATE AS MEASURED BY THE EFA METHOD. THE LENGTH OF THE HORIZONTAL AND VERTICAL LINES INDICATE THE STANDARD DEVIATION OF THE UNCERTAINTY IN CRITICAL SHEAR STRESS AND ERODIBILITY COEFFICIENT, RESPECTIVELY. EROSION-RESISTANCE PARAMETERS ARE BASED ON GRAIN SHEAR STRESS ESTIMATES.

BET method

Figure 70 through Figure 75 compare the erosion-resistance parameters derived when accounting and not accounting for uncertainty in shear stress estimates and erosion rate measurements for both total shear- and grain shear-based erosion functions.

EROSION-RESISTANCE PARAMETERS DERIVED FROM TOTAL SHEAR STRESS ESTIMATES

On average, the critical shear stresses when uncertainty in shear stress and erosion rate is taken into account are similar to those without accounting for uncertainty (Figure 70). Three trendlines of BET tests that originally had positive intercepts with the erosion rate axis (critical shear stress set at 0.06 Pa), had negative intercepts with the erosion rate axis (i.e. positive critical shear stress) when accounting for uncertainty in estimated shear stress and erosion rate. The erodibility coefficient generally increased when accounting for uncertainty (Figure 71). The increase in erodibility coefficient resulted in a shift towards larger erodibility coefficients when plotting erodibility coefficient versus critical shear stress (Figure 72).

EROSION-RESISTANCE PARAMETERS DERIVED FROM GRAIN SHEAR STRESS ESTIMATES

The effects of uncertainty on erosion-resistance parameters based on grain shear estimates were similar to those based on total shear stress estimates. On average, the critical shear stresses when uncertainty in shear stress and erosion rate is taken into account are similar to those without accounting for uncertainty (Figure 73). Four trendlines of EFA tests that originally had positive intercepts with the erosion rate axis (critical shear stress set at 0.06 Pa), had negative intercepts with the erosion rate axis when accounting for uncertainty in estimated shear stress and erosion rate. The erodibility coefficient generally increased when accounting for uncertainty (Figure 74). Plotting erodibility coefficient versus critical shear stress shows a small reduction in scatter as smaller critical shear stresses do not show a trend in how measurement/approximation uncertainty affects the relationship between erodibility coefficient and critical shear stress (Figure 75).

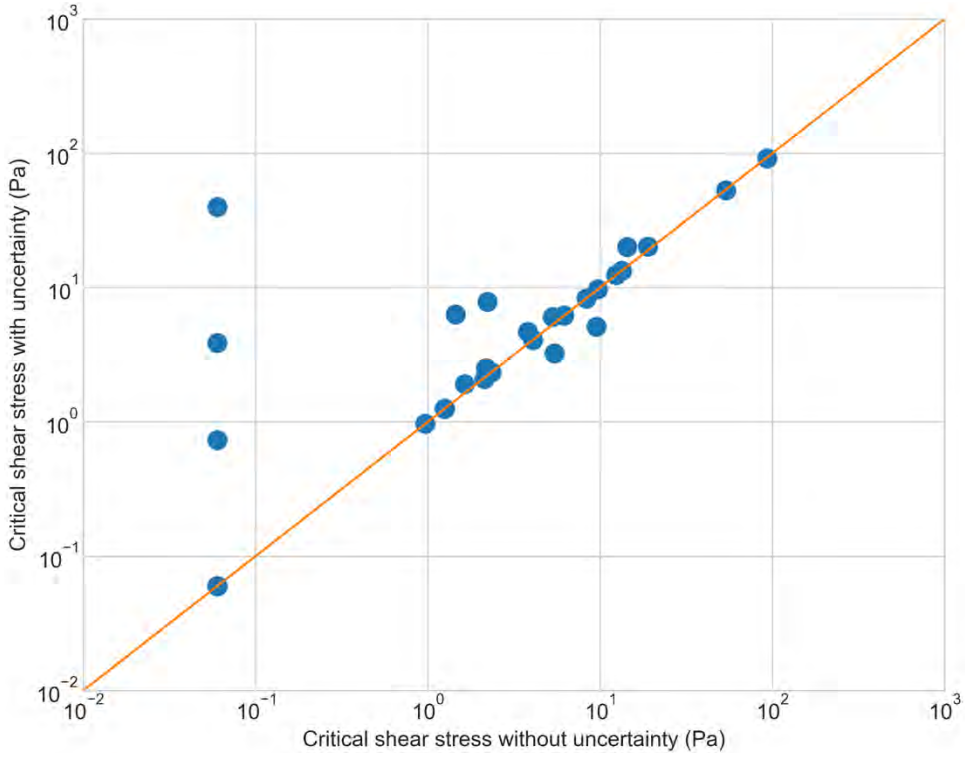

FIGURE 70 – COMPARISON OF CRITICAL SHEAR STRESS DERIVED WITHOUT AND WITH ACCOUNTING FOR UNCERTAINTY IN SHEAR STRESS AND EROSION RATE AS MEASURED BY THE BET METHOD. THE CRITICAL SHEAR STRESS IS BASED ON TOTAL SHEAR STRESS ESTIMATES.

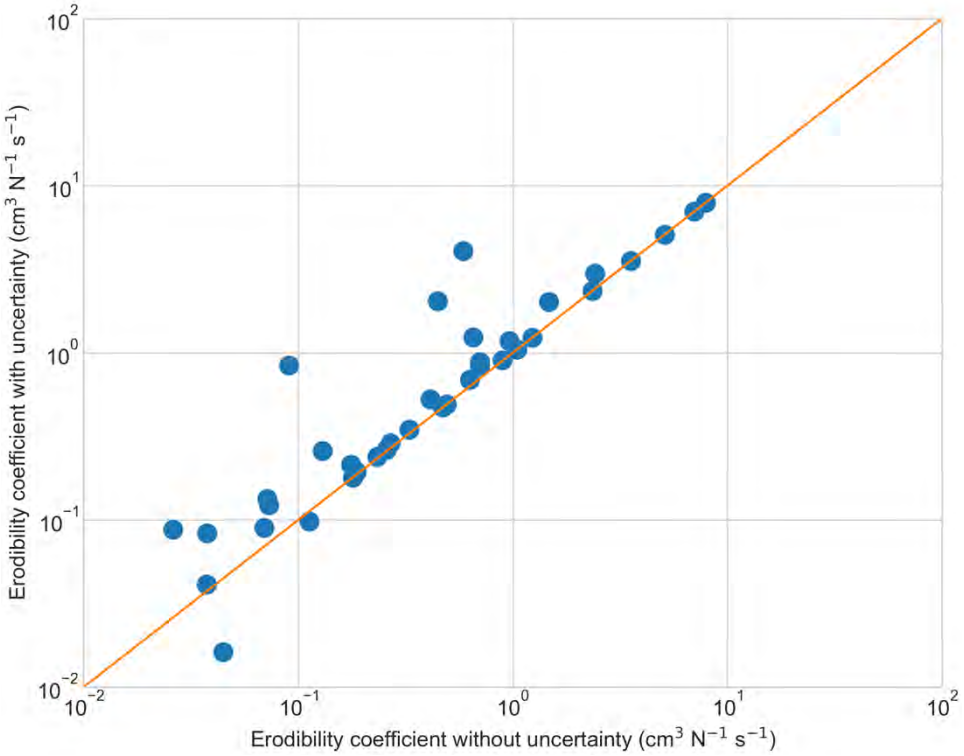

FIGURE 71 – COMPARISON OF ERODIBILITY COEFFICIENT DERIVED WITHOUT AND WITH ACCOUNTING FOR UNCERTAINTY IN SHEAR STRESS AND EROSION RATE AS MEASURED BY THE BET METHOD. THE ERODIBILITY COEFFICIENT IS BASED ON TOTAL SHEAR STRESS ESTIMATES.

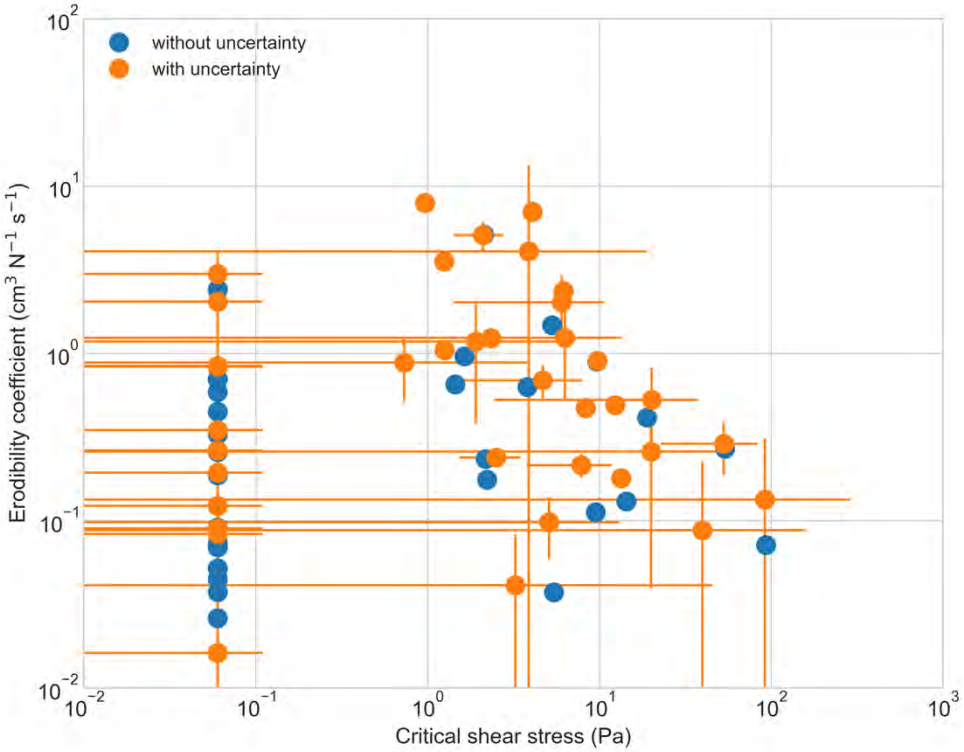

FIGURE 72 – COMPARISON OF ERODIBILITY COEFFICIENT VERSUS CRITICAL SHEAR STRESS DERIVED WITHOUT AND WITH ACCOUNTING FOR UNCERTAINTY IN SHEAR STRESS AND EROSION RATE AS MEASURED BY THE BET METHOD. THE LENGTH OF THE HORIZONTAL AND VERTICAL LINES INDICATE THE STANDARD DEVIATION OF THE UNCERTAINTY IN CRITICAL SHEAR STRESS AND ERODIBILITY COEFFICIENT, RESPECTIVELY. EROSION-RESISTANCE PARAMETERS ARE BASED ON TOTAL SHEAR STRESS ESTIMATES.

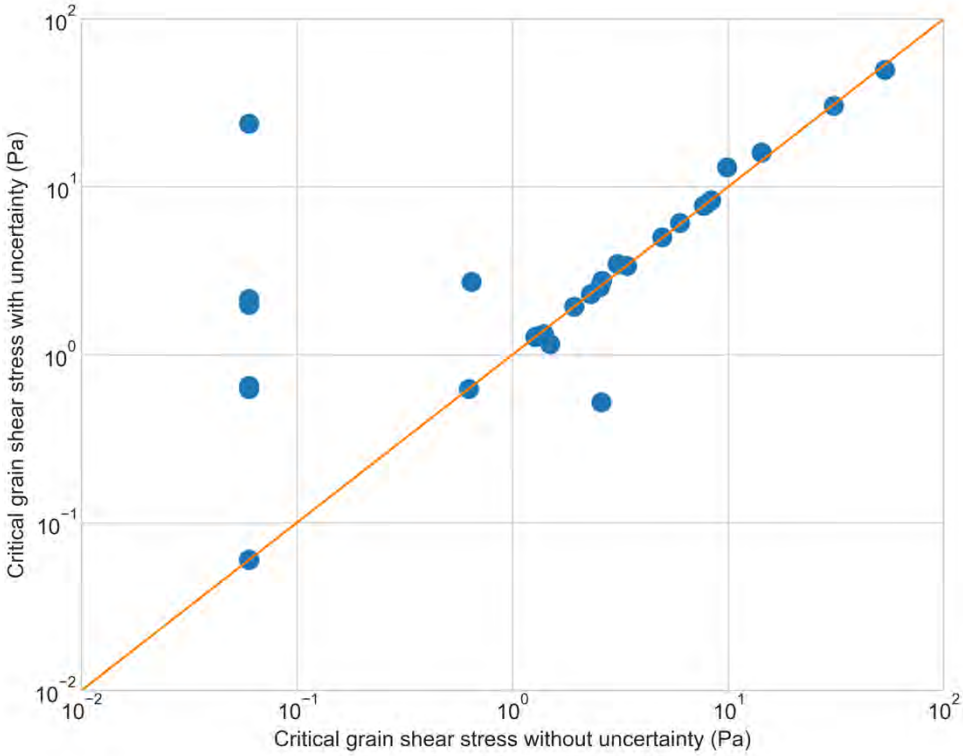

FIGURE 73 – COMPARISON OF CRITICAL SHEAR STRESS DERIVED WITHOUT AND WITH ACCOUNTING FOR UNCERTAINTY IN SHEAR STRESS AND EROSION RATE AS MEASURED BY THE BET METHOD. THE CRITICAL SHEAR STRESS IS BASED ON GRAIN SHEAR STRESS ESTIMATES.

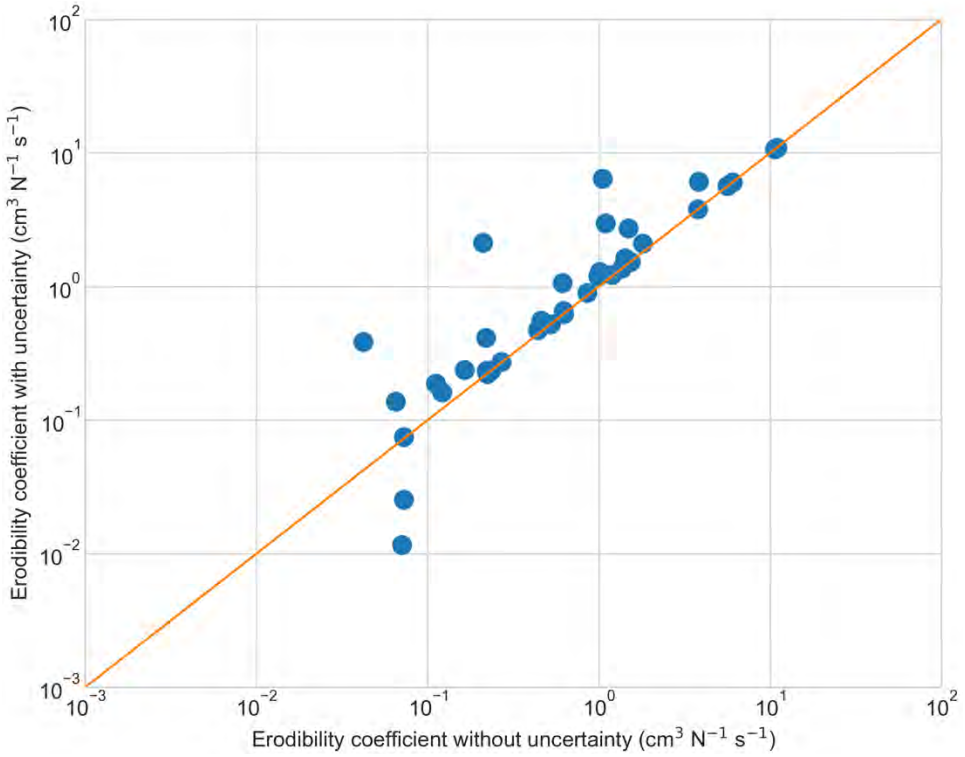

FIGURE 74 – COMPARISON OF ERODIBILITY COEFFICIENT DERIVED WITHOUT AND WITH ACCOUNTING FOR UNCERTAINTY IN SHEAR STRESS AND EROSION RATE AS MEASURED BY THE BET METHOD. THE ERODIBILITY COEFFICIENT IS BASED ON GRAIN SHEAR STRESS ESTIMATES.

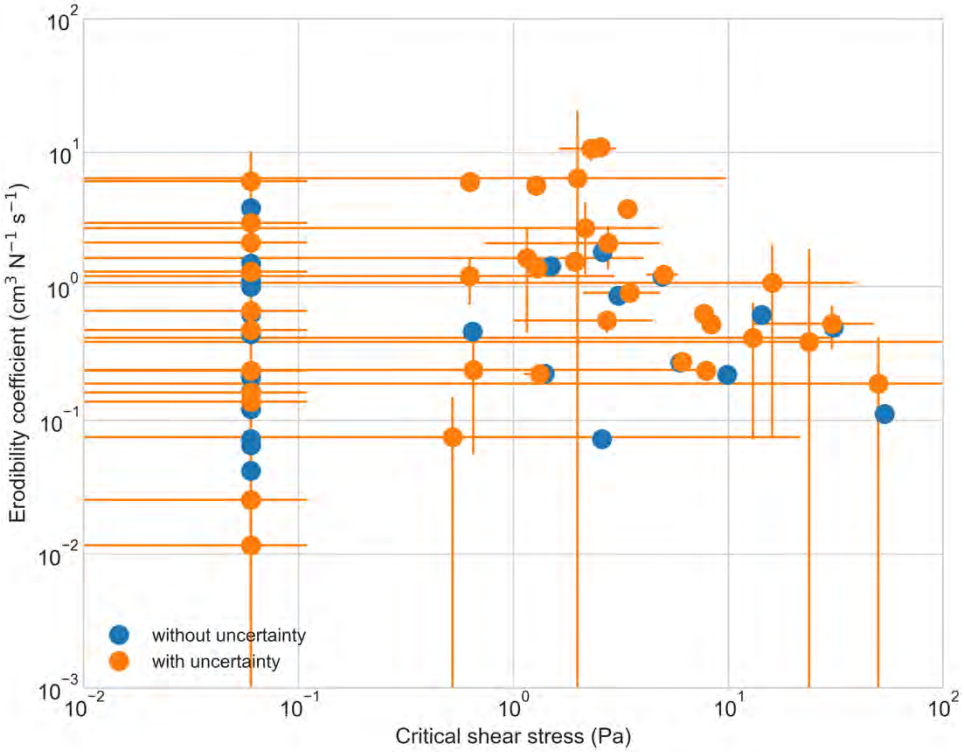

FIGURE 75 – COMPARISON OF ERODIBILITY COEFFICIENT VERSUS CRITICAL SHEAR STRESS DERIVED WITHOUT AND WITH ACCOUNTING FOR UNCERTAINTY IN SHEAR STRESS AND EROSION RATE AS MEASURED BY THE BET METHOD. THE LENGTH OF THE HORIZONTAL AND VERTICAL LINES INDICATE THE STANDARD DEVIATION OF THE UNCERTAINTY IN CRITICAL SHEAR STRESS AND ERODIBILITY COEFFICIENT, RESPECTIVELY. EROSION-RESISTANCE PARAMETERS ARE BASED ON GRAIN SHEAR STRESS ESTIMATES.

Comparison between BET, EFA, and JET methods

Figure 76 compares the erosion-resistance parameters derived from BET, EFA, and JET measurement techniques. The presented parameters were derived from erosion functions that include uncertainty in shear stress and erosion rate, represent the mass erosion regime, and are based on grain shear stress (Analysis Step 4). Results from tests that would produce negative critical shear stresses have been omitted. The BET-derived critical shear stresses have a similar range as those derived from EFA and JET methods but have much smaller erodibility coefficients. This appears to be related to the significant uncertainty in both estimated shear stress and erosion rate. The standard deviation of the uncertainties in shear stress and erosion rate have similar magnitudes as the shear stress and erosion rate themselves, which indicates that current approximation and measurement techniques used to quantify BET shear stress and erosion rate are insufficient.

Figure 77 presents the same data as Figure 76, but only for EFA and JET methods. Only silty sands (SM) and silts (ML) were tested multiple times using EFA and JET measurement techniques. Figure 77 shows that the erosion-resistance parameters derived by the EFA and JET methods plot within the cluster of points representing the erosion-resistance region of each soil tested. It can be concluded therefore that both EFA and JET method provide similar erosion resistance parameters for a given soil. This is confirmed by Figure 78 and Figure 79, which show that critical shear stress and erodibility coefficient for EFA and JET methods are reasonably similar when the analysis used by each method: 1) considers the same erosion regime of cohesive soils (here the mass-erosion regime); 2) uses erosion functions that are based on grain shear stress; and 3) includes the effects of measurement uncertainty in erosion rate and estimation uncertainty in applied shear stress.

Table 8 lists the results of two-sample Kolmogorov-Smirnov (KS) tests conducted to compare the critical shear stress and erodibility coefficient distributions for silts (ML) and silty sands (SM) derived using the EFA and JET methods. When the KS statistic α is small or the p-value of the test is large the tested distributions are the same (i.e. we cannot reject the null hypothesis that the two distributions are the same). Generally, the α values are fairly large but improved (i.e. became smaller) for Step 4 compared to Step 1. Also, the p values improved (i.e. increased) for Step 4 relative to Step 1. Therefore, the

distributions of erosion-resistance parameters compare better for Step 4 than they do for Step 1, which is shown in Figure 78 and Figure 79. The KS tests indicate that the EFA- and JET-derived critical shear stress distributions for silty sand soils are different for Step 1 (small p values) but compare reasonably well for Step 4 ($p > 0.11$). The erodibility coefficients determined by EFA and JET methods are different for Step 1, but compare reasonably well for silts and quite well for silty sand soils.

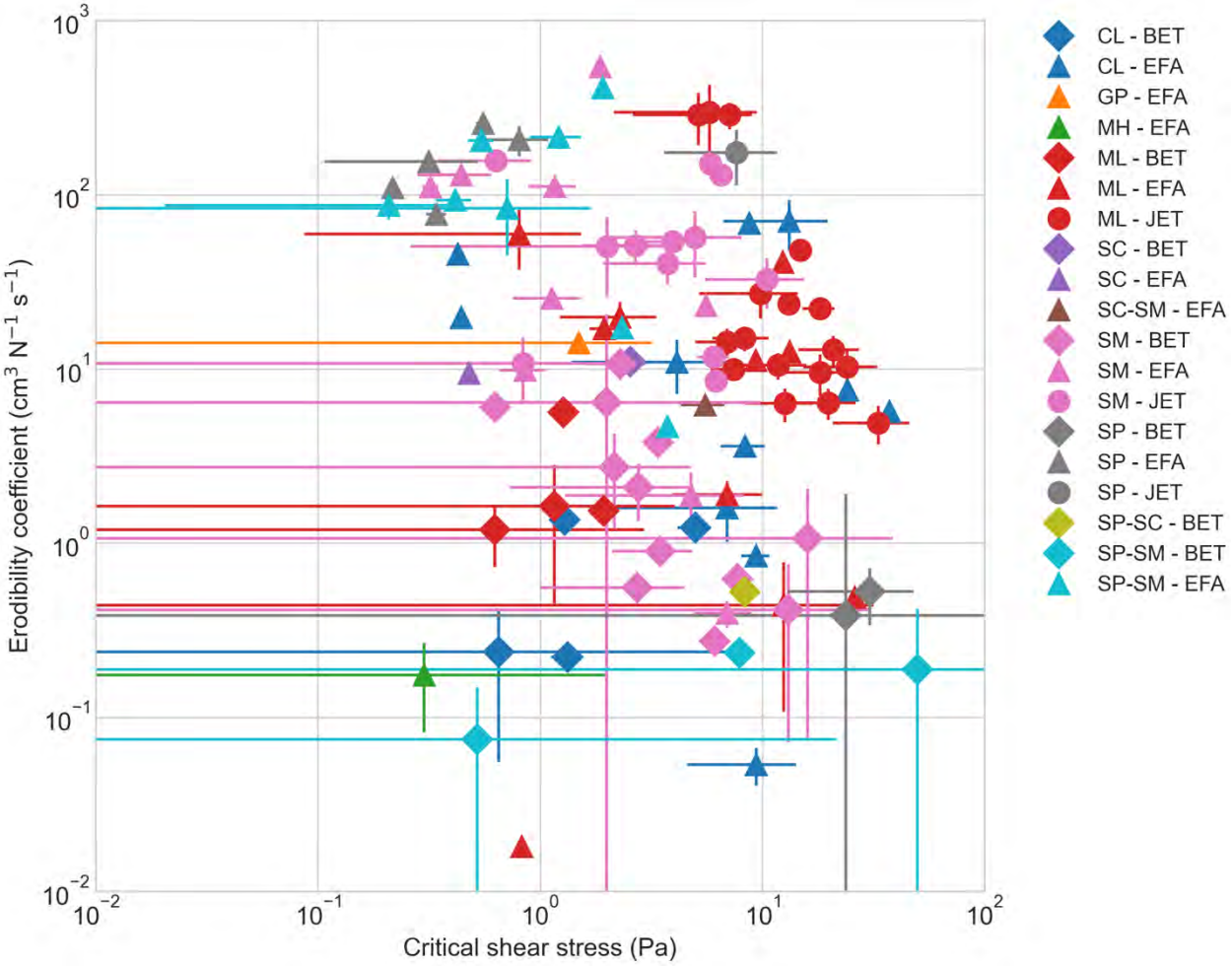

FIGURE 76 – ERODIBILITY COEFFICIENT PLOTTED AGAINST CRITICAL SHEAR STRESS FOR ALL MEASUREMENT TECHNIQUES (BET, EFA, AND JET). EROSION-RESISTANCE PARAMETERS WERE DERIVED FROM AUGMENTED EROSION FUNCTIONS THAT INCLUDE UNCERTAINTY IN SHEAR STRESS AND EROSION RATE, REPRESENT THE MASS EROSION REGIME, AND ARE BASED ON GRAIN SHEAR STRESS. THE LENGTH OF THE HORIZONTAL AND VERTICAL LINES INDICATE THE STANDARD DEVIATION OF THE UNCERTAINTY IN CRITICAL SHEAR STRESS AND ERODIBILITY COEFFICIENT, RESPECTIVELY.

TABLE 8 – OUTPUT PARAMETERS α AND p FROM KOLMOGOROV-SMIRNOV (KS) TESTS INDICATING IF DISTRIBUTIONS OF CRITICAL SHEAR STRESSES AND ERODIBILITY COEFFICIENTS DERIVED BY EFA AND JET METHODS FOR SILT AND SILTY SAND SOIL TYPES ARE THE SAME. THE PARAMETER α IS THE KS STATISTIC AND p IS THE TWO-TAILED p VALUE. IN THE 'STANDARD' METHOD EROSION-RESISTANCE PARAMETERS ARE DERIVED FROM THE ENTIRE EROSION FUNCTION PROVIDED BY THE MEASUREMENT METHOD. IN THE 'FINAL' METHOD EROSION-RESISTANCE PARAMETERS WERE DERIVED FROM EROSION FUNCTIONS REPRESENTING THE MASS EROSION REGIME, BASED ON GRAIN SHEAR STRESS, AND INCLUDE UNCERTAINTY.

	Silt				Silty sand			
	Standard		Final		Standard		Final	
Parameter	α	p	α	p	α	p	α	p
Critical shear stress	0.500	0.088	0.400	0.201	0.833	$4.4\ 10^{-4}$	0.500	0.114
Erodibility coefficient	0.556	0.041	0.400	0.201	0.500	0.114	0.306	0.638

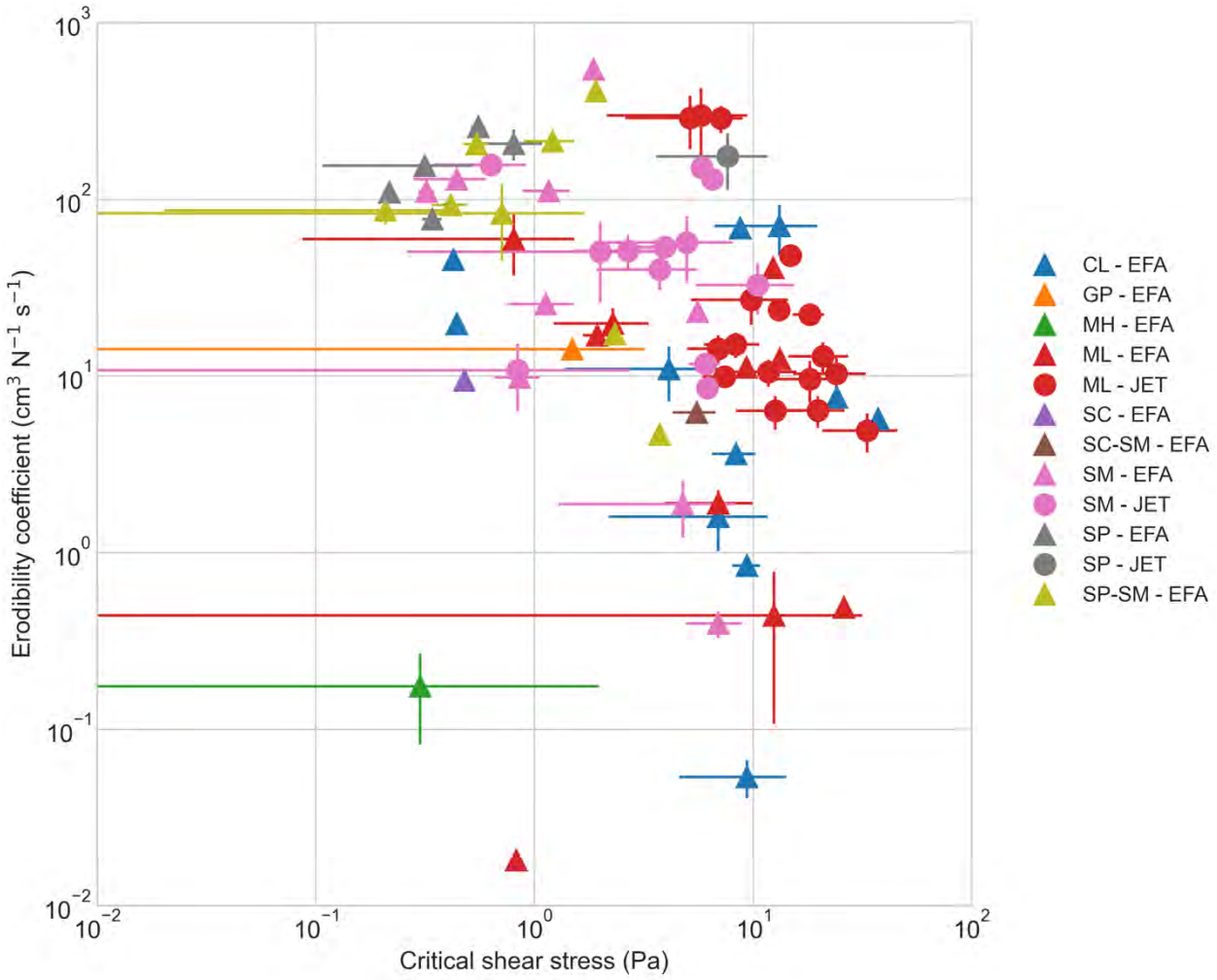

FIGURE 77 – ERODIBILITY COEFFICIENT PLOTTED AGAINST CRITICAL SHEAR STRESS FOR JET AND EFA MEASUREMENT TECHNIQUES. EROSION-RESISTANCE PARAMETERS WERE DERIVED FROM EROSION FUNCTIONS REPRESENTING THE MASS EROSION REGIME AND BASED ON GRAIN SHEAR STRESS. THE LENGTH OF THE HORIZONTAL AND VERTICAL LINES INDICATE THE STANDARD DEVIATION OF THE UNCERTAINTY IN CRITICAL SHEAR STRESS AND ERODIBILITY COEFFICIENT, RESPECTIVELY.

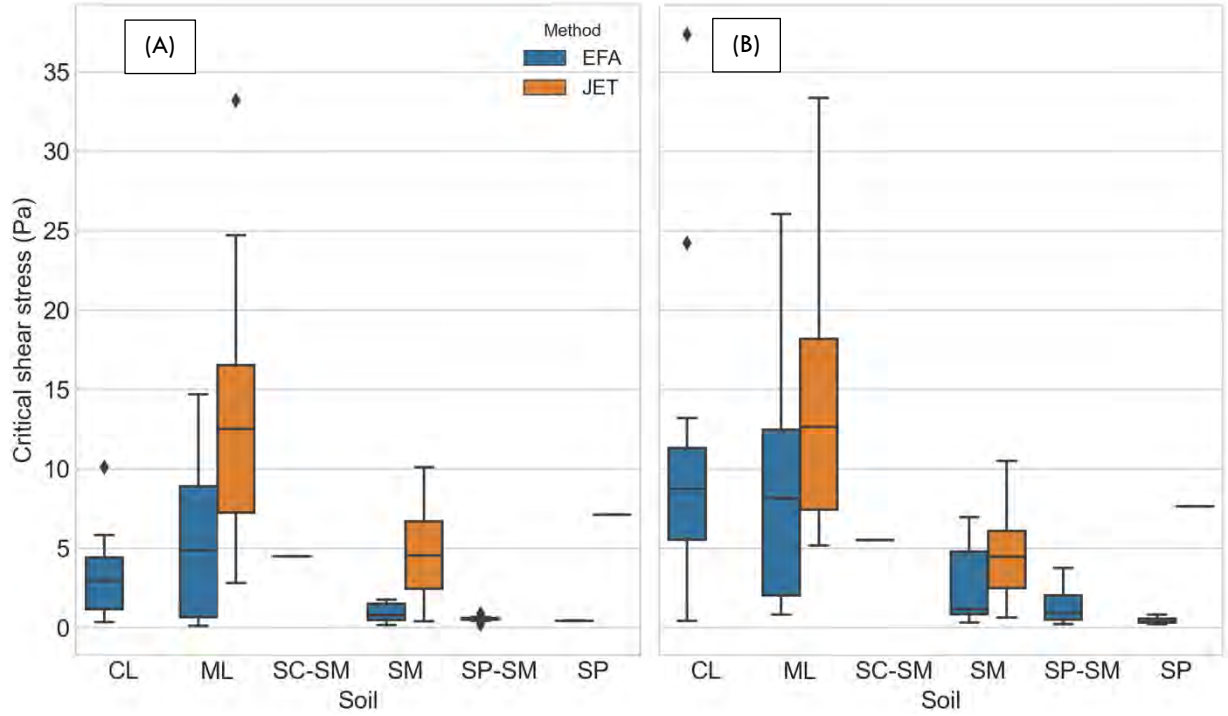

FIGURE 78 – COMPARISON OF (A) CRITICAL SHEAR STRESS DERIVED USING STANDARD EFA AND JET POST-PROCESSING TECHNIQUES AND (B) CRITICAL SHEAR STRESS ASSOCIATED WITH EROSION FUNCTIONS BASED ON GRAIN SHEAR STRESS, MASS SURFACE EROSION REGIME, AND INCLUDE UNCERTAINTY IN ESTIMATED SHEAR STRESS AND MEASURED EROSION RATE. THE STANDARD PROCESSING TECHNIQUES DO NOT INCLUDE THE EFFECTS OF MEASUREMENT UNCERTAINTY AND EFA EROSION-RESISTANCE DATA IS BASED ON TOTAL SHEAR STRESS.

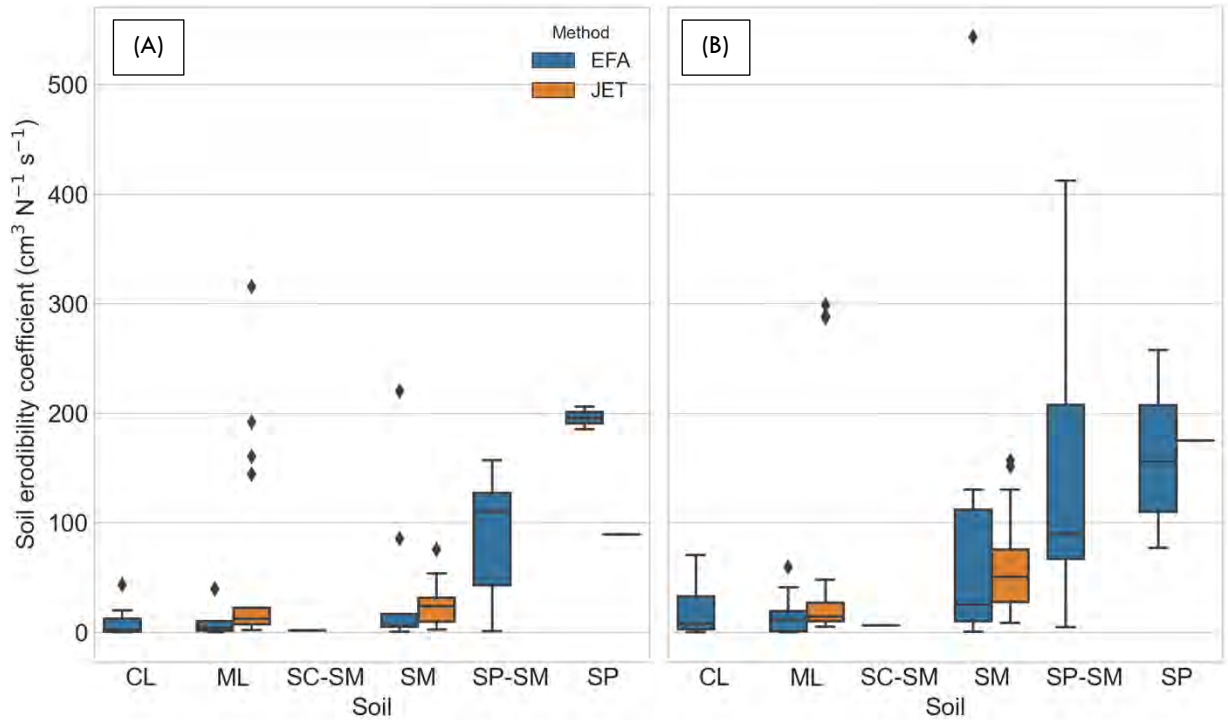

FIGURE 79 – COMPARISON OF (A) ERODIBILITY COEFFICIENT DERIVED USING STANDARD EFA AND JET POST-PROCESSING TECHNIQUES AND (B) ERODIBILITY COEFFICIENT ASSOCIATED WITH EROSION FUNCTIONS BASED ON GRAIN SHEAR STRESS, MASS SURFACE EROSION REGIME, AND INCLUDE UNCERTAINTY IN ESTIMATED SHEAR STRESS AND MEASURED EROSION RATE. THE STANDARD PROCESSING TECHNIQUES DO NOT INCLUDE THE EFFECTS OF MEASUREMENT UNCERTAINTY AND EFA EROSION-RESISTANCE DATA IS BASED ON TOTAL SHEAR STRESS.

Comparison between measured data and calibrated data for the BSTEM model

The third objective of the presented study is to provide recommendations on the use and application of the derived erosion-resistance parameters pertinent to the evaluation of bank erosion on the Lower American River using the BSTEM model. A number of simulations have already been conducted by the USACE-Sacramento District to calibrate erosion-resistance parameters at eight bank erosion sites on the Lower American River (J.S. AuBuchon, pers. comm.). The calibrated erosion-resistance parameters are for the following soil types: CL, ML, SM, and SP.

Figure 80 compares the calibrated erosion-resistance parameters to those measured using EFA and JET methods (cf. Figure 77). The calibrated erosion-resistance parameters for silts compare well with those measured. For silty sands the calibrated erosion-resistance parameters plot towards the larger measured critical shear stresses and smaller measured erodibility coefficients, whereas the calibrated erosion-resistance parameters deviate significantly from those measured for sands and clays. This is also shown by Figure 81 and Figure 82. Similar to the measured critical shear stress values, Figure 81 shows that calibrated critical shear stresses reduce for less cohesive and cohesionless soils. Though, the rate of decrease is much smaller than that observed for the EFA and JET data. Excluding the value for clay soils, the calibrated soil erodibility coefficients reduce for less cohesive and cohesionless soils, which is opposite to the trend in measured soil erodibility coefficients.

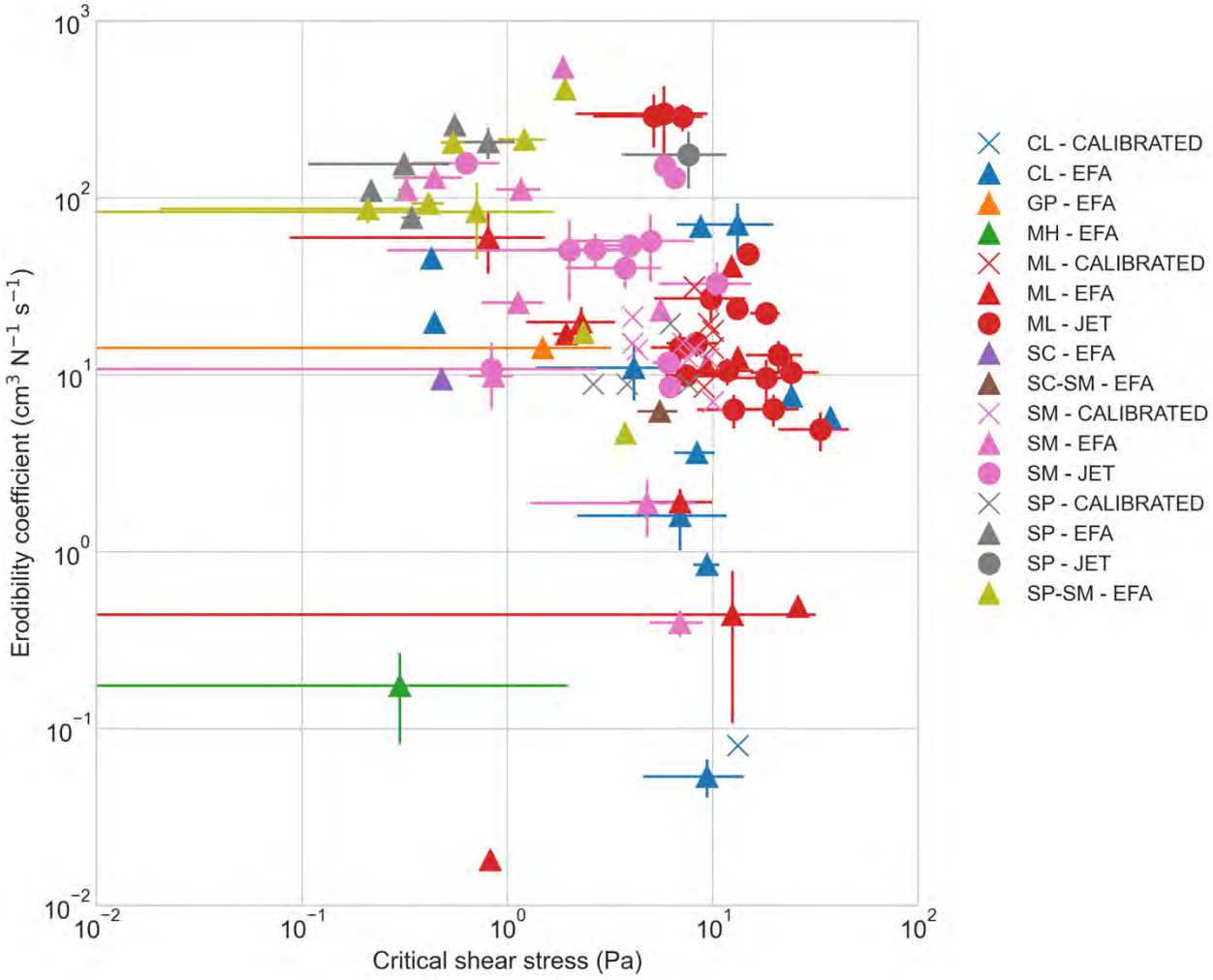

FIGURE 80 – COMPARISION OF EROSION-RESISTANCE PARAMETERS DERIVED BY THE EFA AND JET MEASUREMENT TECHNIQUES AND CALIBRATED VALUES OF BSTEM MODELS FOR THE LOWER AMERICAN RIVER. MEASURED EROSION-RESISTANCE PARAMETERS WERE DERIVED FROM EROSION FUNCTIONS REPRESENTING THE MASS EROSION REGIME AND BASED ON GRAIN SHEAR STRESS. THE LENGTH OF THE HORIZONTAL AND VERTICAL LINES INDICATE THE STANDARD DEVIATION OF THE UNCERTAINTY IN CRITICAL SHEAR STRESS AND ERODIBILITY COEFFICIENT, RESPECTIVELY.

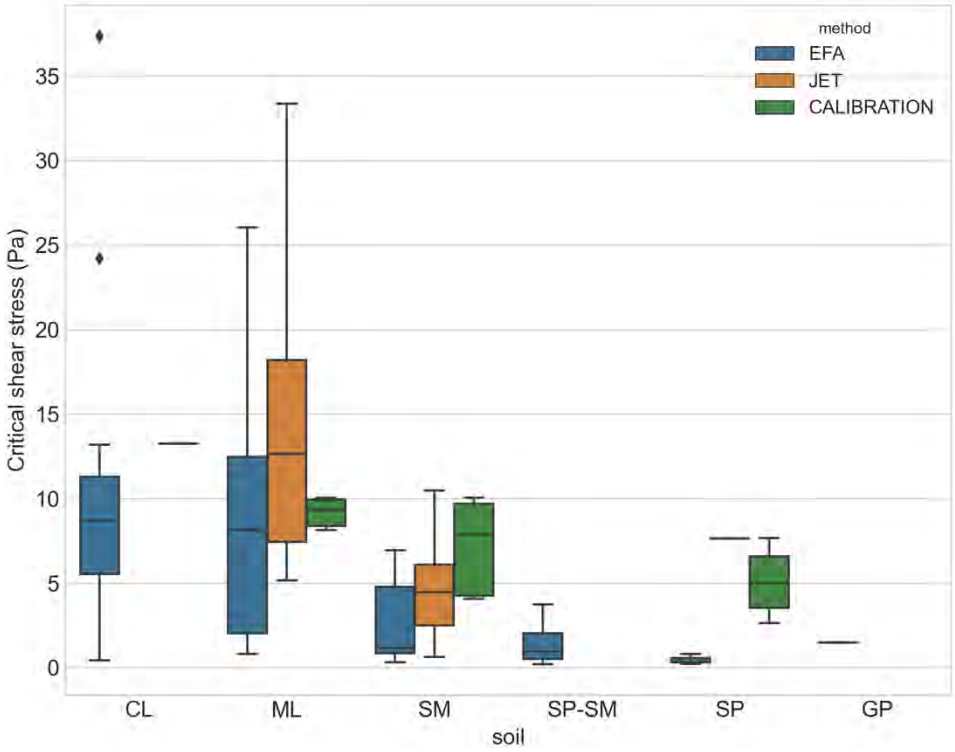

FIGURE 81 – COMPARISON OF CRITICAL SHEAR STRESSES DERIVED USING EFA AND JET METHODS AND THOSE CALIBRATED USING BSTEM MODELS. MEASURED CRITICAL SHEAR STRESSES ARE ASSOCIATED WITH EROSION FUNCTIONS BASED ON GRAIN SHEAR STRESS, MASS SURFACE EROSION REGIME, AND INCLUDE UNCERTAINTY IN ESTIMATED SHEAR STRESS AND MEASURED EROSION RATE.

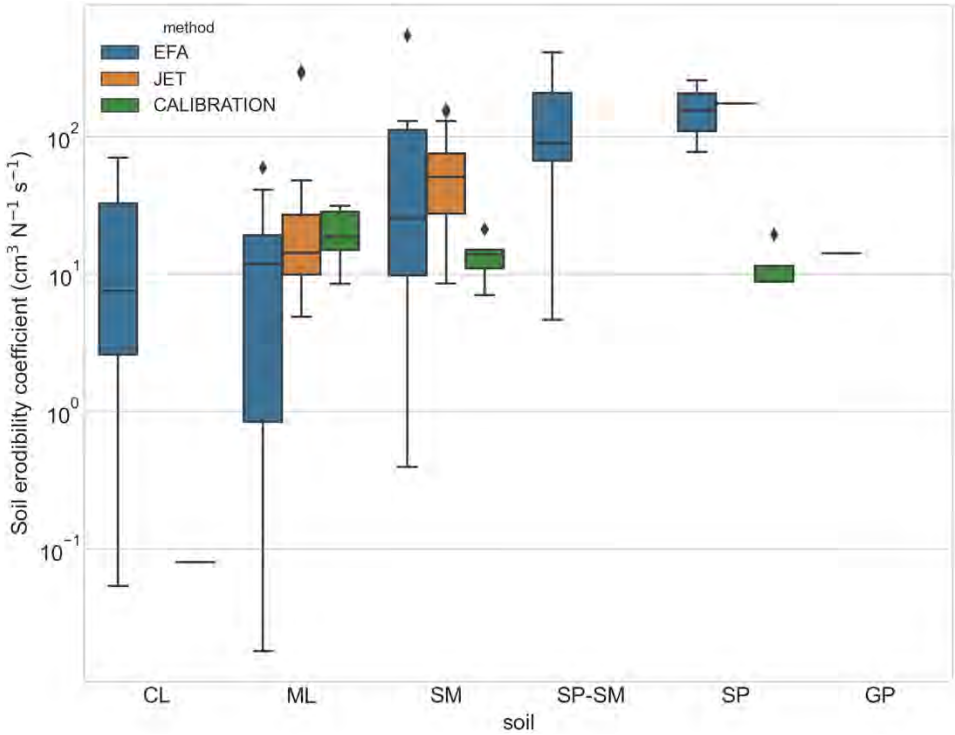

FIGURE 82 – COMPARISON OF ERODIBILITY COEFFICIENTS DERIVED USING EFA AND JET METHODS AND THOSE CALIBRATED USING BSTEM MODELS. MEASURED ERODIBILITY COEFFICIENTS ARE ASSOCIATED WITH EROSION FUNCTIONS BASED ON GRAIN SHEAR STRESS, MASS SURFACE EROSION REGIME, AND INCLUDE UNCERTAINTY IN ESTIMATED SHEAR STRESS AND MEASURED EROSION RATE.

It should be noted that the estimated applied shear stresses in BSTEM are based on the divided channel method typically used in one-dimensional computer models of open-channel flow (e.g. Knight et al., 1984), and therefore can have significant error near streambanks where boundary shear stress can be impacted by complex three-dimensional flow induced by large changes in channel geometry and spatially varying roughness. If we define the ratio of modeled applied shear stress (τ_{BSTEM}) to actual applied shear stress (τ) as:

$$\frac{\tau_{\mathrm{BSTEM}}}{\tau} = \chi \tag{8}$$

Then, substituting Eq. (8) into Eq. (1), we have:

$$E = \begin{cases} k_d\left(\tau_{\mathrm{BSTEM}}/\chi - \tau_c\right) & \tau_{\mathrm{BSTEM}}/\chi > \tau_c \\ 0 & \tau_{\mathrm{BSTEM}}/\chi \leq \tau_c \end{cases} \tag{9}$$

Introducing $\tau_{c,\mathrm{BSTEM}} = \chi\tau_c$ and $k_{d,\mathrm{BSTEM}} = k_d/\chi$ into Eq. (9), we get:

$$E = \begin{cases} k_{d,\mathrm{BSTEM}}\left(\tau_{\mathrm{BSTEM}} - \tau_{c,\mathrm{BSTEM}}\right) & \tau_{\mathrm{BSTEM}} > \tau_{c,\mathrm{BSTEM}} \\ 0 & \tau_{\mathrm{BSTEM}} \leq \tau_{c,\mathrm{BSTEM}} \end{cases} \tag{10}$$

Eq. (10) is equivalent to Eq. (1). Therefore, the coefficient χ can be used to correct for errors in BSTEM's approximation of applied bank shear stress. Note, if we assume erosion rate is related nonlinearly to excess shear through an exponent m on the excess shear stress term, which is common for sediment transport relationships ($1.5 \leq m \leq 2.5$), we have $k_{d,\mathrm{BSTEM}} = k_d/\chi^m$. Figure 81 and Figure 82 show that $m \approx 1$ and $\chi \approx 1$ for ML, $m \approx 1.5$ and $\chi \approx 2$ for SM, and $m \approx 1.5$ and $\chi \approx 5$ for SP soil types. This generally indicates that the bank shear stress is satisfactorily estimated by BSTEM but appears to deviate more, i.e. it is too high, the less cohesive the soil is. Furthermore, the calibrated parameters seem to imply that the relationship between erosion rate and excess shear stress becomes increasingly more exponential the less cohesive the soil is. If the error in estimated shear stress at the bank toe by BSTEM is independent from the sediment classification, χ values are expected to be similar between sediments. This is not the case, the increase in χ from ML to SP soil types implies a greater required reduction in entrainment rates for cohesionless materials than cohesive materials, which is likely due to supply issues.

Coarser, less cohesive or cohesionless materials such as silty sands (SM) and sands (SP) are typically found at lower elevations along a streambank, that is near the streambed; therefore, their entrainment can be transport limited because of both larger particle size and the upstream supply of coarser materials in contrast to fines such as silts. BSTEM does not account for transport limitation and could therefore overestimate the entrainment of sandy bank materials. To prevent this, one would have to increase critical shear stress and/or reduce the erodibility coefficient of cohesionless bank material ($\chi > 1$), which is shown by Figure 81 and Figure 82.

CONCLUSIONS AND RECOMMENDATIONS

Comparisons of soil erosion-resistance parameters derived from the BET, EFA, and JET measurement technologies were made by accounting for differences in hydraulic principles and erosion mechanics of these technologies. First, direct comparisons of raw data, termed erosion function (erosion rate versus shear stress), collected by each REMT were plotted by USCS soil classification and location. Secondly, comparisons were made based on a consistent regressive method to determine erosion-resistance parameters, critical shear stress and erodibility coefficient, from the erosion function for each REMT. Attempts were made to reduce the raw data prior to regression for the EFA and BET. The BET data were reduced to soil layer-averaged erosion rates and shear stress values for each flow sequence at each site where negative erosion rates were removed from consideration. EFA data were regressed with all of the data provided and a reduced dataset where a subjective filter was applied to isolate the mass-erosion regime. This erosion regime is characterized by a rapid increase in erosion rate as aggregates and clods are detached from the eroding soil surface. Thirdly, BET and EFA raw data were based on grain shear stress consistent with the JET analysis procedure. Because grain shear stresses act directly on soil particles, they are generally used to calculate entrainment and transport of sediment grains and soil particles. Finally, BET, EFA, and JET methods can have significant uncertainty in measured erosion rate and estimated applied shear stresses, which could affect the erosion-resistance parameters derived by regression. Therefore, the erosion-resistance parameters were also determined by accounting for measurement uncertainty. Comparisons were made at each of the four levels and analyses were conducted to determine agreement between methods.

BET and EFA methods were used on both cohesive and cohesionless soils, whereas the JET method was limited to silts (ML) and silty sands (SM) though one test was performed on a poorly graded sand. While no single step of the analysis procedure provided perfect agreement between erosion-resistance parameters provided by the REMTs, the distributions of the erosion-resistance parameters by soil showed progressive improved agreement when applied shear forces were scaled similarly and the assessed erosion regime was the same. Grouping the raw data by soil, there was, in general, lack of agreement for the cohesionless soils and agreement for the cohesive soils. Comparison of erosion-resistance parameters showed that the JET was consistently 2-4 Pa larger than the EFA for the two soils that could be compared (ML and SM). BET results indicated that critical shear stress estimates were reasonable when regressions resulted in positive erodibility parameters, but the erodibility coefficient was consistently much lower than that derived using the EFA and JET, which illustrated general agreement. Since the erodibility coefficient is the slope of the erosion function (erosion rate versus applied shear stress plot), and erosion rates are measured directly, it can be deduced that relative changes in estimated shear stress for a given change in erosion rate are similar for EFA and JET methods. Uncertainty analyses also illustrated large errors for higher applied shear stresses than for lower values which implies that a critical shear stress value is likely to be more consistent than the erodibility coefficient for a linear regressive technique. JET and USACE JET results, while different in application, provided similar consistent results by soil type. EFA and USACE EFA results were significantly different, which may be attributed to differences in measurement procedures or geological differences. The USACE EFA tests were conducted on Pleistocene era sediments, which are older, and likely more consolidated than the Holocene era sediments tested by Briaud et al. (2020). USACE EFA results, in general, plotted in a higher erosion regime, that is more erosion-resistant material, than EFA results for the same soil type.

Definitive guidance to the practical application of the analyses conducted is inherently difficult due to the limitations associated with each REMT. While it is not the purpose of this document to shed light on the limitations of each REMT it should be noted that there is no right way to determine erodibility parameters. However, it is encouraging that the EFA and JET results, while considerably different in terms of hydraulic application, are generally in agreement and consistent between soil types, and either method could be used to determine the erosion-resistance parameters of bank soils as long as these parameters represent the mass-erosion regime and are based on grain shear stress (Step 3 of the Analysis Procedure). It is recommended not to use BET-derived erosion parameters for quantitative bank erosion assessment. However, the BET is useful to identify more erodible soil layers that could then be evaluated using EFA and JET methods.

For bank erosion assessment using models such as BSTEM, the parameters for cohesive soils appear not to need much calibration. However, for cohesionless soils, erosion-resistance parameters should be calibrated carefully as the rate of erosion is sensitive to the model's bank shear stress approximation and transport-capacity limitation effects on entrainment.

REFERENCES

Ariathurai, R., and K. Arulanandan. 1978. "Erosion rates of cohesive soils." *Journal of the Hydraulics Division* 104 (HY2): 279-283.

ASTM Standard D1587. 1999. *Standard practice for thin-walled geotechnical sampling of soils*. West Conshohocken, PA: ASTM International.

ASTM Standard D2487. 2000. *Standard Practice for Classification of Soils for Engineering Purposes (Unified Soil Classification System)*. West Conshohocken, PA: ASTM International.

ASTM Standard D2488. 2009. *Standard Practice for Description and Identification of Soils (Visual-Manual Procedures)*. West Conshohocken, PA: ASTM International.

ASTM Standard D4318. 2005. *Standard Test Methods for Liquid Limit, Plastic Limit, and Plasticity Index of Soils*. West Conshohocken, PA: ASTM International.

Bankhead, N., A. Simon, R. Thomas, L. Klimetz, and D. Klimetz. 2010. *Sediment loadings from streambanks and levees along the Sacramento River and selected tributaries*. Oxford, MS: U.S. Department of Agriculture, Agricultural Research Service, National Sedimentation Laboratory.

Boggs, P.T., R.H. Byrd, and R.B. Schnabel. 1987. "A stable and efficient algorithm for nonlinear orthogonal distance regression." *SIAM J. Sci. and Stat. Comput.* 8 (6): 1052-1078.

Briaud, J.-L. 2008. "Case histories in soil and rock erosion: Woodrow Wilson Bridge, Brazos River Meander, Normandy Cliffs, and New Orleans Levees." *Journal of Geotechnical and Geoenvironmental Engineering* (ASCE) 134 (10).

Briaud, J.-L., A. Shidlovskaya, and A. Timchenko. 2020. *Assessing erosion resistance of bank materials on American and Sacramento Rivers*. College Station, TX: Texas A&M University.

Briaud, J.-L., F. Ting, H.C. Chen, S.R. Gudavalli, S. Perugu, and G. Wei. 1999. "SRICOS: Prediction of scour rate in cohesive soils at bridge piers." *J. Geotech Eng., ASCE* 125: 237-246.

Briaud, J.-L., F.C.K. Ting, H.C. Chen, Y. Cao, S.W. Han, and K.W. Kwak. 2001. "Erosion function apparatus for scour rate predictions." *Journal of Geotechnical and Geoenvironmental Engineering* 127 (2): 105-113.

Briaud, J.-L., M. Chedid, H.C. Chen, and A. Shidlovskaya. 2017. "The Borhole Erosion Test." *Journal of Geotechnical and Geoenvironmental Engineering,* (ASCE) 143 (8).

Brunner, G.W. 2016. *HEC-RAS River Analysis System User's Manual Version 5.0*. Davis: US Army Corps of Engineers.

Chow, V.T. 1959. *Open Channel Hydraulics*. New York: McGraw-Hill.

Einstein, H.A, and R.B. Banks. 1950. "Fluid resistance of composite roughness." *Transactions, American Geophysical Union* 31 (4): 603-610.

Einstein, H.A. 1950. *The bed-load function for sediment transportation in open channel flows*. Technical Bulletin, Washington, D.C.: United States Department of Agriculture, Soil Conservation Service.

Haaland, S.E. 1983. "Simple and explicit formulas for the friction factor in turbulent flow." *Journal of Fluids Engineering* 105 (1): 89-90.

Hanson, G.J., and A. Simon. 2001. "Erodibility of cohesive streambeds in the loess area of the midwestern USA." *Hydrological Processes* 15 (1): 23-38. Doi:10.1002/hyp.149.

Hanson, G.J., K.M. Robinson, and D.M. Temple. 1990. "Pressure and stress distributions due to a submerged impinging jet." *Proceedings of the 1990 National Conference on Hydraulic Engineering*. Washington: ASCE. 525-530.

Hanson, G.J., and K.R. Cook. 2004. "Apparatus, test procedures, and analytical methods to measure soil erodibility in situ." *Applied Engineering in Agriculture* 20 (4): 455-462.

Hanson, G.J. 1990. "Surface erodibility of earthen channels at high stress. Part II – Developing an in situ testing device." *Transactions of ASAE* 33 (1): 132-137.

Knight D.W., J.D. Demetriou, and M.E. Hamed. 1984. "Stage discharge relationships for compound channels." *In Channels and channel control structures*, edited by K.V.H. Smith, 445–459. Berlin, Germany: Springer.

Lai, Y.G., R.E. Thomas, Y. Ozeren, A. Simon, B.P. Greimann, and K. Wu. 2015. "Modeling of multilayer cohesive bank erosion with a coupled bank stability and mobile-bed model." *Geomorphology* 243: 116-129.

Langendoen, E.J., and M.E. Ursic. 2020. *Erodibility of bank materials on the Lower American and Sacramento Rivers, adjacent to the City of Sacramento, California*. Research Report No. 80, Oxford, MS: U.S. Department of Agriculture, Agricultural Research Service, National Sedimentation Laboratory, 138.

Langendoen, E.J., and A. Simon. 2008. "Modeling the evolution of incised streams. II: Streambank erosion." *Journal of Hydraulic Engineering* 134 (7): 905-915. Doi:10.1061/(ASCE)0733-9429(2008)134:7(905).

Langendoen, E.J., and C.V. Alonso. 2008. "Modeling the evolution of incised streams. I: Model formulation and validation of flow and streambed evolution components." *Journal of Hydraulic Engineering* 134 (6): 749-762. Doi:10.1061/(ASCE)0733-9429(2008)134:6(749).

Mercier, F., S. Bonelli, P. Pinettes, F. Golay, F. Anselmet, and P. Philippe. 2014. "Comparison of computational fluid dynamic simulations with experimental jet erosion tests results." *J. Hydr. Eng.* 140 (5): 04014006.

Moody, L.F. 1944. "Friction factors for pipe flow." *Trans. Am. Soc. Of Mech. Engrs.* 66.

Motta, D., J.D. Abad, E.J. Langendoen, and M.H. Garcia. 2012. "A simplified 2D model for meander migration with physically-based bank evolution." *Geomorphology* 163-164: 10-25. Doi:10.1016/j.geomorph.2011.06.036.

Munson, B., D. Young, T. Okiishi, and W. Huebsch. 2009. *Fundamentals of Fluid Mechanics*. Sixth Edition. Wiley.

Papanicolaou, A.N., C.G. Wilson, A.G. Tsakaris, T.E. Sutarto, F. Bertrand, M. Rinaldi, S. Dey, and E.J. Langendoen. 2017. "Understanding mass fluvial erosion along a bank profile: using PEEP technology for quantifying retreat lengths and identifying event timing." *Earth Surface Processes and Landforms* 42 (11): 1717-1732.

Simon, A., N. Pollen-Bankhead, and R.E. Thomas. 2011. "Development and application of a deterministic bank stability and toe erosion model for stream restoration." In *Stream Restoration in Dynamic Fluvial Systems: Scientific Approaches, Analyses, and Tools*, edited by A. Simon, S.J. Bennett and J.M. Castro, 453-474. Washington, DC: American Geophysical Union.

Simon, A., R.E. Thomas, and L. Klimetz. 2010. "Comparison and experiences with field techniques to measure critical shear stress and erodibility of cohesive deposits." *Joint Federal Interagency Conference 2010*. Washington, DC: Advisory Committee on Water Information. 1-13.

USACE. 2016. *American River Common Features General Reevaluation Report: Final environmental impact statement/environmental impoact report*. Washington, DC: Department of the Army, Chief of Engineers, U.S. Army Corps of Engineers.

Vanoni, V.A., and N.H. Brooks. 1957. *Laboratory studies of the roughness and suspended load of alluvial streams*. Pasadena, CA: California Institute of Technology.

Weidner, K.L. 2012. "Evaluation of the jet test method for determining the erosional properties of cohesive soils: A numerical approach." MSc Thesis, Virginia Polytechnic Institute and State University, Blacksburg, VA, 84.

Wibowo, J.L., and B.A. Robbins. 2012. *Laboratory Jet Erosion Tests on American River Soil Samples, Sacramento, CA*. Vicksburg, MS: USACE Engineer Research and Development Center.

Wibowo, J.L., and B.A. Robbins. 2017. *Laboratory Jet Erosion Tests on the Lower American River Soil Samples, Sacramento, CA - Phase 2*. Engineer Research and Development Center: USACE.

Work, P.A., and D.N. Livsey. 2020. *Sediment lithology and borehole erosion testing, American and Sacramento Rivers, California.* Scientific Investigations Report 2020-5063, Reston, Virginia: U.S. Geological Survey, 92.

APPENDIX A

All erodibility parameter results are provided including negative results. It should be noted that all analyses only utilized positive values as negative erodibility parameters are not reasonable. The Steps represent the following analysis procedure: Step 1, Calculate the erosion-resistance parameters from the 'as-is' erosion function measured (or output) by the BET, EFA, and JET methods; Step 2, Same as Step 1 but limit the erosion function to the portion representing the mass soil erosion regime; Step 3, Same as Step 2 but base the erosion function on the shear stress acting at grain or (small) soil particle roughness length scales; and Step 4, Same as Step 3 but account for uncertainty in measured erosion rate and estimated applied shear stress. The variable τ_c is critical shear stress and k_d is erodibility coefficient.

TABLE 9 – ERODIBILITY PARAMETERS FOR ALL REMT TESTS.

					Step 1		Step 2		Step 3		Step 4	
Site	Test type (REMT)	USCS soil classification	Test reference	Elevation range (m)	τ_c (Pa)	k_d (cm^3 N^{-1} s^{-1})	τ_c (Pa)	k_d (cm^3 N^{-1} s^{-1})	τ_c (Pa)	k_d (cm^3 N^{-1} s^{-1})	τ_c (Pa)	k_d (cm^3 N^{-1} s^{-1})
LAR1	EFA	SM	SS#12	3.8-6.7	0.55	8.36	0.64	8.51	0.53	8.85	0.86	9.81
LAR1	EFA	SM	SS#13	2.6-3.7	0.80	16.59	0.94	16.91	0.40	21.40	1.13	25.49
LAR1	JET	SM	1(1)	7.6	10.10	2.32	-	-	10.10	2.32	10.48	32.72
LAR1	JET	SM	1(3)	7.6	2.57	32.96	-	-	2.57	32.96	2.68	51.06
LAR1*	JET	ML	B-2F-11-180 U-T-2-Jet-1	11.52	6.93	12.56	-	-	6.93	12.56	6.94	14.26
LAR1/LAR2*	EFA	ML	2F-11-130 (#7)		10.73	0.06	28.52	0.08	19.55	0.27	26.04	0.49
LAR2	BET	SM	2F 19 LAR 2 B	12.5-11.88	2.13	5.11	-	-	2.31	10.65	2.30	10.70
LAR2	BET	ML	2F 19 LAR 2 B	11.88-11.28	2.26	0.99	-	-	2.42	1.51	1.16	1.63
LAR2	BET	SM	2F 19 LAR 2 B	11.28-10.67	3.81	0.63	-	-	3.08	0.85	3.48	0.90
LAR2	BET	ML	2F 19 LAR 2 B	10.67-10.36	-14.70	0.40	-	-	-5.18	0.99	0.06	2.97
LAR2	JET	SM	2(1)	8.08	2.05	24.25	-	-	2.05	24.25	2.01	50.46
LAR2*	JET	ML	B-2F-11-141U-T-1-Jet-1	15.09	5.62	160.48	-	-	5.62	160.48	5.79	298.59
LAR2*	JET	SM	B-2F-11-175U-T-2-Jet-2	14	4.84	36.53	-	-	4.84	36.53	4.99	56.92
LAR2/LAR3*	EFA	CL	2F-11-129B		10.12	0.70	39.27	5.43	37.34	5.72	37.34	5.72
LAR2/LAR3*	EFA	SM	2F-11-129C		1.49	0.50	3.30	0.62	5.09	0.32	6.95	0.40
LAR3	BET	CL	2F 19 LAR 3 B	12.8-12.19	-53.15	0.03	-	-	-14.63	0.09	0.65	0.24
LAR3	BET	SM	2F 19 LAR 3 B	11.9-11.7	1.45	0.65	-	-	0.04	1.48	2.16	2.73
LAR3	BET	CL	2F 19 LAR 3 B	11.7-11.5	9.72	0.89	-	-	4.94	1.19	5.00	1.23
LAR3	BET	SM	2F 19 LAR 3 B	11.5-7.6	15.00	0.14	-	-	10.28	0.23	13.08	0.41

Site	Test type (REMT)	USCS soil classification	Test reference	Elevation range (m)	Step 1		Step 2		Step 3		Step 4	
					τ_c (Pa)	k_d (cm³ N⁻¹ s⁻¹)	τ_c (Pa)	k_d (cm³ N⁻¹ s⁻¹)	τ_c (Pa)	k_d (cm³ N⁻¹ s⁻¹)	τ_c (Pa)	k_d (cm³ N⁻¹ s⁻¹)
LAR3	EFA	SP-SM	SS#17	10.97-9.9	0.52	109.77	0.52	109.78	0.53	119.65	0.21	86.86
LAR3	EFA	SP-SM	SS#18	9.07-9.75	0.42	127.00	0.48	131.22	0.41	179.04	0.55	205.30
LAR3*	EFA	SM	2F-11-128B		1.58	2.56	3.21	3.46	4.82	2.13	4.78	1.88
LAR3/LAR4*	EFA	CL	2F-11-128A		1.90	2.02	3.96	3.07	6.54	1.69	6.94	1.60
LAR3/LAR4*	EFA	SP-SM	2F-11-137 (#2)		0.54	0.83	0.54	0.83	0.92	2.22	3.75	4.67
LAR3/LAR4*	EFA	ML	2F-11-137 (#3)		-4.70	0.01	-4.70	0.01	-2.23	0.02	0.83	0.02
LAR3/LAR4*	JET	ML	B-2F-11-128B-T-1-Jet-2	-	5.00	144.19	-	-	5.00	144.19	5.16	288.71
LAR4	EFA	SM	SS#24	6.4-4.72	0.43	85.41	0.43	85.41	0.30	111.99	0.32	111.04
LAR4	JET	SM	4(1)	7.8	6.38	11.20	-	-	6.38	11.20	6.06	11.72
LAR4*	EFA	MH	2F-11-126B (#2)		1.10	0.58	1.62	0.61	2.08	0.42	0.30	0.17
LAR5	BET	SC	2F 19 LAR 5 B	8.83-7.62	4.08	7.02	-	-	2.54	10.98	2.54	10.98
LAR5	BET	SP-SC	2F 19 LAR 5 B	7.62-7.01	8.33	0.47	-	-	8.34	0.52	8.34	0.52
LAR5	BET	SM	2F 19 LAR 5 B	7.01-6.4	12.37	0.49	-	-	7.71	0.62	7.71	0.62
LAR5	BET	SP-SM	2F 19 LAR 5 B	6.4-5.79	13.39	0.18	-	-	7.89	0.23	7.89	0.23
LAR5	BET	SM	2F 19 LAR 5 B	5.79-5.18	6.19	2.35	-	-	3.39	3.79	3.39	3.79
LAR5	JET	SM	5(1)	6	7.42	58.00	-	-	7.42	58.00	6.52	130.35
LAR5	JET	SM	5(3)	6	6.07	53.68	-	-	6.07	53.68	5.84	151.12
LAR5	JET	SM	5(4)	6	0.41	75.53	-	-	0.41	75.53	0.63	156.72
LAR5*	EFA	ML	2F-11-126A		14.71	1.01	36.53	1.43	13.26	12.51	13.26	12.51
LAR5*	EFA	CL	2F-11-135		1.34	0.02	1.56	0.02	4.84	0.05	9.39	0.05
LAR5*	JET	ML	B-2F-11-135-T-2-Jet-2A	-	2.78	311.60	-	-	2.78	311.60	-	-
LAR5/LAR7*	EFA	ML	2F-11-125		3.47	0.81	7.52	1.20	12.79	0.61	12.50	0.44
LAR6	BET	SM	2F 19 LAR 6 B	8.55-7.95	-12.14	0.32	-	-	-7.93	0.52	1.99	6.42
LAR6	BET	SM	2F 19 LAR 6 B	7.95-7.15	5.31	1.47	-	-	2.60	1.80	2.76	2.10
LAR6	BET	SM	2F 19 LAR 6 B	7.15-6.75	2.22	0.18	-	-	0.65	0.46	2.73	0.56
LAR6	BET	SP	2F 19 LAR 6 B	6.75-5.85	53.90	0.27	-	-	30.91	0.49	30.44	0.53
LAR6	BET	SP	2F 19 LAR 6 B	5.85-5.55	-32.57	0.02	-	-	-39.51	0.03	23.80	0.38

Site	Test type (REMT)	USCS soil classification	Test reference	Elevation range (m)	Step 1		Step 2		Step 3		Step 4	
					τ_c (Pa)	k_d (cm³ N⁻¹ s⁻¹)	τ_c (Pa)	k_d (cm³ N⁻¹ s⁻¹)	τ_c (Pa)	k_d (cm³ N⁻¹ s⁻¹)	τ_c (Pa)	k_d (cm³ N⁻¹ s⁻¹)
LAR6	BET	SP-SM	2F 19 LAR 6 B	5.55-4.35	93.25	0.07	-	-	53.47	0.11	49.91	0.19
LAR6	EFA	SP-SM	SS#10	8.55-6.85	0.55	157.07	1.10	265.81	1.27	231.63	1.21	213.99
LAR6	EFA	ML	ST1	-0.9--1.22	0.11	39.61	0.38	43.72	0.35	47.29	0.81	59.56
LAR6	EFA	GP	SS#11	3.44-0.40			2.12	14.69	3.01	10.44	1.49	14.16
LAR7	BET	SP	2F 19 LAR 7 B	8.84-7.34	-8.29	0.43	-	-	-7.58	0.55	0.06	1.29
LAR7	BET	CL	2F 19 LAR 7 B	7.34-5.44	24.61	-0.24	-	-	17.68	-0.32	0.06	0.01
LAR7	BET	SC	2F 19 LAR 7 B	5.44-4.24	42.30	-0.15	-	-	25.97	-0.24	0.06	0.03
LAR7	BET	SP	2F 19 LAR 7 B	4.24-3.34	29.91	-0.40	-	-	12.46	-0.95	0.06	2.13
LAR7	EFA	SP-SM	SS#7	-0.06--1.66	0.87	11.33	3.36	15.93	2.34	17.26	2.34	17.27
LAR7	EFA	SM	SS#3	8.53-6.86	0.49	220.28	1.50	872.46	1.87	543.63	1.87	543.63
LAR7	EFA	SP	SS#5	3.05-1.98	0.43	206.13	0.71	317.62	0.87	235.74	0.81	207.20
LAR7	EFA	SP-SM	SS#6	1.82-0.9	0.60	110.49	1.12	162.57	1.11	123.36	0.71	83.54
LAR7	EFA	SC	SS#4	5.24-4.33	-0.74	5.51	0.43	8.68	0.48	9.42	0.48	9.43
LAR7*	EFA	CL	2F-11-134		4.60	0.16	13.26	0.22	9.12	0.79	9.41	0.84
LAR7*	JET	ML	A1_B-2F-11-124-T-1-Jet-1B	-	18.25	8.79	-	-	18.25	8.79	18.18	9.58
LAR7*	JET	SP	B-2F-11-124-T-1-Jet-2	-	6.63	89.14	-	-	6.63	89.14	7.64	174.81
LAR7*	JET	ML	B-2F-11-125-T-2-Jet-2	-	33.20	3.55	-	-	33.20	3.55	33.35	4.91
LAR7/LAR5*	JET	ML	B-2F-11-126A-T2-Jet-2A	-	7.12	191.84	-	-	7.12	191.84	7.13	287.29
LAR8	JET	SM	8(1)	7.11	4.23	29.84	-	-	4.23	29.84	3.94	53.78
LAR8	JET	SM	8(2)	7.11	1.45	10.11	-	-	1.45	10.11	0.84	10.77
LAR8	JET	SM	8(3.3)	7.11	8.03	8.81	-	-	8.03	8.81	6.19	8.54
LAR9	BET	SM	2F 19 LAR 9 B	9.75-7.45	-3.74	0.93	-	-	-3.29	1.20	0.06	6.12
LAR9	BET	CL	2F 19 LAR 9 B	7.45-5.75	-4.78	0.14	-	-	-6.27	0.14	0.06	0.23
LAR9	BET	SM	2F 19 LAR 9 B	5.75-1.75	1.25	3.55	-	-	0.63	6.05	0.63	6.05
LAR9	EFA	SM	SS#8	5.75-3.55	0.16	4.96	8.55	15.10	5.58	23.14	5.58	23.14
LAR9	EFA	CL	ST2	6.4-5.79	0.36	43.44	0.36	43.44	0.43	45.62	0.43	45.62
LAR9	EFA	CL	ST1	7.01-6.4	0.50	18.36	0.50	18.36	0.44	19.70	0.44	19.70

Site	Test type (REMT)	USCS soil classification	Test reference	Elevation range (m)	Step 1		Step 2		Step 3		Step 4	
					τ_c (Pa)	k_d (cm^3 N^{-1} s^{-1})	τ_c (Pa)	k_d (cm^3 N^{-1} s^{-1})	τ_c (Pa)	k_d (cm^3 N^{-1} s^{-1})	τ_c (Pa)	k_d (cm^3 N^{-1} s^{-1})
LAR9	EFA	CL	SS#9	3.35-1.95	4.02	6.33	16.53	14.92	8.73	68.72	8.73	68.72
LAR9	JET	SM	9(1)	4.5	4.27	23.40	-	-	4.27	23.40	3.74	40.21
LAR9	JET	ML	9(2.2)	3	20.49	4.85	-	-	20.49	4.85	19.78	6.40
LAR9	JET	ML	9(3)	3	20.25	6.96	-	-	20.25	6.96	20.88	12.90
LAR10	BET	SM	2F 19 LAR 10 B	6.71-5.21	-479.05	0.01	-	-	-270.65	0.02	0.06	0.14
LAR10	BET	ML	2F 19 LAR 10 B	5.21-3.81	-4.43	0.30	-	-	-2.51	0.56	0.06	0.66
LAR10	BET	CH	2F 19 LAR 10 B	3.81-2.61	-63.21	0.04	-	-	-37.88	0.07	0.06	0.16
LAR10	EFA	SP	SS#16	-2.13--3.2	-0.15	44.59	0.10	51.20	0.20	70.97	0.34	77.16
LAR10	EFA	SP-SM	SS#14	-0.9--1.98	0.23	53.24	0.23	54.62	0.09	73.42	0.41	93.08
LAR12	EFA	SP	SS#2	1.52--0.15	0.44	185.41	0.60	209.46	0.53	250.62	0.55	257.49
LAR12	EFA	SP-SM	SS#1	5.18-3.05	0.67	127.78	2.53	311.81	1.91	412.24	1.91	412.24
SAC1	BET	SM	0-3.5m	8.84-5.34	18.92	0.41	-	-	14.32	0.61	16.02	1.06
SAC1	BET	CL	3.5-9m	5.34--0.16	2.16	0.23	-	-	1.39	0.22	1.33	0.22
SAC1	EFA	CL	ST6: 29-31 ft	0--0.6	4.23	1.91	4.22	1.91	4.14	3.09	8.36	3.61
SAC1	EFA	ML	ST2: 11-13ft	5.49-4.88	6.79	1.66	15.72	2.24	10.93	2.84	6.95	1.90
SAC3	BET	ML	2F 19 SAC 3 B	6.4-5.5	2.53	1.94	-	-	3.29	-7.20	-	-
SAC3	BET	SM	2F 19 SAC 3 B	5.5-2.4	-2.52	0.24	-	-	-5.02	0.36	0.06	0.47
SAC3	BET	ML	2F 19 SAC 3 B2	6.4-5.5	-1.66	0.16	-	-	-0.56	0.45	1.27	5.64
SAC3	BET	SM	2F 19 SAC 3 B2	5.5-2.4	14.29	0.08	-	-	5.87	0.22	6.10	0.27
SAC3	BET	SP-SM	2F 19 SAC 3 B2	2.4-1.4	-10.43	0.02	-	-	-2.00	0.05	0.52	0.07
SAC3	EFA	SM	SS#22	1.8-1.4	0.80	5.82	1.70	72.64	1.21	115.25	1.17	111.70
SAC3	EFA	SM	SS#21	4.9-3.8	-0.48	76.23	1.20	158.12	0.50	135.64	0.44	130.31
SAC3	JET	ML	3(1)	2.83	9.92	12.39	-	-	9.92	12.39	9.81	27.03
SAC3	JET	ML	3(2)	3.89	15.43	22.42	-	-	15.43	22.42	14.84	47.99
SAC3	JET	ML	3(3)	3.86	10.08	19.05	-	-	10.08	19.05	8.33	15.08
SAC3	JET	ML	3(4)	3.95	14.20	21.60	-	-	14.20	21.60	13.16	23.63
SAC3	JET	ML	3(5)	3.6	7.64	9.77	-	-	7.64	9.77	7.43	9.92

Site	Test type (REMT)	USCS soil classification	Test reference	Elevation range (m)	Step 1		Step 2		Step 3		Step 4	
					τ_c (Pa)	k_d (cm³ N⁻¹ s⁻¹)	τ_c (Pa)	k_d (cm³ N⁻¹ s⁻¹)	τ_c (Pa)	k_d (cm³ N⁻¹ s⁻¹)	τ_c (Pa)	k_d (cm³ N⁻¹ s⁻¹)
SAC3	JET	ML	3(6)	3.6	12.34	4.50	-	-	12.34	4.50	12.65	6.34
SAC5	EFA	SC-SM	ST3: 53-55ft	-6.14--6.74	4.49	1.42	12.45	1.81	5.24	6.15	5.52	6.20
SAC5	EFA	CL	SS#25	1.86--0.86	5.84	20.11	20.96	54.43	13.68	83.41	13.19	70.54
SAC5	EFA	SM	SS#26	-2.94--4.54	1.76	6.17	2.33	6.38	1.76	8.43	0.06	6.00
SAC7	BET	ML	2F 19 SAC 7 B	6.71-4.11	-2.61	0.62	-	-	-1.34	0.90	0.63	1.19
SAC7	BET	CL	2F 19 SAC 7 B	4.11-3.66	-44.90	0.16	-	-	-43.06	0.17	1.29	1.36
SAC7	BET	ML	2F 19 SAC 7 B	3.66-2.11	-30.79	0.21	-	-	-24.32	0.26	1.94	1.53
SAC7	EFA	ML	ST1: 9-11 ft	4-3.11	0.65	10.19	2.23	17.45	2.06	18.06	1.94	17.00
SAC7	EFA	ML	ST2: 15-17 ft	2.11-1.51	8.90	9.92	8.90	9.92	9.33	11.18	9.33	11.19
SAC7	JET	ML	7(1)	3.466	24.69	7.04	-	-	24.69	7.04	24.05	10.30
SAC7	JET	ML	7(4)	3.466	16.90	13.05	-	-	16.90	13.05	18.18	22.28
SAC7	JET	ML	7(5)	3.466	14.03	7.56	-	-	14.03	7.56	11.77	10.51
SAC8	EFA	SP	SS#19	3.4-2.3	-0.99	67.56	0.24	101.53	0.22	109.82	0.22	109.82
SAC8	EFA	SP	SS#20	4-3.5	-0.30	117.91	0.43	150.43	0.40	162.73	0.32	155.63
SAC8	EFA	ML	ST1: 27-28.7ft	-2.1--2.6	4.86	3.82	32.43	16.45	12.35	41.02	12.35	41.02
SAC8	EFA	ML	ST2: 47-49ft	-8.2--8.8	0.30	4.40	1.66	4.68	2.30	20.85	2.28	19.88
SAC9	EFA	CL	9-11ft	2.79-1.89	0.99	0.37	41.47	4.41	24.21	7.56	24.21	7.56
SAC9	EFA	CL	15-17ft	0.89-0.29	2.97	2.82	6.83	3.38	2.61	8.84	4.13	10.94

* Estimated location based on aerial imagery provided in summary reports (Wibowo & Robbins 2012; 2017)

APPENDIX B

Figure 83 through Figure 106 plot the measured erosion functions for grain shear stress estimates to explore consistencies in individual tests by location. A maximum of two figures per location are presented; if a dominant soil is present at a given location then a figure was dedicated to that soil as described in the figure caption. However, if a variety of soils is present at a given location then the individual soil types are identified in the legend rather than the figure caption. Approximate NAVD88 elevations are provided for each test.

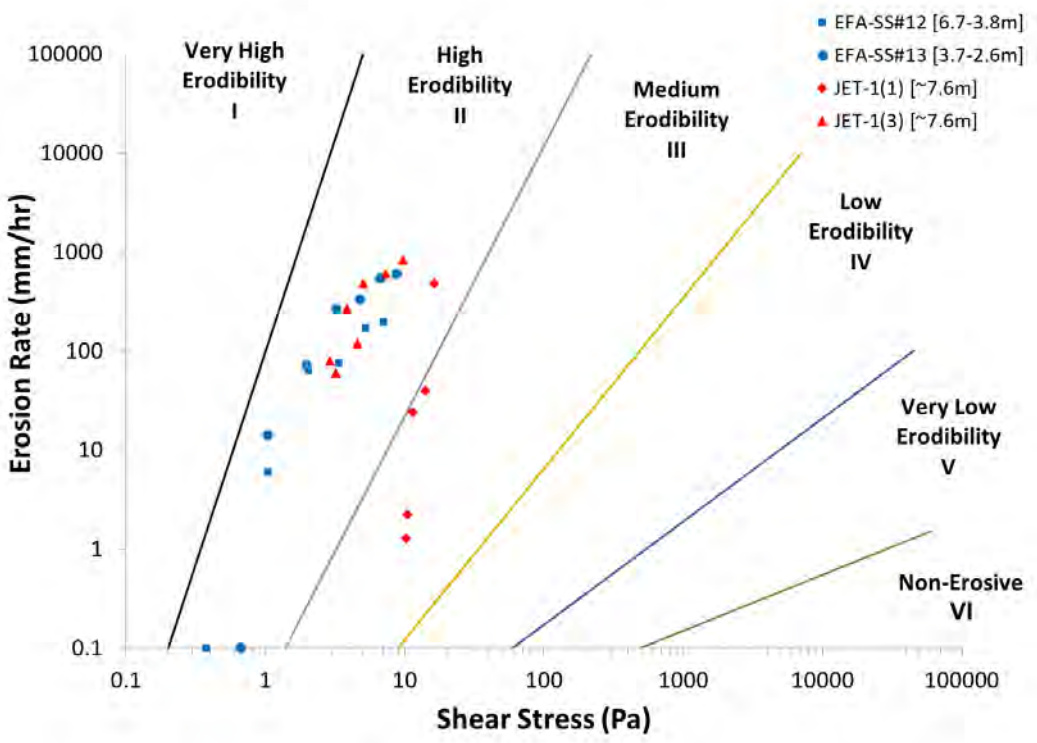

FIGURE 83 – LOWER AMERICAN RIVER SITE 1 (LAR1) – SILTY SAND (USCS SM) – GRAIN SHEAR STRESS

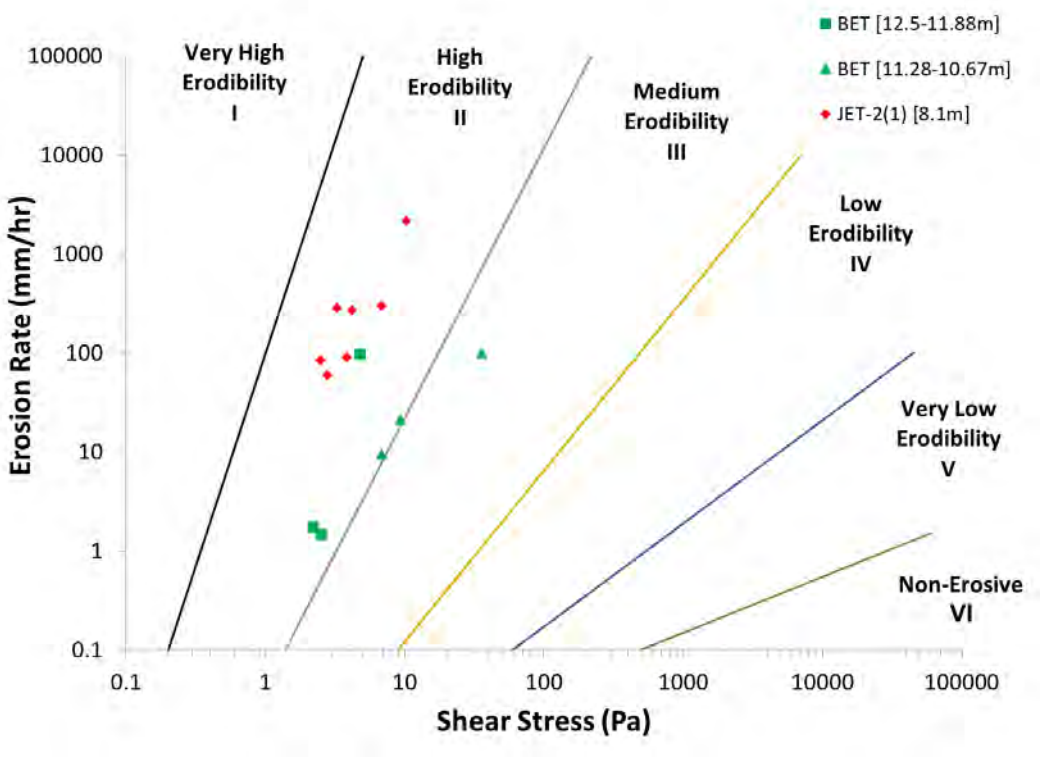

FIGURE 84 – LOWER AMERICAN RIVER SITE 2 (LAR2) – SILTY SAND (USCS SM) – GRAIN SHEAR STRESS

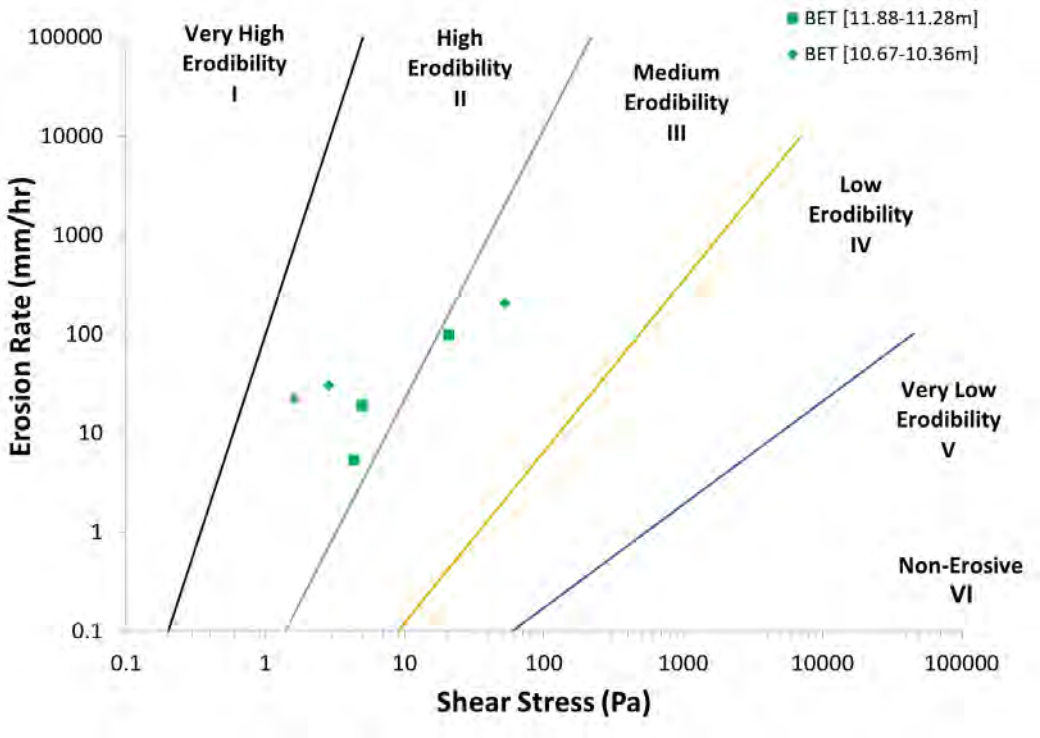

FIGURE 85 – LOWER AMERICAN RIVER SITE 2 (LAR2) – SILT (USCS ML) – GRAIN SHEAR STRESS

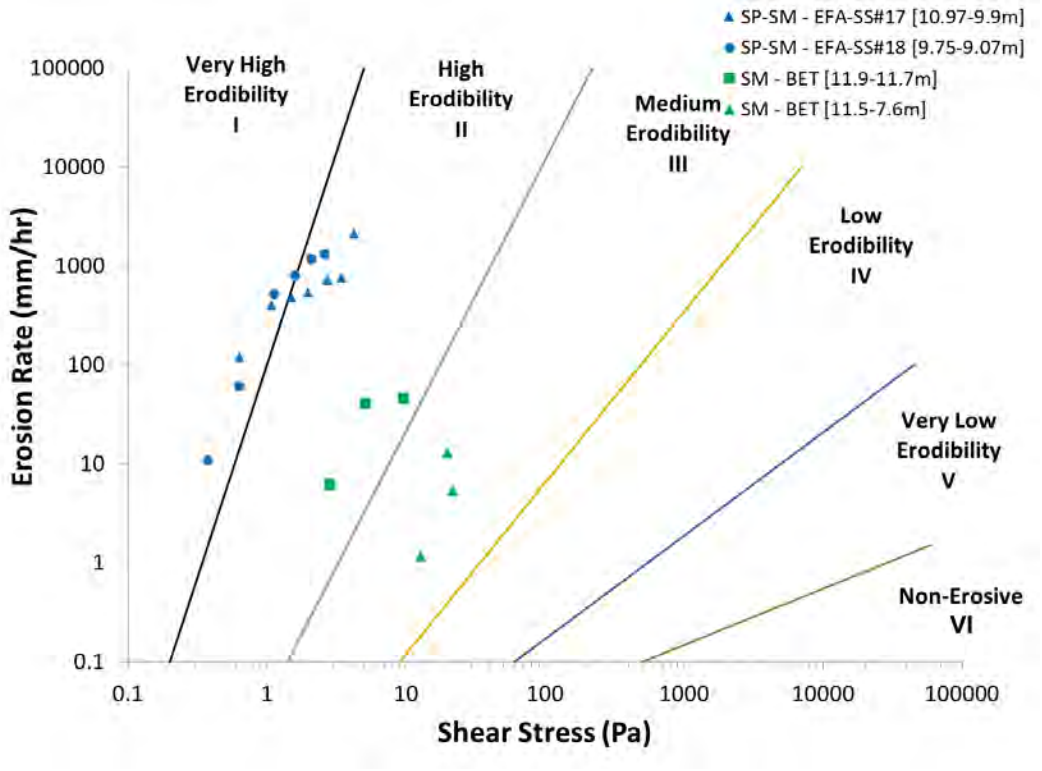

FIGURE 86 – LOWER AMERICAN RIVER SITE 3 (LAR3) – SILTY SAND (USCS SM) – GRAIN SHEAR STRESS

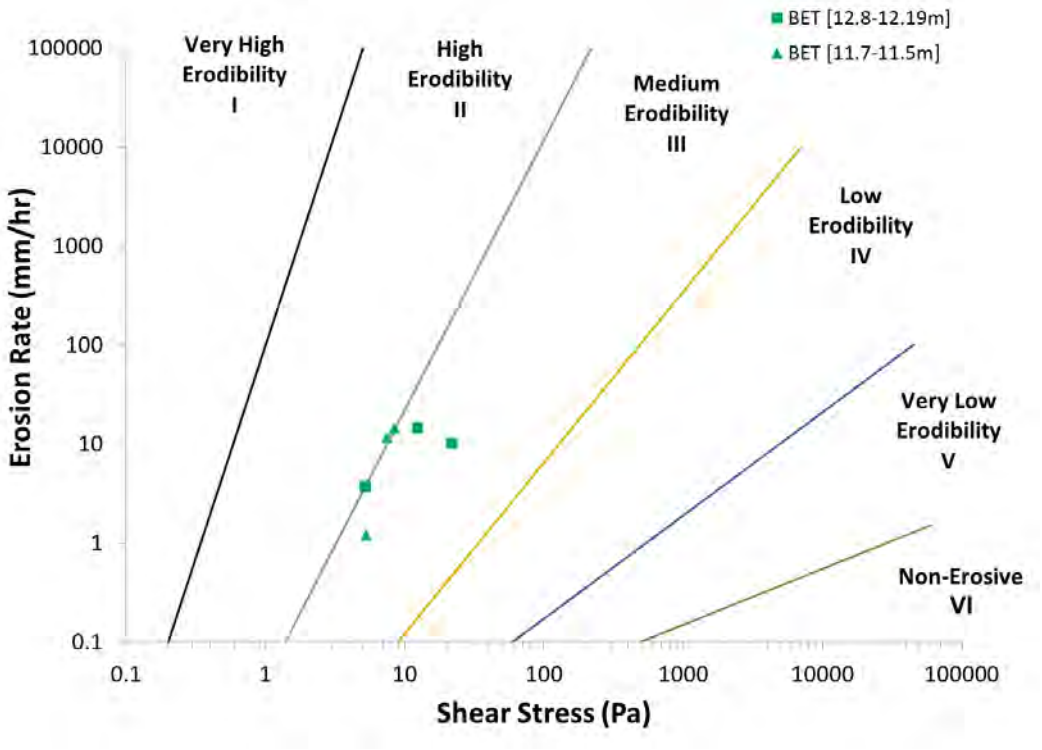

FIGURE 87 - LOWER AMERICAN RIVER SITE 3 (LAR3) – LEAN CLAY (USCS CL) – GRAIN SHEAR STRESS

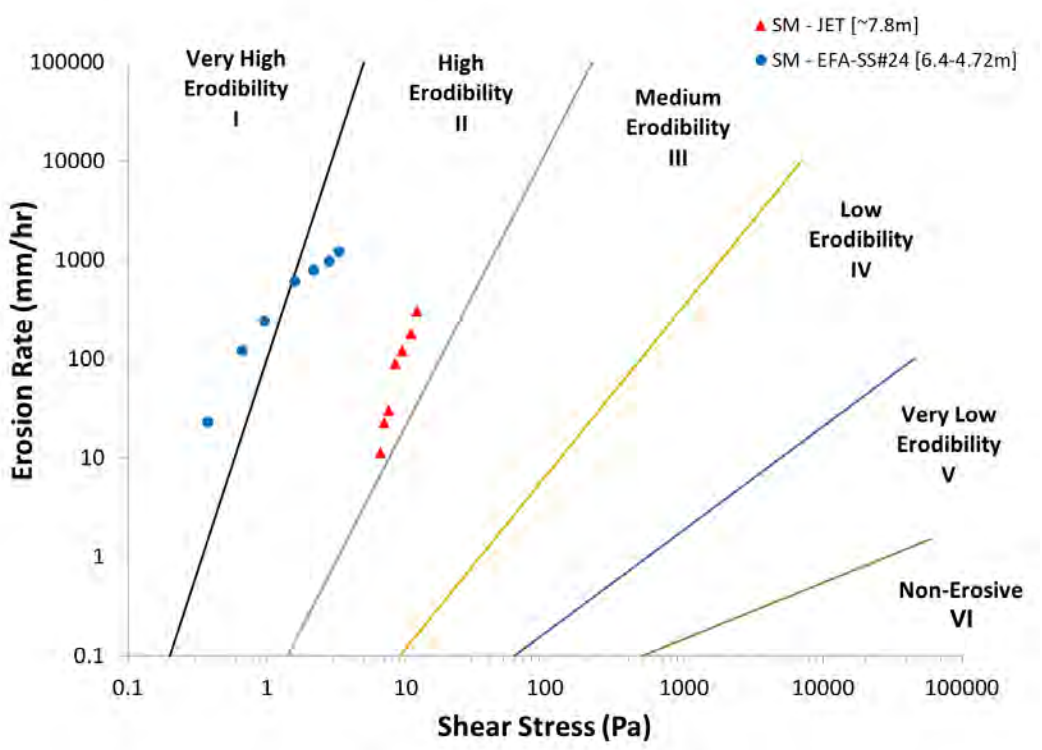

FIGURE 88 – LOWER AMERICAN RIVER SITE 4 (LAR4) – OTHER USCS CLASSIFICATIONS – GRAIN SHEAR STRESS

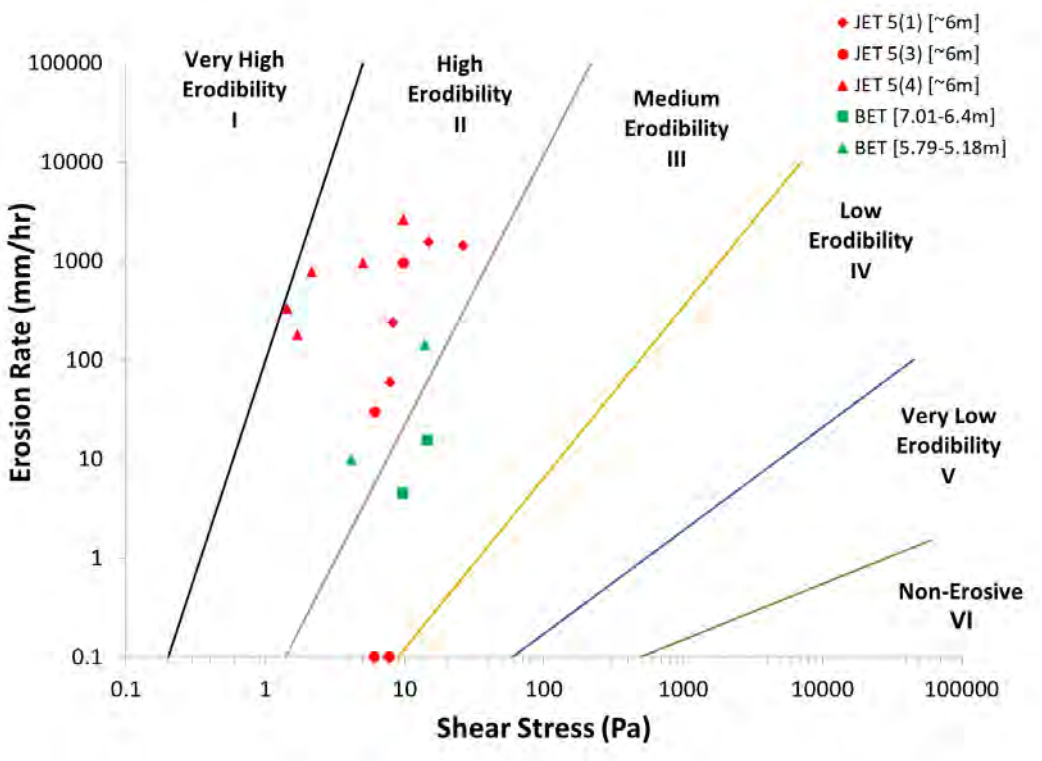

FIGURE 89 - LOWER AMERICAN RIVER SITE 5 (LAR5) – SILTY SAND (USCS SM) – GRAIN SHEAR STRESS

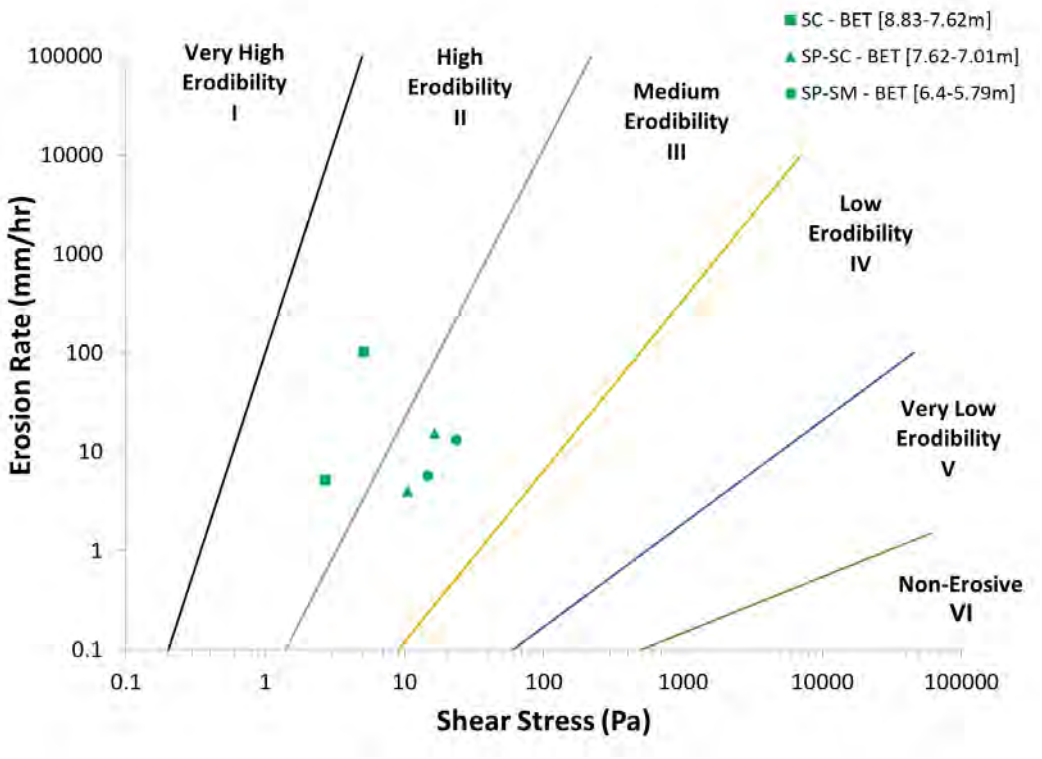

FIGURE 90 - LOWER AMERICAN RIVER SITE 5 (LAR5) – OTHER USCS CLASSIFICATIONS – GRAIN SHEAR STRESS

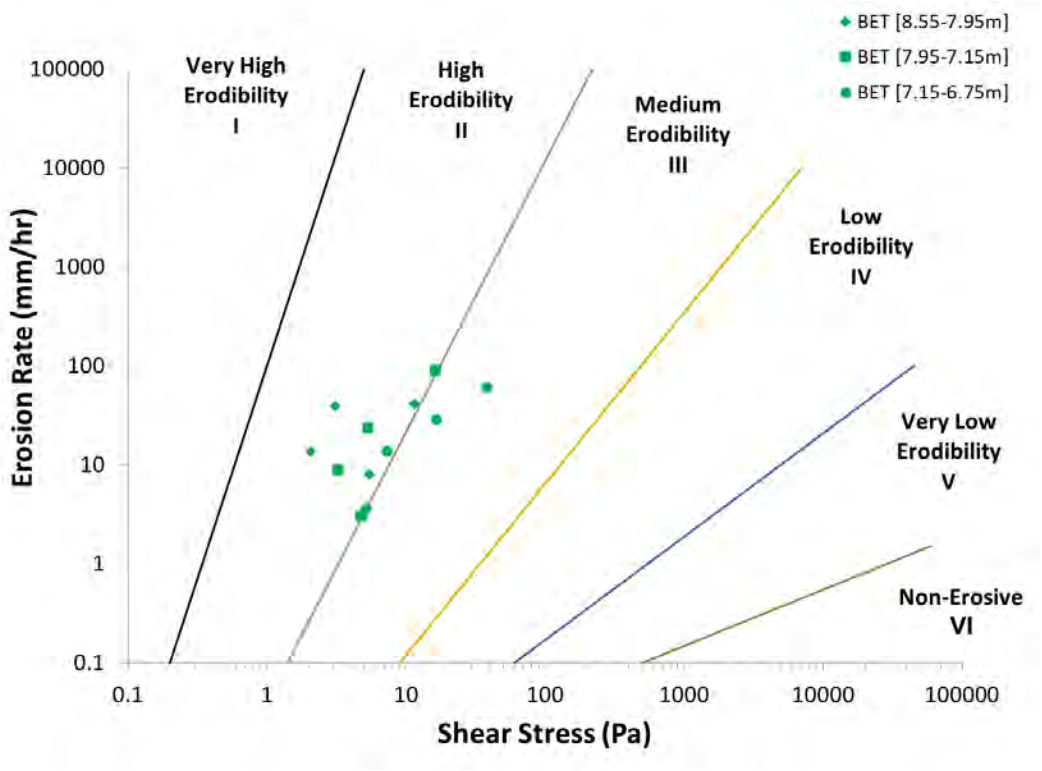

FIGURE 91 - LOWER AMERICAN RIVER SITE 6 (LAR6) – SILTY SAND (USCS SM). *QUESTIONABLE BET DATA* - GRAIN SHEAR STRESS

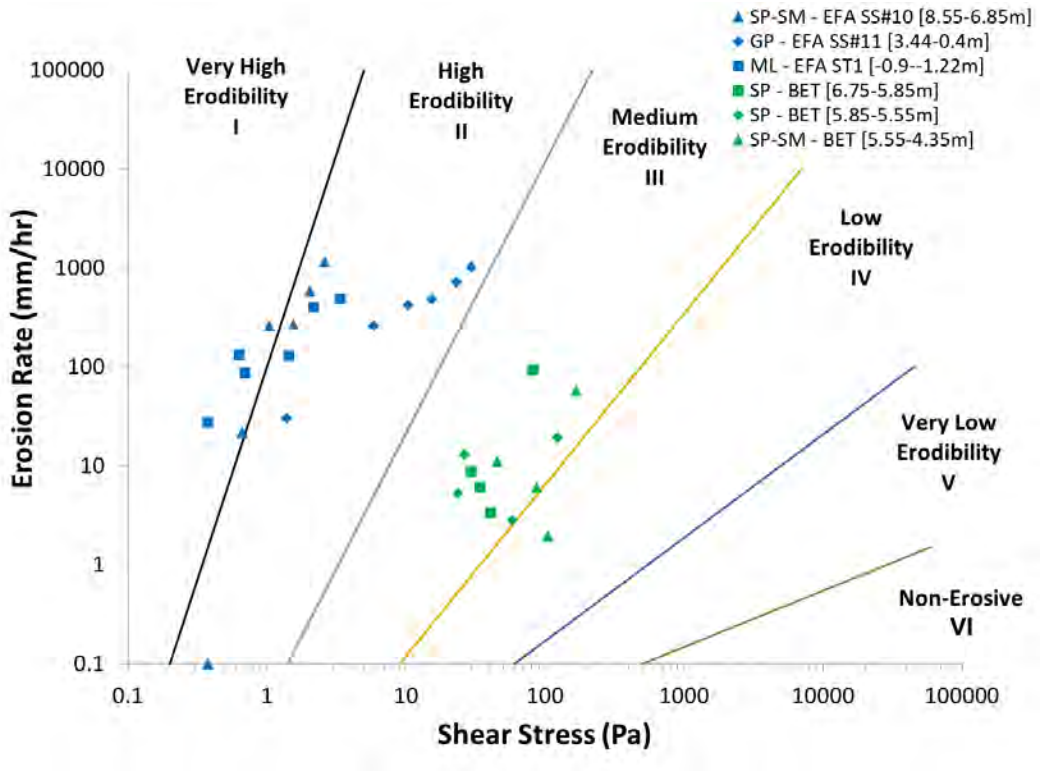

FIGURE 92 - LOWER AMERICAN RIVER SITE 6 (LAR6) – OTHER USCS CLASSIFICATIONS. *QUESTIONABLE BET DATA* - GRAIN SHEAR STRESS

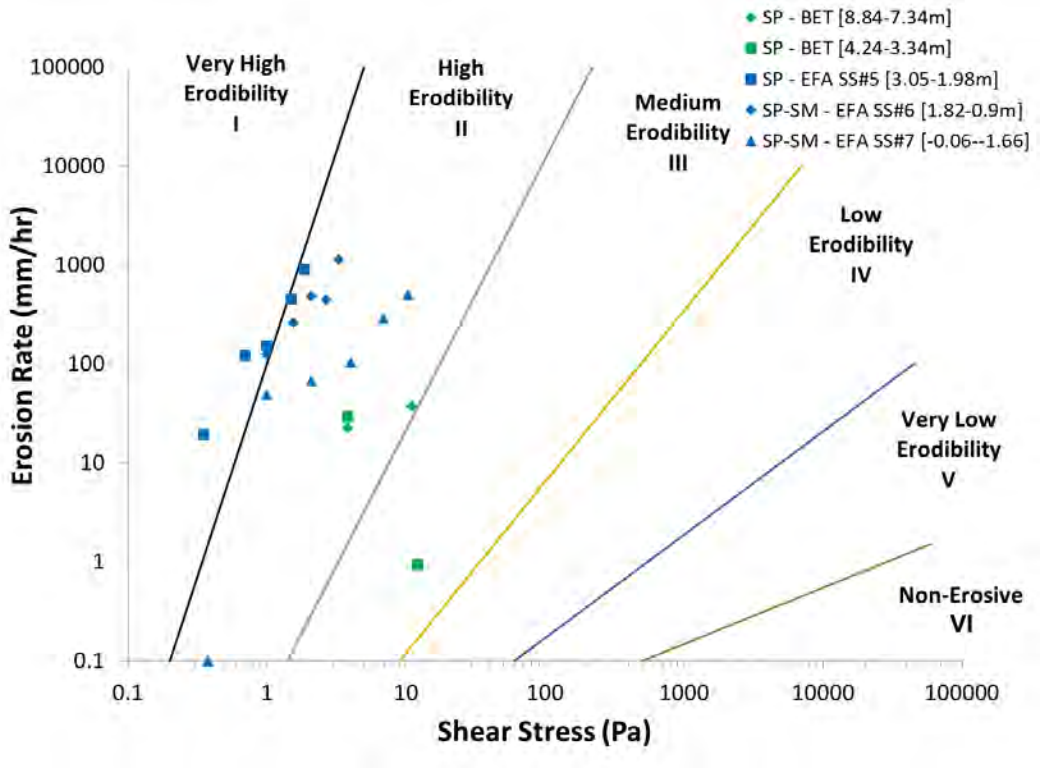

FIGURE 93 - LOWER AMERICAN RIVER SITE 7 (LAR7) – (USCS SP & SP-SM) – GRAIN SHEAR STRESS

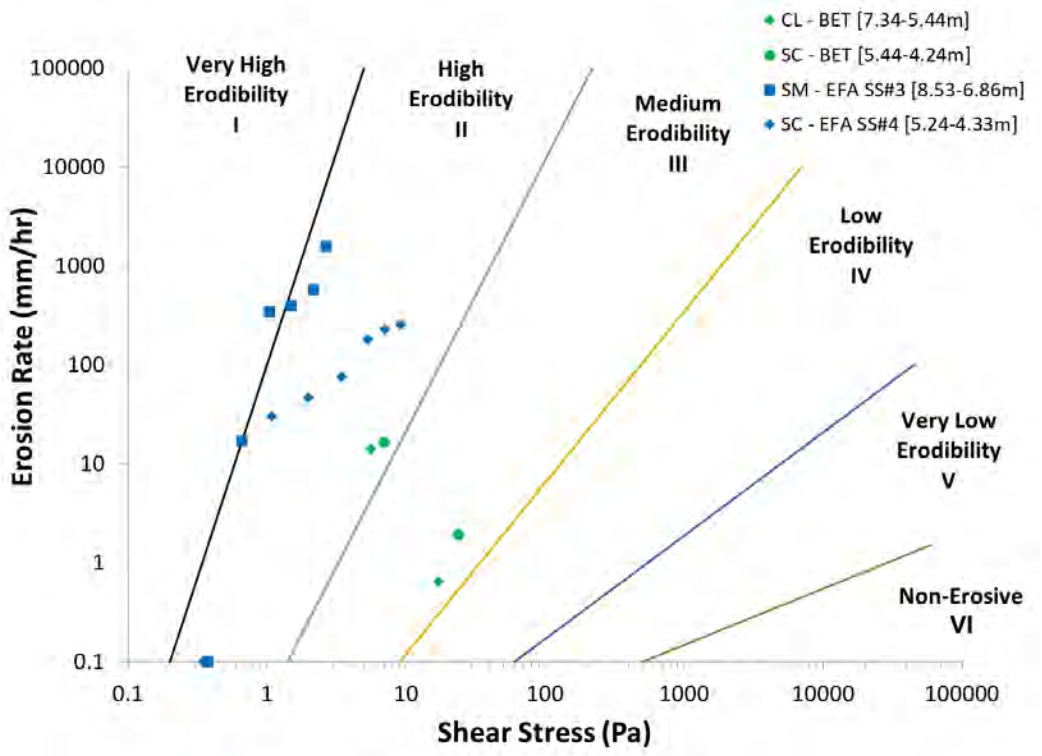

FIGURE 94 - LOWER AMERICAN RIVER SITE 7 (LAR7) – OTHER USCS CLASSIFICATIONS – GRAIN SHEAR STRESS

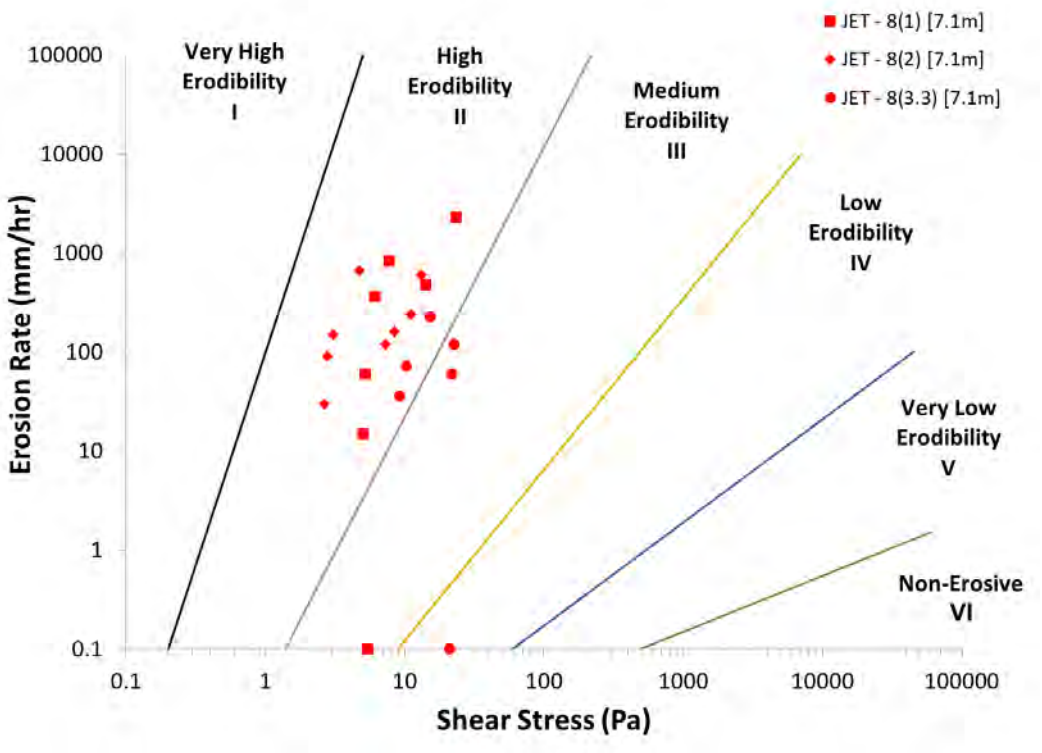

FIGURE 95 - LOWER AMERICAN RIVER SITE 8 (LAR8) – SILTY SAND (USCS SM) – GRAIN SHEAR STRESS

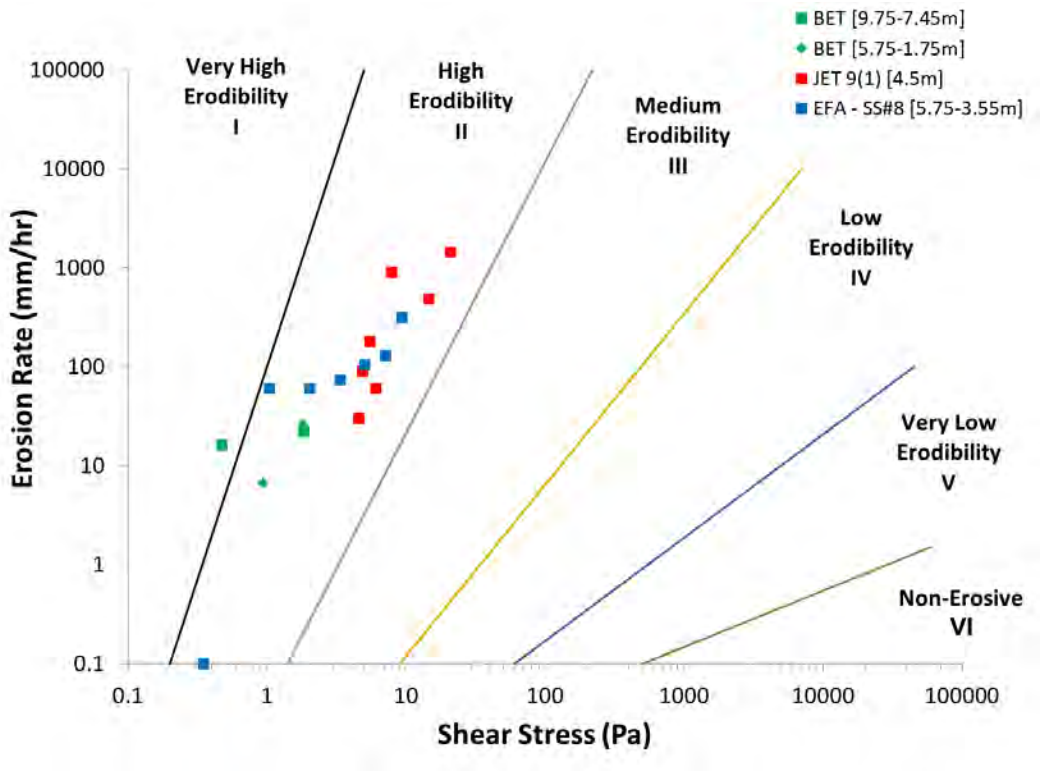

FIGURE 96 - LOWER AMERICAN RIVER SITE 9 (LAR9) – SILTY SAND (USCS SM) – GRAIN SHEAR STRESS

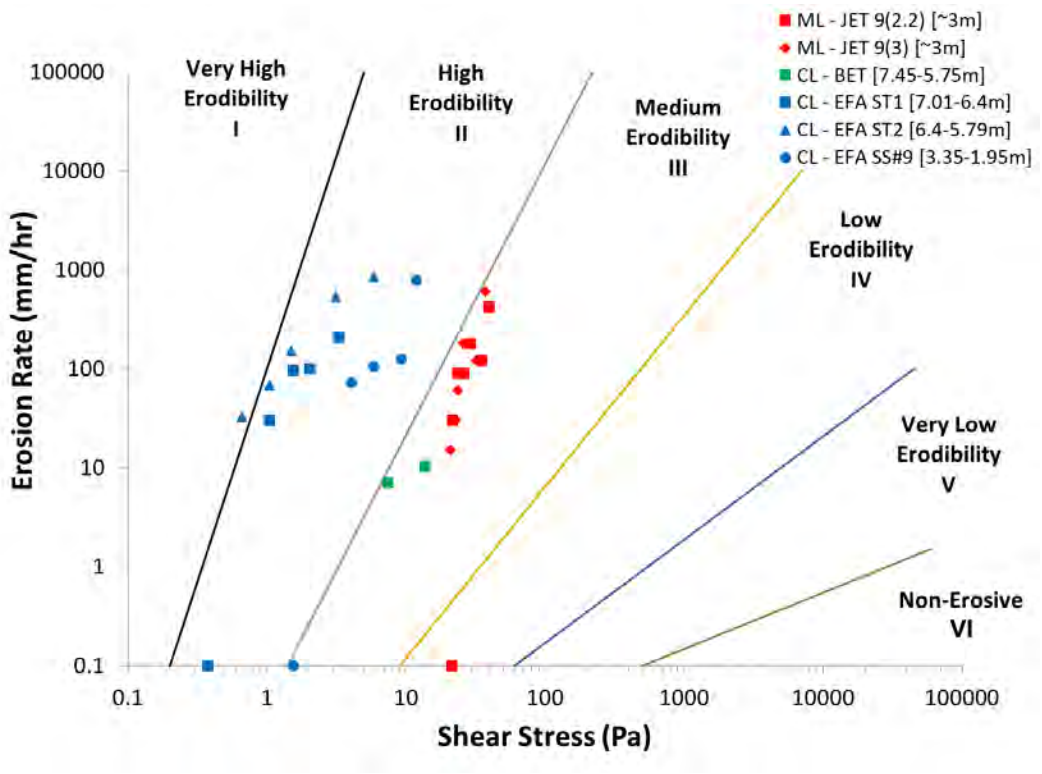

FIGURE 97 - LOWER AMERICAN RIVER SITE 9 (LAR9) – OTHER USCS CLASSIFICATIONS – GRAIN SHEAR STRESS

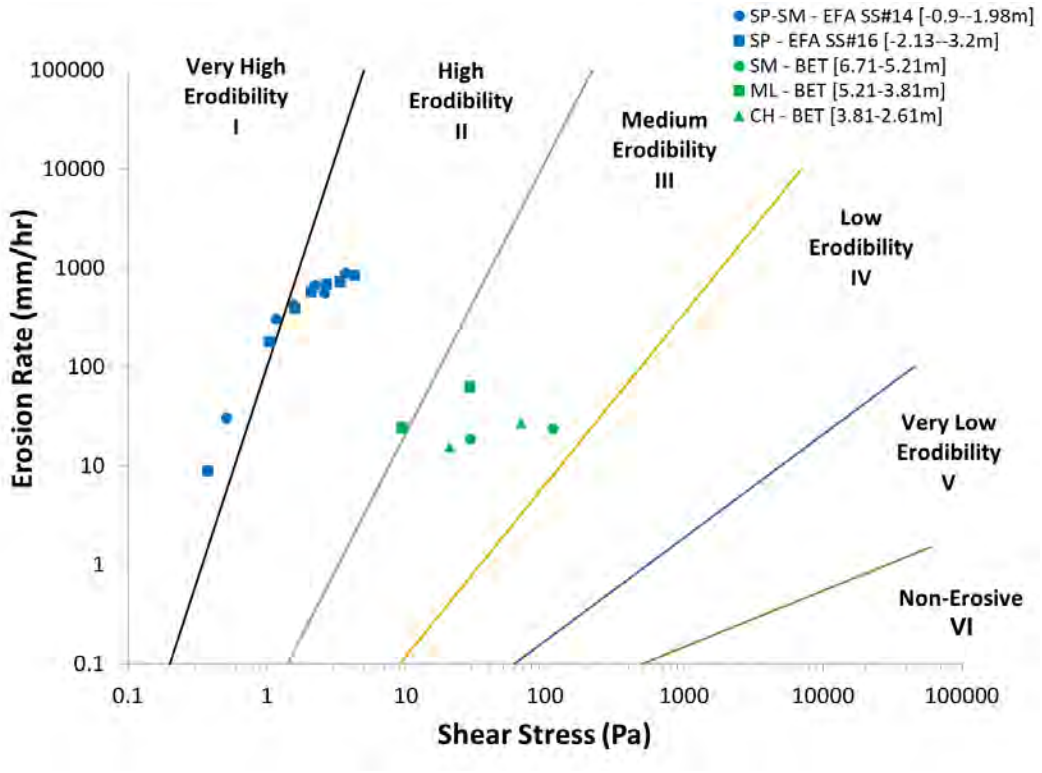

FIGURE 98 - LOWER AMERICAN RIVER SITE 10 (LAR10) – OTHER USCS CLASSIFICATIONS – GRAIN SHEAR STRESS

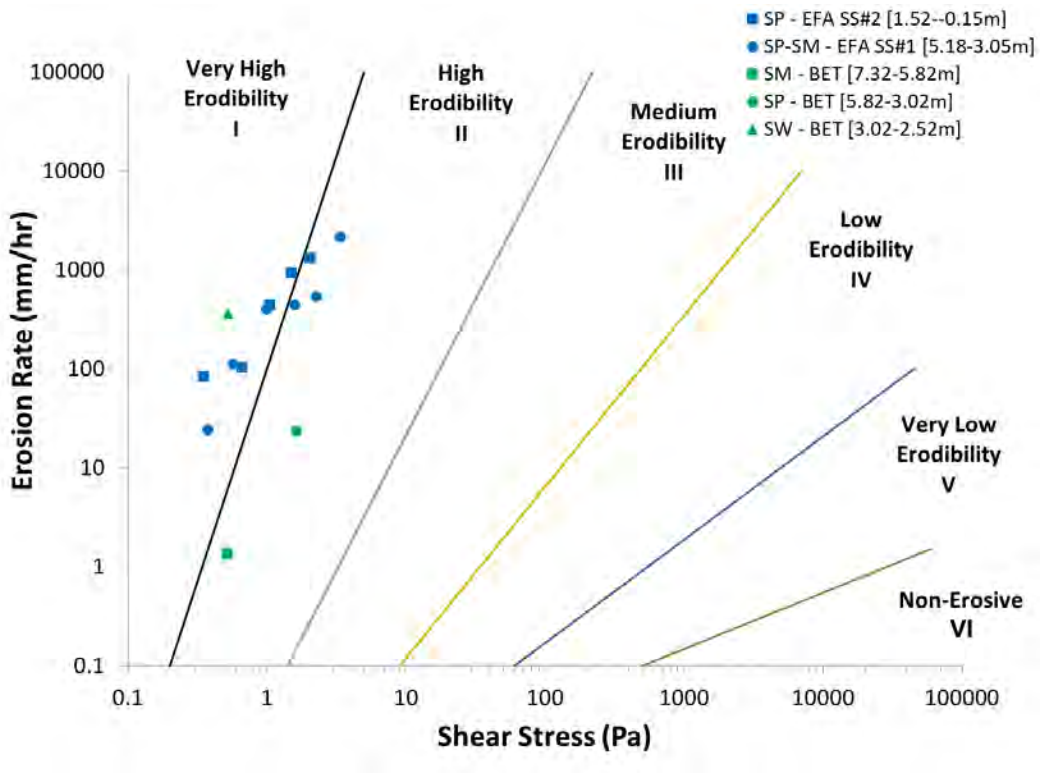

FIGURE 99 - LOWER AMERICAN RIVER SITE 12 (LAR12) – OTHER USCS CLASSIFICATIONS – GRAIN SHEAR STRESS

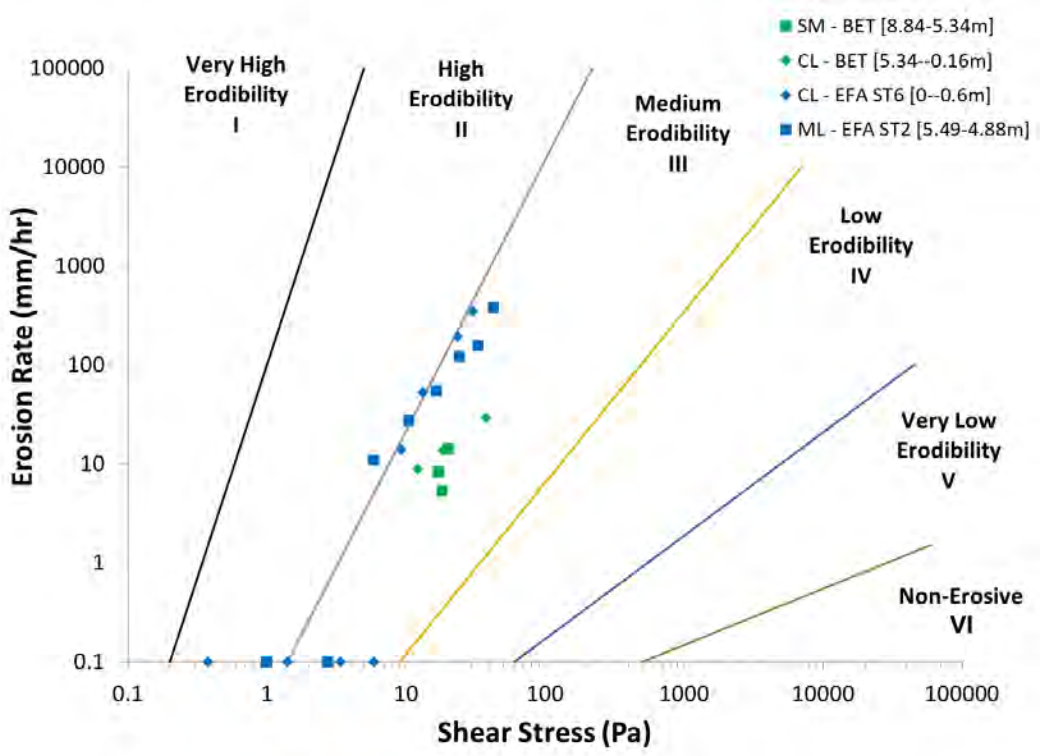

FIGURE 100 – SACRAMENTO RIVER SITE 1 (SAC1) – OTHER USCS CLASSIFICATIONS – GRAIN SHEAR STRESS

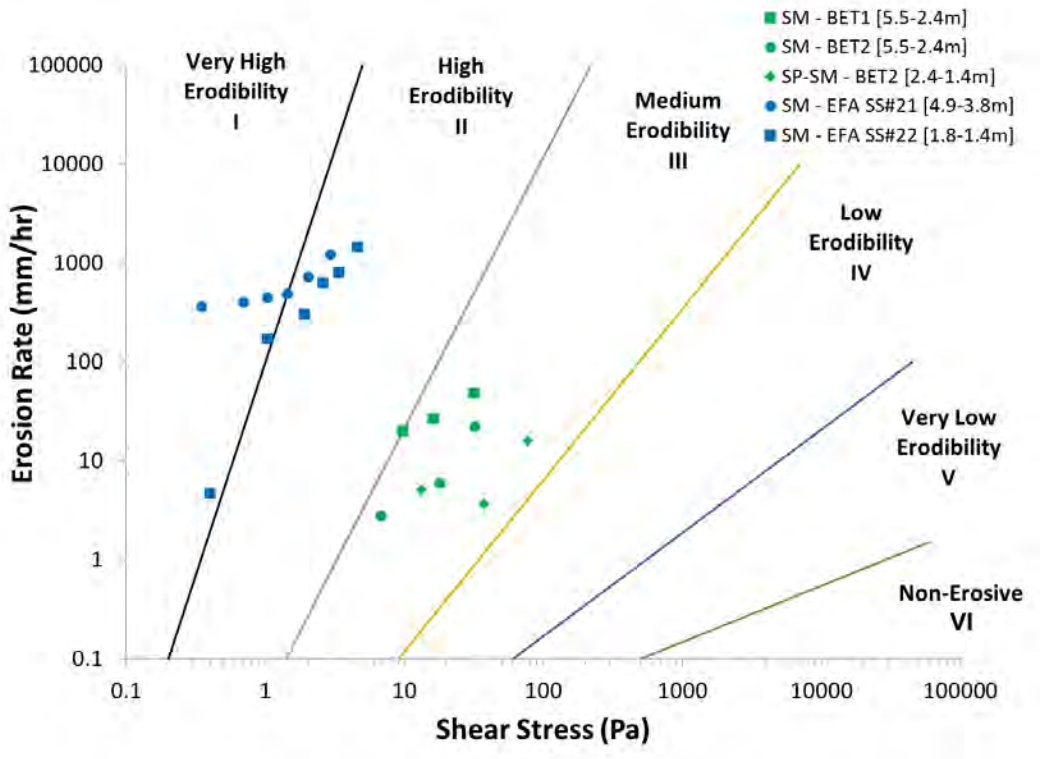

FIGURE 101 – SACRAMENTO RIVER SITE 3 (SAC3) – OTHER USCS CLASSIFICATIONS – GRAIN SHEAR STRESS

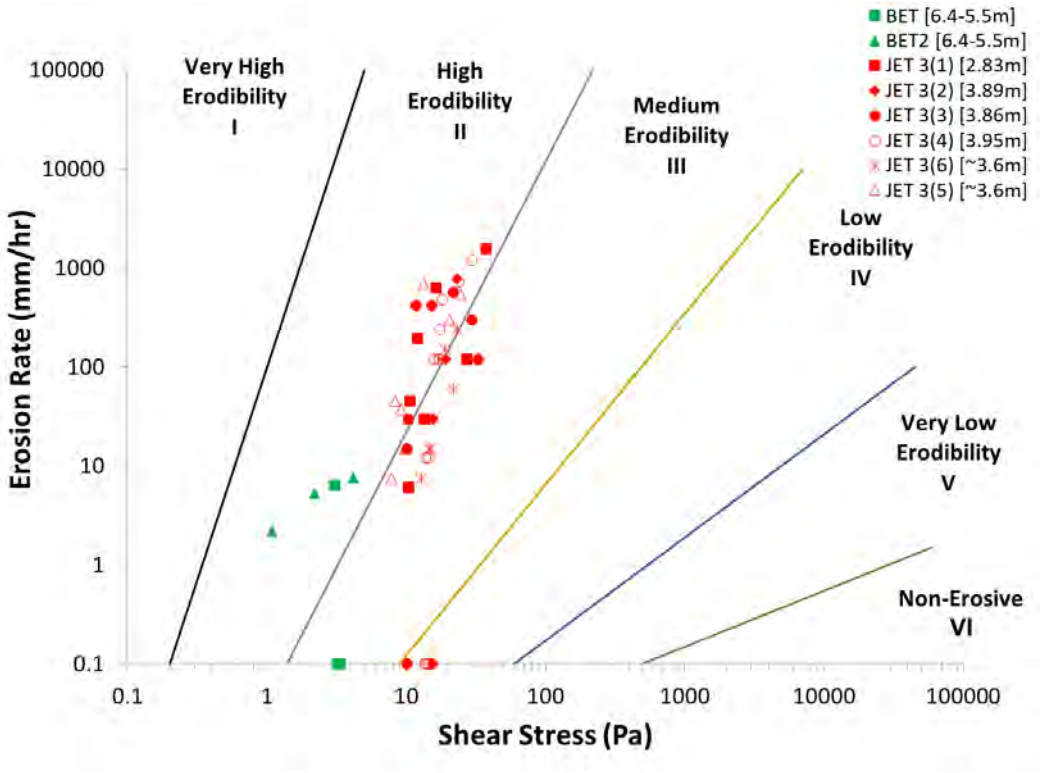

FIGURE 102 – SACRAMENTO RIVER SITE 3 (SAC3) – SILT (USCS ML) – GRAIN SHEAR STRESS

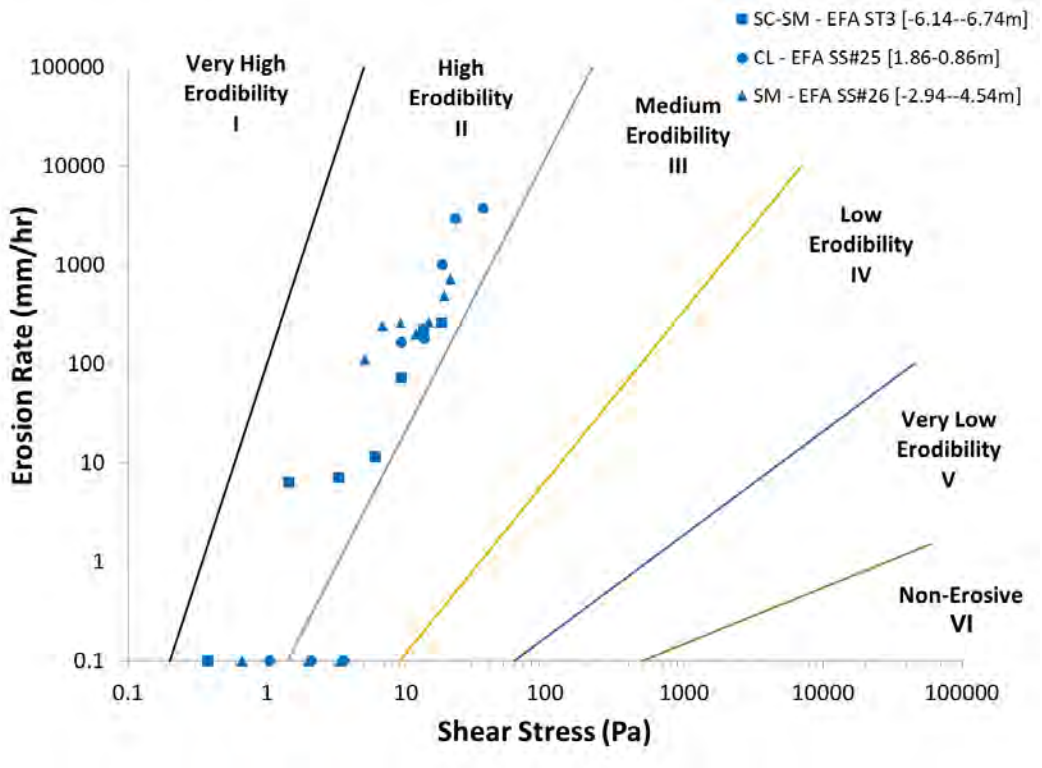

FIGURE 103 – SACRAMENTO RIVER SITE 5 (SAC5) – OTHER USCS CLASSIFICATIONS – GRAIN SHEAR STRESS

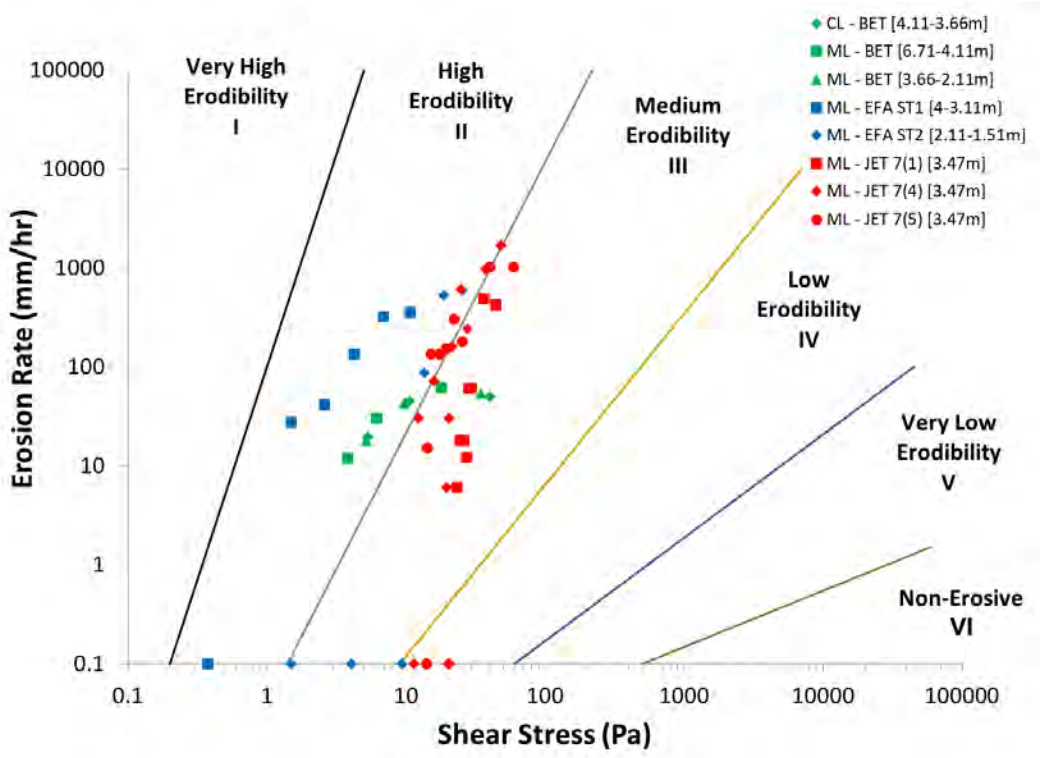

FIGURE 104 – SACRAMENTO RIVER SITE 7 (SAC7) – SILT AND LEAN CLAY (USCS ML, CL) – GRAIN SHEAR STRESS

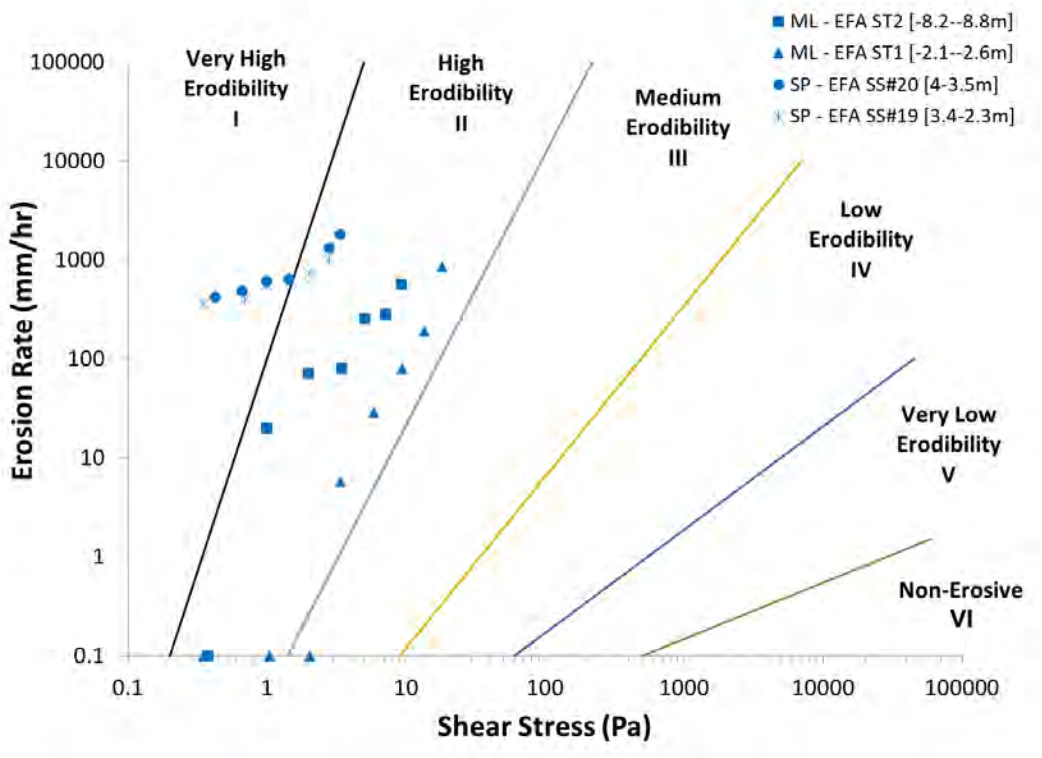

FIGURE 105 – SACRAMENTO RIVER SITE 8 (SAC8) – OTHER USCS CLASSIFICATIONS – GRAIN SHEAR STRESS

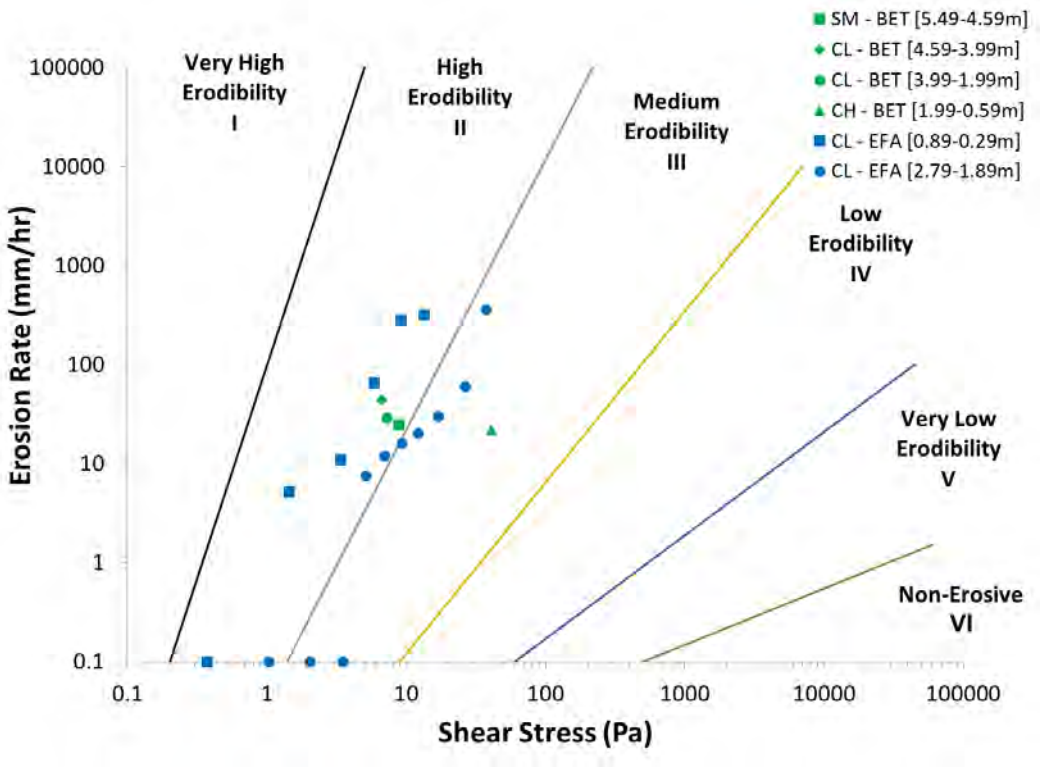

FIGURE 106 – SACRAMENTO RIVER SITE 9 (SAC9) – OTHER USCS CLASSIFICATIONS – GRAIN SHEAR STRESS

APPENDIX C

Erosion functions are generally non-linear as they cover different erosion regimes (Papanicolaou et al., 2017): (1) particle-by-particle at low excess shear stress, (2) mass erosion when applied shear stress exceeds a critical shear stress to entrain aggregates and clods, and (3) limited detachment because of large sediment concentrations near the soil surface at very large shear stresses. EFA data were filtered based on interpreted erosion regimes in order to regress erosion of the second regime. Table 10 provides results of the filter in a simple Boolean format.

TABLE 10 – EFA FILTER RESULTS BY DATA POINT.

EFA Test ID	Shear stress (Pa)	Erosion rate (mm hr^{-1})	Data used for regression (Y/N)
2F-19-LAR6A-ST1 34-35ft	0.4	27.3	N
2F-19-LAR6A-ST1 34-35ft	0.7	132	N
2F-19-LAR6A-ST1 34-35ft	0.8	86.7	N
2F-19-LAR6A-ST1 34-35ft	1.6	128.6	Y
2F-19-LAR6A-ST1 34-35ft	2.3	400	Y
2F-19-LAR6A-ST1 34-35ft	3.6	480	Y
2F-19-LAR9A-ST2 11-13ft	0.4	0	Y
2F-19-LAR9A-ST2 11-13ft	0.7	33	Y
2F-19-LAR9A-ST2 11-13ft	1	68.2	Y
2F-19-LAR9A-ST2 11-13ft	1.4	150	Y
2F-19-LAR9A-ST2 11-13ft	2.9	540	Y
2F-19-LAR9A-ST2 11-13ft	6.2	860	Y
2F-19-SAC7A-ST1 9-11ft	0.3	0	N
2F-19-SAC7A-ST1 9-11ft	1.6	27.3	N
2F-19-SAC7A-ST1 9-11ft	2.8	40.9	Y
2F-19-SAC7A-ST1 9-11ft	4.5	132.9	Y
2F-19-SAC7A-ST1 9-11ft	7.3	320	Y
2F-19-SAC7A-ST1 9-11ft	11.3	356	N
2F-19-SAC7A-ST2 15-17ft	0.3	0	N
2F-19-SAC7A-ST2 15-17ft	1	0	N
2F-19-SAC7A-ST2 15-17ft	3.4	0	N
2F-19-SAC7A-ST2 15-17ft	8.4	0	Y
2F-19-SAC7A-ST2 15-17ft	14.3	87.3	Y
2F-19-SAC7A-ST2 15-17ft	19.7	528	Y
2F-19-SAC7A-ST2 15-17ft	26.9	590	Y
2F-19-LAR9A-ST1 9-11ft	0.4	0	Y
2F-19-LAR9A-ST1 9-11ft	1.2	30	Y
2F-19-LAR9A-ST1 9-11ft	1.7	96	Y

EFA Test ID	Shear stress (Pa)	Erosion rate (mm hr^{-1})	Data used for regression (Y/N)
2F-19-LAR9A-ST1 9-11ft	2.2	100	Y
2F-19-LAR9A-ST1 9-11ft	3.6	205.7	Y
2F-19-LAR9A-ST1 9-11ft	6.3	270	N
2F-19-LAR9A_Sand sample #9	0.3	0	N
2F-19-LAR9A_Sand sample #9	1	0	N
2F-19-LAR9A_Sand sample #9	8.3	72	N
2F-19-LAR9A_Sand sample #9	12	105	N
2F-19-LAR9A_Sand sample #9	18.9	125.5	Y
2F-19-LAR9A_Sand sample #9	31.1	780	Y
2F-19-LAR7A_Sand Sample #7	0.4	0	N
2F-19-LAR7A_Sand Sample #7	1.1	49.1	N
2F-19-LAR7A_Sand Sample #7	2.8	73.3	N
2F-19-LAR7A_Sand Sample #7	5.3	102.9	Y
2F-19-LAR7A_Sand Sample #7	8.1	285	Y
2F-19-LAR7A_Sand Sample #7	12.2	500	Y
2F-19-LAR9A_Sand Sample #8	0.3	0	N
2F-19-LAR9A_Sand Sample #8	1.4	60	N
2F-19-LAR9A_Sand Sample #8	3.5	60	N
2F-19-LAR9A_Sand Sample #8	4.5	73.3	N
2F-19-LAR9A_Sand Sample #8	7.7	105	N
2F-19-LAR9A_Sand Sample #8	10.9	130	Y
2F-19-LAR9A_Sand Sample #8	14.3	315	Y
2F-19-LAR7A_Sand Sample #4	0.3	0	Y
2F-19-LAR7A_Sand Sample #4	1	30	Y
2F-19-LAR7A_Sand Sample #4	2.1	46.7	Y
2F-19-LAR7A_Sand Sample #4	3.7	75	Y
2F-19-LAR7A_Sand Sample #4	5.6	180	Y
2F-19-LAR7A_Sand Sample #4	9.3	230	N
2F-19-LAR7A_Sand Sample #4	14	255	N
2F-19-LAR6A_Sand Sample #10	0.4	0	N
2F-19-LAR6A_Sand Sample #10	0.6	21.8	N
2F-19-LAR6A_Sand Sample #10	0.9	257.1	N
2F-19-LAR6A_Sand Sample #10	1.3	270	Y
2F-19-LAR6A_Sand Sample #10	1.8	580	Y
2F-19-LAR6A_Sand Sample #10	2.3	1140	Y
2F-19-LAR7A-Sand Sample #5 19-22.5 ft	0.3	19.2	N

EFA Test ID	Shear stress (Pa)	Erosion rate (mm hr^{-1})	Data used for regression (Y/N)
2F-19-LAR7A-Sand Sample #5 19-22.5 ft	0.6	120	N
2F-19-LAR7A-Sand Sample #5 19-22.5 ft	0.8	150	Y
2F-19-LAR7A-Sand Sample #5 19-22.5 ft	1.2	450	Y
2F-19-LAR7A-Sand Sample #5 19-22.5 ft	1.5	900	Y
2F-19-LAR1A-Sand Sample #12 13-22.5 ft	0.4	0	N
2F-19-LAR1A-Sand Sample #12 13-22.5 ft	1.2	6	Y
2F-19-LAR1A-Sand Sample #12 13-22.5 ft	2.2	63.2	Y
2F-19-LAR1A-Sand Sample #12 13-22.5 ft	3.6	75.8	Y
2F-19-LAR1A-Sand Sample #12 13-22.5 ft	5.5	171.4	Y
2F-19-LAR1A-Sand Sample #12 13-22.5 ft	7.4	195	Y
2F-19-LAR12A-Sand Sample #1 7-14 ft	0.4	24	N
2F-19-LAR12A-Sand Sample #1 7-14 ft	0.6	111.4	N
2F-19-LAR12A-Sand Sample #1 7-14 ft	1.4	400	N
2F-19-LAR12A-Sand Sample #1 7-14 ft	2.2	440	N
2F-19-LAR12A-Sand Sample #1 7-14 ft	3	540	Y
2F-19-LAR12A-Sand Sample #1 7-14 ft	4.5	2160	Y
2F-19-LAR7A-Sand Sample #3 1-6.5 ft	0.3	0	N
2F-19-LAR7A-Sand Sample #3 1-6.5 ft	0.6	17.1	N
2F-19-LAR7A-Sand Sample #3 1-6.5 ft	0.8	340	N
2F-19-LAR7A-Sand Sample #3 1-6.5 ft	1.2	390	N
2F-19-LAR7A-Sand Sample #3 1-6.5 ft	1.7	570	Y
2F-19-LAR7A-Sand Sample #3 1-6.5 ft	2	1560	Y
2F-19-LAR7A-Sand Sample #6 23-26 ft	0.4	19.2	N
2F-19-LAR7A-Sand Sample #6 23-26 ft	1	126	N
2F-19-LAR7A-Sand Sample #6 23-26 ft	1.5	260	Y
2F-19-LAR7A-Sand Sample #6 23-26 ft	1.8	480	Y
2F-19-LAR7A-Sand Sample #6 23-26 ft	2.3	440	Y
2F-19-LAR7A-Sand Sample #6 23-26 ft	2.8	1120	Y
2F-19-LAR12A-Sand Sample #2 19-24.5 ft	0.4	84	N
2F-19-LAR12A-Sand Sample #2 19-24.5 ft	0.7	102.9	Y
2F-19-LAR12A-Sand Sample #2 19-24.5 ft	1.2	440	Y
2F-19-LAR12A-Sand Sample #2 19-24.5 ft	2	936	Y
2F-19-LAR12A-Sand Sample #2 19-24.5 ft	2.2	1320	Y
2F-19-SAC5A 53-55 ft	0.5	0	N
2F-19-SAC5A 53-55 ft	2	6.3	N
2F-19-SAC5A 53-55 ft	5.6	7.1	N

EFA Test ID	Shear stress (Pa)	Erosion rate (mm hr^{-1})	Data used for regression (Y/N)
2F-19-SAC5A 53-55 ft	15.7	11.4	Y
2F-19-SAC5A 53-55 ft	24.1	72	Y
2F-19-SAC5A 53-55 ft	41.3	222.9	Y
2F-19-SAC5A 53-55 ft	55.7	260	Y
2F-19-SAC8A 47-49 ft	0.4	0	N
2F-19-SAC8A 47-49 ft	1.4	20	N
2F-19-SAC8A 47-49 ft	4	70.6	N
2F-19-SAC8A 47-49 ft	9	80	Y
2F-19-SAC8A 47-49 ft	15.7	255	Y
2F-19-SAC8A 47-49 ft	27.5	280	Y
2F-19-SAC8A 47-49 ft	24.1	560	Y
2F-19-SAC8A-ST1 27-28.67 ft	0.3	0	N
2F-19-SAC8A-ST1 27-28.67 ft	0.8	0	N
2F-19-SAC8A-ST1 27-28.67 ft	1.6	0	N
2F-19-SAC8A-ST1 27-28.67 ft	3.6	5.7	N
2F-19-SAC8A-ST1 27-28.67 ft	10.1	28.6	N
2F-19-SAC8A-ST1 27-28.67 ft	24.5	80	N
2F-19-SAC8A-ST1 27-28.67 ft	35.6	189.2	Y
2F-19-SAC8A-ST1 27-28.67 ft	47	860	Y
2F-19-SAC9A-ST2 15-17 ft	0.4	0	N
2F-19-SAC9A-ST2 15-17 ft	2.3	5.2	N
2F-19-SAC9A-ST2 15-17 ft	6.9	10.9	N
2F-19-SAC9A-ST2 15-17 ft	15.4	65.5	Y
2F-19-SAC9A-ST2 15-17 ft	24.1	280	Y
2F-19-SAC9A-ST2 15-17 ft	35.2	315	Y
2F-19-SAC1A-ST6 29-31 ft	0.3	0	N
2F-19-SAC1A-ST6 29-31 ft	1	0	N
2F-19-SAC1A-ST6 29-31 ft	2	0	N
2F-19-SAC1A-ST6 29-31 ft	3.4	0	N
2F-19-SAC1A-ST6 29-31 ft	12.2	13.8	Y
2F-19-SAC1A-ST6 29-31 ft	20.2	52.2	Y
2F-19-SAC1A-ST6 29-31 ft	24.2	3000	N
2F-19-SAC1A-ST6 29-31 ft	36.4	192	Y
2F-19-SAC1A-ST6 29-31 ft	46.5	346.7	Y
2F-19-SAC9A-ST1 9-11 ft	0.3	0	N
2F-19-SAC9A-ST1 9-11 ft	0.9	0	N

EFA Test ID	Shear stress (Pa)	Erosion rate (mm hr^{-1})	Data used for regression (Y/N)
2F-19-SAC9A-ST1 9-11 ft	2.2	0	N
2F-19-SAC9A-ST1 9-11 ft	3.8	0	N
2F-19-SAC9A-ST1 9-11 ft	5.4	7.5	N
2F-19-SAC9A-ST1 9-11 ft	7.4	12	N
2F-19-SAC9A-ST1 9-11 ft	12.4	16	N
2F-19-SAC9A-ST1 9-11 ft	16.1	20	N
2F-19-SAC9A-ST1 9-11 ft	26	30	N
2F-19-SAC9A-ST1 9-11 ft	45.2	60	Y
2F-19-SAC9A-ST1 9-11 ft	64.1	360	Y
2F-19-SAC1A-ST2 11-13 ft	0.9	0	N
2F-19-SAC1A-ST2 11-13 ft	3	0	N
2F-19-SAC1A-ST2 11-13 ft	6.2	10.9	N
2F-19-SAC1A-ST2 11-13 ft	16.1	27.3	Y
2F-19-SAC1A-ST2 11-13 ft	21.8	54.5	Y
2F-19-SAC1A-ST2 11-13 ft	31.9	120	Y
2F-19-SAC1A-ST2 11-13 ft	43.4	156	Y
2F-19-SAC1A-ST2 11-13 ft	56.7	380	Y
2F-19-LAR6A-Sand Sample #11 19.7-29.7 ft	1	30	N
2F-19-LAR6A-Sand Sample #11 19.7-29.7 ft	4.2	260	N
2F-19-LAR6A-Sand Sample #11 19.7-29.7 ft	7.3	420	N
2F-19-LAR6A-Sand Sample #11 19.7-29.7 ft	10.9	480	Y
2F-19-LAR6A-Sand Sample #11 19.7-29.7 ft	16.5	720	Y
2F-19-LAR6A-Sand Sample #11 19.7-29.7 ft	21	1020	Y
2F-19-LAR10A-Sand Sample #16 29-32.5 ft	0.3	8.9	Y
2F-19-LAR10A-Sand Sample #16 29-32.5 ft	1.2	180	Y
2F-19-LAR10A-Sand Sample #16 29-32.5 ft	2.2	384	Y
2F-19-LAR10A-Sand Sample #16 29-32.5 ft	2.8	570	Y
2F-19-LAR10A-Sand Sample #16 29-32.5 ft	3.5	680	Y
2F-19-LAR10A-Sand Sample #16 29-32.5 ft	4.5	720	Y
2F-19-LAR10A-Sand Sample #16 29-32.5 ft	5.6	840	N
2F-19-LAR3A-Sand Sample #18 11-16.5 ft	0.4	10.9	N
2F-19-LAR3A-Sand Sample #18 11-16.5 ft	0.7	60	Y
2F-19-LAR3A-Sand Sample #18 11-16.5 ft	1.5	520	Y
2F-19-LAR3A-Sand Sample #18 11-16.5 ft	2.2	800	Y
2F-19-LAR3A-Sand Sample #18 11-16.5 ft	2.8	1160	Y
2F-19-LAR3A-Sand Sample #18 11-16.5 ft	3.4	1320	Y

EFA Test ID	Shear stress (Pa)	Erosion rate (mm hr^{-1})	Data used for regression (Y/N)
2F-19-LAR10A-Sand Sample #14 25-28.5 ft	0.6	30	Y
2F-19-LAR10A-Sand Sample #14 25-28.5 ft	1.6	300	Y
2F-19-LAR10A-Sand Sample #14 25-28.5 ft	2.4	420	Y
2F-19-LAR10A-Sand Sample #14 25-28.5 ft	3.4	660	Y
2F-19-LAR10A-Sand Sample #14 25-28.5 ft	3.4	552	N
2F-19-LAR10A-Sand Sample #14 25-28.5 ft	4.9	880	Y
2F-19-LAR4A-Sand Sample #24 17-22.5 ft	0.5	22.9	Y
2F-19-LAR4A-Sand Sample #24 17-22.5 ft	0.9	120	Y
2F-19-LAR4A-Sand Sample #24 17-22.5 ft	1.3	240	Y
2F-19-LAR4A-Sand Sample #24 17-22.5 ft	2.2	600	Y
2F-19-LAR4A-Sand Sample #24 17-22.5 ft	2.9	780	Y
2F-19-LAR4A-Sand Sample #24 17-22.5 ft	3.7	960	Y
2F-19-LAR4A-Sand Sample #24 17-22.5 ft	4.4	1200	Y
2F-19-LARA1-Sand Sample #13 23-26.5 ft	0.6	0	N
2F-19-LARA1-Sand Sample #13 23-26.5 ft	1.2	14.1	N
2F-19-LARA1-Sand Sample #13 23-26.5 ft	3.4	72	Y
2F-19-LARA1-Sand Sample #13 23-26.5 ft	4.3	264	Y
2F-19-LARA1-Sand Sample #13 23-26.5 ft	6.3	330	Y
2F-19-LARA1-Sand Sample #13 23-26.5 ft	8.9	540	Y
2F-19-LARA1-Sand Sample #13 23-26.5 ft	11.6	600	Y
2F-19-LAR5A-Sand Sample #25 27-30 ft	0.7	0	N
2F-19-LAR5A-Sand Sample #25 27-30 ft	1.6	0	N
2F-19-LAR5A-Sand Sample #25 27-30 ft	3	0	N
2F-19-LAR5A-Sand Sample #25 27-30 ft	7	11.4	N
2F-19-LAR5A-Sand Sample #25 27-30 ft	12.2	165	N
2F-19-LAR5A-Sand Sample #25 27-30 ft	20.9	180	Y
2F-19-LAR5A-Sand Sample #25 27-30 ft	28.1	1000	Y
2F-19-LAR5A-Sand Sample #25 27-30 ft	34.9	2940	Y
2F-19-LAR5A-Sand Sample #25 27-30 ft	54.7	3720	Y
2F-19-LAR3A-Sand Sample #17 7-10.5 ft	0.6	120	Y
2F-19-LAR3A-Sand Sample #17 7-10.5 ft	1.2	400	Y
2F-19-LAR3A-Sand Sample #17 7-10.5 ft	1.6	480	Y
2F-19-LAR3A-Sand Sample #17 7-10.5 ft	2.1	540	Y
2F-19-LAR3A-Sand Sample #17 7-10.5 ft	3	720	Y
2F-19-LAR3A-Sand Sample #17 7-10.5 ft	3.7	760	Y
2F-19-LAR3A-Sand Sample #17 7-10.5 ft	4.5	2120	Y

EFA Test ID	Shear stress (Pa)	Erosion rate (mm hr^{-1})	Data used for regression (Y/N)
2F-19-SAC8A-Sand Sample #19 9-12.5 ft	0.4	360	N
2F-19-SAC8A-Sand Sample #19 9-12.5 ft	0.8	400	N
2F-19-SAC8A-Sand Sample #19 9-12.5 ft	1.1	560	N
2F-19-SAC8A-Sand Sample #19 9-12.5 ft	1.6	600	N
2F-19-SAC8A-Sand Sample #19 9-12.5 ft	2.2	720	Y
2F-19-SAC8A-Sand Sample #19 9-12.5 ft	3	1020	Y
2F-19-SAC8A-Sand Sample #20 7-8.5 ft	0.5	420	N
2F-19-SAC8A-Sand Sample #20 7-8.5 ft	0.7	480	N
2F-19-SAC8A-Sand Sample #20 7-8.5 ft	1.1	600	N
2F-19-SAC8A-Sand Sample #20 7-8.5 ft	1.6	640	Y
2F-19-SAC8A-Sand Sample #20 7-8.5 ft	3	1320	Y
2F-19-SAC8A-Sand Sample #20 7-8.5 ft	3.6	1800	Y
2F-19-SAC3A-Sand Sample #21 5-8.5 ft	0.5	360	N
2F-19-SAC3A-Sand Sample #21 5-8.5 ft	0.9	400	N
2F-19-SAC3A-Sand Sample #21 5-8.5 ft	1.4	440	N
2F-19-SAC3A-Sand Sample #21 5-8.5 ft	2	480	Y
2F-19-SAC3A-Sand Sample #21 5-8.5 ft	2.7	720	Y
2F-19-SAC3A-Sand Sample #21 5-8.5 ft	3.2	1200	Y
2F-19-SAC3A-Sand Sample #22 15-16.5 ft	0.5	4.6	N
2F-19-SAC3A-Sand Sample #22 15-16.5 ft	1.4	171.4	N
2F-19-SAC3A-Sand Sample #22 15-16.5 ft	3.3	300	Y
2F-19-SAC3A-Sand Sample #22 15-16.5 ft	3.4	630	Y
2F-19-SAC3A-Sand Sample #22 15-16.5 ft	5.2	800	Y
2F-19-SAC3A-Sand Sample #22 15-16.5 ft	7	1440	Y
2F-19-SAC5A-Sand Sample #26 42.5-48 ft	0.5	0	N
2F-19-SAC5A-Sand Sample #26 42.5-48 ft	1.3	0	N
2F-19-SAC5A-Sand Sample #26 42.5-48 ft	2.8	0	N
2F-19-SAC5A-Sand Sample #26 42.5-48 ft	6.7	110.8	Y
2F-19-SAC5A-Sand Sample #26 42.5-48 ft	9	240	Y
2F-19-SAC5A-Sand Sample #26 42.5-48 ft	12	260	Y
2F-19-SAC5A-Sand Sample #26 42.5-48 ft	15.7	171.4	Y
2F-19-SAC5A-Sand Sample #26 42.5-48 ft	19.4	264	Y
2F-19-SAC5A-Sand Sample #26 42.5-48 ft	25	480	Y
2F-19-SAC5A-Sand Sample #26 42.5-48 ft	27.6	720	Y
USACE 2011 - 2F-11-125	0.3	0.0	N
USACE 2011 - 2F-11-125	1.7	0.0	N

EFA Test ID	Shear stress (Pa)	Erosion rate (mm hr^{-1})	Data used for regression (Y/N)
USACE 2011 - 2F-11-125	6.2	2.0	Y
USACE 2011 - 2F-11-125	10.5	11.0	Y
USACE 2011 - 2F-11-125	15.2	18.0	Y
USACE 2011 - 2F-11-125	21.6	70.0	Y
USACE 2011 - 2F-11-126A	2.8	1.5	N
USACE 2011 - 2F-11-126A	14.1	4.0	N
USACE 2011 - 2F-11-126A	38.5	10.0	Y
USACE 2011 - 2F-11-126A	106.6	360.0	Y
USACE 2011 - 2F-11-126B	0.3	0.0	N
USACE 2011 - 2F-11-126B	1.5	1.0	Y
USACE 2011 - 2F-11-126B	4.2	9.0	Y
USACE 2011 - 2F-11-126B	7.6	4.0	Y
USACE 2011 - 2F-11-126B	11.2	25.0	Y
USACE 2011 - 2F-11-126B	13.9	28.0	Y
USACE 2011 - 2F-11-128A	0.3	0.0	N
USACE 2011 - 2F-11-128A	1.4	0.0	N
USACE 2011 - 2F-11-128A	3.6	2.5	Y
USACE 2011 - 2F-11-128A	5.7	16.0	Y
USACE 2011 - 2F-11-128A	7.9	32.0	Y
USACE 2011 - 2F-11-128A	10.5	80.0	Y
USACE 2011 - 2F-11-128B	0.3	0.0	N
USACE 2011 - 2F-11-128B	1.0	2.5	N
USACE 2011 - 2F-11-128B	3.1	6.0	Y
USACE 2011 - 2F-11-128B	4.7	18.0	Y
USACE 2011 - 2F-11-128B	6.5	30.0	Y
USACE 2011 - 2F-11-128B	11.0	102.0	Y
USACE 2011 - 2F-11-129B	1.1	0.0	N
USACE 2011 - 2F-11-129B	4.3	0.3	N
USACE 2011 - 2F-11-129B	9.6	0.5	N
USACE 2011 - 2F-11-129B	13.4	1.0	N
USACE 2011 - 2F-11-129B	27.4	1.0	N
USACE 2011 - 2F-11-129B	39.4	2.0	Y
USACE 2011 - 2F-11-129B	48.5	180.0	Y
USACE 2011 - 2F-11-129C	0.3	0.0	N
USACE 2011 - 2F-11-129C	1.3	0.5	N
USACE 2011 - 2F-11-129C	4.7	1.0	Y

EFA Test ID	Shear stress (Pa)	Erosion rate (mm hr^{-1})	Data used for regression (Y/N)
USACE 2011 - 2F-11-129C	6.6	10.0	Y
USACE 2011 - 2F-11-129C	11.4	18.0	Y
USACE 2011 - 2F-11-129C	14.7	25.0	Y
USACE 2011 - 2F-11-130	0.8	0.3	N
USACE 2011 - 2F-11-130	5.1	0.3	N
USACE 2011 - 2F-11-130	12.4	1.0	N
USACE 2011 - 2F-11-130	27.1	1.0	Y
USACE 2011 - 2F-11-130	41.6	2.0	Y
USACE 2011 - 2F-11-130	96.7	20.0	Y
USACE 2011 - 2F-11-134	0.7	0.0	N
USACE 2011 - 2F-11-134	3.1	1.0	N
USACE 2011 - 2F-11-134	4.8	1.0	N
USACE 2011 - 2F-11-134	13.0	2.5	N
USACE 2011 - 2F-11-134	18.5	4.0	Y
USACE 2011 - 2F-11-134	33.0	16.0	Y
USACE 2011 - 2F-11-134	51.1	30.0	Y
USACE 2011 - 2F-11-135	0.7	0.0	N
USACE 2011 - 2F-11-135	5.4	0.5	Y
USACE 2011 - 2F-11-135	11.0	1.0	Y
USACE 2011 - 2F-11-135	21.0	1.0	Y
USACE 2011 - 2F-11-135	30.3	1.5	Y
USACE 2011 - 2F-11-135	62.4	5.0	Y
USACE 2011 - 2F-11-135	113.7	8.0	Y
USACE 2011 - 2F-11-137 (2)	0.3	1.0	Y
USACE 2011 - 2F-11-137 (2)	0.7	2.0	Y
USACE 2011 - 2F-11-137 (2)	1.5	4.5	Y
USACE 2011 - 2F-11-137 (2)	9.9	18.8	Y
USACE 2011 - 2F-11-137 (2)	19.1	60.0	Y
USACE 2011 - 2F-11-137 (3)	0.8	0.1	Y
USACE 2011 - 2F-11-137 (3)	5.9	0.5	Y
USACE 2011 - 2F-11-137 (3)	11.6	0.5	Y
USACE 2011 - 2F-11-137 (3)	24.7	1.0	Y

APPENDIX D

This Appendix presents the regressions of the excess shear stress equation through all measured erosion functions using both standard linear regression (does not account for measurement uncertainty) and error-in-variables regression (does account for measurement uncertainty).

Jet erosion tests

USACE ERDC jet erosion tests

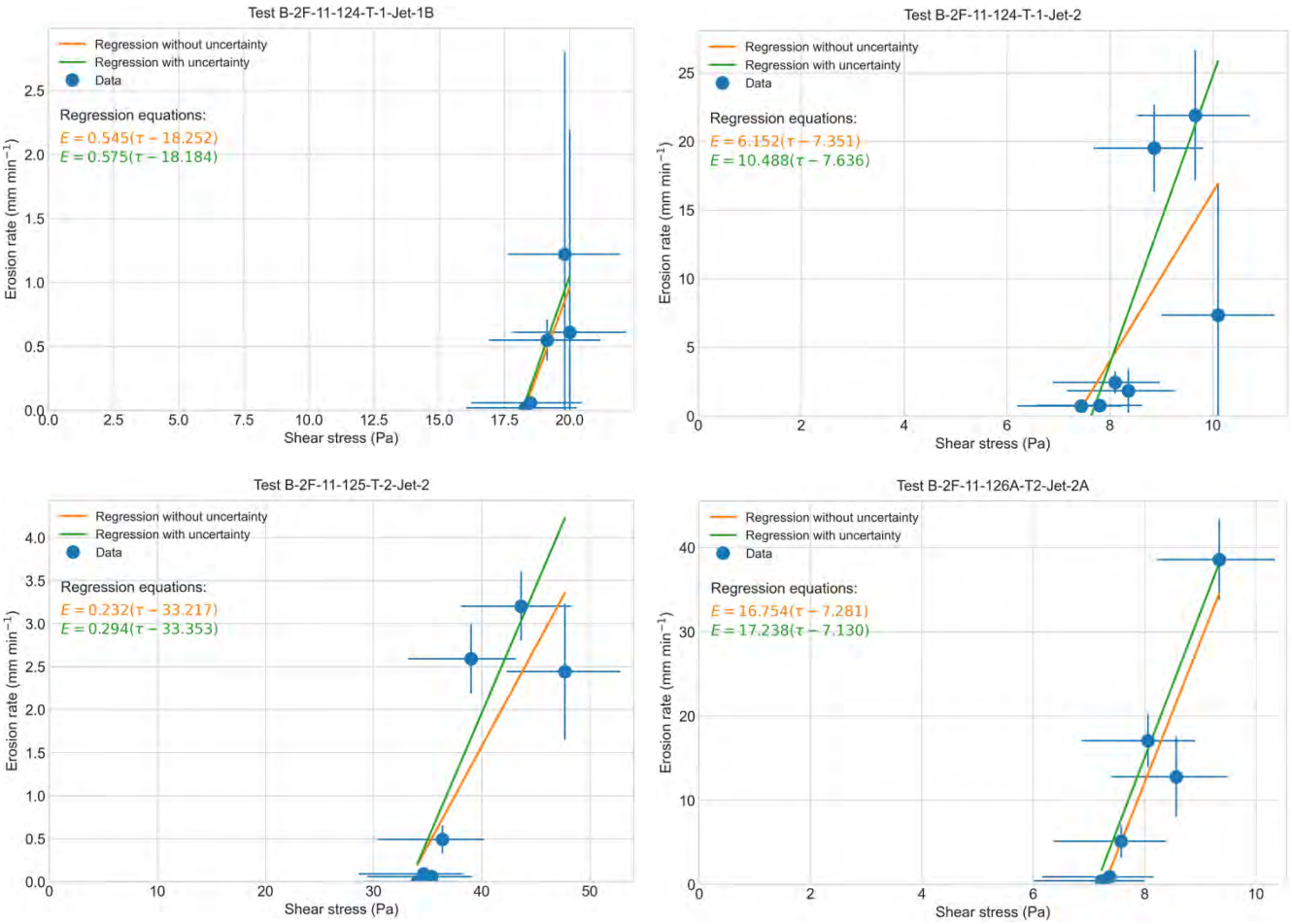

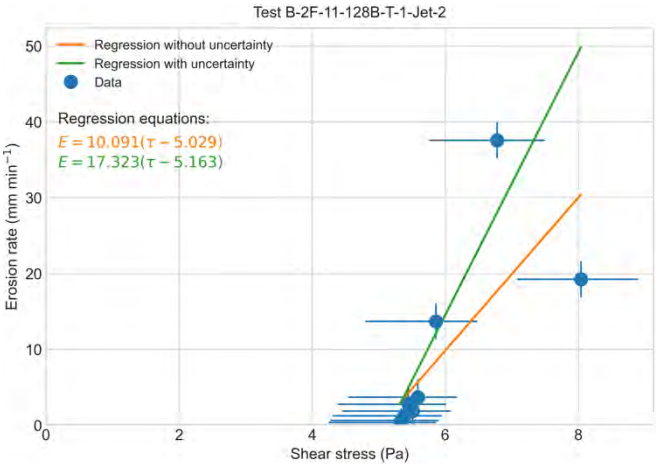

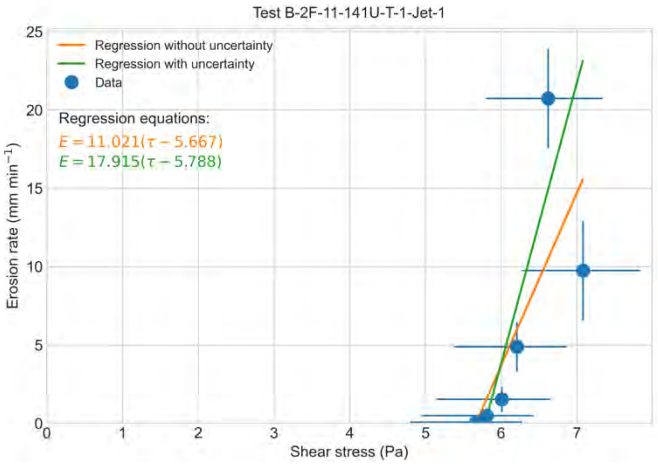

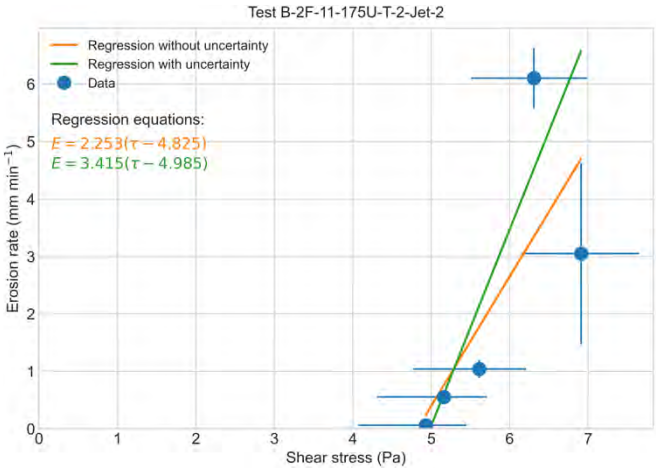

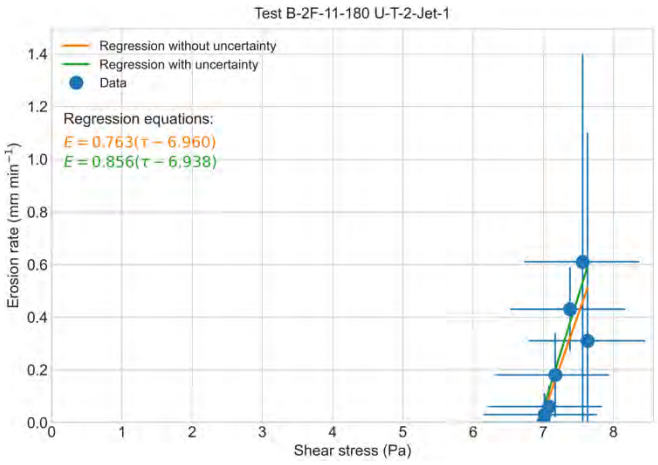

USDA ARS mini-jet erosion tests

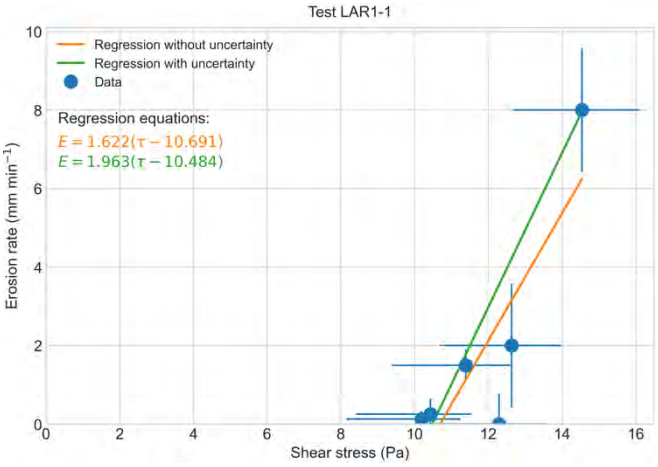

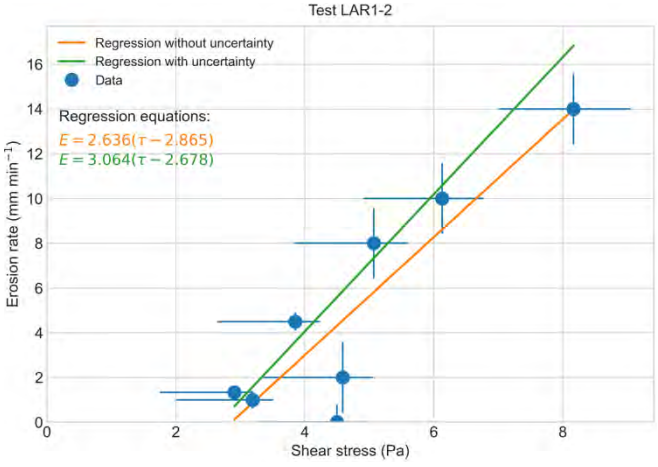

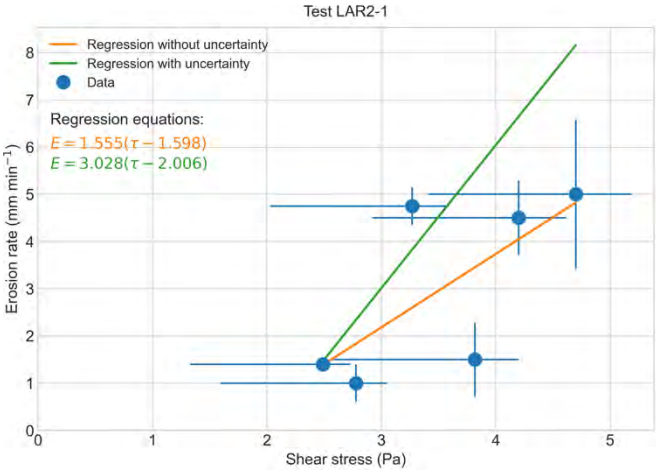
Test LAR2-1
Regression without uncertainty
Regression with uncertainty
Data
Regression equations:
$E = 1.555(\tau - 1.598)$
$E = 3.028(\tau - 2.006)$
Erosion rate (mm min^{-1})
Shear stress (Pa)

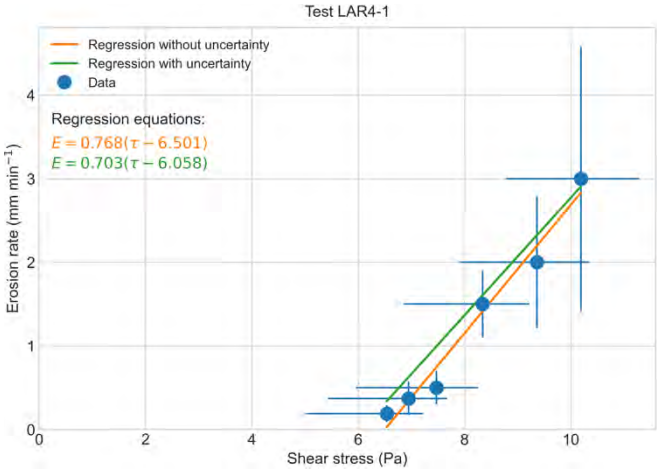
Test LAR4-1
Regression without uncertainty
Regression with uncertainty
Data
Regression equations:
$E = 0.768(\tau - 6.501)$
$E = 0.703(\tau - 6.058)$
Erosion rate (mm min^{-1})
Shear stress (Pa)

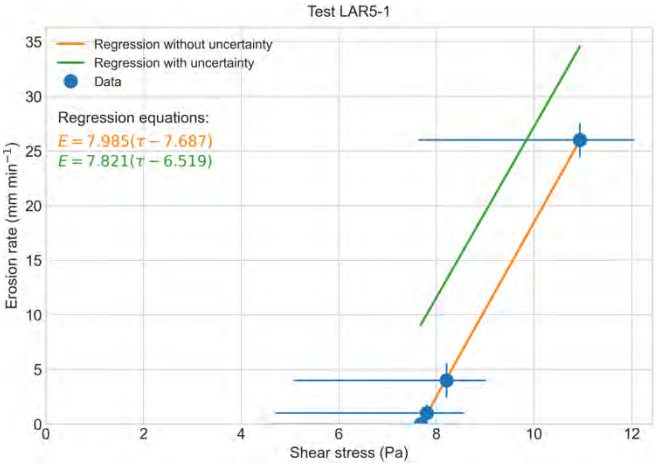
Test LAR5-1
Regression without uncertainty
Regression with uncertainty
Data
Regression equations:
$E = 7.985(\tau - 7.687)$
$E = 7.821(\tau - 6.519)$
Erosion rate (mm min^{-1})
Shear stress (Pa)

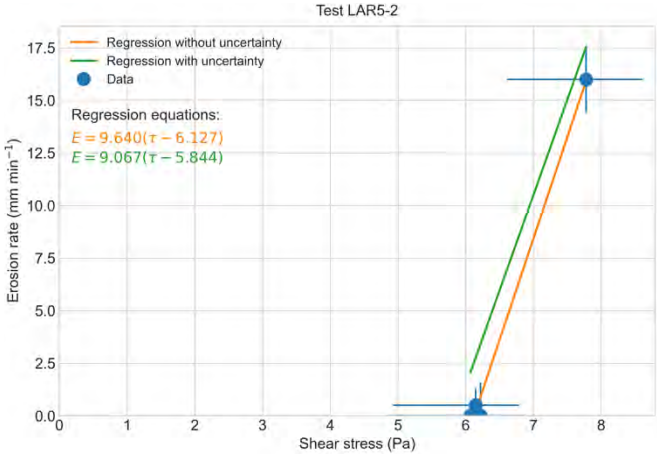
Test LAR5-2
Regression without uncertainty
Regression with uncertainty
Data
Regression equations:
$E = 9.640(\tau - 6.127)$
$E = 9.067(\tau - 5.844)$
Erosion rate (mm min^{-1})
Shear stress (Pa)

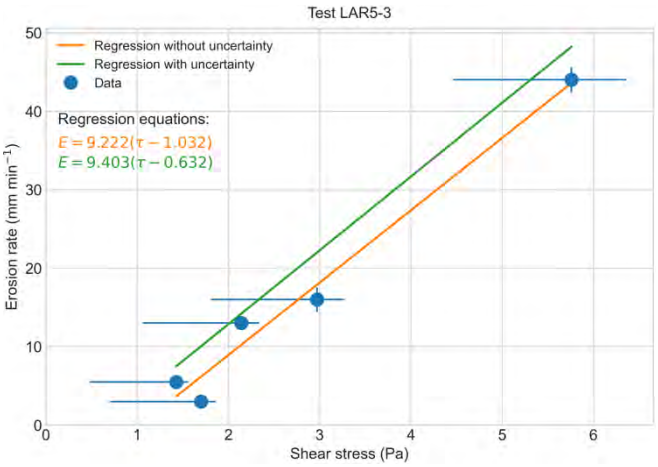
Test LAR5-3
Regression without uncertainty
Regression with uncertainty
Data
Regression equations:
$E = 9.222(\tau - 1.032)$
$E = 9.403(\tau - 0.632)$
Erosion rate (mm min^{-1})
Shear stress (Pa)

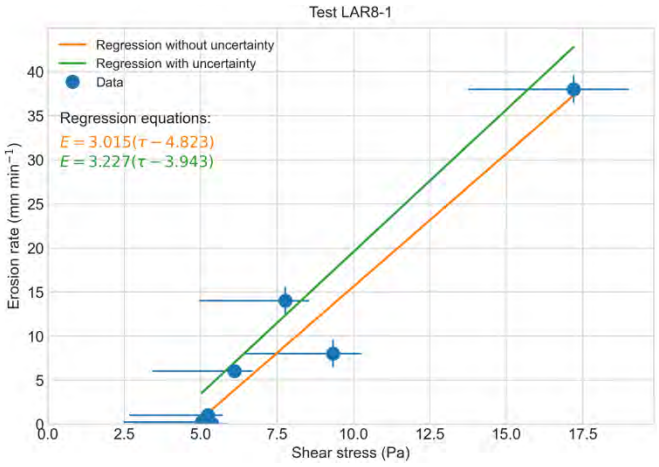
Test LAR8-1
Regression without uncertainty
Regression with uncertainty
Data
Regression equations:
$E = 3.015(\tau - 4.823)$
$E = 3.227(\tau - 3.943)$
Erosion rate (mm min^{-1})
Shear stress (Pa)

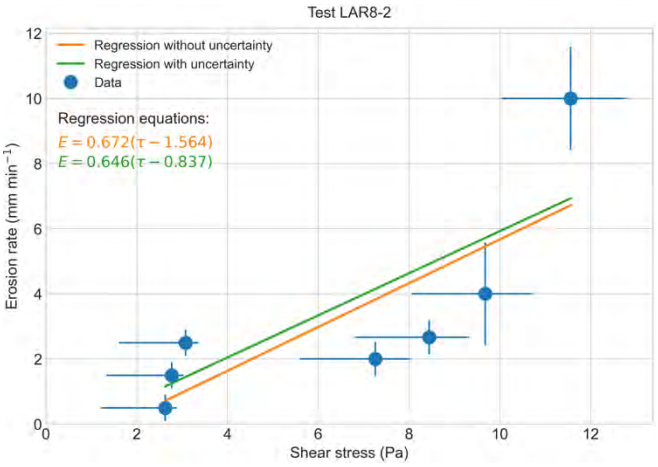
Test LAR8-2
Regression without uncertainty
Regression with uncertainty
Data
Regression equations:
$E = 0.672(\tau - 1.564)$
$E = 0.646(\tau - 0.837)$
Erosion rate (mm min^{-1})
Shear stress (Pa)

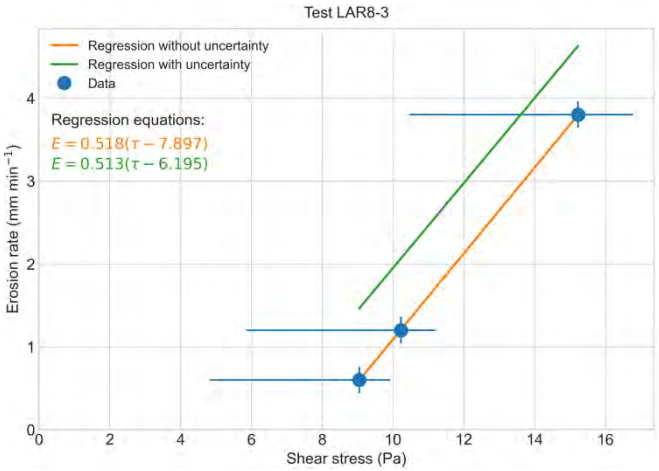
Test LAR8-3
Regression without uncertainty
Regression with uncertainty
Data
Regression equations:
$E = 0.518(\tau - 7.897)$
$E = 0.513(\tau - 6.195)$
Erosion rate (mm min^{-1})
Shear stress (Pa)

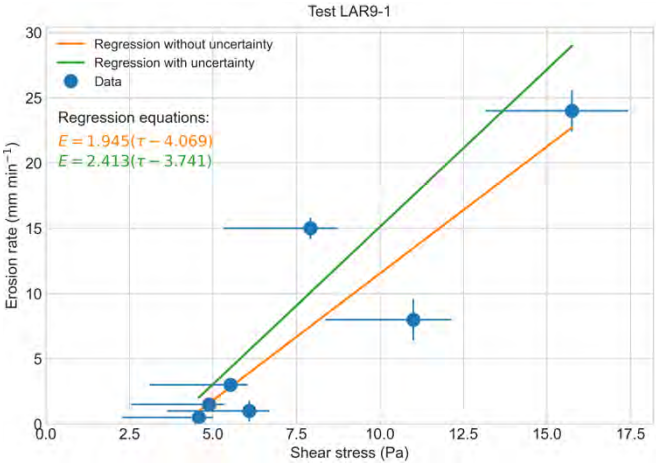
Test LAR9-1
Regression without uncertainty
Regression with uncertainty
Data
Regression equations:
$E = 1.945(\tau - 4.069)$
$E = 2.413(\tau - 3.741)$
Erosion rate (mm min^{-1})
Shear stress (Pa)

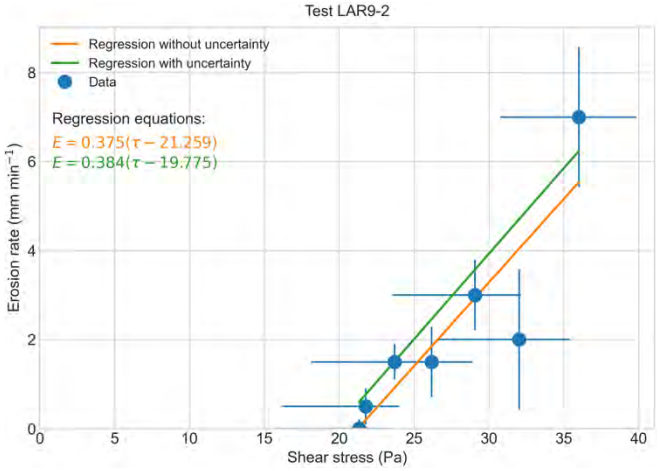
Test LAR9-2
Regression without uncertainty
Regression with uncertainty
Data
Regression equations:
$E = 0.375(\tau - 21.259)$
$E = 0.384(\tau - 19.775)$
Erosion rate (mm min^{-1})
Shear stress (Pa)

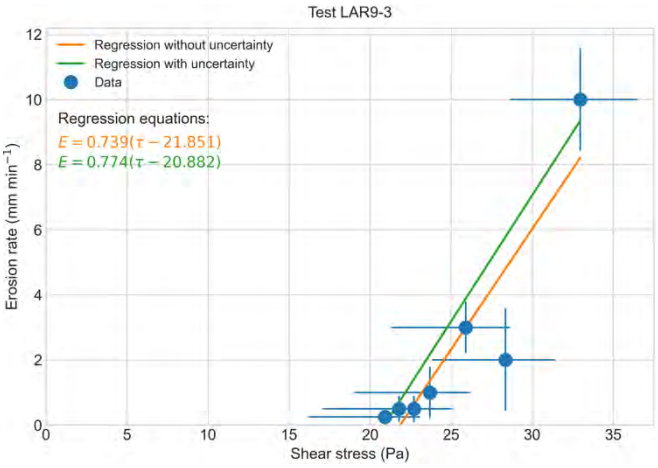
Test LAR9-3
Regression without uncertainty
Regression with uncertainty
Data
Regression equations:
$E = 0.739(\tau - 21.851)$
$E = 0.774(\tau - 20.882)$
Erosion rate (mm min^{-1})
Shear stress (Pa)

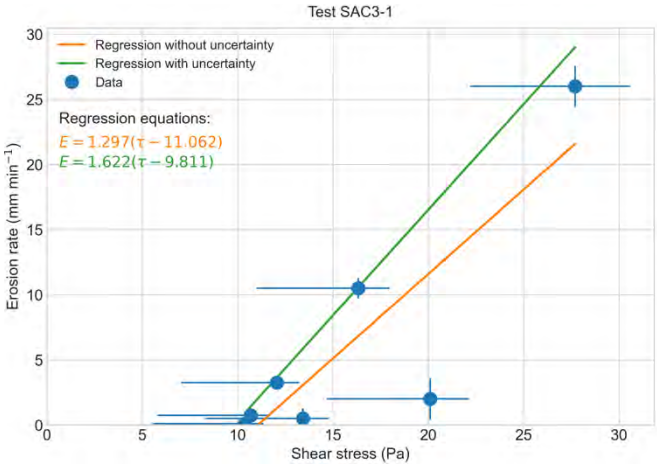
Test SAC3-1
Regression without uncertainty
Regression with uncertainty
Data
Regression equations:
$E = 1.297(\tau - 11.062)$
$E = 1.622(\tau - 9.811)$
Erosion rate (mm min^{-1})
Shear stress (Pa)

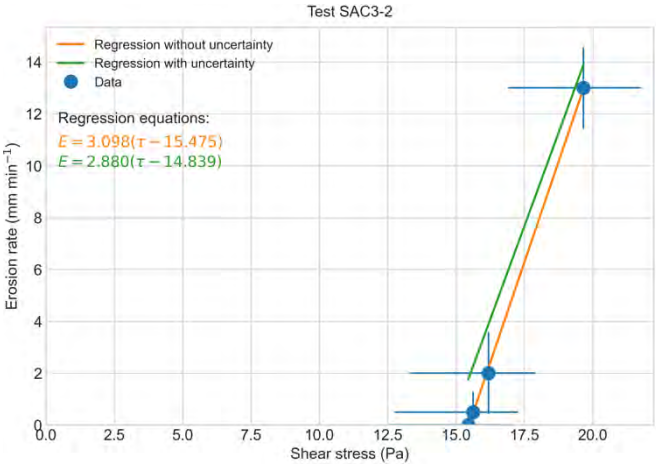
Test SAC3-2
Regression without uncertainty
Regression with uncertainty
Data
Regression equations:
$E = 3.098(\tau - 15.475)$
$E = 2.880(\tau - 14.839)$
Erosion rate (mm min^{-1})
Shear stress (Pa)

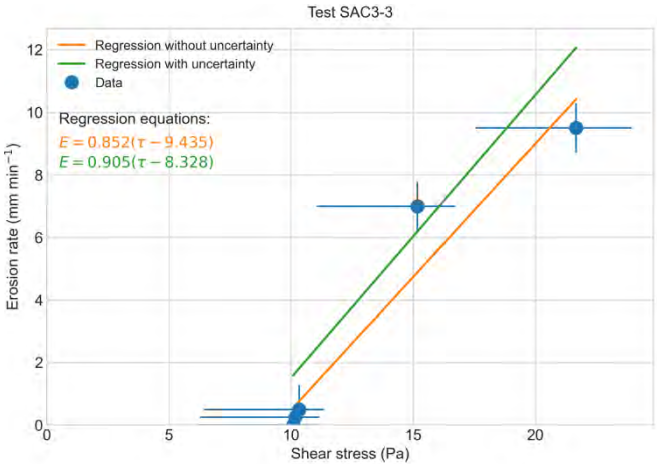
Test SAC3-3
Regression without uncertainty
Regression with uncertainty
Data
Regression equations:
$E = 0.852(\tau - 9.435)$
$E = 0.905(\tau - 8.328)$
Erosion rate (mm min^{-1})
Shear stress (Pa)

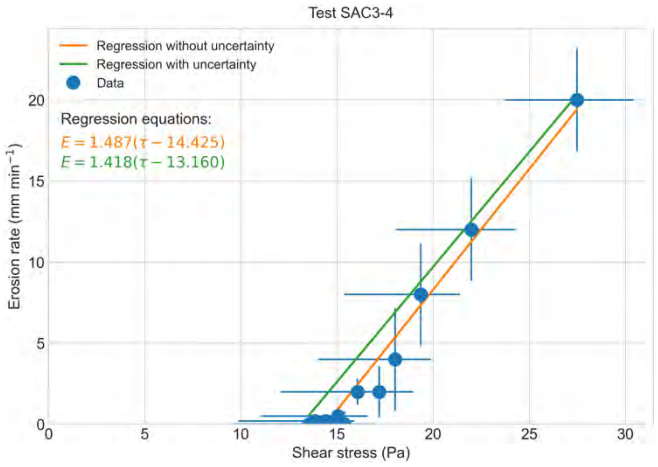
Test SAC3-4
Regression without uncertainty
Regression with uncertainty
Data
Regression equations:
$E = 1.487(\tau - 14.425)$
$E = 1.418(\tau - 13.160)$
Erosion rate (mm min^{-1})
Shear stress (Pa)

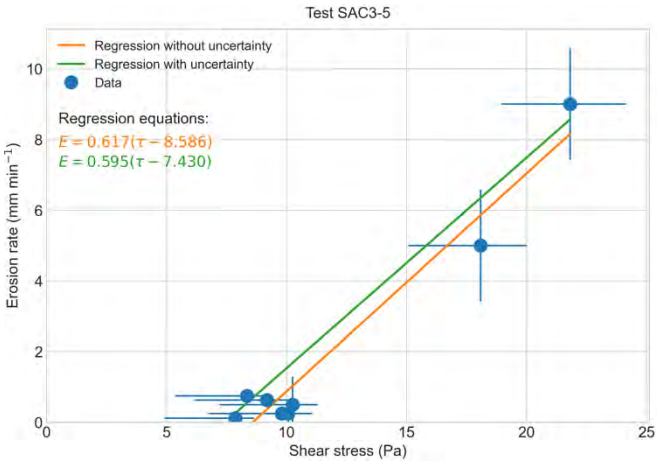
Test SAC3-5
Regression without uncertainty
Regression with uncertainty
Data
Regression equations:
$E = 0.617(\tau - 8.586)$
$E = 0.595(\tau - 7.430)$
Erosion rate (mm min^{-1})
Shear stress (Pa)

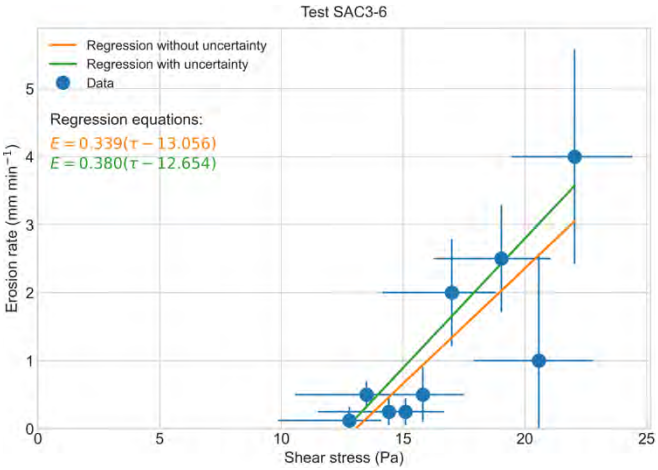
Test SAC3-6
Regression without uncertainty
Regression with uncertainty
Data
Regression equations:
$E = 0.339(\tau - 13.056)$
$E = 0.380(\tau - 12.654)$
Erosion rate (mm min^{-1})
Shear stress (Pa)

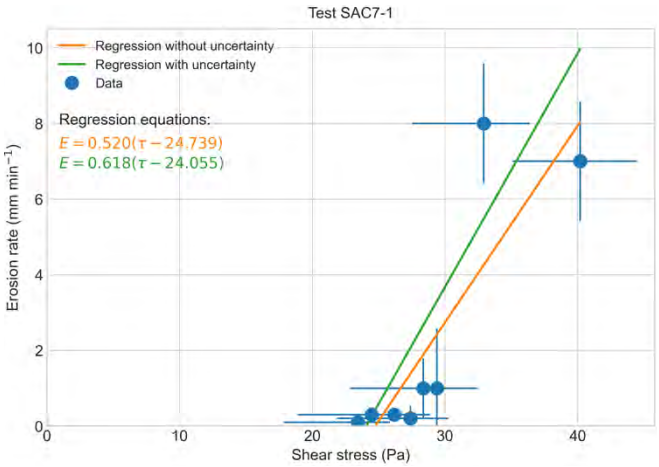
Test SAC7-1
Regression without uncertainty
Regression with uncertainty
Data
Regression equations:
$E = 0.520(\tau - 24.739)$
$E = 0.618(\tau - 24.055)$
Erosion rate (mm min^{-1})
Shear stress (Pa)

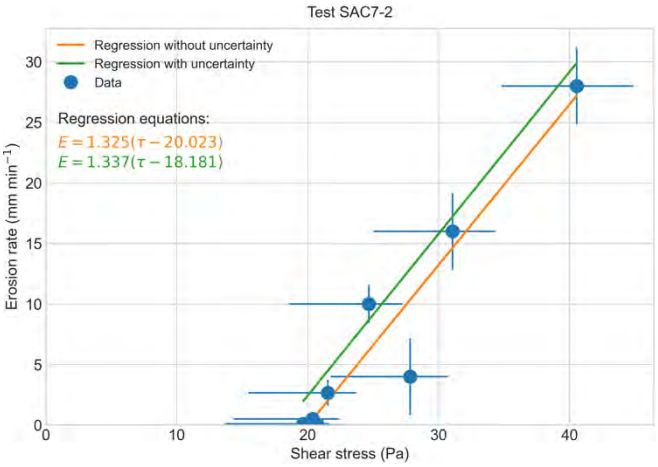

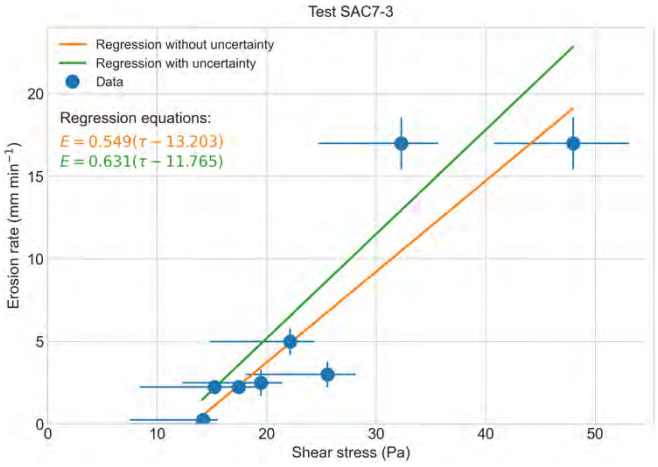

Erosion function apparatus tests – total shear stress

TAMU erosion function apparatus tests

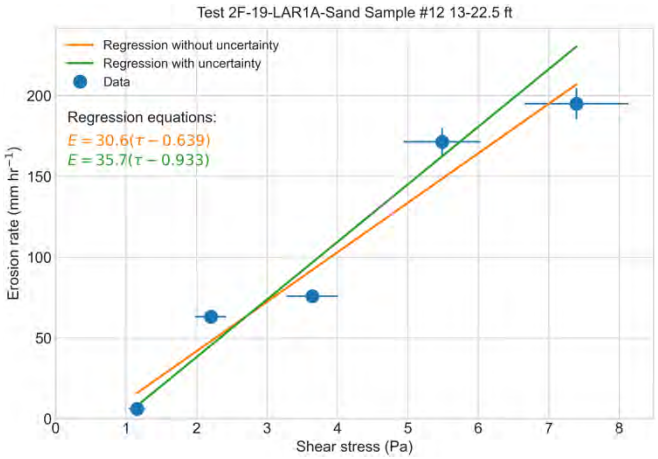

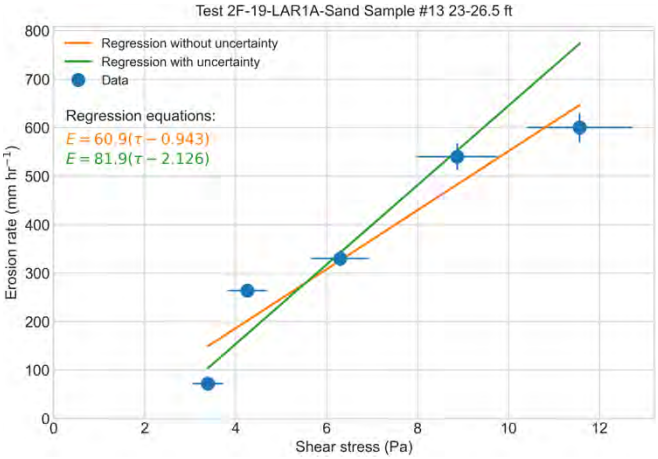

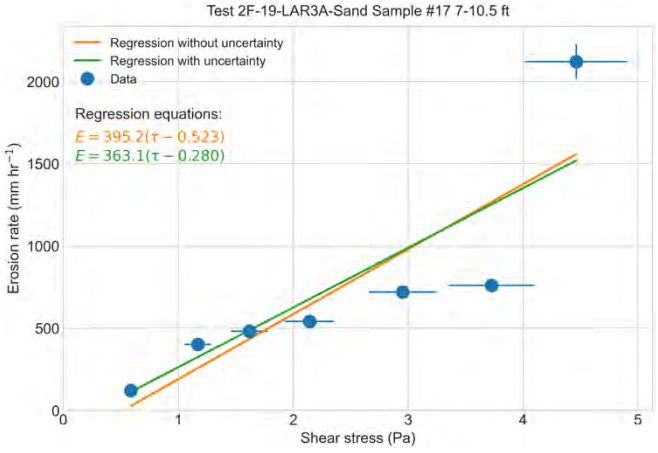

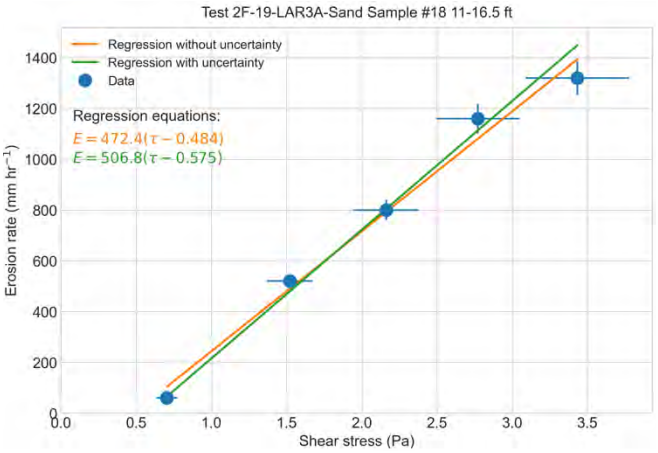

Test 2F-19-LAR4A-Sand Sample #24 17-22.5 ft

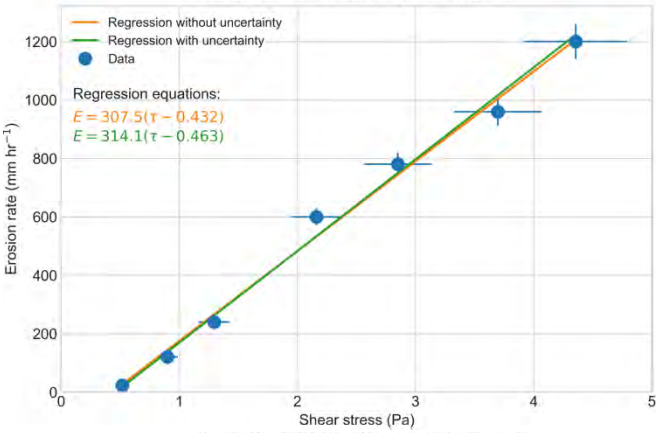

Test 2F-19-LAR6A-Sand Sample #10

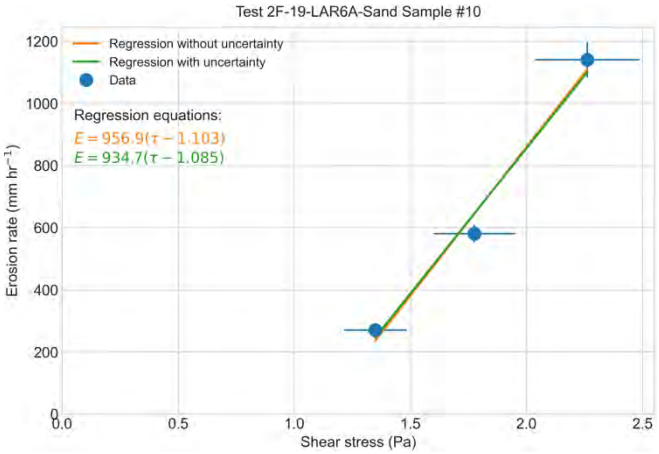

Test 2F-19-LAR6A-Sand Sample #11 19.7-29.7 ft

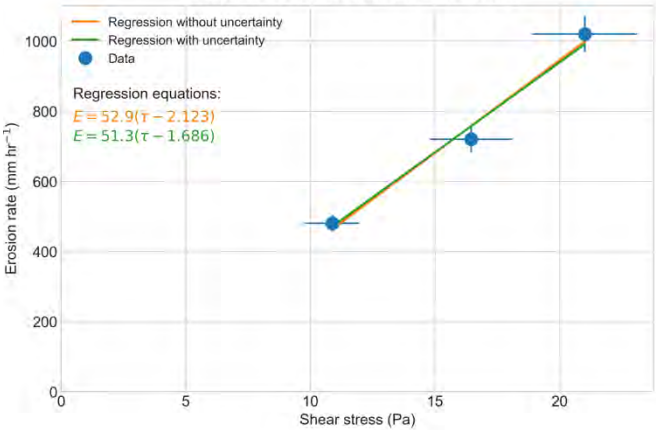

Test 2F-19-LAR6A-ST1 34-35ft

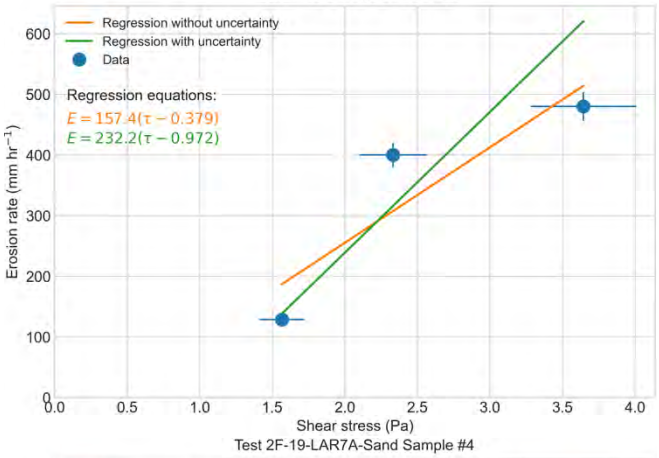

Test 2F-19-LAR7A-Sand Sample #3 1-6.5 ft

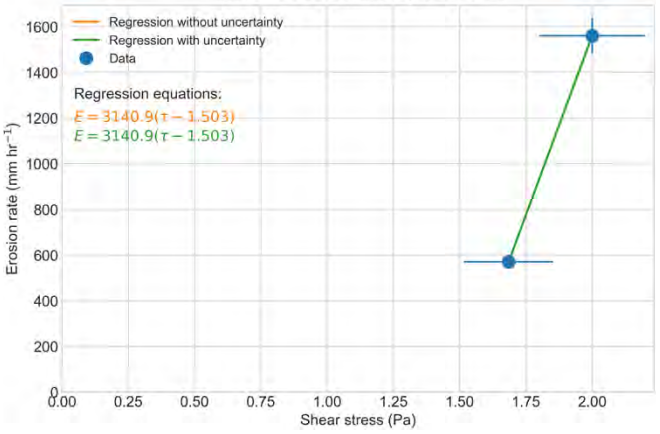

Test 2F-19-LAR7A-Sand Sample #4

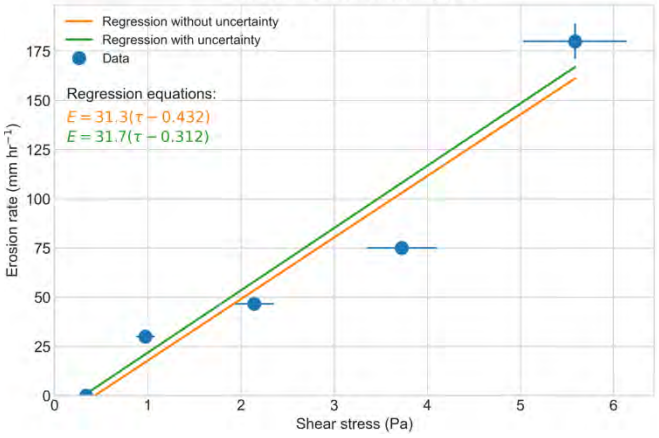

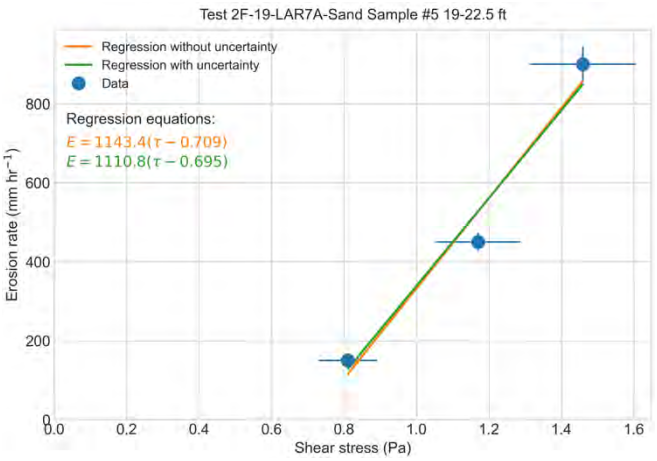
Test 2F-19-LAR7A-Sand Sample #5 19-22.5 ft
Regression without uncertainty
Regression with uncertainty
Data
Regression equations:
$E = 1143.4(\tau - 0.709)$
$E = 1110.8(\tau - 0.695)$
Erosion rate (mm hr^{-1})
Shear stress (Pa)

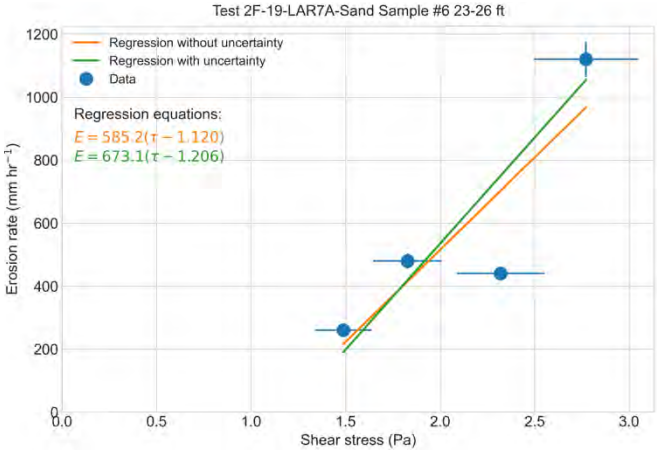
Test 2F-19-LAR7A-Sand Sample #6 23-26 ft
Regression without uncertainty
Regression with uncertainty
Data
Regression equations:
$E = 585.2(\tau - 1.120)$
$E = 673.1(\tau - 1.206)$
Erosion rate (mm hr^{-1})
Shear stress (Pa)

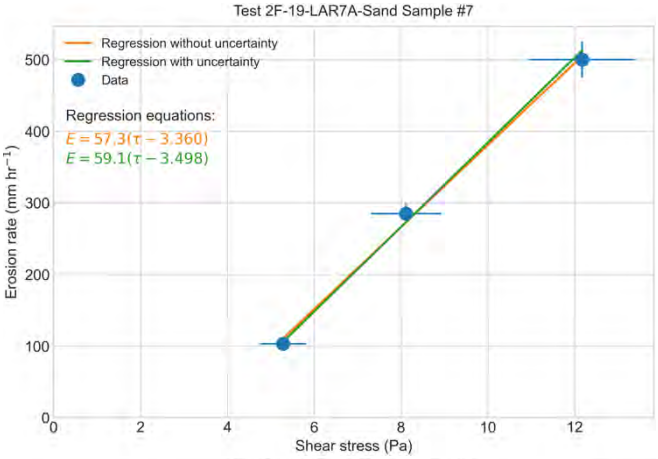
Test 2F-19-LAR7A-Sand Sample #7
Regression without uncertainty
Regression with uncertainty
Data
Regression equations:
$E = 57.3(\tau - 3.360)$
$E = 59.1(\tau - 3.498)$
Erosion rate (mm hr^{-1})
Shear stress (Pa)

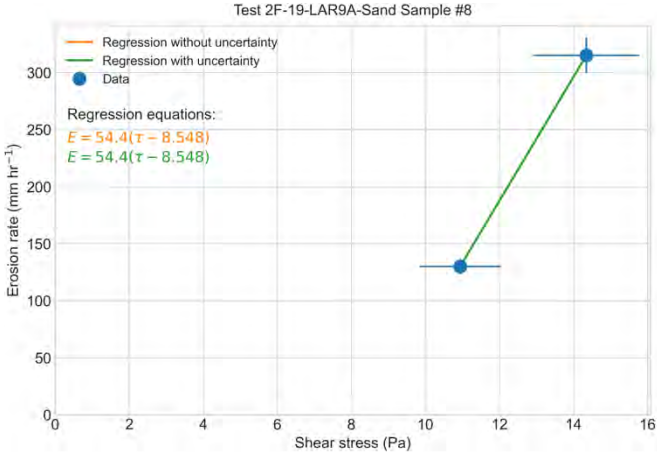
Test 2F-19-LAR9A-Sand Sample #8
Regression without uncertainty
Regression with uncertainty
Data
Regression equations:
$E = 54.4(\tau - 8.548)$
$E = 54.4(\tau - 8.548)$
Erosion rate (mm hr^{-1})
Shear stress (Pa)

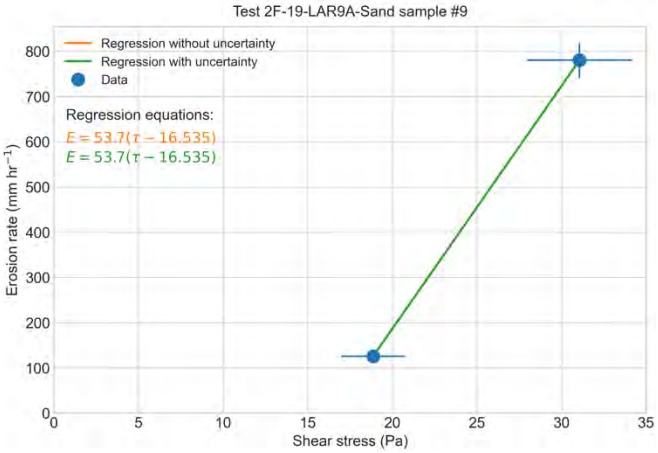
Test 2F-19-LAR9A-Sand sample #9
Regression without uncertainty
Regression with uncertainty
Data
Regression equations:
$E = 53.7(\tau - 16.535)$
$E = 53.7(\tau - 16.535)$
Erosion rate (mm hr^{-1})
Shear stress (Pa)

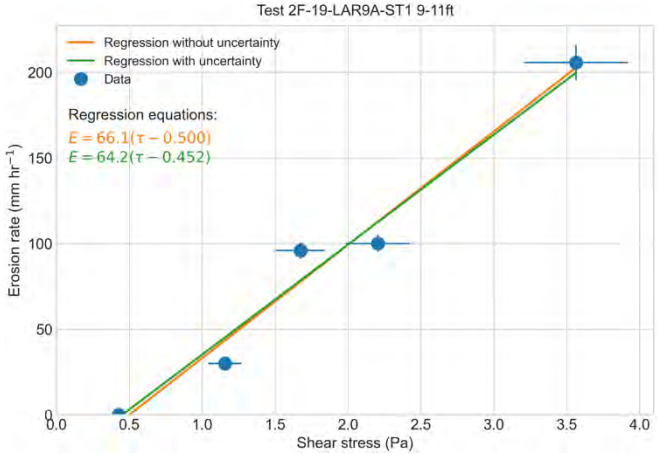
Test 2F-19-LAR9A-ST1 9-11ft
Regression without uncertainty
Regression with uncertainty
Data
Regression equations:
$E = 66.1(\tau - 0.500)$
$E = 64.2(\tau - 0.452)$
Erosion rate (mm hr^{-1})
Shear stress (Pa)

Test 2F-19-LAR9A-ST2 11-13ft

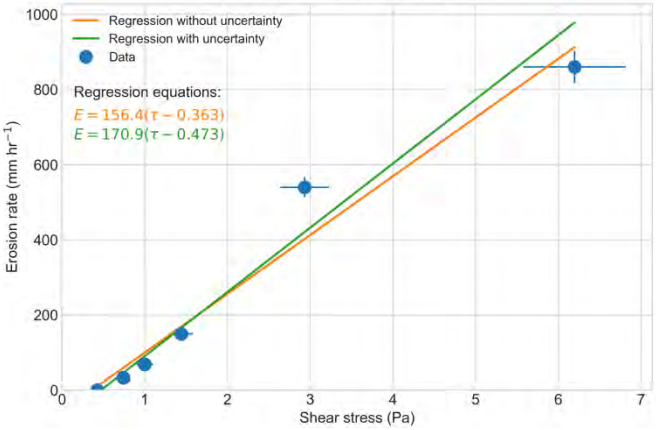

Test 2F-19-LAR10A-Sand Sample #14 25-28.5 ft

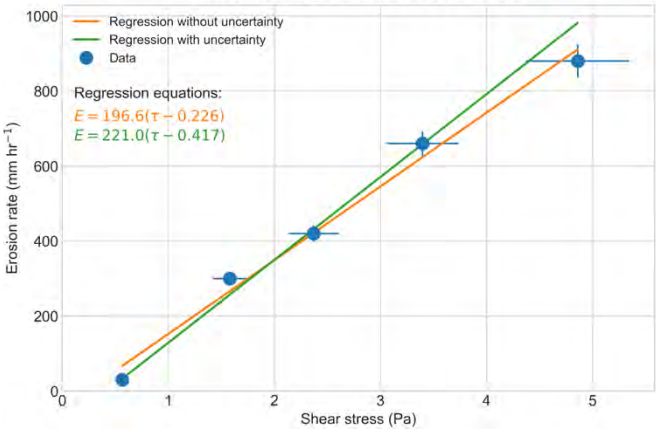

Test 2F-19-LAR10A-Sand Sample #16 29-32.5 ft

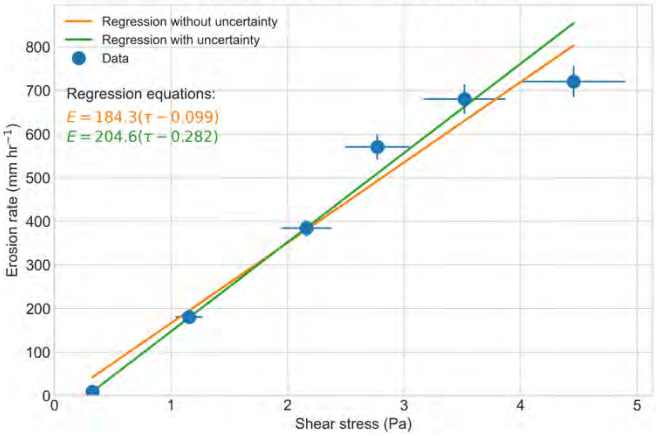

Test 2F-19-LAR12A-Sand Sample #1 7-14 ft

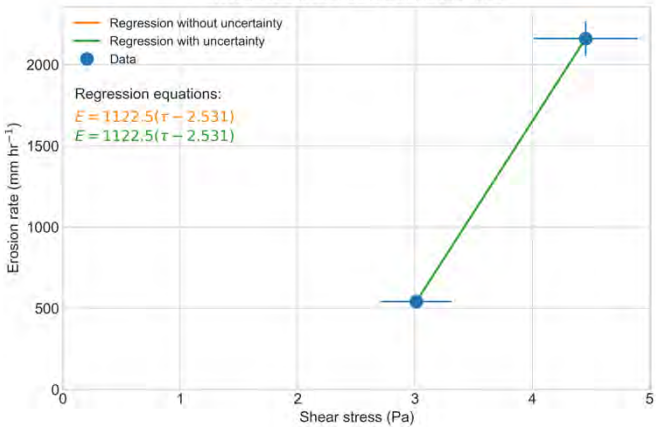

Test 2F-19-LAR12A-Sand Sample #2 19-24.5 ft

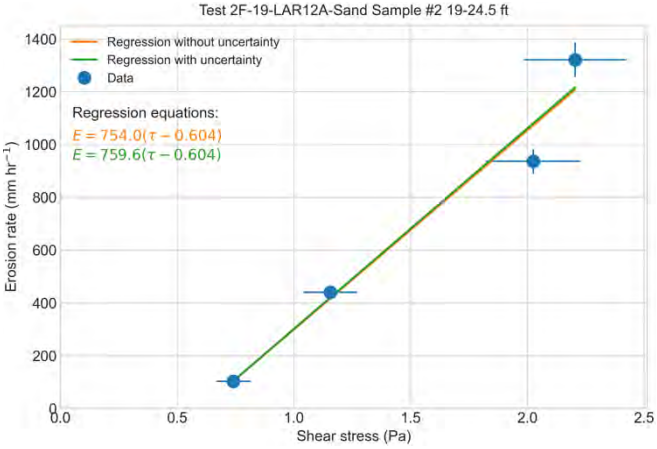

Test 2F-19-SAC1A-ST2 11-13 ft

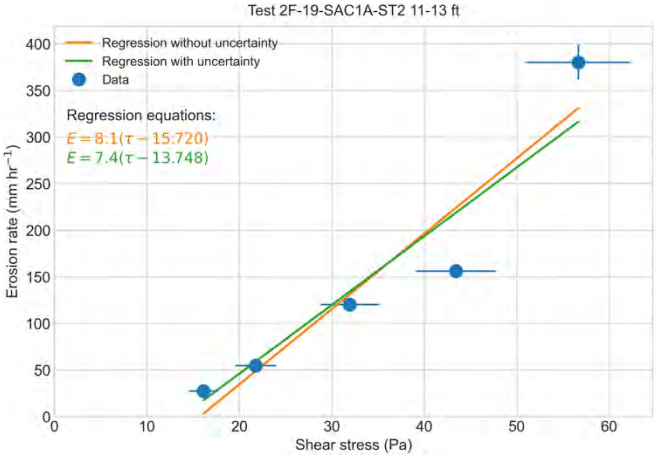

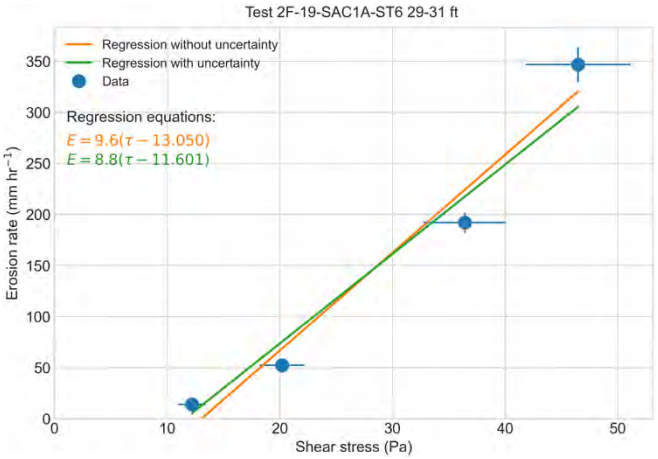
Test 2F-19-SAC1A-ST6 29-31 ft
Regression without uncertainty
Regression with uncertainty
Data
Regression equations:
$E = 9.6(\tau - 13.050)$
$E = 8.8(\tau - 11.601)$
Erosion rate (mm hr^{-1})
Shear stress (Pa)

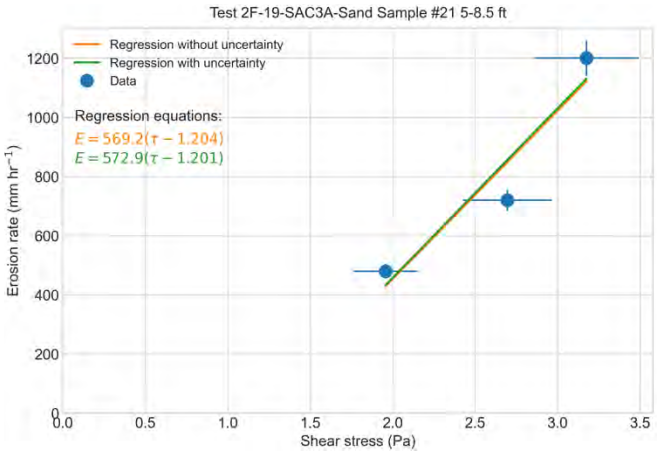
Test 2F-19-SAC3A-Sand Sample #21 5-8.5 ft
Regression without uncertainty
Regression with uncertainty
Data
Regression equations:
$E = 569.2(\tau - 1.204)$
$E = 572.9(\tau - 1.201)$
Erosion rate (mm hr^{-1})
Shear stress (Pa)

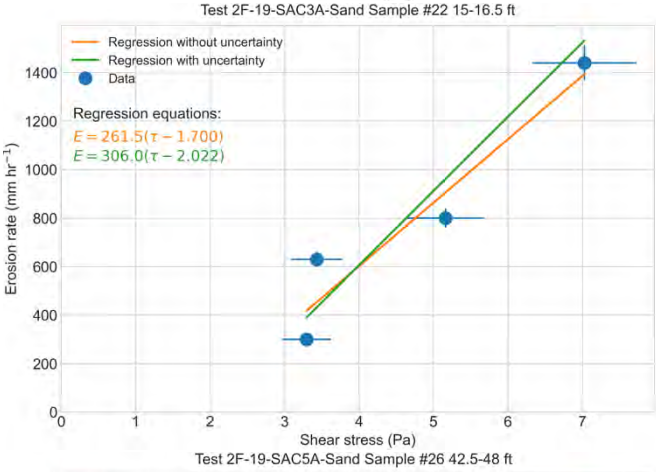
Test 2F-19-SAC3A-Sand Sample #22 15-16.5 ft
Regression without uncertainty
Regression with uncertainty
Data
Regression equations:
$E = 261.5(\tau - 1.700)$
$E = 306.0(\tau - 2.022)$
Erosion rate (mm hr^{-1})
Shear stress (Pa)

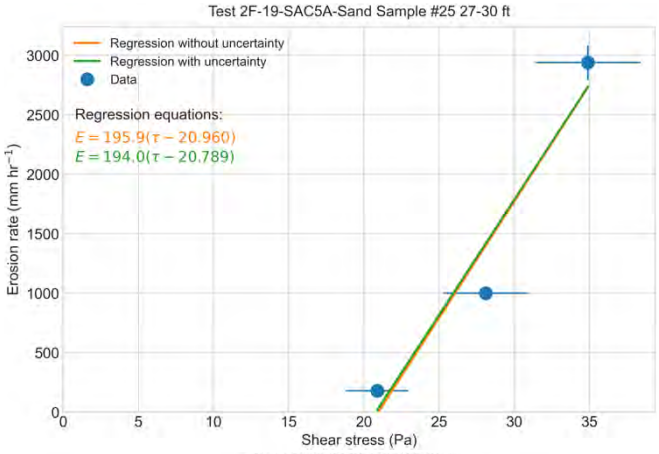
Test 2F-19-SAC5A-Sand Sample #25 27-30 ft
Regression without uncertainty
Regression with uncertainty
Data
Regression equations:
$E = 195.9(\tau - 20.960)$
$E = 194.0(\tau - 20.789)$
Erosion rate (mm hr^{-1})
Shear stress (Pa)

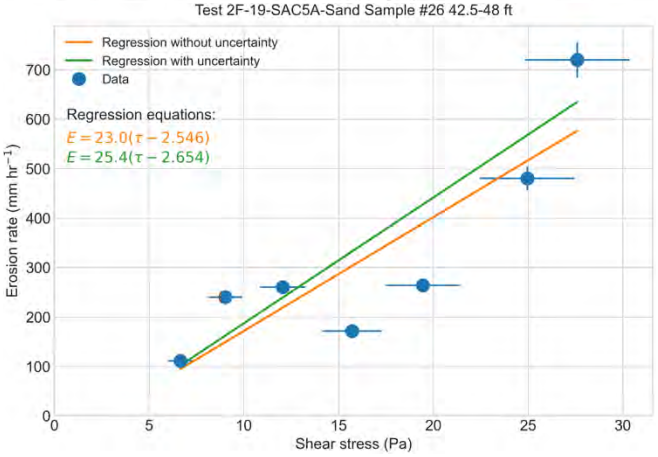
Test 2F-19-SAC5A-Sand Sample #26 42.5-48 ft
Regression without uncertainty
Regression with uncertainty
Data
Regression equations:
$E = 23.0(\tau - 2.546)$
$E = 25.4(\tau - 2.654)$
Erosion rate (mm hr^{-1})
Shear stress (Pa)

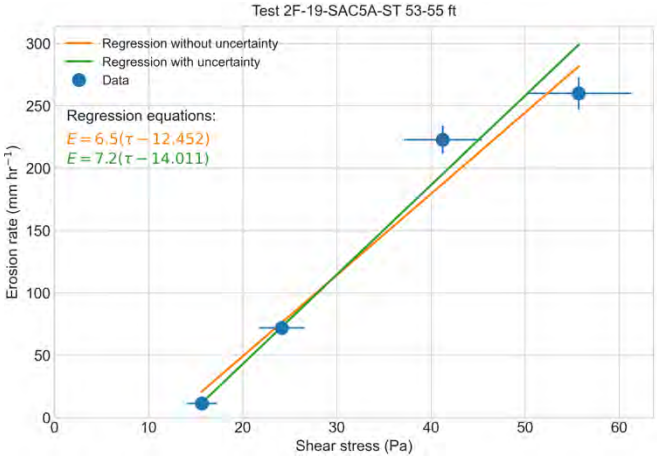
Test 2F-19-SAC5A-ST 53-55 ft
Regression without uncertainty
Regression with uncertainty
Data
Regression equations:
$E = 6.5(\tau - 12.452)$
$E = 7.2(\tau - 14.011)$
Erosion rate (mm hr^{-1})
Shear stress (Pa)

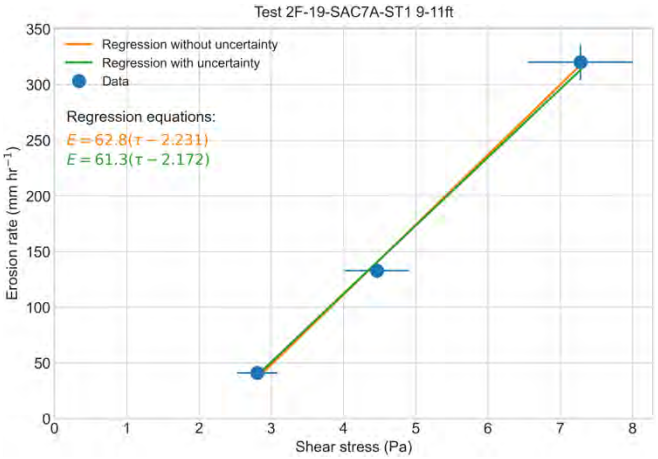
Test 2F-19-SAC7A-ST1 9-11ft
Regression without uncertainty
Regression with uncertainty
Data
Regression equations:
$E = 62.8(\tau - 2.231)$
$E = 61.3(\tau - 2.172)$
Erosion rate (mm hr^{-1})
Shear stress (Pa)

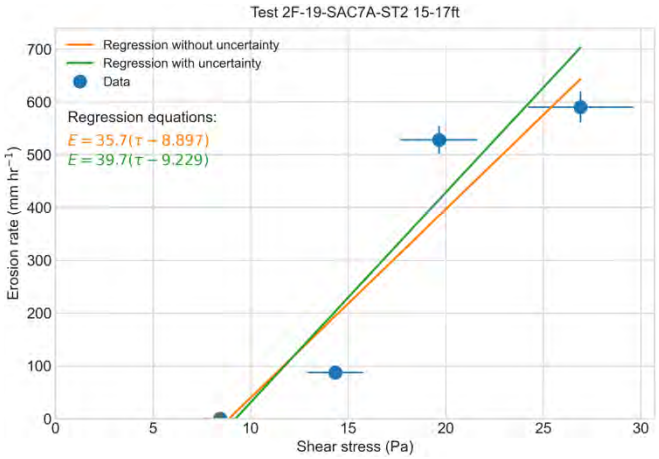
Test 2F-19-SAC7A-ST2 15-17ft
Regression without uncertainty
Regression with uncertainty
Data
Regression equations:
$E = 35.7(\tau + 8.897)$
$E = 39.7(\tau - 9.229)$
Erosion rate (mm hr^{-1})
Shear stress (Pa)

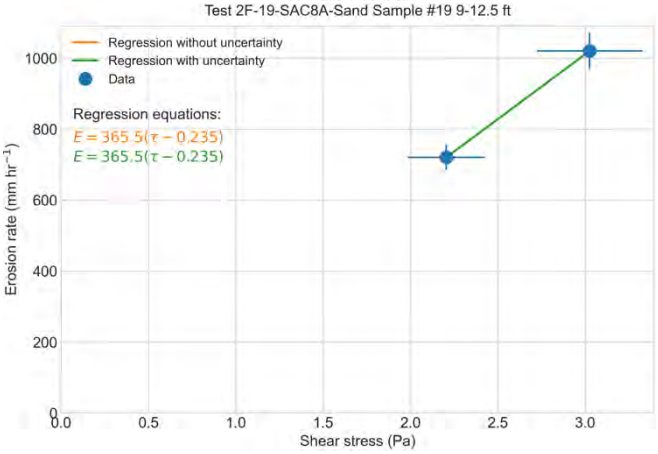
Test 2F-19-SAC8A-Sand Sample #19 9-12.5 ft
Regression without uncertainty
Regression with uncertainty
Data
Regression equations:
$E = 365.5(\tau - 0.235)$
$E = 365.5(\tau - 0.235)$
Erosion rate (mm hr^{-1})
Shear stress (Pa)

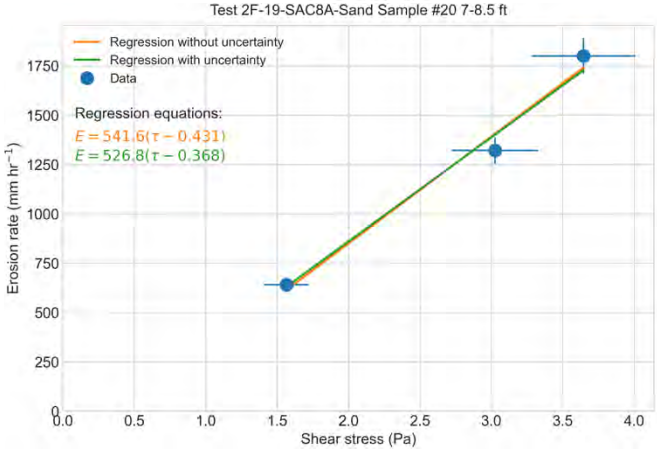
Test 2F-19-SAC8A-Sand Sample #20 7-8.5 ft
Regression without uncertainty
Regression with uncertainty
Data
Regression equations:
$E = 541.6(\tau - 0.431)$
$E = 526.8(\tau - 0.368)$
Erosion rate (mm hr^{-1})
Shear stress (Pa)

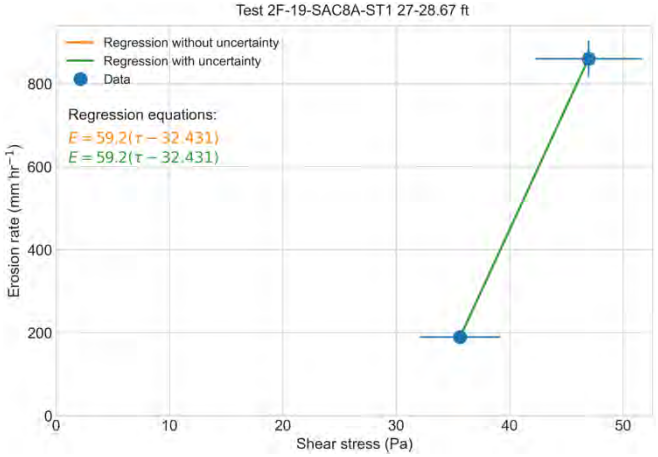
Test 2F-19-SAC8A-ST1 27-28.67 ft
Regression without uncertainty
Regression with uncertainty
Data
Regression equations:
$E = 59.2(\tau - 32.431)$
$E = 59.2(\tau - 32.431)$
Erosion rate (mm hr^{-1})
Shear stress (Pa)

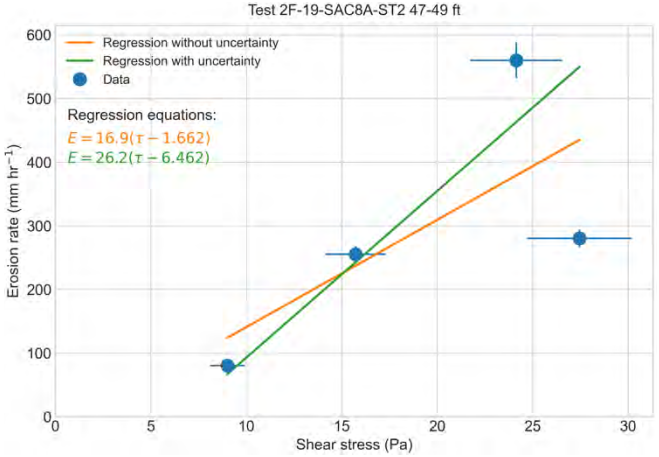
Test 2F-19-SAC8A-ST2 47-49 ft
Regression without uncertainty
Regression with uncertainty
Data
Regression equations:
$E = 16.9(\tau - 1.662)$
$E = 26.2(\tau - 6.462)$
Erosion rate (mm hr^{-1})
Shear stress (Pa)

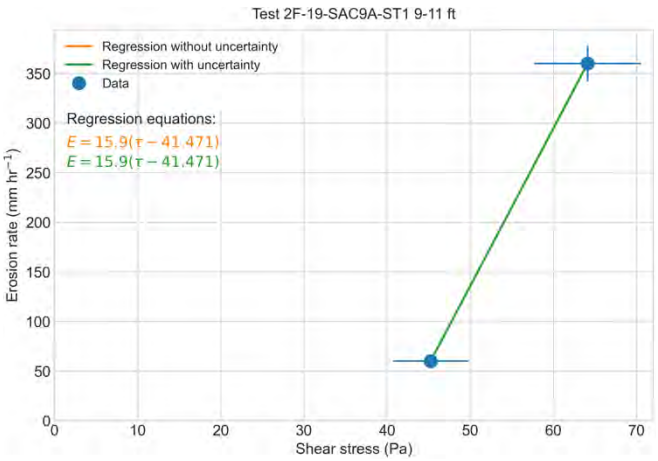

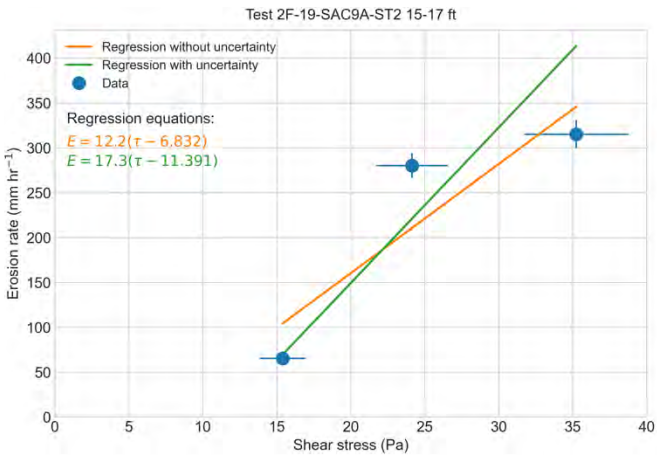

USACE ERDC erosion function apparatus tests

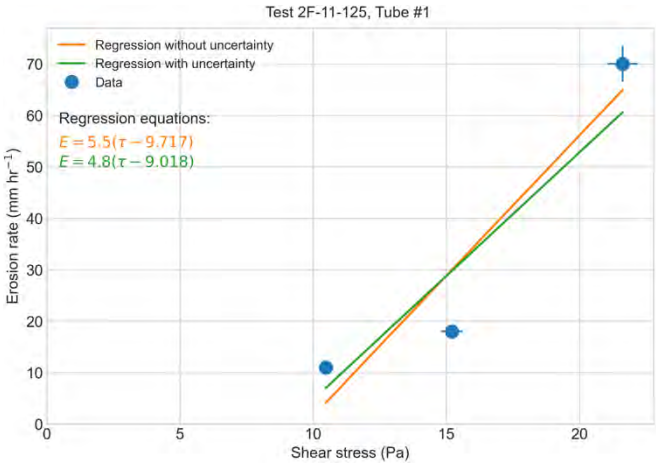

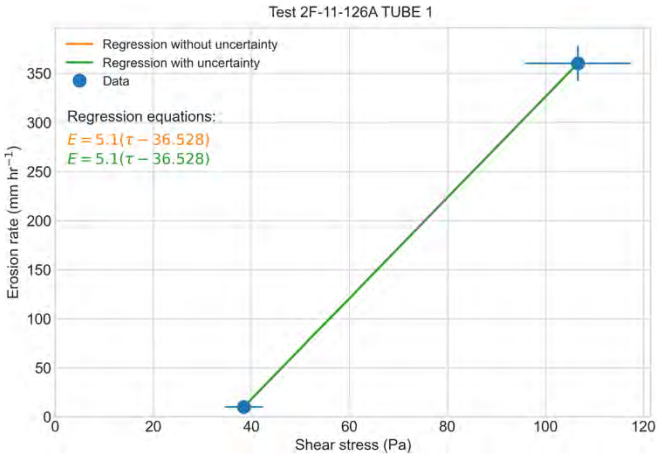

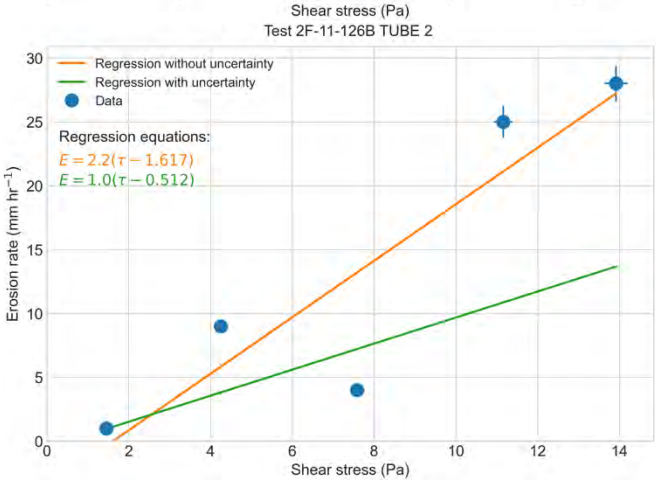

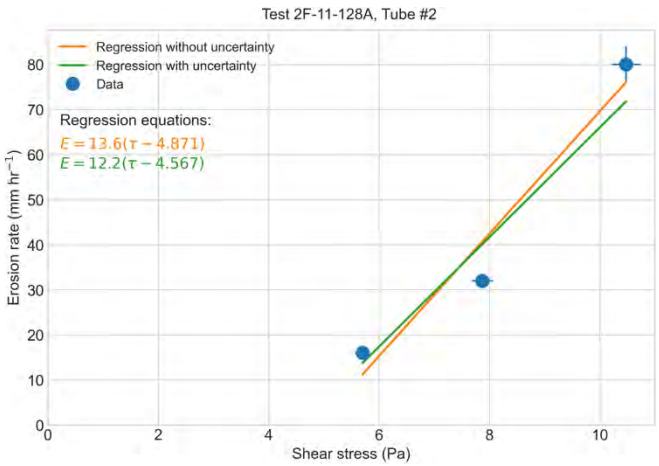

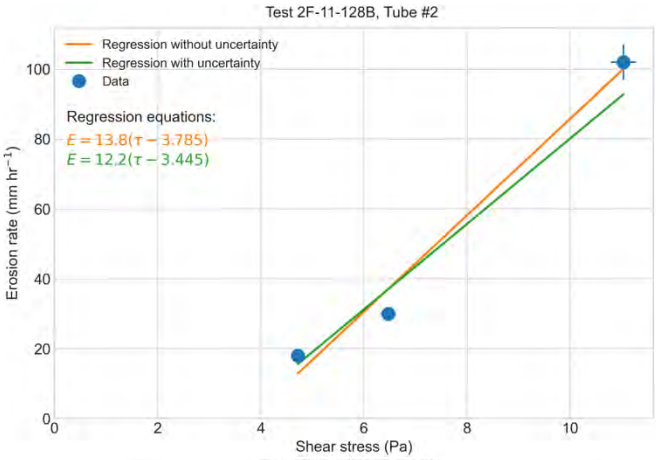
Test 2F-11-128B, Tube #2
Regression without uncertainty
Regression with uncertainty
Data
Regression equations:
$\dot{E} = 13.8(\tau - 3.785)$
$\dot{E} = 12.2(\tau - 3.445)$
Erosion rate (mm hr^{-1})
Shear stress (Pa)

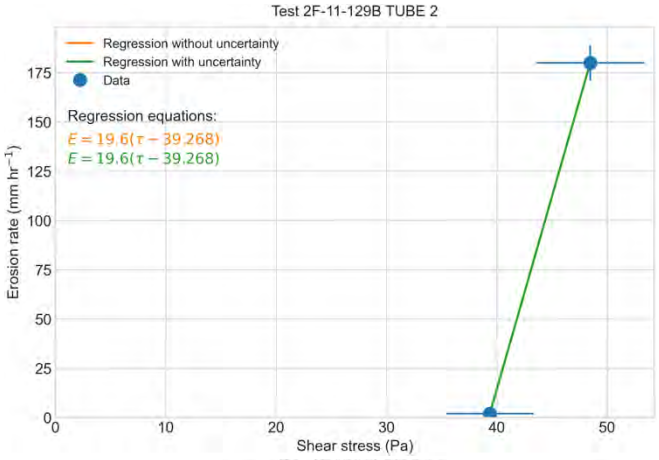
Test 2F-11-129B TUBE 2
Regression without uncertainty
Regression with uncertainty
Data
Regression equations:
$\dot{E} = 19.6(\tau - 39.268)$
$\dot{E} = 19.6(\tau - 39.268)$
Erosion rate (mm hr^{-1})
Shear stress (Pa)

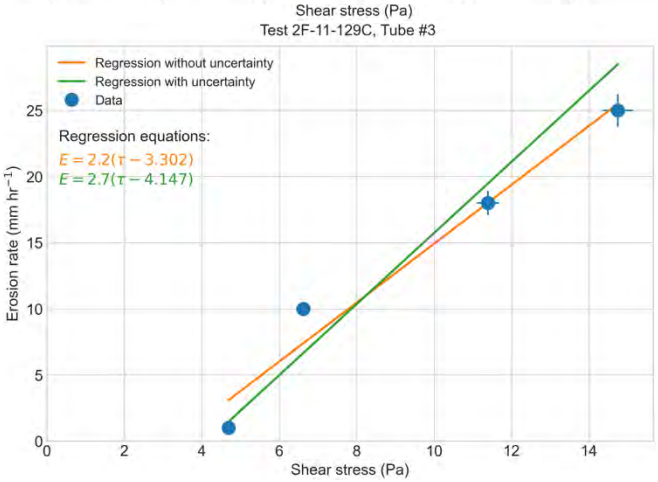
Test 2F-11-129C, Tube #3
Regression without uncertainty
Regression with uncertainty
Data
Regression equations:
$\dot{E} = 2.2(\tau - 3.302)$
$\dot{E} = 2.7(\tau - 4.147)$
Erosion rate (mm hr^{-1})
Shear stress (Pa)

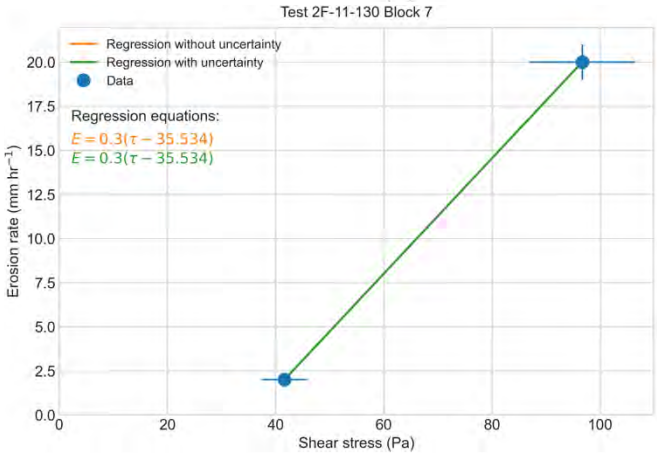
Test 2F-11-130 Block 7
Regression without uncertainty
Regression with uncertainty
Data
Regression equations:
$\dot{E} = 0.3(\tau - 35.534)$
$\dot{E} = 0.3(\tau - 35.534)$
Erosion rate (mm hr^{-1})
Shear stress (Pa)

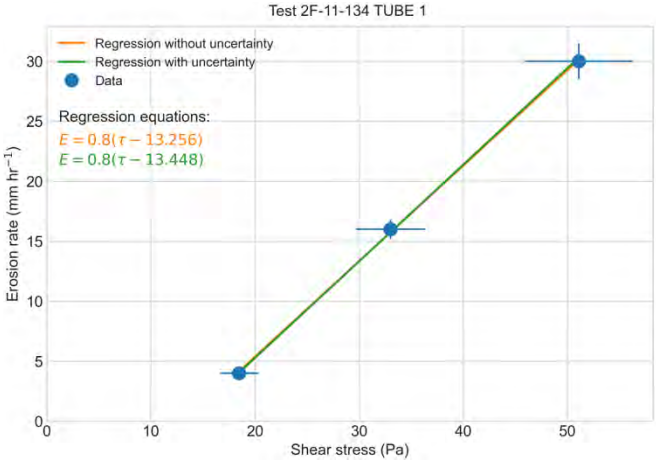
Test 2F-11-134 TUBE 1
Regression without uncertainty
Regression with uncertainty
Data
Regression equations:
$\dot{E} = 0.8(\tau - 13.256)$
$\dot{E} = 0.8(\tau - 13.448)$
Erosion rate (mm hr^{-1})
Shear stress (Pa)

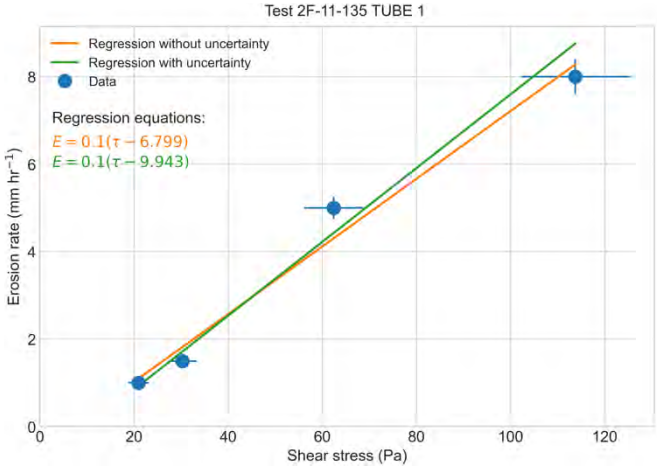
Test 2F-11-135 TUBE 1
Regression without uncertainty
Regression with uncertainty
Data
Regression equations:
$\dot{E} = 0.1(\tau - 6.799)$
$\dot{E} = 0.1(\tau - 9.943)$
Erosion rate (mm hr^{-1})
Shear stress (Pa)

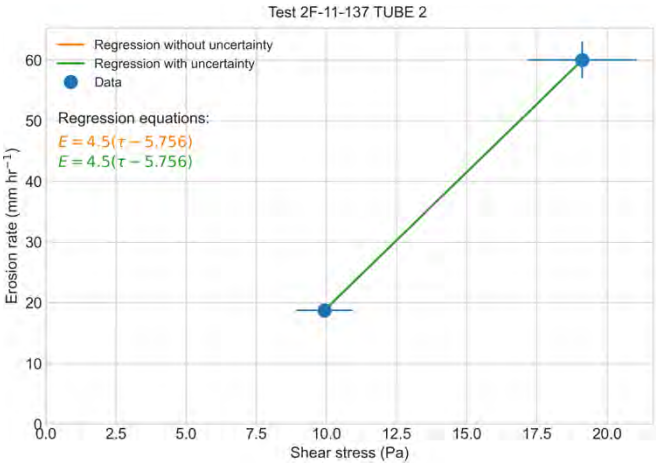

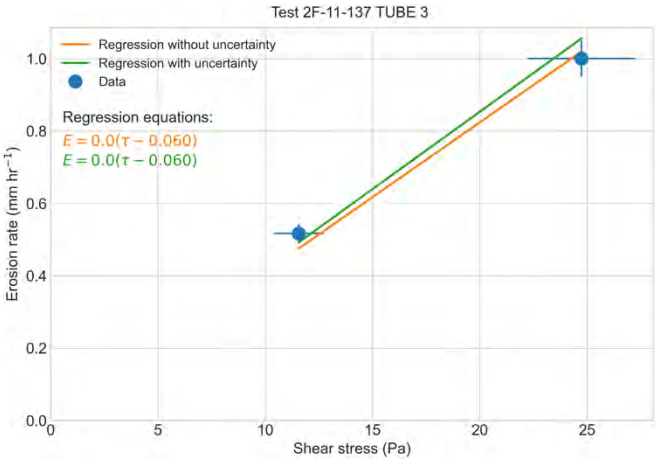

Erosion function apparatus tests – grain shear stress

TAMU erosion function apparatus tests

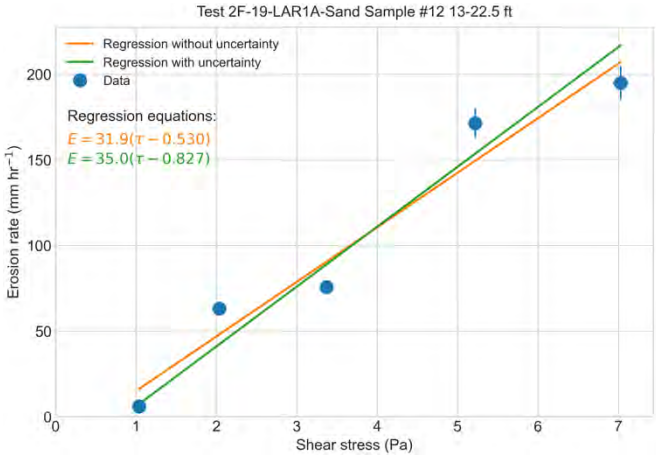

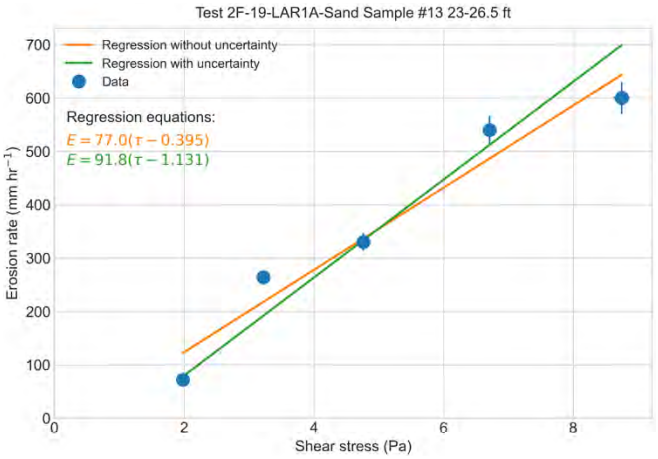

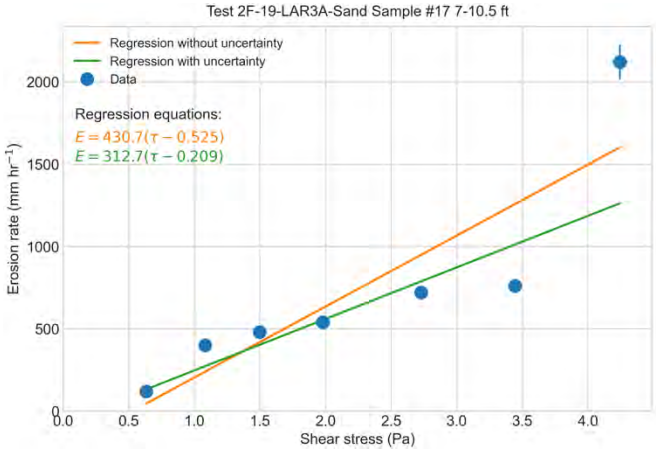

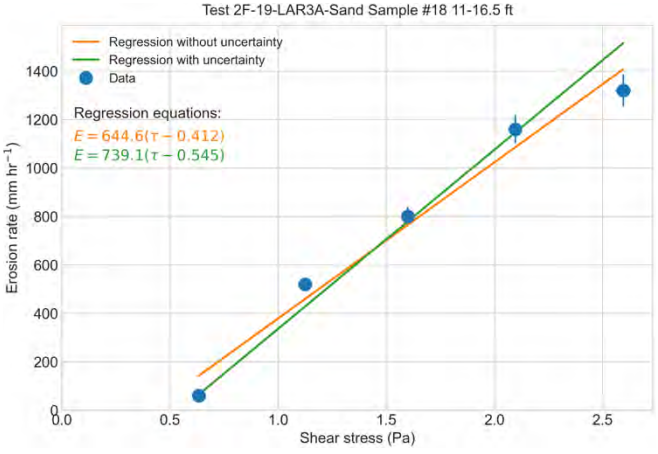

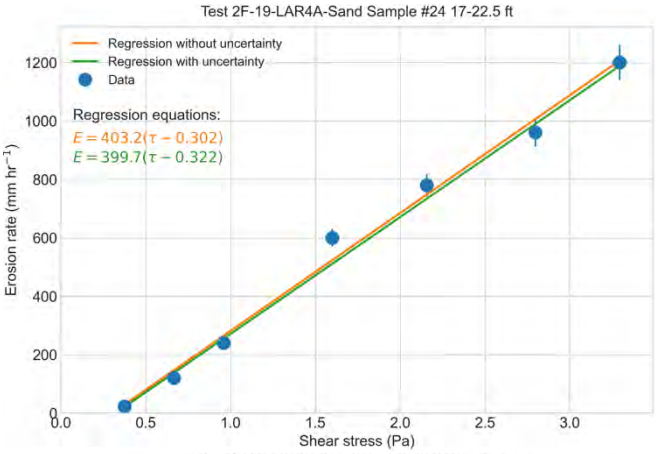
Test 2F-19-LAR4A-Sand Sample #24 17-22.5 ft
Regression without uncertainty
Regression with uncertainty
Data
Regression equations:
$E = 403.2(\tau - 0.302)$
$E = 399.7(\tau - 0.322)$
Erosion rate (mm hr^{-1})
Shear stress (Pa)

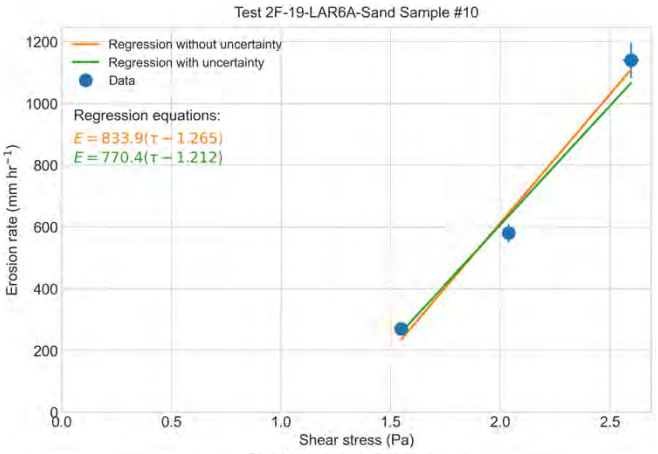
Test 2F-19-LAR6A-Sand Sample #10
Regression without uncertainty
Regression with uncertainty
Data
Regression equations:
$E = 833.9(\tau - 1.265)$
$E = 770.4(\tau - 1.212)$
Erosion rate (mm hr^{-1})
Shear stress (Pa)

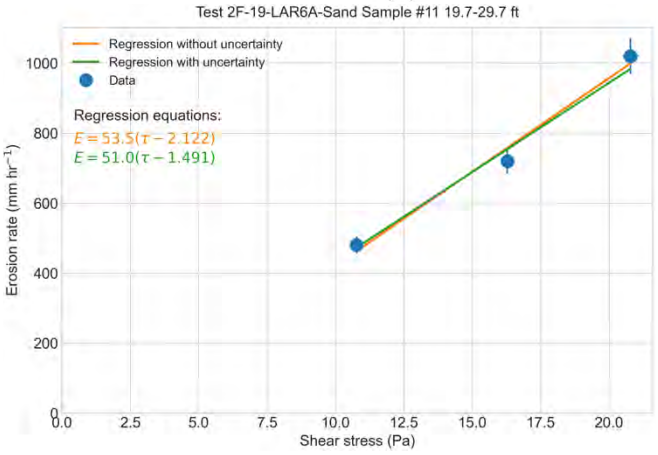
Test 2F-19-LAR6A-Sand Sample #11 19.7-29.7 ft
Regression without uncertainty
Regression with uncertainty
Data
Regression equations:
$E = 53.5(\tau - 2.122)$
$E = 51.0(\tau - 1.491)$
Erosion rate (mm hr^{-1})
Shear stress (Pa)

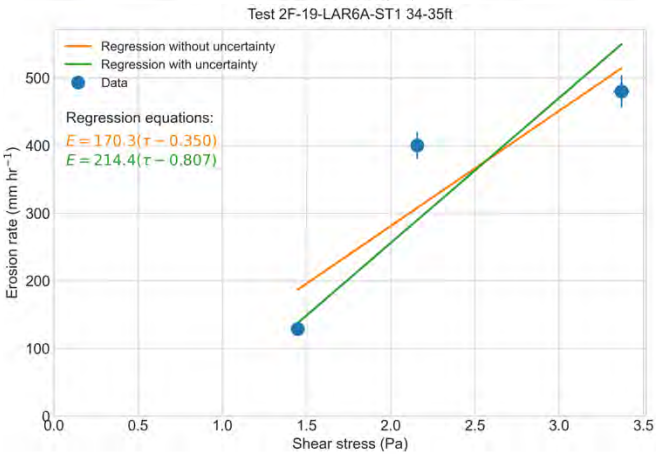
Test 2F-19-LAR6A-ST1 34-35ft
Regression without uncertainty
Regression with uncertainty
Data
Regression equations:
$E = 170.3(\tau - 0.350)$
$E = 214.4(\tau - 0.807)$
Erosion rate (mm hr^{-1})
Shear stress (Pa)

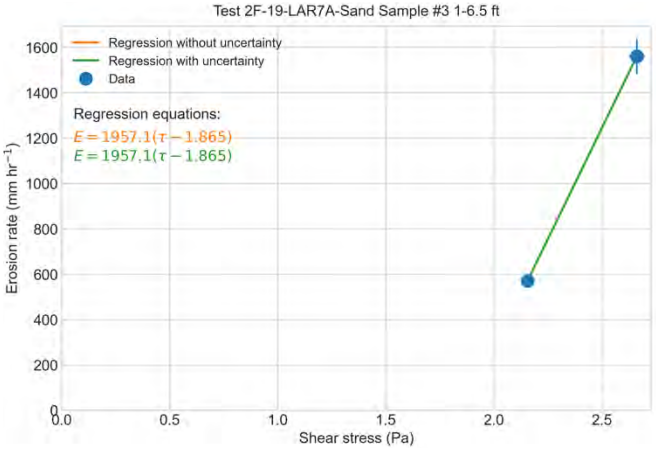
Test 2F-19-LAR7A-Sand Sample #3 1-6.5 ft
Regression without uncertainty
Regression with uncertainty
Data
Regression equations:
$E = 1957.1(\tau - 1.865)$
$E = 1957.1(\tau - 1.865)$
Erosion rate (mm hr^{-1})
Shear stress (Pa)

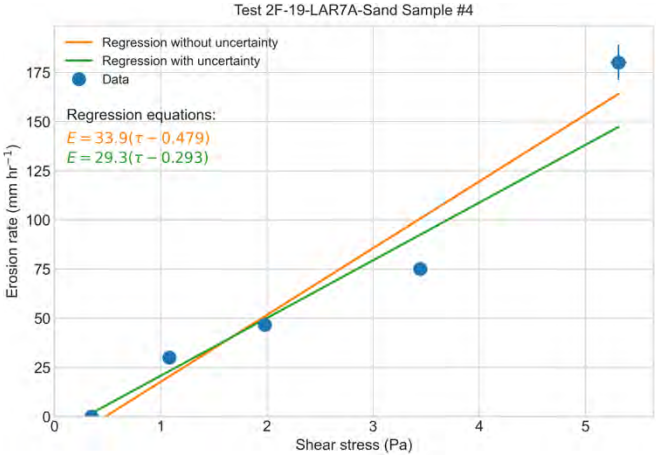
Test 2F-19-LAR7A-Sand Sample #4
Regression without uncertainty
Regression with uncertainty
Data
Regression equations:
$E = 33.9(\tau - 0.479)$
$E = 29.3(\tau - 0.293)$
Erosion rate (mm hr^{-1})
Shear stress (Pa)

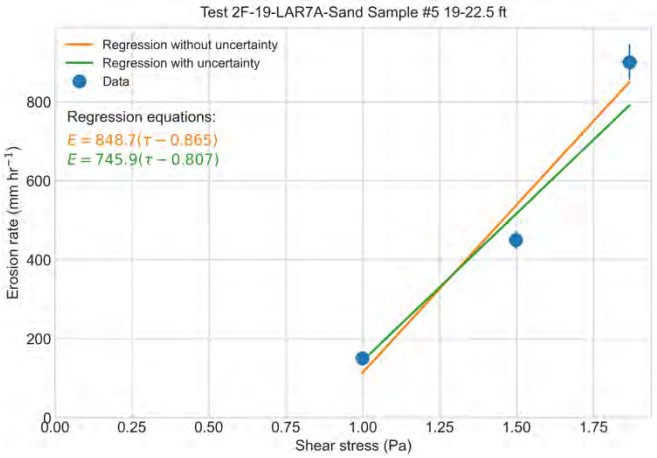
Test 2F-19-LAR7A-Sand Sample #5 19-22.5 ft
Regression without uncertainty
Regression with uncertainty
Data
Regression equations:
$E = 848.7(\tau - 0.865)$
$E = 745.9(\tau - 0.807)$
Erosion rate (mm hr^{-1})
Shear stress (Pa)

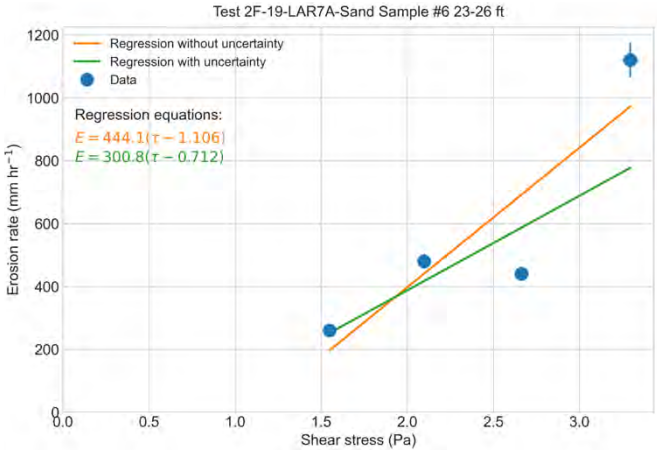
Test 2F-19-LAR7A-Sand Sample #6 23-26 ft
Regression without uncertainty
Regression with uncertainty
Data
Regression equations:
$E = 444.1(\tau - 1.106)$
$E = 300.8(\tau - 0.712)$
Erosion rate (mm hr^{-1})
Shear stress (Pa)

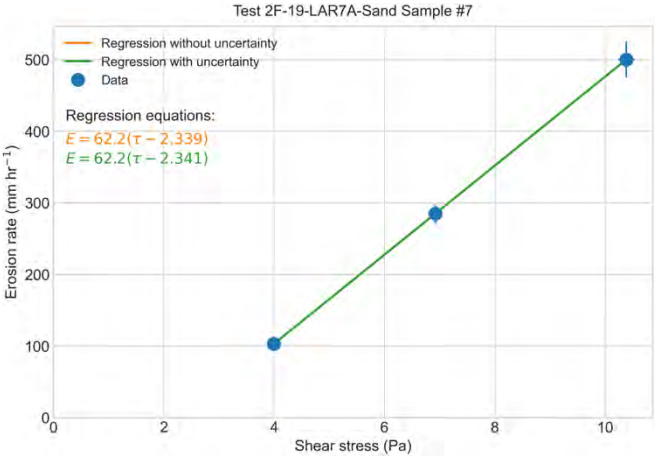
Test 2F-19-LAR7A-Sand Sample #7
Regression without uncertainty
Regression with uncertainty
Data
Regression equations:
$E = 62.2(\tau - 2.339)$
$E = 62.2(\tau - 2.341)$
Erosion rate (mm hr^{-1})
Shear stress (Pa)

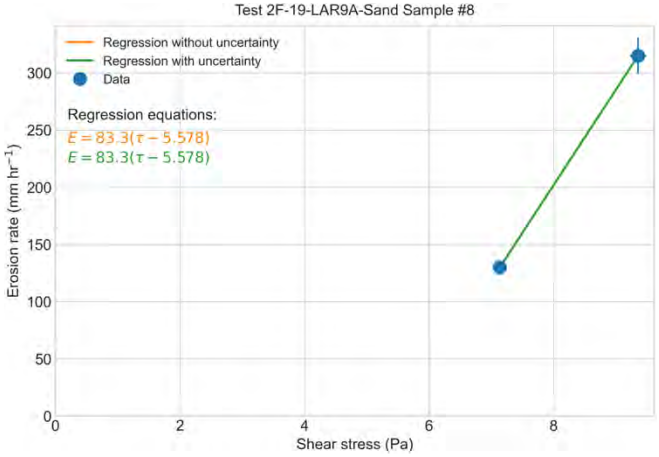
Test 2F-19-LAR9A-Sand Sample #8
Regression without uncertainty
Regression with uncertainty
Data
Regression equations:
$E = 83.3(\tau - 5.578)$
$E = 83.3(\tau - 5.578)$
Erosion rate (mm hr^{-1})
Shear stress (Pa)

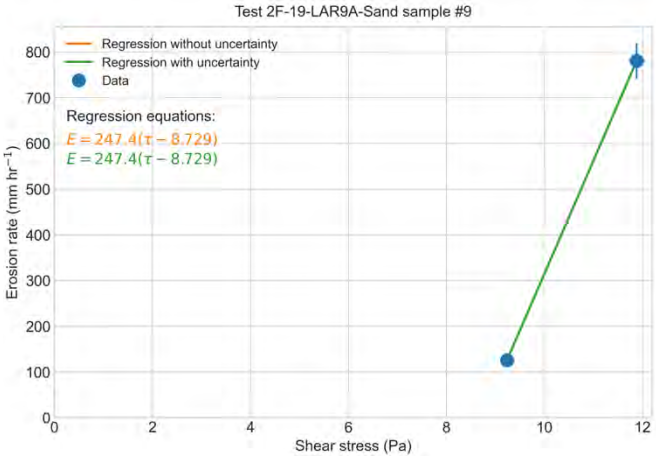
Test 2F-19-LAR9A-Sand sample #9
Regression without uncertainty
Regression with uncertainty
Data
Regression equations:
$E = 247.4(\tau - 8.729)$
$E = 247.4(\tau - 8.729)$
Erosion rate (mm hr^{-1})
Shear stress (Pa)

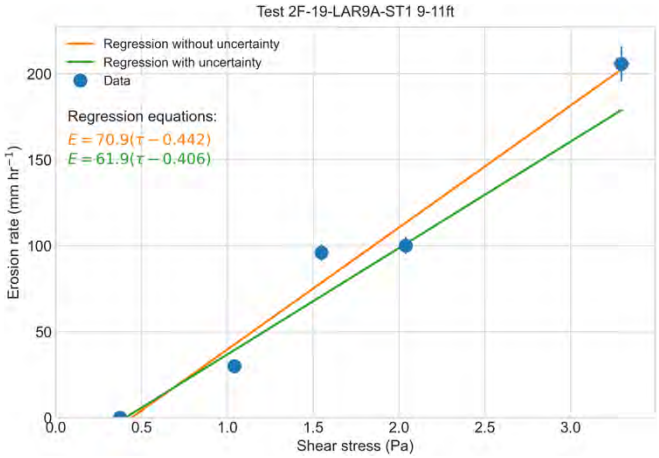
Test 2F-19-LAR9A-ST1 9-11ft
Regression without uncertainty
Regression with uncertainty
Data
Regression equations:
$E = 70.9(\tau - 0.442)$
$E = 61.9(\tau - 0.406)$
Erosion rate (mm hr^{-1})
Shear stress (Pa)

Test 2F-19-LAR9A-ST2 11-13ft

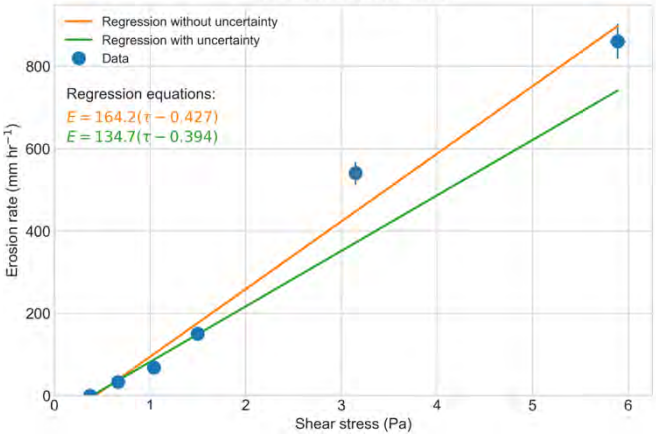

Test 2F-19-LAR10A-Sand Sample #14 25-28.5 ft

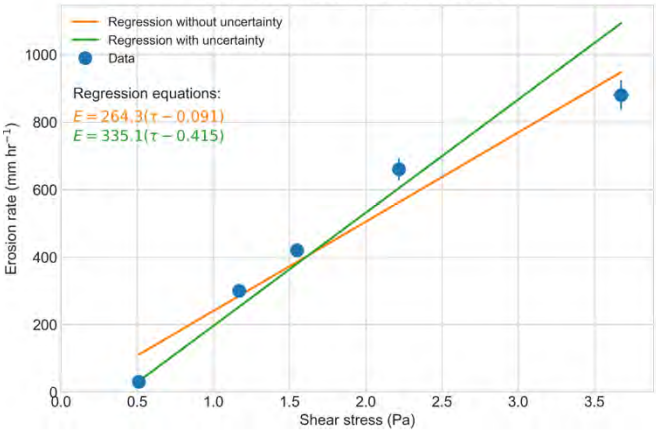

Test 2F-19-LAR10A-Sand Sample #16 29-32.5 ft

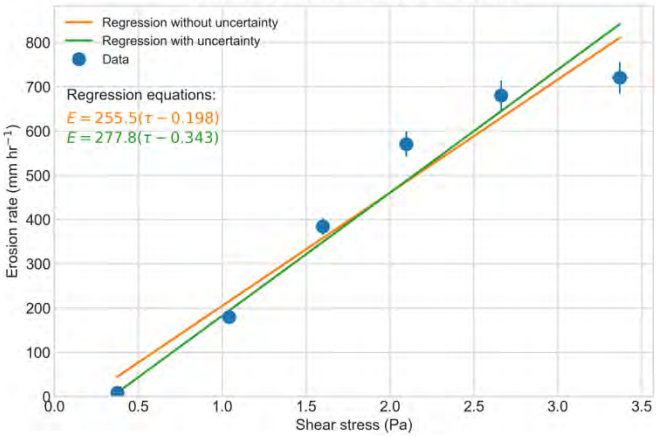

Test 2F-19-LAR12A-Sand Sample #1 7-14 ft

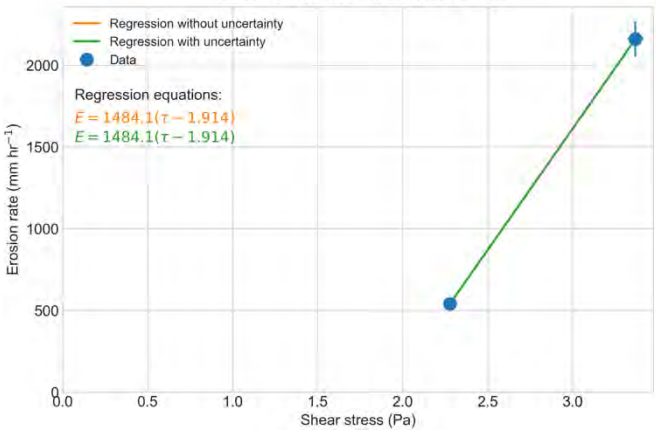

Test 2F-19-LAR12A-Sand Sample #2 19-24.5 ft

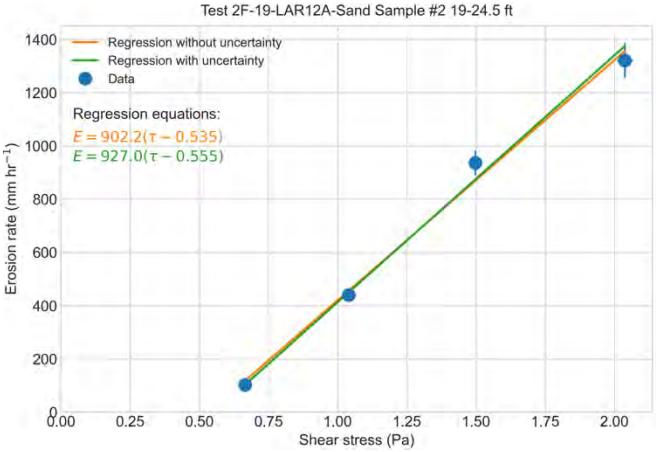

Test 2F-19-SAC1A-ST2 11-13 ft

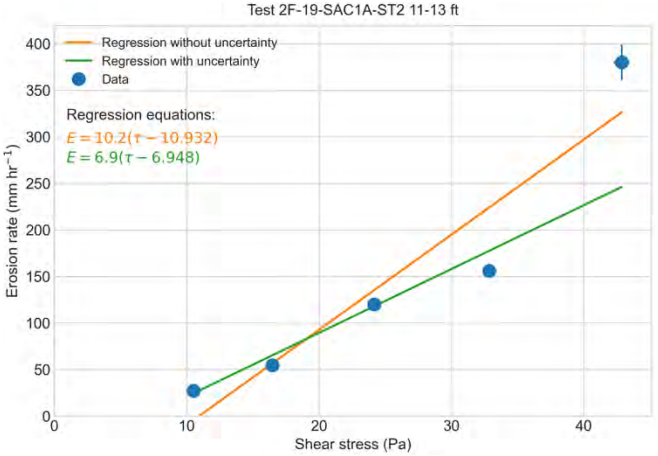

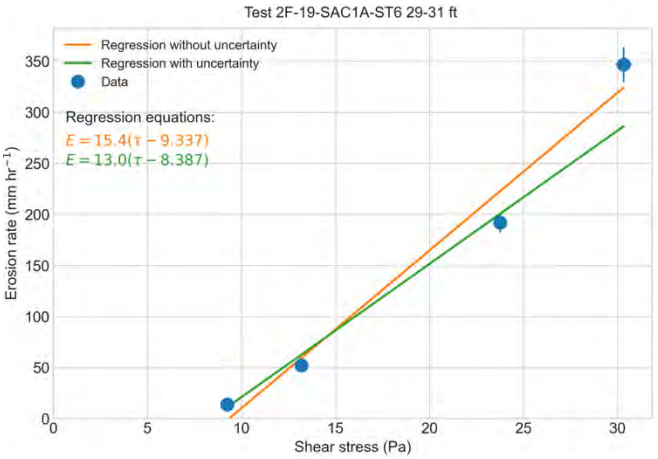
Test 2F-19-SAC1A-ST6 29-31 ft
Regression without uncertainty
Regression with uncertainty
Data
Regression equations:
$E = 15.4(\tau - 9.337)$
$E = 13.0(\tau - 8.387)$
Erosion rate (mm hr^{-1})
Shear stress (Pa)

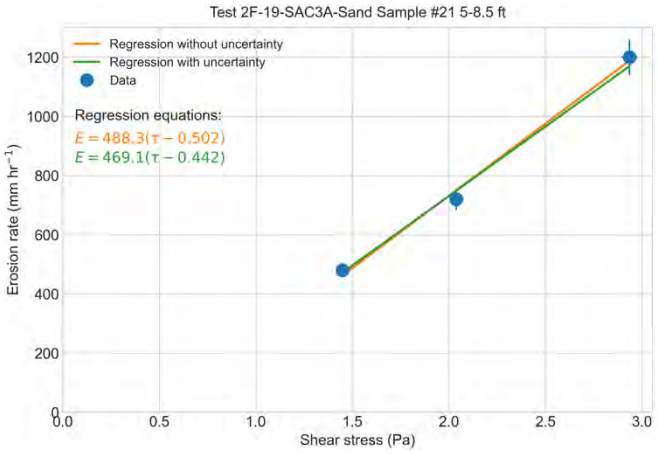
Test 2F-19-SAC3A-Sand Sample #21 5-8.5 ft
Regression without uncertainty
Regression with uncertainty
Data
Regression equations:
$E = 488.3(\tau - 0.502)$
$E = 469.1(\tau - 0.442)$
Erosion rate (mm hr^{-1})
Shear stress (Pa)

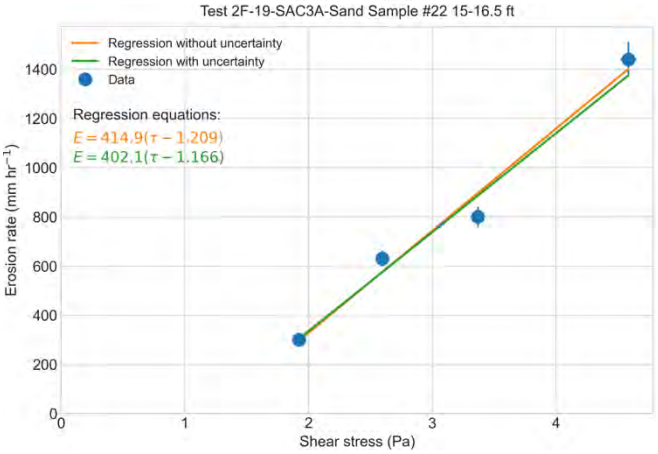
Test 2F-19-SAC3A-Sand Sample #22 15-16.5 ft
Regression without uncertainty
Regression with uncertainty
Data
Regression equations:
$E = 414.9(\tau - 1.209)$
$E = 402.1(\tau - 1.166)$
Erosion rate (mm hr^{-1})
Shear stress (Pa)

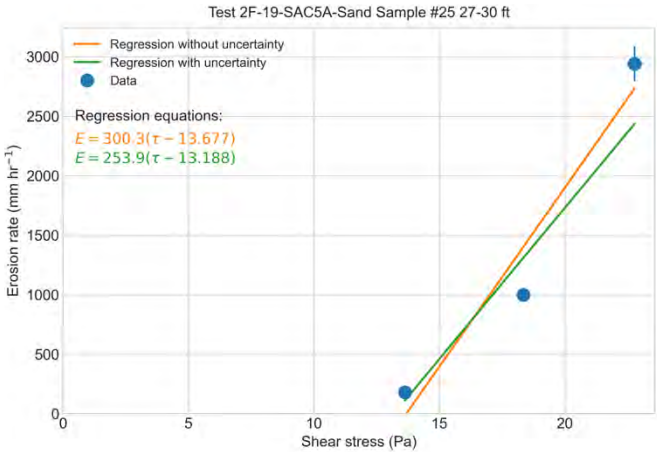
Test 2F-19-SAC5A-Sand Sample #25 27-30 ft
Regression without uncertainty
Regression with uncertainty
Data
Regression equations:
$E = 300.3(\tau - 13.677)$
$E = 253.9(\tau - 13.188)$
Erosion rate (mm hr^{-1})
Shear stress (Pa)

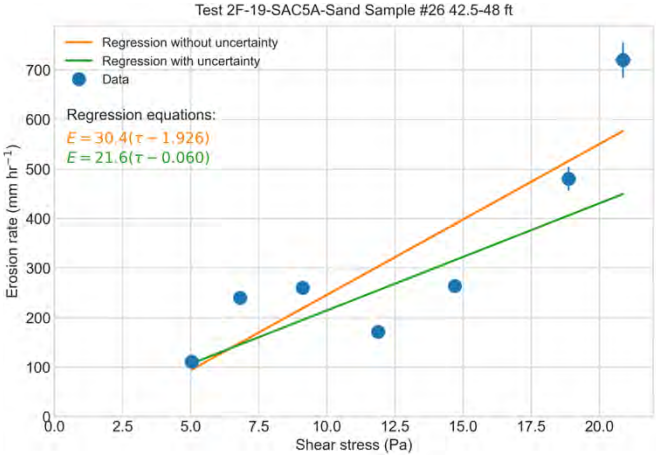
Test 2F-19-SAC5A-Sand Sample #26 42.5-48 ft
Regression without uncertainty
Regression with uncertainty
Data
Regression equations:
$E = 30.4(\tau - 1.926)$
$E = 21.6(\tau - 0.060)$
Erosion rate (mm hr^{-1})
Shear stress (Pa)

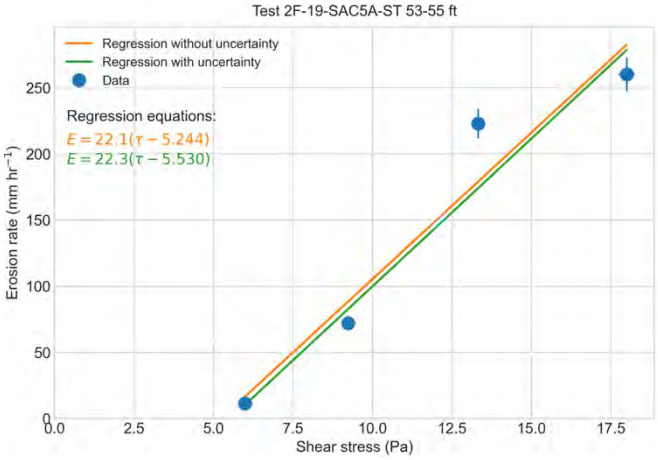
Test 2F-19-SAC5A-ST 53-55 ft
Regression without uncertainty
Regression with uncertainty
Data
Regression equations:
$E = 22.1(\tau - 5.244)$
$E = 22.3(\tau - 5.530)$
Erosion rate (mm hr^{-1})
Shear stress (Pa)

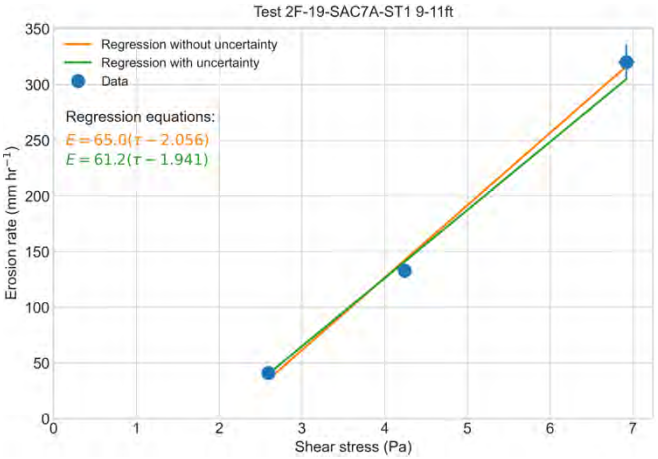
Test 2F-19-SAC7A-ST1 9-11ft
Regression without uncertainty
Regression with uncertainty
Data
Regression equations:
$E = 65.0(\tau - 2.056)$
$E = 61.2(\tau - 1.941)$
Erosion rate (mm hr^{-1})
Shear stress (Pa)

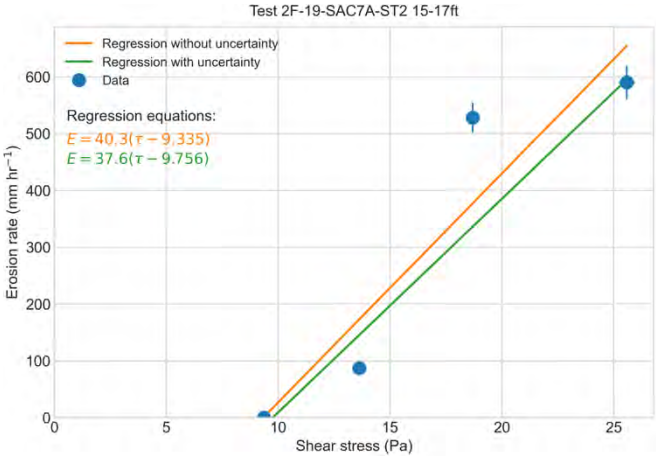
Test 2F-19-SAC7A-ST2 15-17ft
Regression without uncertainty
Regression with uncertainty
Data
Regression equations:
$E = 40.3(\tau - 9.335)$
$E = 37.6(\tau - 9.756)$
Erosion rate (mm hr^{-1})
Shear stress (Pa)

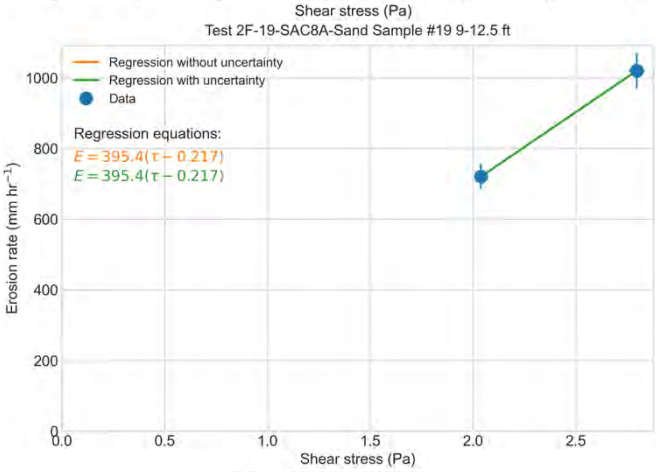
Test 2F-19-SAC8A-Sand Sample #19 9-12.5 ft
Regression without uncertainty
Regression with uncertainty
Data
Regression equations:
$E = 395.4(\tau - 0.217)$
$E = 395.4(\tau - 0.217)$
Erosion rate (mm hr^{-1})
Shear stress (Pa)

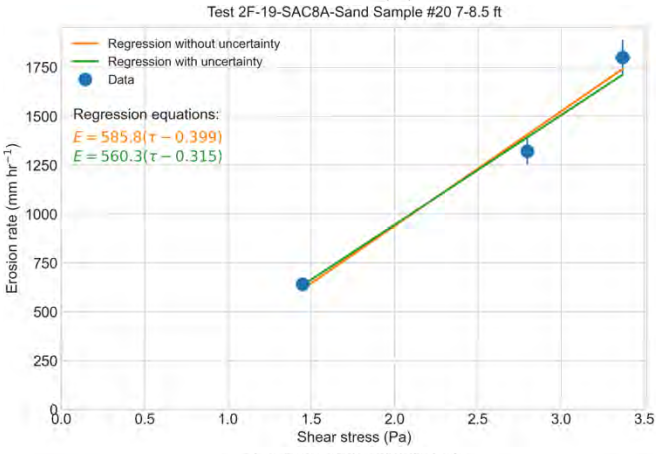
Test 2F-19-SAC8A-Sand Sample #20 7-8.5 ft
Regression without uncertainty
Regression with uncertainty
Data
Regression equations:
$E = 585.8(\tau - 0.399)$
$E = 560.3(\tau - 0.315)$
Erosion rate (mm hr^{-1})
Shear stress (Pa)

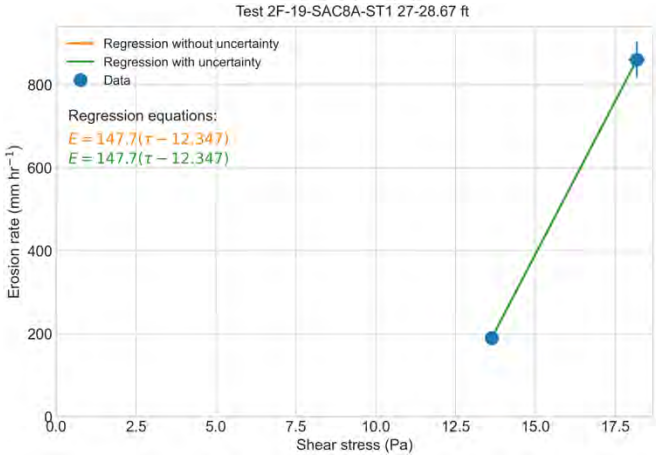
Test 2F-19-SAC8A-ST1 27-28.67 ft
Regression without uncertainty
Regression with uncertainty
Data
Regression equations:
$E = 147.7(\tau - 12.347)$
$E = 147.7(\tau - 12.347)$
Erosion rate (mm hr^{-1})
Shear stress (Pa)

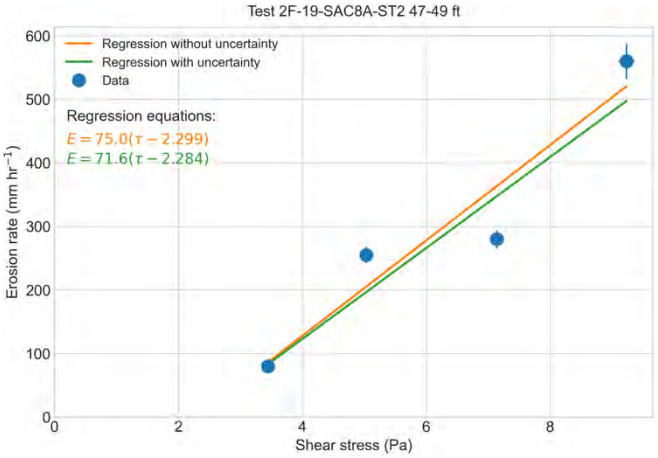
Test 2F-19-SAC8A-ST2 47-49 ft
Regression without uncertainty
Regression with uncertainty
Data
Regression equations:
$E = 75.0(\tau - 2.299)$
$E = 71.6(\tau - 2.284)$
Erosion rate (mm hr^{-1})
Shear stress (Pa)

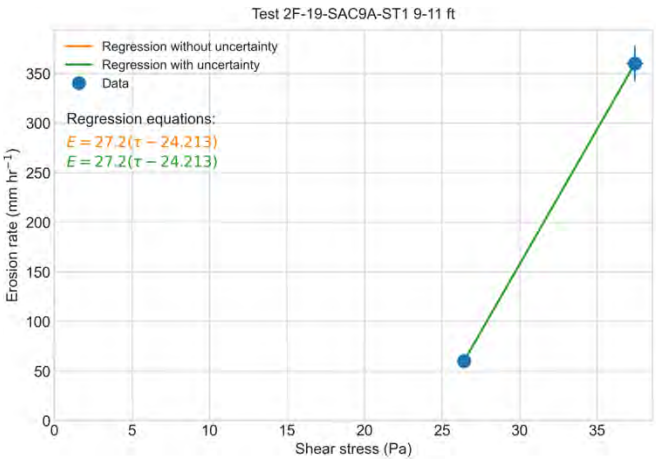

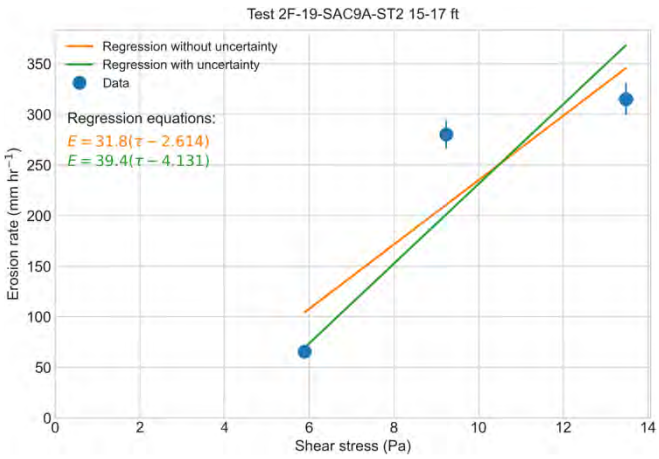

USACE ERDC erosion function apparatus tests

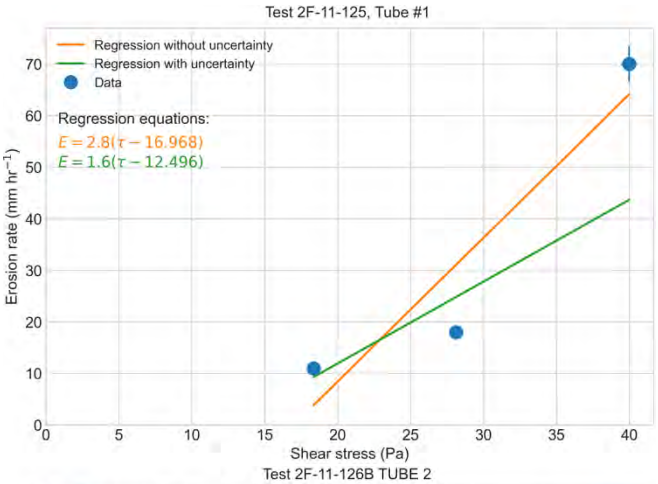

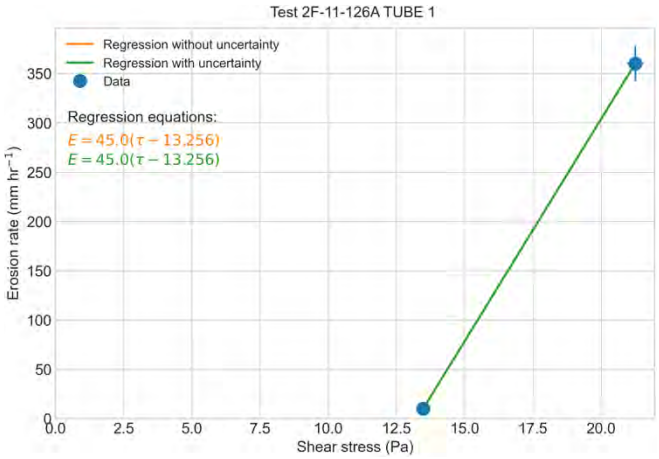

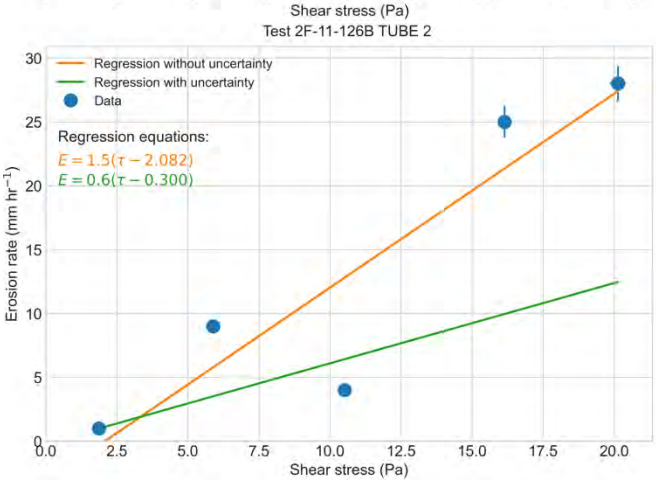

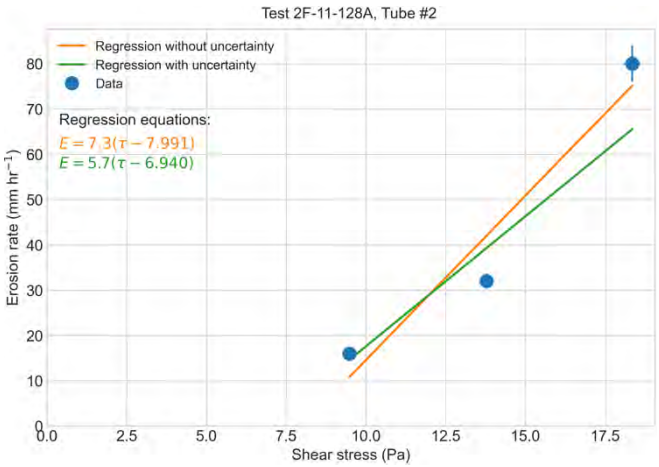

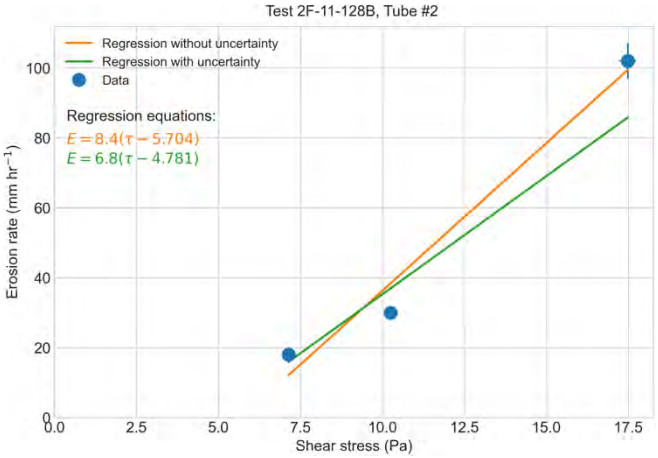
Test 2F-11-128B, Tube #2
Regression without uncertainty
Regression with uncertainty
Data
Regression equations:
$E = 8.4(\tau - 5.704)$
$E = 6.8(\tau - 4.781)$
Erosion rate (mm hr^{-1})
Shear stress (Pa)

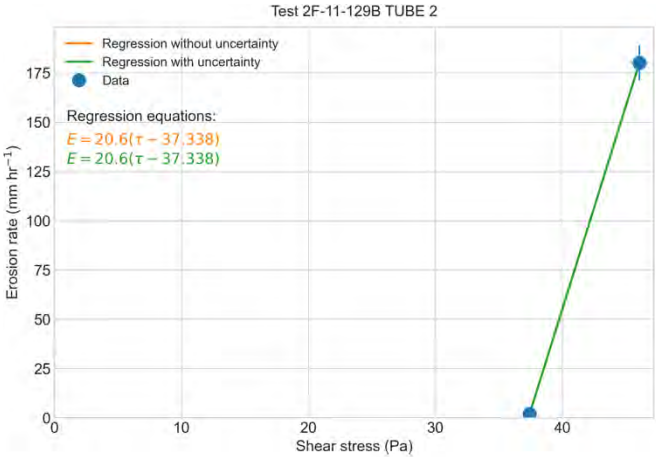
Test 2F-11-129B TUBE 2
Regression without uncertainty
Regression with uncertainty
Data
Regression equations:
$E = 20.6(\tau - 37.338)$
$E = 20.6(\tau - 37.338)$
Erosion rate (mm hr^{-1})
Shear stress (Pa)

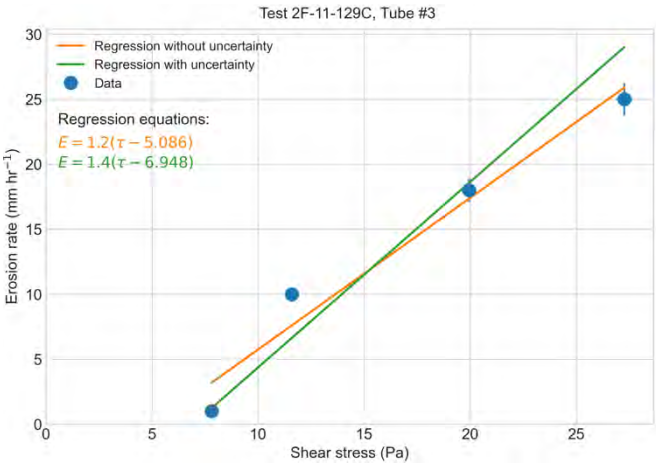
Test 2F-11-129C, Tube #3
Regression without uncertainty
Regression with uncertainty
Data
Regression equations:
$E = 1.2(\tau - 5.086)$
$E = 1.4(\tau - 6.948)$
Erosion rate (mm hr^{-1})
Shear stress (Pa)

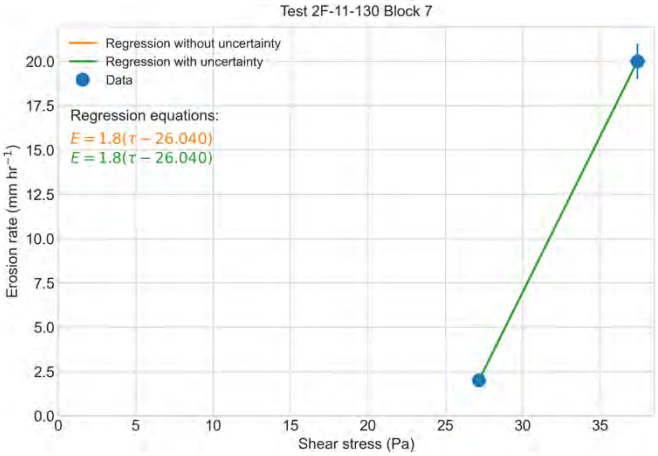
Test 2F-11-130 Block 7
Regression without uncertainty
Regression with uncertainty
Data
Regression equations:
$E = 1.8(\tau - 26.040)$
$E = 1.8(\tau - 26.040)$
Erosion rate (mm hr^{-1})
Shear stress (Pa)

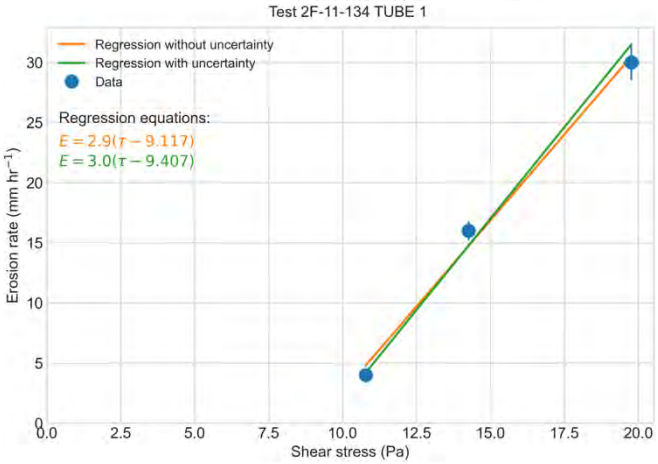
Test 2F-11-134 TUBE 1
Regression without uncertainty
Regression with uncertainty
Data
Regression equations:
$E = 2.9(\tau - 9.117)$
$E = 3.0(\tau - 9.407)$
Erosion rate (mm hr^{-1})
Shear stress (Pa)

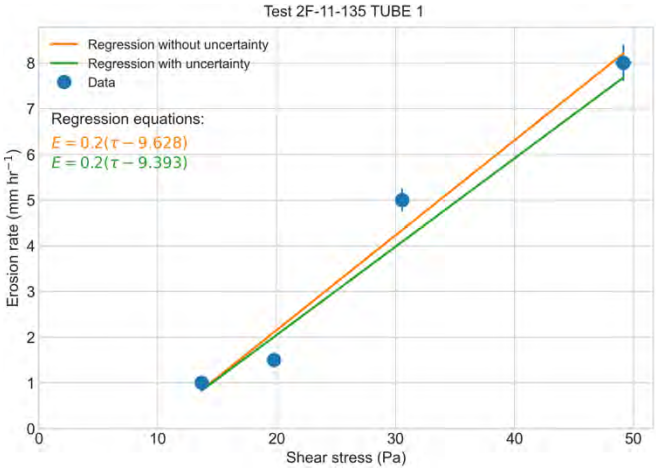
Test 2F-11-135 TUBE 1
Regression without uncertainty
Regression with uncertainty
Data
Regression equations:
$E = 0.2(\tau - 9.628)$
$E = 0.2(\tau - 9.393)$
Erosion rate (mm hr^{-1})
Shear stress (Pa)

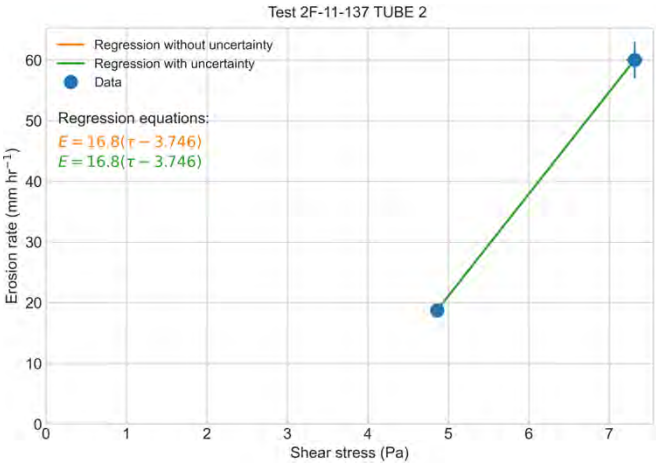

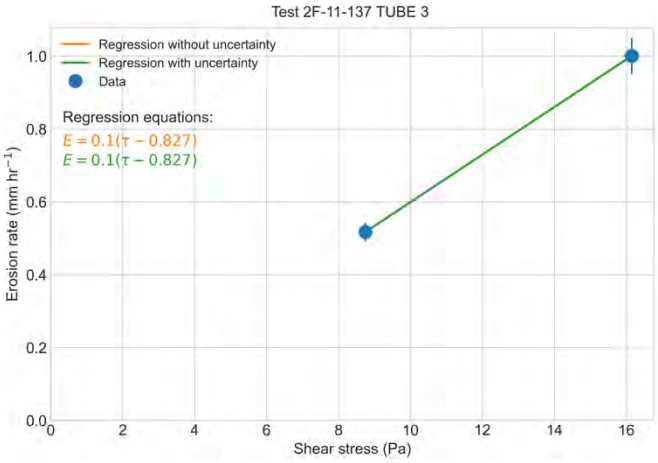

Borehole erosion tests – total shear stress

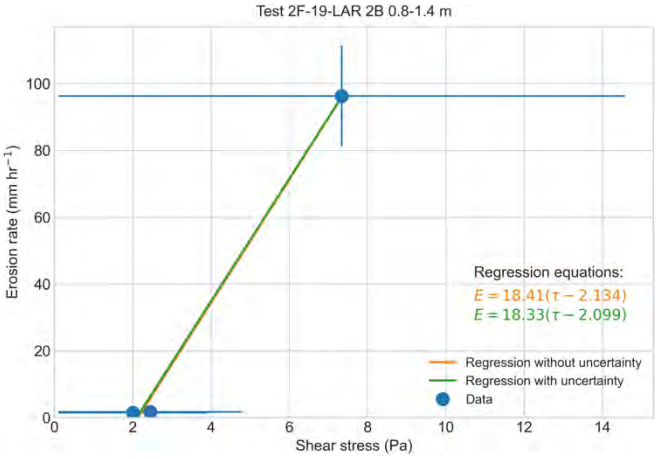

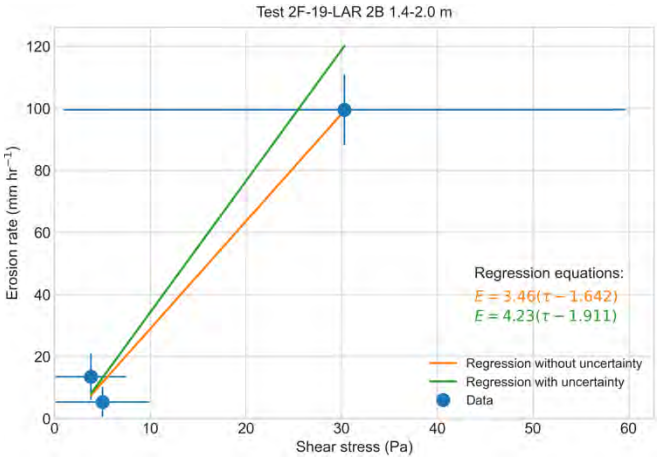

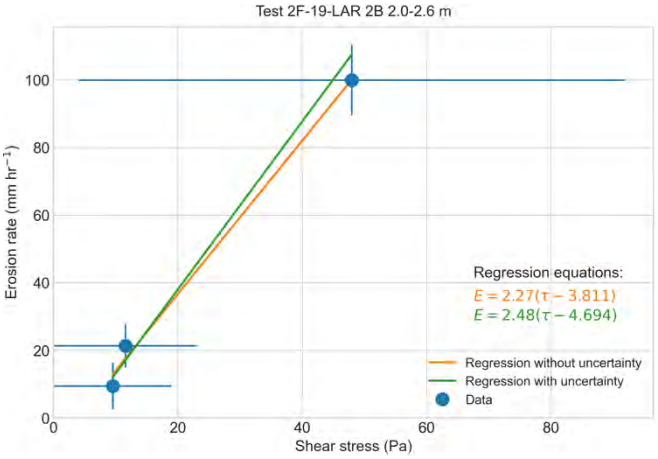

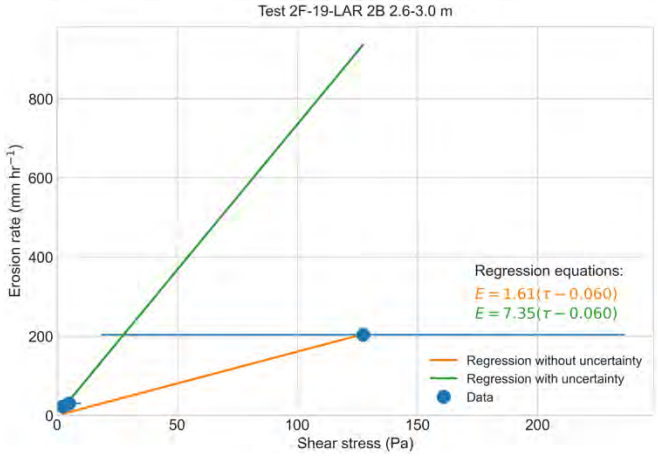

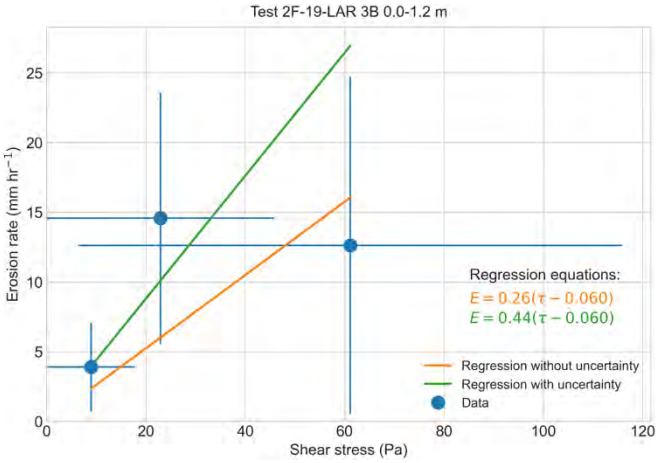
Test 2F-19-LAR 3B 0.0-1.2 m
Erosion rate (mm hr^{-1})
Shear stress (Pa)
Regression equations:
$E = 0.26(\tau - 0.060)$
$E = 0.44(\tau - 0.060)$
Regression without uncertainty
Regression with uncertainty
Data

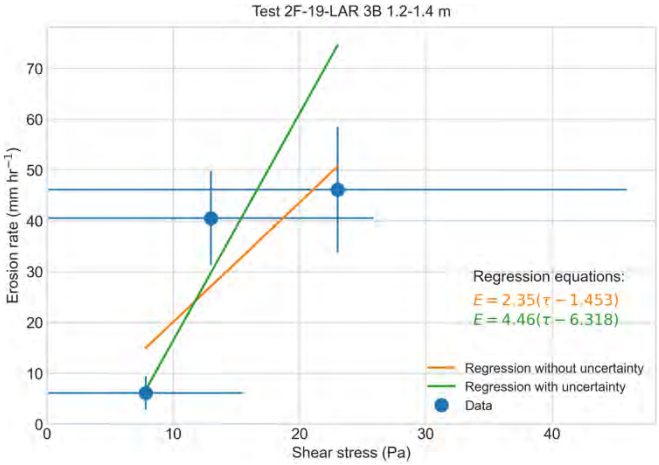
Test 2F-19-LAR 3B 1.2-1.4 m
Erosion rate (mm hr^{-1})
Shear stress (Pa)
Regression equations:
$E = 2.35(\tau - 1.453)$
$E = 4.46(\tau - 6.318)$
Regression without uncertainty
Regression with uncertainty
Data

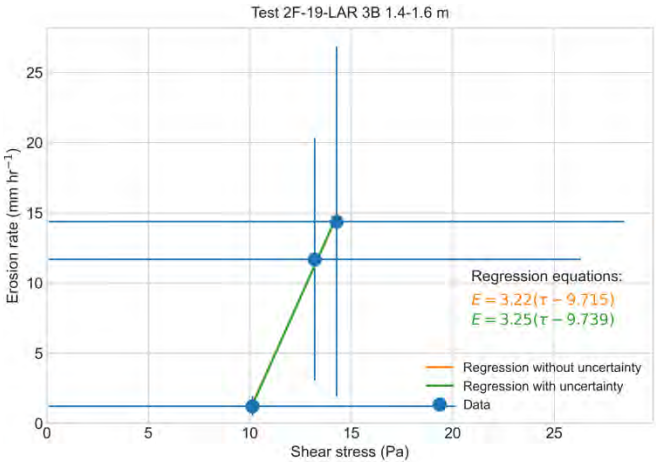
Test 2F-19-LAR 3B 1.4-1.6 m
Erosion rate (mm hr^{-1})
Shear stress (Pa)
Regression equations:
$E = 3.22(\tau - 9.715)$
$E = 3.25(\tau - 9.739)$
Regression without uncertainty
Regression with uncertainty
Data

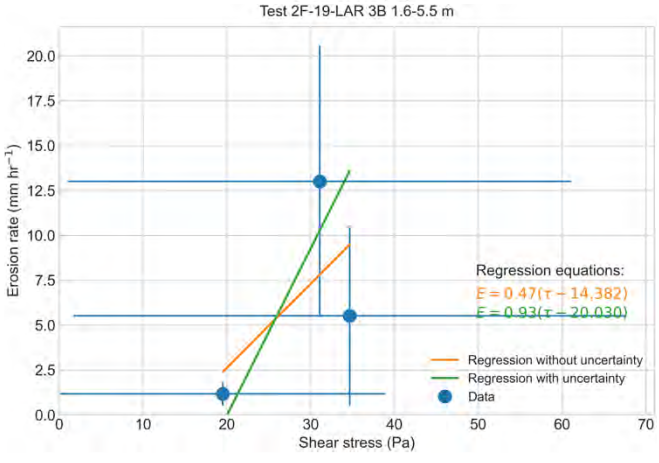
Test 2F-19-LAR 3B 1.6-5.5 m
Erosion rate (mm hr^{-1})
Shear stress (Pa)
Regression equations:
$E = 0.47(\tau - 14.382)$
$E = 0.93(\tau - 20.030)$
Regression without uncertainty
Regression with uncertainty
Data

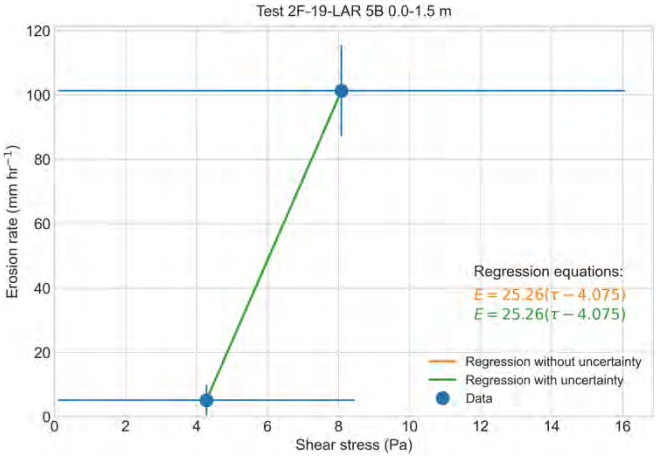
Test 2F-19-LAR 5B 0.0-1.5 m
Erosion rate (mm hr^{-1})
Shear stress (Pa)
Regression equations:
$E = 25.26(\tau - 4.075)$
$E = 25.26(\tau - 4.075)$
Regression without uncertainty
Regression with uncertainty
Data

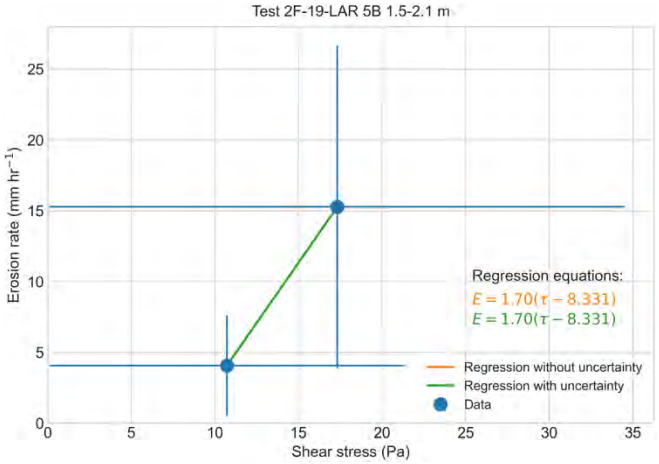
Test 2F-19-LAR 5B 1.5-2.1 m
Erosion rate (mm hr^{-1})
Shear stress (Pa)
Regression equations:
$E = 1.70(\tau - 8.331)$
$E = 1.70(\tau - 8.331)$
Regression without uncertainty
Regression with uncertainty
Data

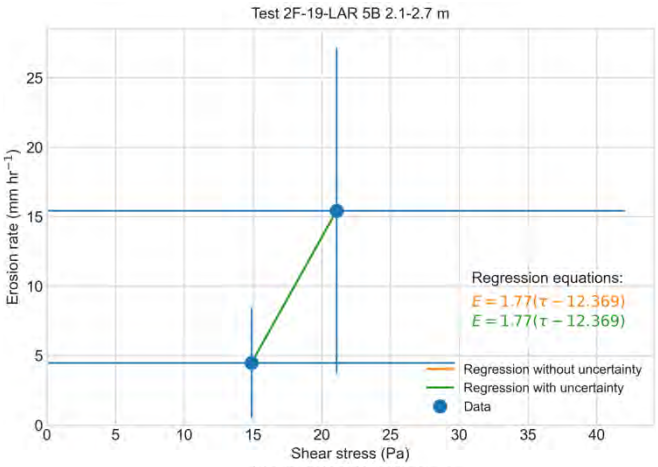
Test 2F-19-LAR 5B 2.1-2.7 m
Erosion rate (mm hr⁻¹)
Shear stress (Pa)
Regression equations:
E = 1.77(τ − 12.369)
E = 1.77(τ − 12.369)
Regression without uncertainty
Regression with uncertainty
Data

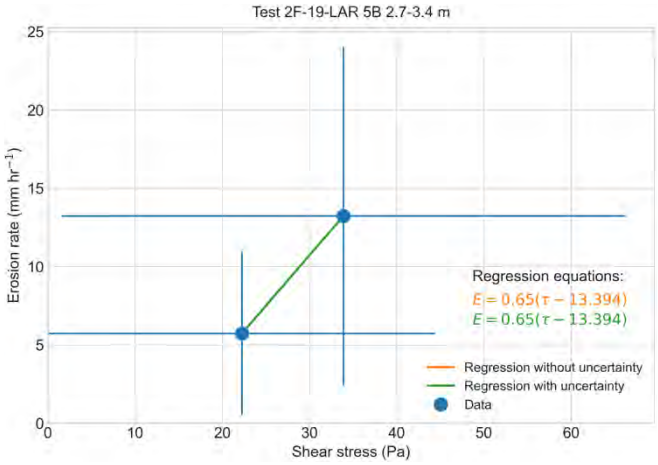
Test 2F-19-LAR 5B 2.7-3.4 m
Erosion rate (mm hr⁻¹)
Shear stress (Pa)
Regression equations:
E = 0.65(τ − 13.394)
E = 0.65(τ − 13.394)
Regression without uncertainty
Regression with uncertainty
Data

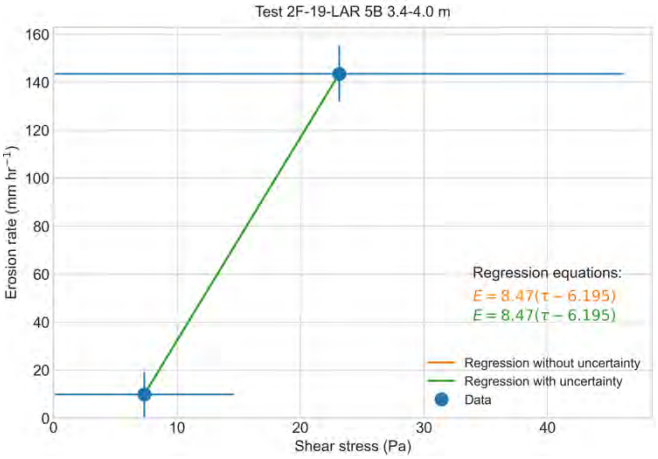
Test 2F-19-LAR 5B 3.4-4.0 m
Erosion rate (mm hr⁻¹)
Shear stress (Pa)
Regression equations:
E = 8.47(τ − 6.195)
E = 8.47(τ − 6.195)
Regression without uncertainty
Regression with uncertainty
Data

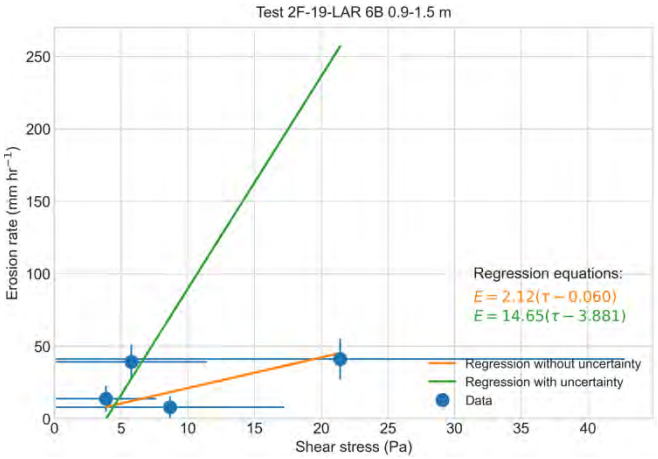
Test 2F-19-LAR 6B 0.9-1.5 m
Erosion rate (mm hr⁻¹)
Shear stress (Pa)
Regression equations:
E = 2.12(τ − 0.060)
E = 14.65(τ − 3.881)
Regression without uncertainty
Regression with uncertainty
Data

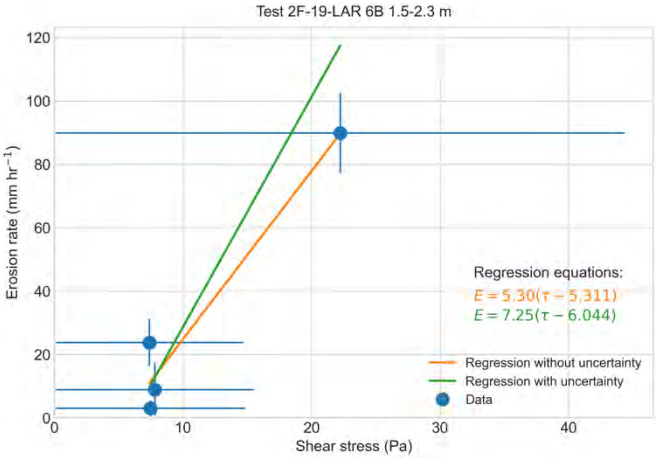
Test 2F-19-LAR 6B 1.5-2.3 m
Erosion rate (mm hr⁻¹)
Shear stress (Pa)
Regression equations:
E = 5.30(τ − 5.311)
E = 7.25(τ − 6.044)
Regression without uncertainty
Regression with uncertainty
Data

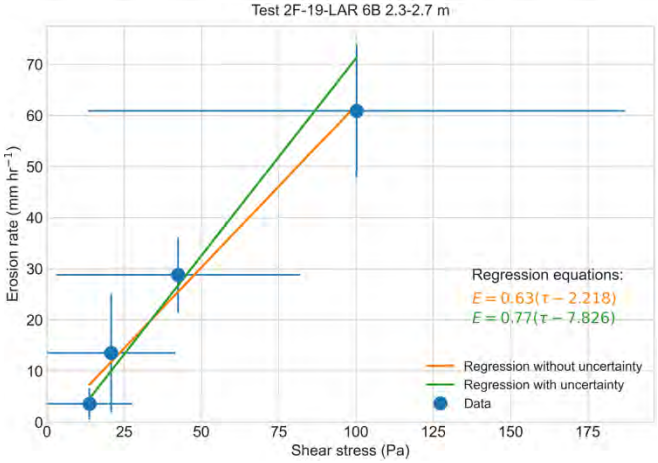
Test 2F-19-LAR 6B 2.3-2.7 m
Erosion rate (mm hr⁻¹)
Shear stress (Pa)
Regression equations:
E = 0.63(τ − 2.218)
E = 0.77(τ − 7.826)
Regression without uncertainty
Regression with uncertainty
Data

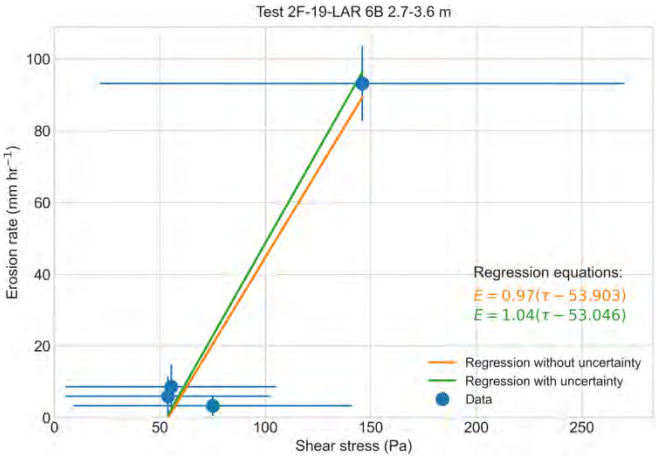
Test 2F-19-LAR 6B 2.7-3.6 m
Erosion rate (mm hr^{-1})
Shear stress (Pa)
Regression equations:
$\dot{E} = 0.97(\tau - 53.903)$
$\dot{E} = 1.04(\tau - 53.046)$
Regression without uncertainty
Regression with uncertainty
Data

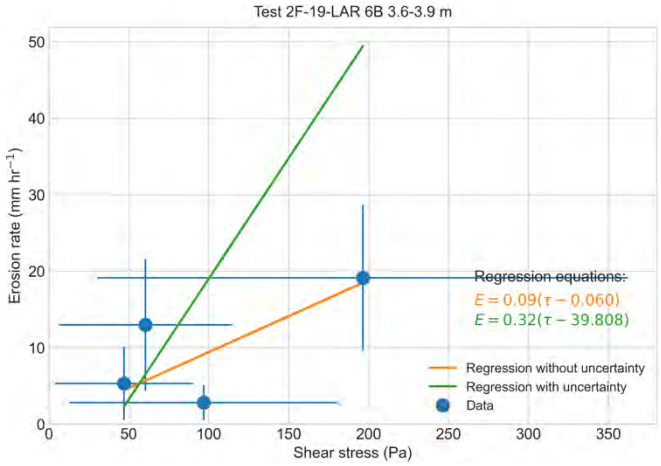
Test 2F-19-LAR 6B 3.6-3.9 m
Erosion rate (mm hr^{-1})
Shear stress (Pa)
Regression equations:
$\dot{E} = 0.09(\tau - 0.060)$
$\dot{E} = 0.32(\tau - 39.808)$
Regression without uncertainty
Regression with uncertainty
Data

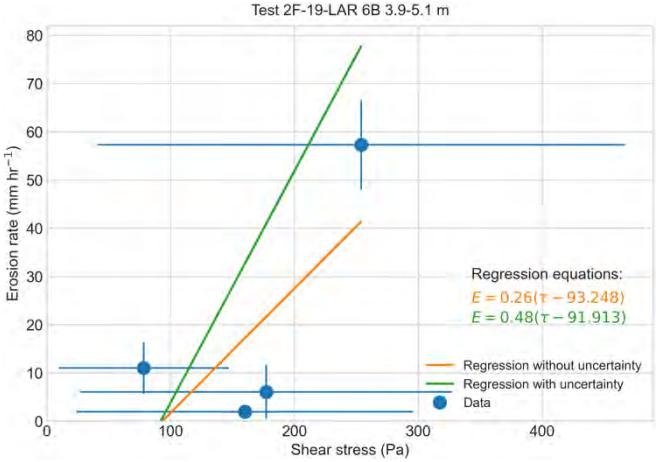
Test 2F-19-LAR 6B 3.9-5.1 m
Erosion rate (mm hr^{-1})
Shear stress (Pa)
Regression equations:
$\dot{E} = 0.26(\tau - 93.248)$
$\dot{E} = 0.48(\tau - 91.913)$
Regression without uncertainty
Regression with uncertainty
Data

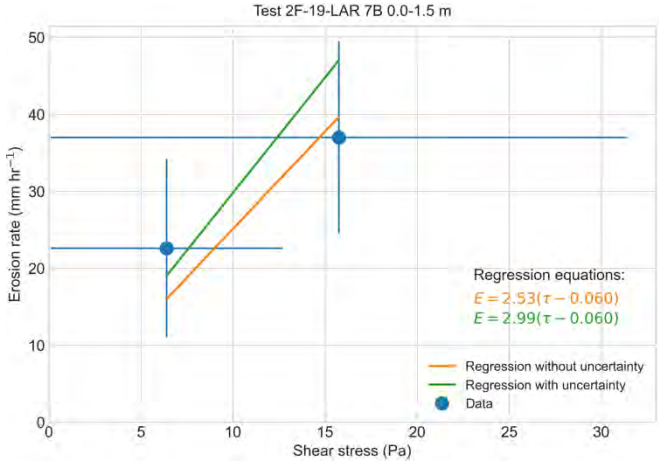
Test 2F-19-LAR 7B 0.0-1.5 m
Erosion rate (mm hr^{-1})
Shear stress (Pa)
Regression equations:
$\dot{E} = 2.53(\tau - 0.060)$
$\dot{E} = 2.99(\tau - 0.060)$
Regression without uncertainty
Regression with uncertainty
Data

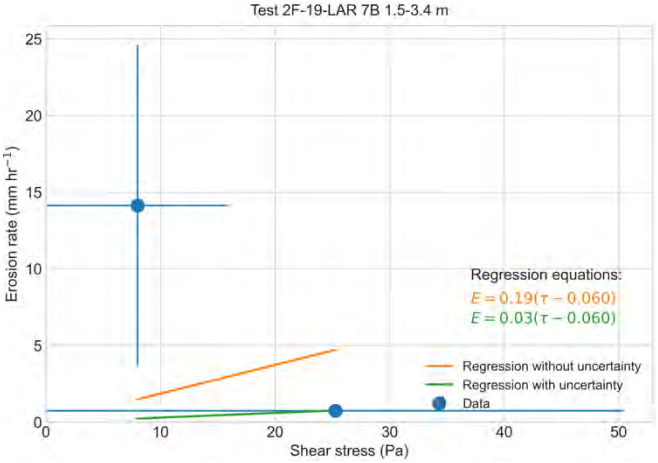
Test 2F-19-LAR 7B 1.5-3.4 m
Erosion rate (mm hr^{-1})
Shear stress (Pa)
Regression equations:
$\dot{E} = 0.19(\tau - 0.060)$
$\dot{E} = 0.03(\tau - 0.060)$
Regression without uncertainty
Regression with uncertainty
Data

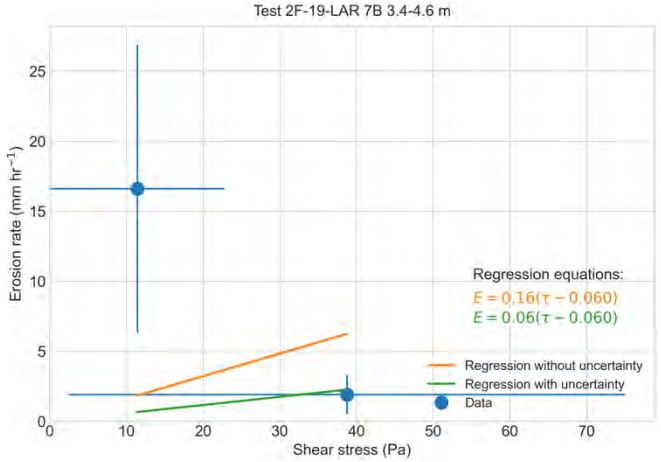
Test 2F-19-LAR 7B 3.4-4.6 m
Erosion rate (mm hr^{-1})
Shear stress (Pa)
Regression equations:
$\dot{E} = 0.16(\tau - 0.060)$
$\dot{E} = 0.06(\tau - 0.060)$
Regression without uncertainty
Regression with uncertainty
Data

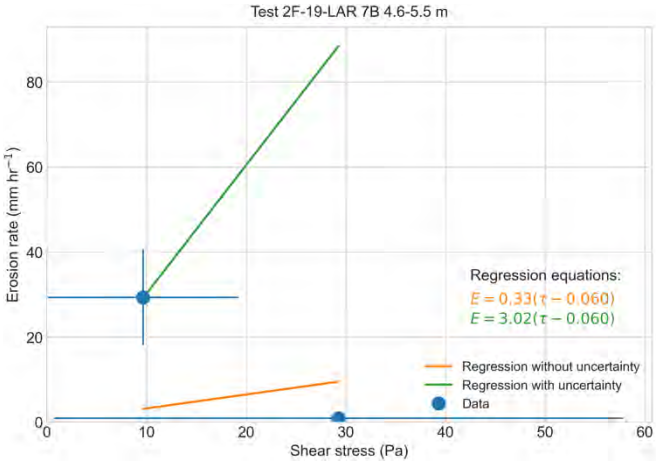
Test 2F-19-LAR 7B 4.6-5.5 m
Erosion rate (mm hr^{-1})
Shear stress (Pa)
Regression equations:
$E = 0.33(\tau - 0.060)$
$E = 3.02(\tau - 0.060)$
Regression without uncertainty
Regression with uncertainty
Data

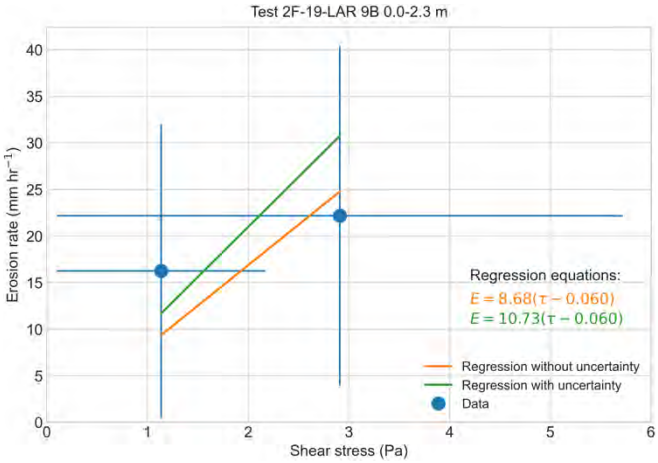
Test 2F-19-LAR 9B 0.0-2.3 m
Erosion rate (mm hr^{-1})
Shear stress (Pa)
Regression equations:
$E = 8.68(\tau - 0.060)$
$E = 10.73(\tau - 0.060)$
Regression without uncertainty
Regression with uncertainty
Data

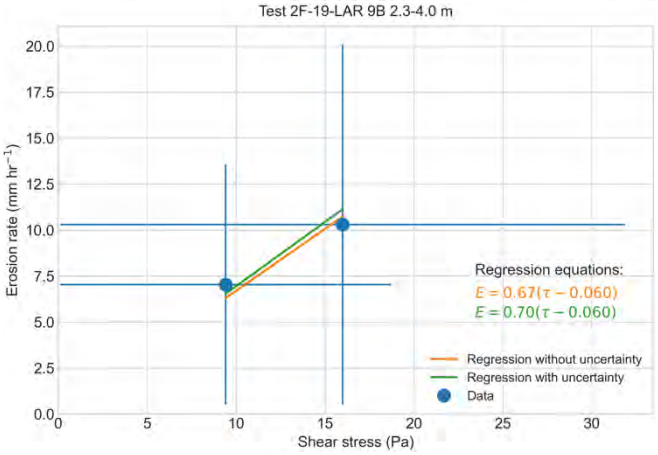
Test 2F-19-LAR 9B 2.3-4.0 m
Erosion rate (mm hr^{-1})
Shear stress (Pa)
Regression equations:
$E = 0.67(\tau - 0.060)$
$E = 0.70(\tau - 0.060)$
Regression without uncertainty
Regression with uncertainty
Data

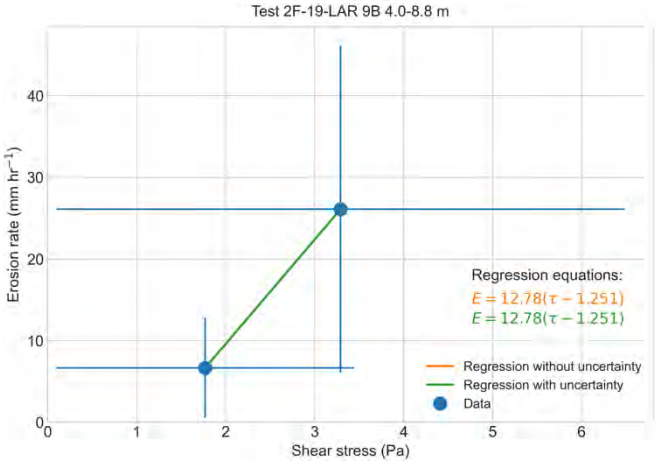
Test 2F-19-LAR 9B 4.0-8.8 m
Erosion rate (mm hr^{-1})
Shear stress (Pa)
Regression equations:
$E = 12.78(\tau - 1.251)$
$E = 12.78(\tau - 1.251)$
Regression without uncertainty
Regression with uncertainty
Data

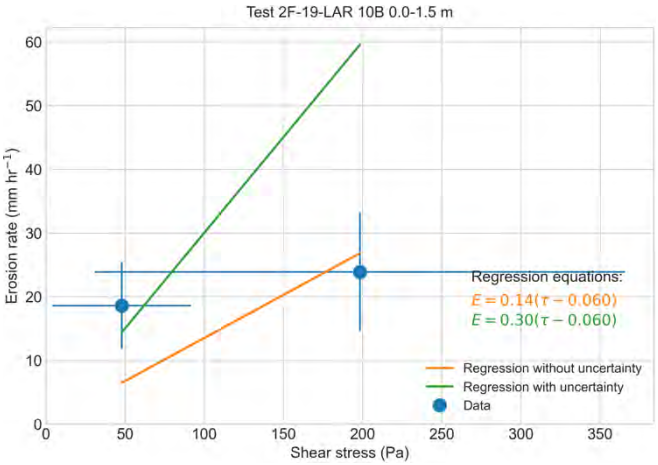
Test 2F-19-LAR 10B 0.0-1.5 m
Erosion rate (mm hr^{-1})
Shear stress (Pa)
Regression equations:
$E = 0.14(\tau - 0.060)$
$E = 0.30(\tau - 0.060)$
Regression without uncertainty
Regression with uncertainty
Data

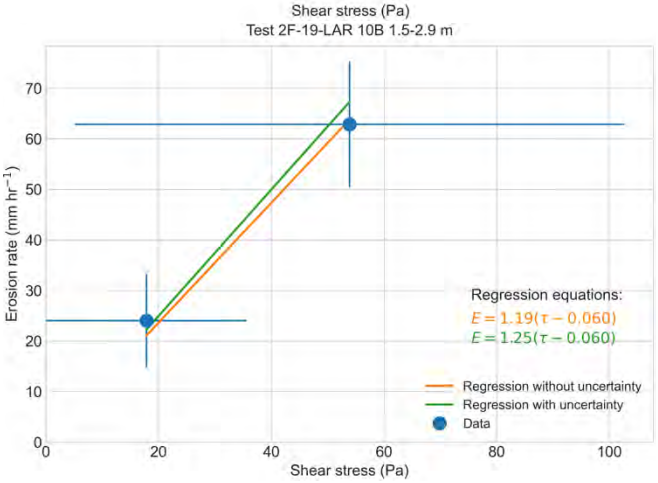
Test 2F-19-LAR 10B 1.5-2.9 m
Erosion rate (mm hr^{-1})
Shear stress (Pa)
Regression equations:
$E = 1.19(\tau - 0.060)$
$E = 1.25(\tau - 0.060)$
Regression without uncertainty
Regression with uncertainty
Data

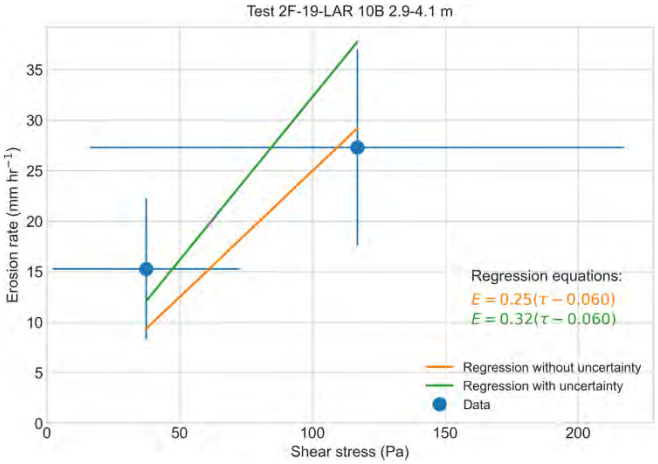
Test 2F-19-LAR 10B 2.9-4.1 m
Erosion rate (mm hr^{-1})
Shear stress (Pa)
Regression equations:
$E = 0.25(\tau - 0.060)$
$E = 0.32(\tau - 0.060)$
Regression without uncertainty
Regression with uncertainty
Data

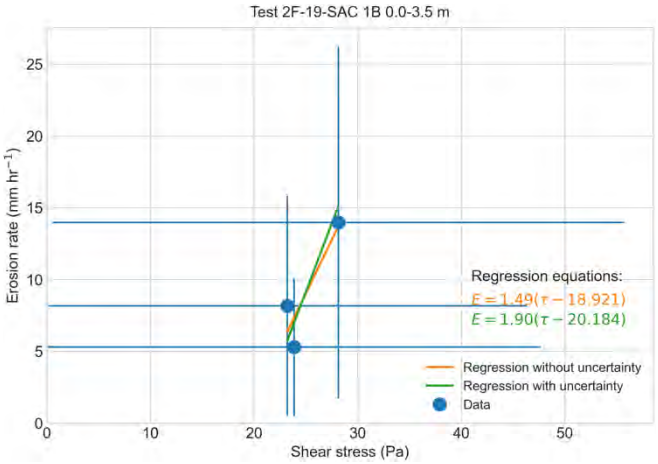
Test 2F-19-SAC 1B 0.0-3.5 m
Erosion rate (mm hr^{-1})
Shear stress (Pa)
Regression equations:
$E = 1.49(\tau - 18.921)$
$E = 1.90(\tau - 20.184)$
Regression without uncertainty
Regression with uncertainty
Data

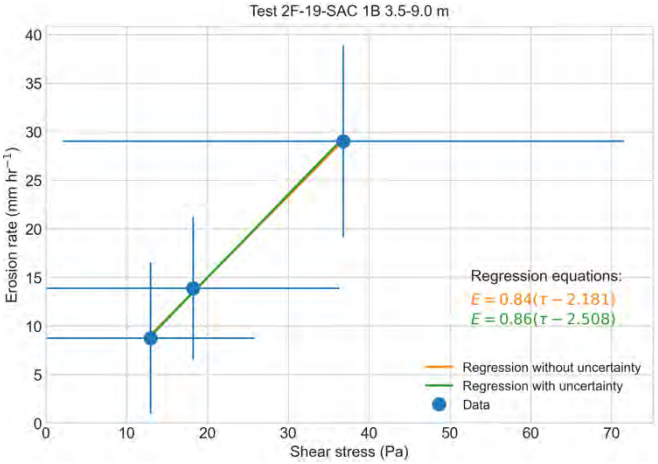
Test 2F-19-SAC 1B 3.5-9.0 m
Erosion rate (mm hr^{-1})
Shear stress (Pa)
Regression equations:
$E = 0.84(\tau - 2.181)$
$E = 0.86(\tau - 2.508)$
Regression without uncertainty
Regression with uncertainty
Data

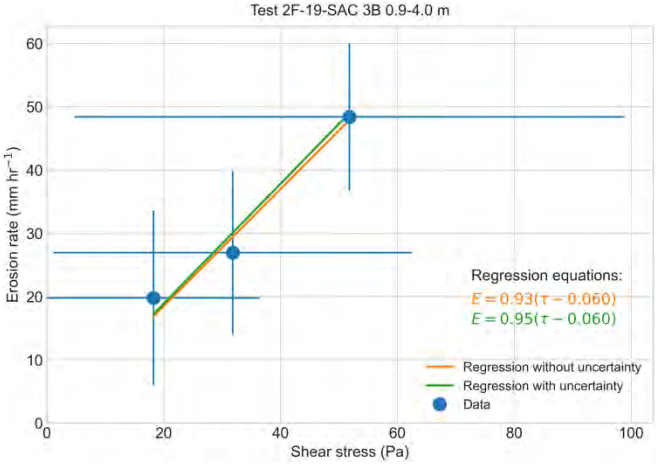
Test 2F-19-SAC 3B 0.9-4.0 m
Erosion rate (mm hr^{-1})
Shear stress (Pa)
Regression equations:
$E = 0.93(\tau - 0.060)$
$E = 0.95(\tau - 0.060)$
Regression without uncertainty
Regression with uncertainty
Data

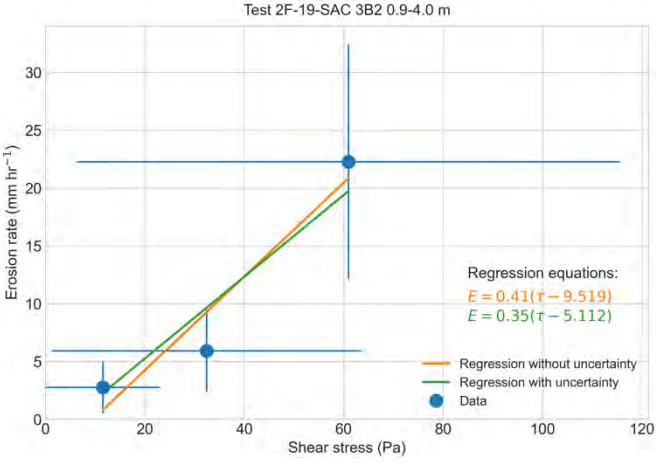
Test 2F-19-SAC 3B2 0.9-4.0 m
Erosion rate (mm hr^{-1})
Shear stress (Pa)
Regression equations:
$E = 0.41(\tau - 9.519)$
$E = 0.35(\tau - 5.112)$
Regression without uncertainty
Regression with uncertainty
Data

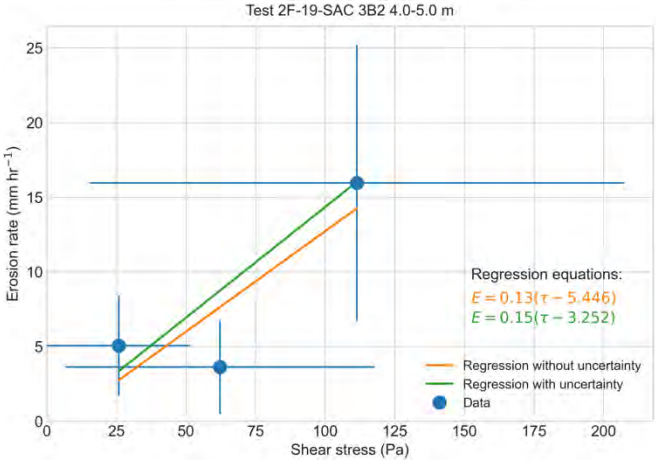
Test 2F-19-SAC 3B2 4.0-5.0 m
Erosion rate (mm hr^{-1})
Shear stress (Pa)
Regression equations:
$E = 0.13(\tau - 5.446)$
$E = 0.15(\tau - 3.252)$
Regression without uncertainty
Regression with uncertainty
Data

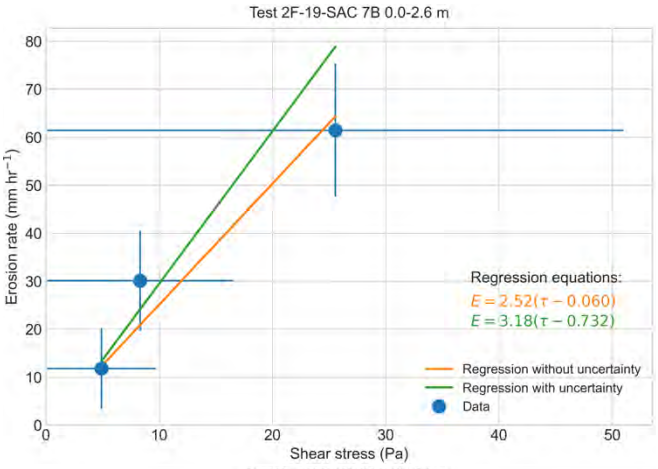

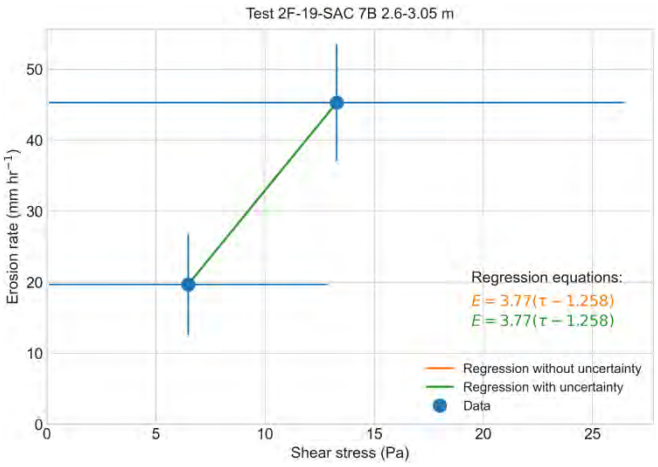

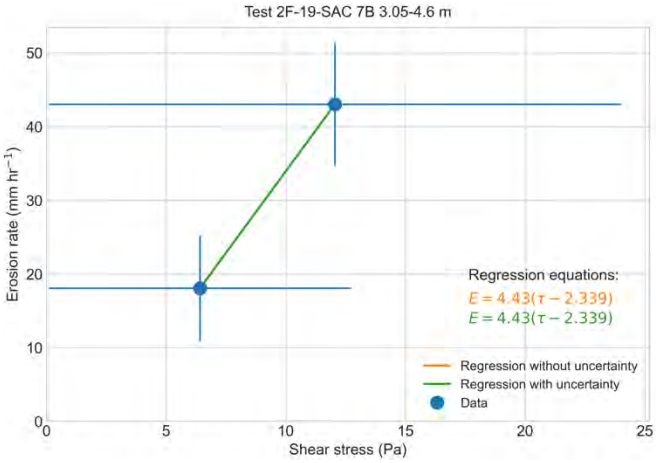

Borehole erosion tests – grain shear stress

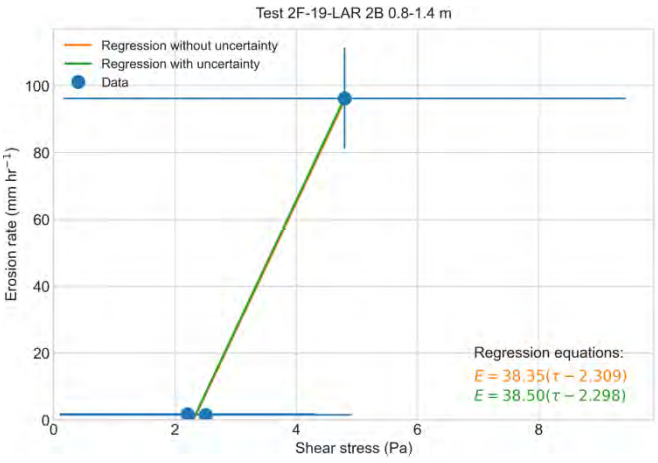

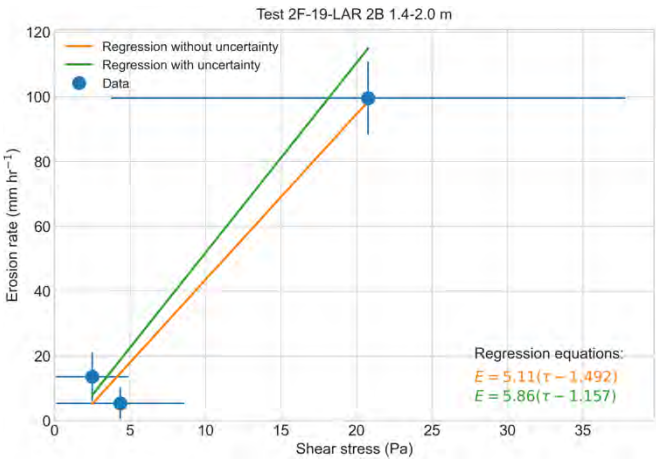

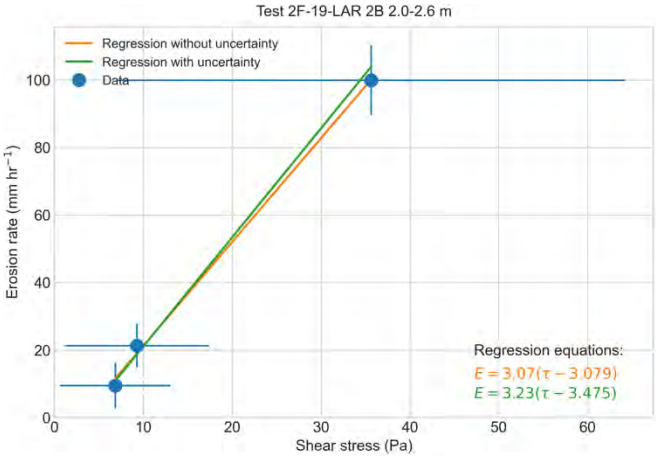
Test 2F-19-LAR 2B 2.0-2.6 m
Regression without uncertainty
Regression with uncertainty
Data
Erosion rate (mm hr⁻¹)
Shear stress (Pa)
Regression equations:
E = 3.07(τ − 3.079)
E = 3.23(τ − 3.475)

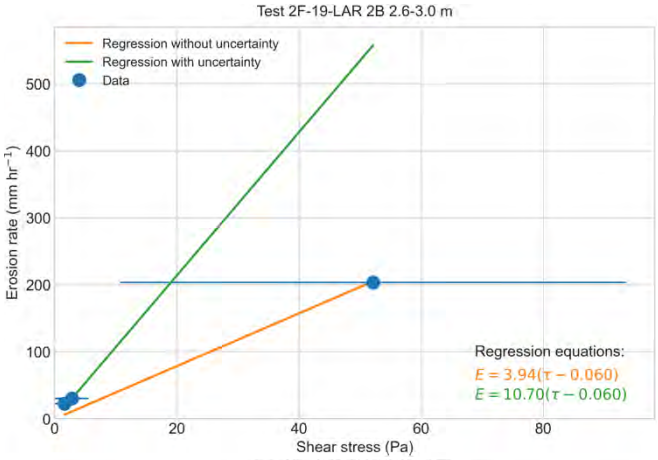
Test 2F-19-LAR 2B 2.6-3.0 m
Regression without uncertainty
Regression with uncertainty
Data
Erosion rate (mm hr⁻¹)
Shear stress (Pa)
Regression equations:
E = 3.94(τ − 0.060)
E = 10.70(τ − 0.060)

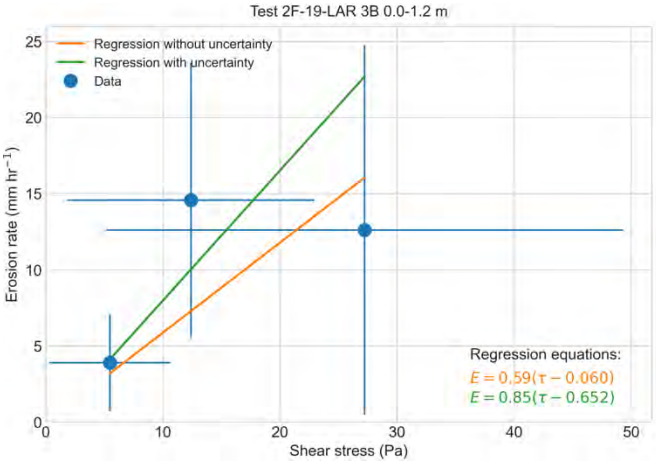
Test 2F-19-LAR 3B 0.0-1.2 m
Regression without uncertainty
Regression with uncertainty
Data
Erosion rate (mm hr⁻¹)
Shear stress (Pa)
Regression equations:
E = 0.59(τ − 0.060)
E = 0.85(τ − 0.652)

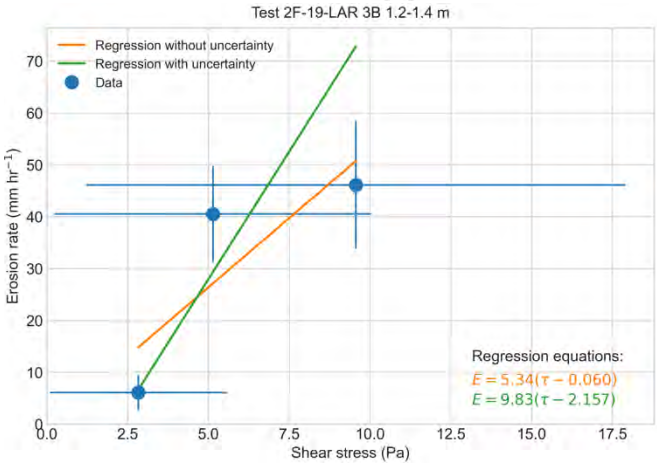
Test 2F-19-LAR 3B 1.2-1.4 m
Regression without uncertainty
Regression with uncertainty
Data
Erosion rate (mm hr⁻¹)
Shear stress (Pa)
Regression equations:
E = 5.34(τ − 0.060)
E = 9.83(τ − 2.157)

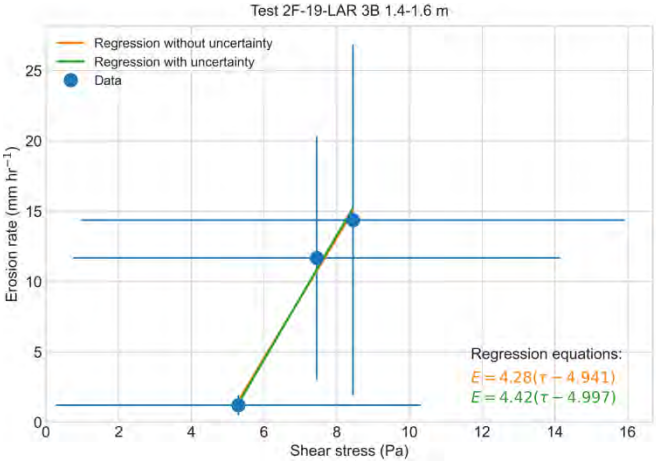
Test 2F-19-LAR 3B 1.4-1.6 m
Regression without uncertainty
Regression with uncertainty
Data
Erosion rate (mm hr⁻¹)
Shear stress (Pa)
Regression equations:
E = 4.28(τ − 4.941)
E = 4.42(τ − 4.997)

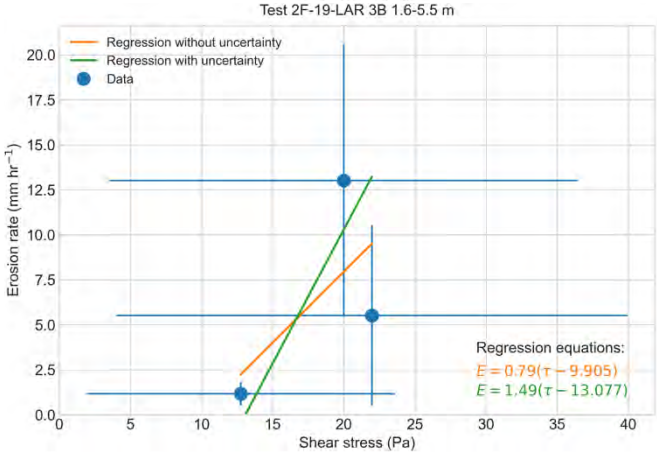
Test 2F-19-LAR 3B 1.6-5.5 m
Regression without uncertainty
Regression with uncertainty
Data
Erosion rate (mm hr⁻¹)
Shear stress (Pa)
Regression equations:
E = 0.79(τ − 9.905)
E = 1.49(τ − 13.077)

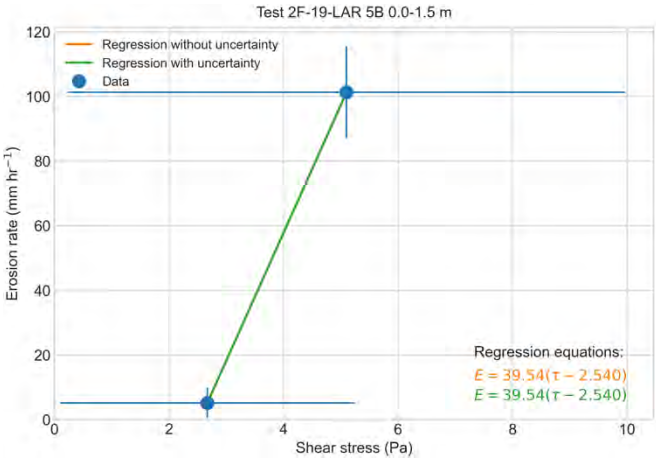
Test 2F-19-LAR 5B 0.0-1.5 m
Regression without uncertainty
Regression with uncertainty
Data
Erosion rate (mm hr^{-1})
Shear stress (Pa)
Regression equations:
$E = 39.54(\tau - 2.540)$
$E = 39.54(\tau - 2.540)$

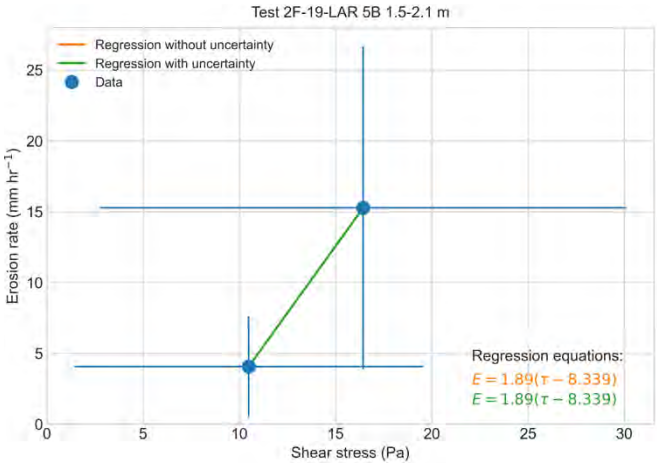
Test 2F-19-LAR 5B 1.5-2.1 m
Regression without uncertainty
Regression with uncertainty
Data
Erosion rate (mm hr^{-1})
Shear stress (Pa)
Regression equations:
$E = 1.89(\tau - 8.339)$
$E = 1.89(\tau - 8.339)$

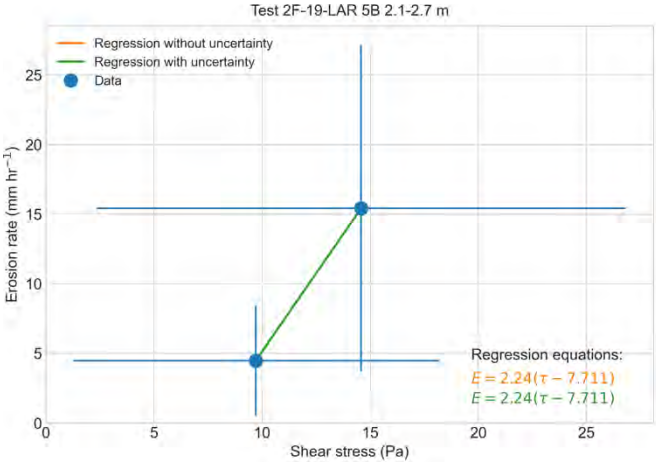
Test 2F-19-LAR 5B 2.1-2.7 m
Regression without uncertainty
Regression with uncertainty
Data
Erosion rate (mm hr^{-1})
Shear stress (Pa)
Regression equations:
$E = 2.24(\tau - 7.711)$
$E = 2.24(\tau - 7.711)$

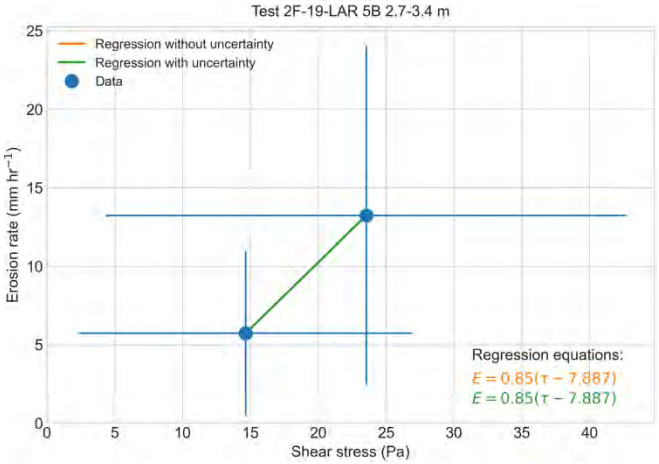
Test 2F-19-LAR 5B 2.7-3.4 m
Regression without uncertainty
Regression with uncertainty
Data
Erosion rate (mm hr^{-1})
Shear stress (Pa)
Regression equations:
$E = 0.85(\tau - 7.887)$
$E = 0.85(\tau - 7.887)$

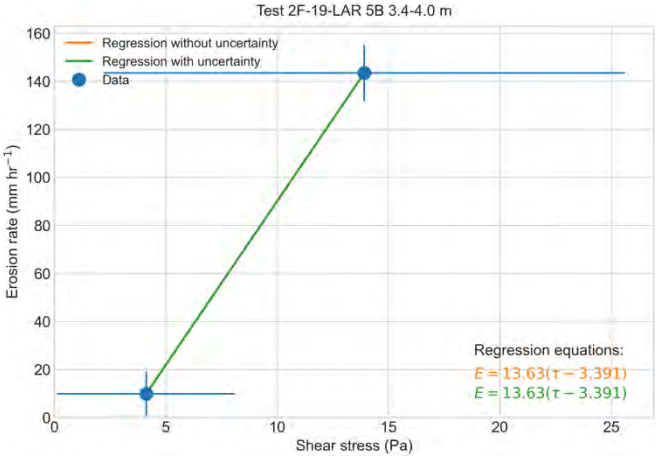
Test 2F-19-LAR 5B 3.4-4.0 m
Regression without uncertainty
Regression with uncertainty
Data
Erosion rate (mm hr^{-1})
Shear stress (Pa)
Regression equations:
$E = 13.63(\tau - 3.391)$
$E = 13.63(\tau - 3.391)$

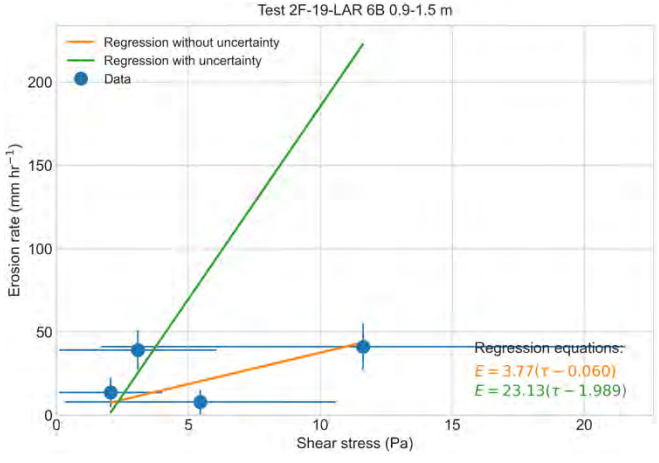
Test 2F-19-LAR 6B 0.9-1.5 m
Regression without uncertainty
Regression with uncertainty
Data
Erosion rate (mm hr^{-1})
Shear stress (Pa)
Regression equations:
$E = 3.77(\tau - 0.060)$
$E = 23.13(\tau - 1.989)$

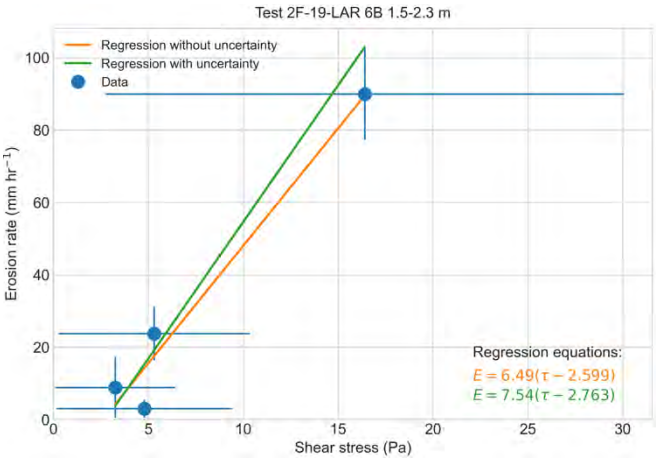
Test 2F-19-LAR 6B 1.5-2.3 m
Regression without uncertainty
Regression with uncertainty
Data
Erosion rate (mm hr⁻¹)
Shear stress (Pa)
Regression equations:
E = 6.49(τ − 2.599)
E = 7.54(τ − 2.763)

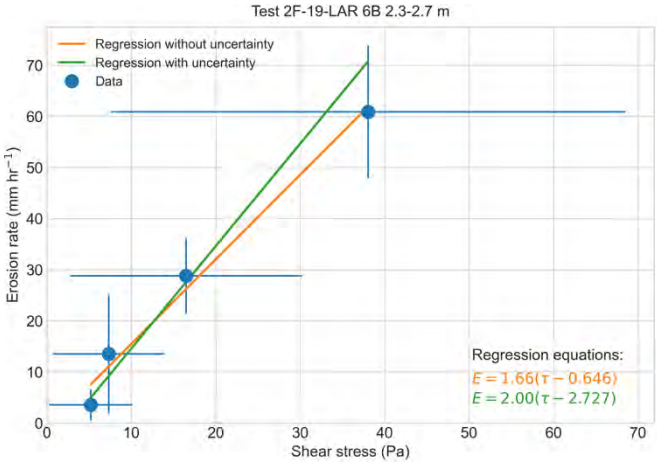
Test 2F-19-LAR 6B 2.3-2.7 m
Regression without uncertainty
Regression with uncertainty
Data
Erosion rate (mm hr⁻¹)
Shear stress (Pa)
Regression equations:
E = 1.66(τ − 0.646)
E = 2.00(τ − 2.727)

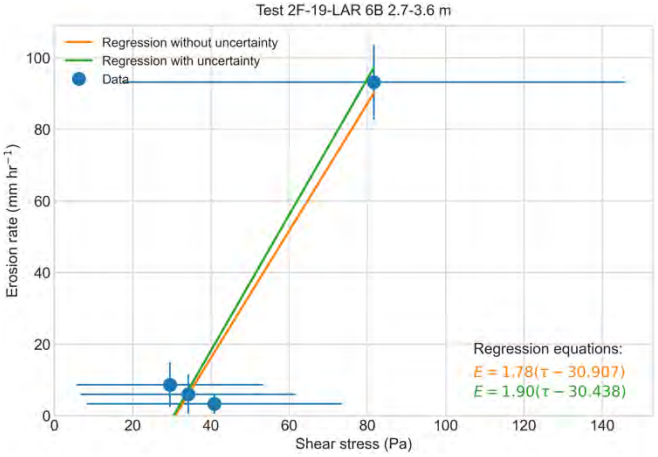
Test 2F-19-LAR 6B 2.7-3.6 m
Regression without uncertainty
Regression with uncertainty
Data
Erosion rate (mm hr⁻¹)
Shear stress (Pa)
Regression equations:
E = 1.78(τ − 30.907)
E = 1.90(τ − 30.438)

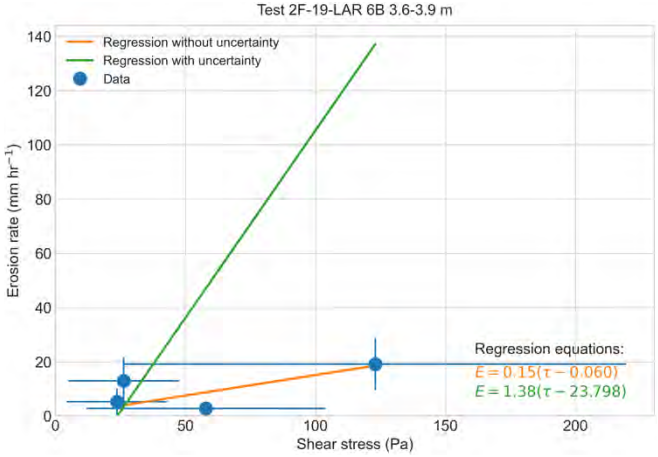
Test 2F-19-LAR 6B 3.6-3.9 m
Regression without uncertainty
Regression with uncertainty
Data
Erosion rate (mm hr⁻¹)
Shear stress (Pa)
Regression equations:
E = 0.15(τ − 0.060)
E = 1.38(τ − 23.798)

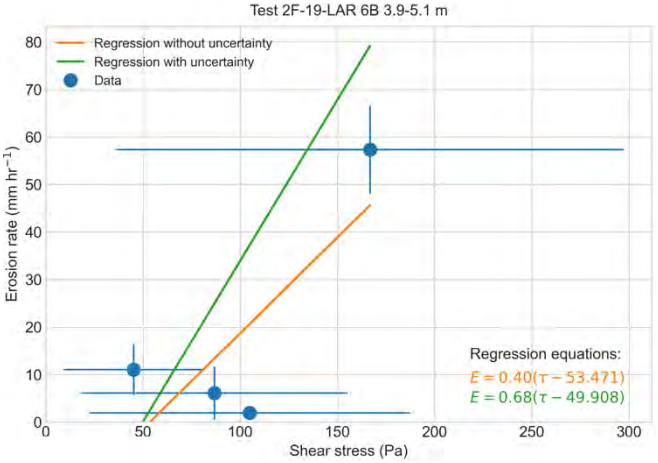
Test 2F-19-LAR 6B 3.9-5.1 m
Regression without uncertainty
Regression with uncertainty
Data
Erosion rate (mm hr⁻¹)
Shear stress (Pa)
Regression equations:
E = 0.40(τ − 53.471)
E = 0.68(τ − 49.908)

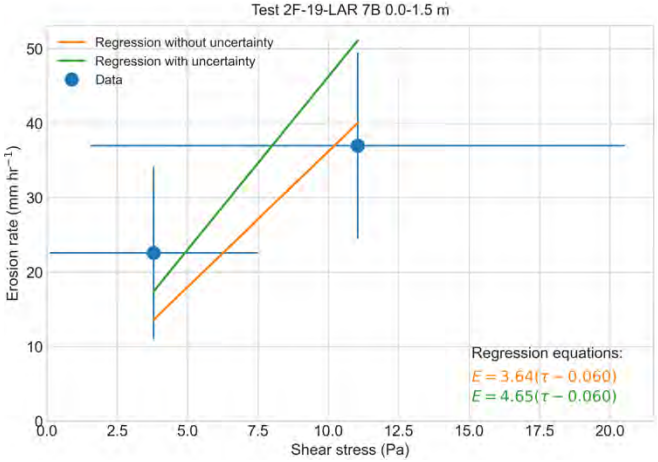
Test 2F-19-LAR 7B 0.0-1.5 m
Regression without uncertainty
Regression with uncertainty
Data
Erosion rate (mm hr⁻¹)
Shear stress (Pa)
Regression equations:
E = 3.64(τ − 0.060)
E = 4.65(τ − 0.060)

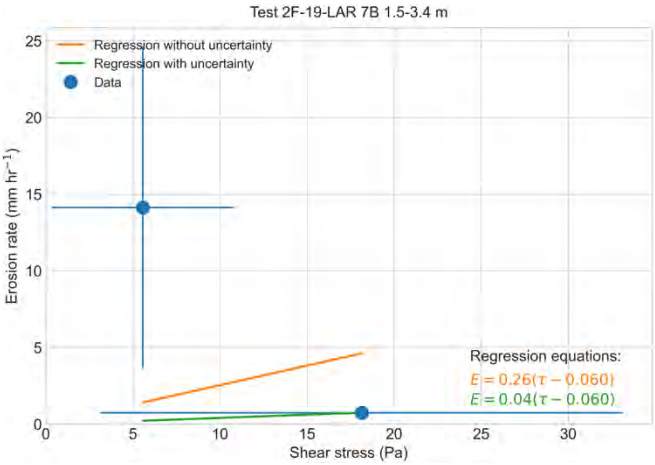
Test 2F-19-LAR 7B 1.5-3.4 m
Regression without uncertainty
Regression with uncertainty
Data
Erosion rate (mm hr^{-1})
Shear stress (Pa)
Regression equations:
$E = 0.26(\tau - 0.060)$
$E = 0.04(\tau - 0.060)$

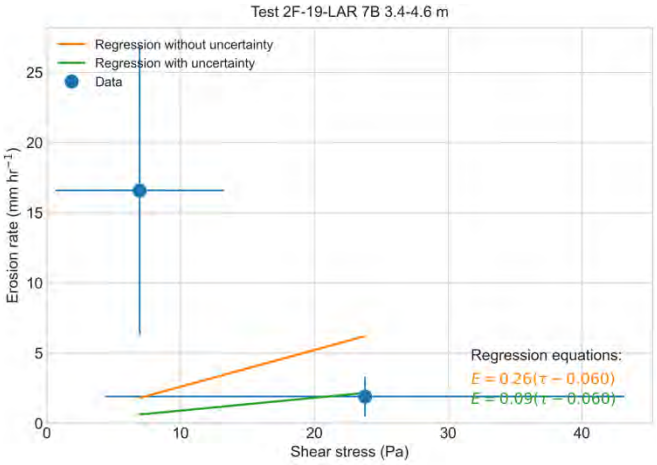
Test 2F-19-LAR 7B 3.4-4.6 m
Regression without uncertainty
Regression with uncertainty
Data
Erosion rate (mm hr^{-1})
Shear stress (Pa)
Regression equations:
$E = 0.26(\tau - 0.060)$
$E = 0.09(\tau - 0.060)$

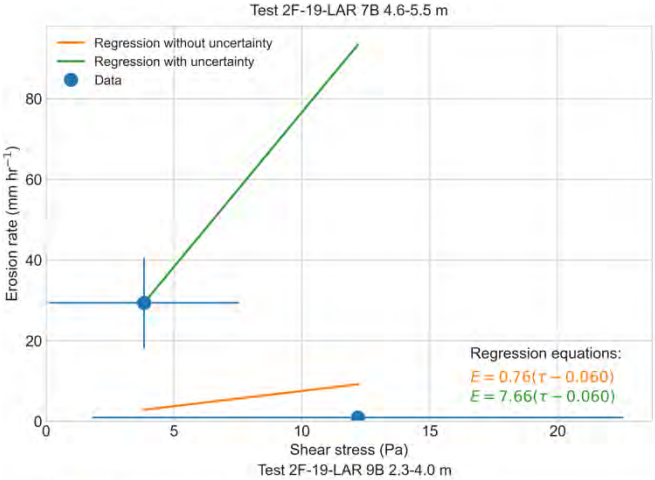
Test 2F-19-LAR 7B 4.6-5.5 m
Regression without uncertainty
Regression with uncertainty
Data
Erosion rate (mm hr^{-1})
Shear stress (Pa)
Regression equations:
$E = 0.76(\tau - 0.060)$
$E = 7.66(\tau - 0.060)$

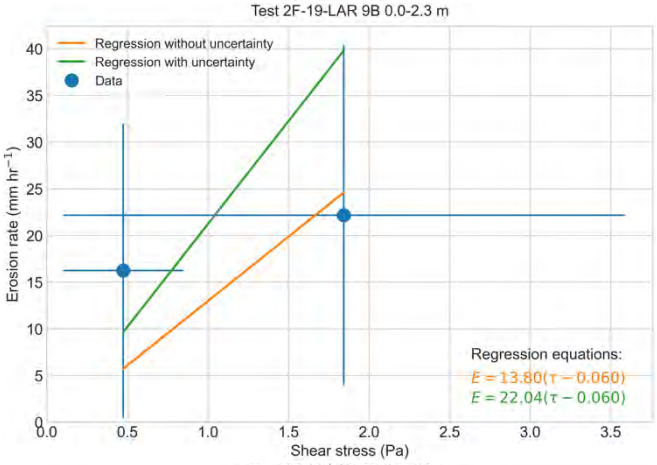
Test 2F-19-LAR 9B 0.0-2.3 m
Regression without uncertainty
Regression with uncertainty
Data
Erosion rate (mm hr^{-1})
Shear stress (Pa)
Regression equations:
$E = 13.80(\tau - 0.060)$
$E = 22.04(\tau - 0.060)$

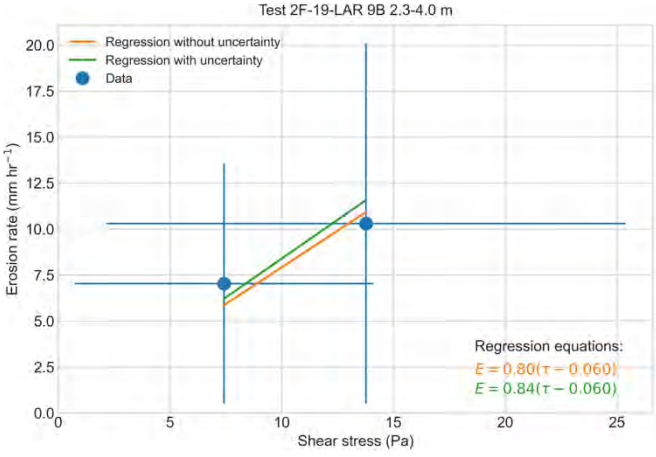
Test 2F-19-LAR 9B 2.3-4.0 m
Regression without uncertainty
Regression with uncertainty
Data
Erosion rate (mm hr^{-1})
Shear stress (Pa)
Regression equations:
$E = 0.80(\tau - 0.060)$
$E = 0.84(\tau - 0.060)$

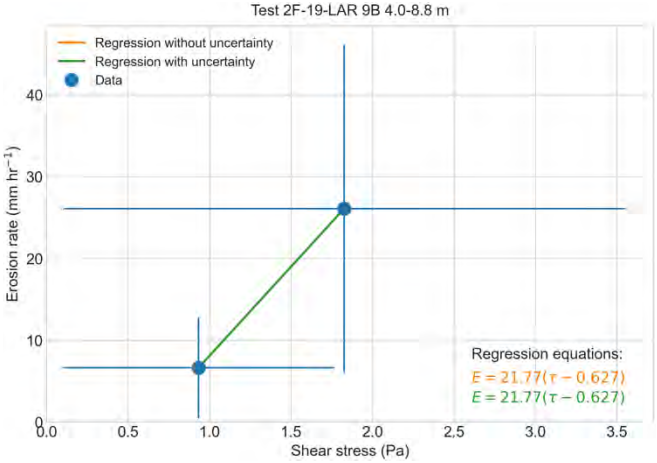
Test 2F-19-LAR 9B 4.0-8.8 m
Regression without uncertainty
Regression with uncertainty
Data
Erosion rate (mm hr^{-1})
Shear stress (Pa)
Regression equations:
$E = 21.77(\tau - 0.627)$
$E = 21.77(\tau - 0.627)$

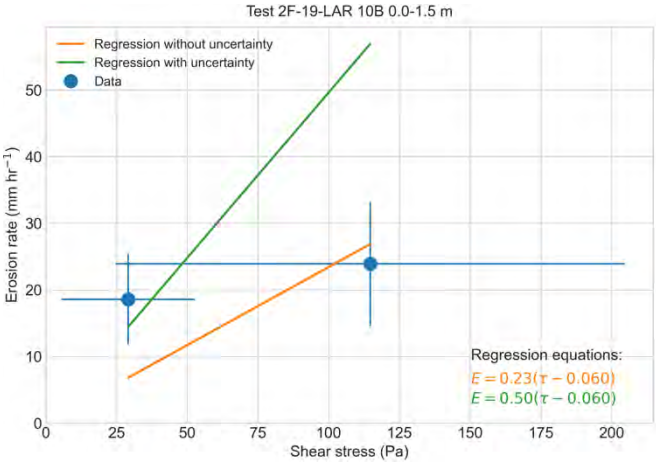
Test 2F-19-LAR 10B 0.0-1.5 m
Regression without uncertainty
Regression with uncertainty
Data
Erosion rate (mm hr^{-1})
Shear stress (Pa)
Regression equations:
$E = 0.23(\tau - 0.060)$
$E = 0.50(\tau - 0.060)$

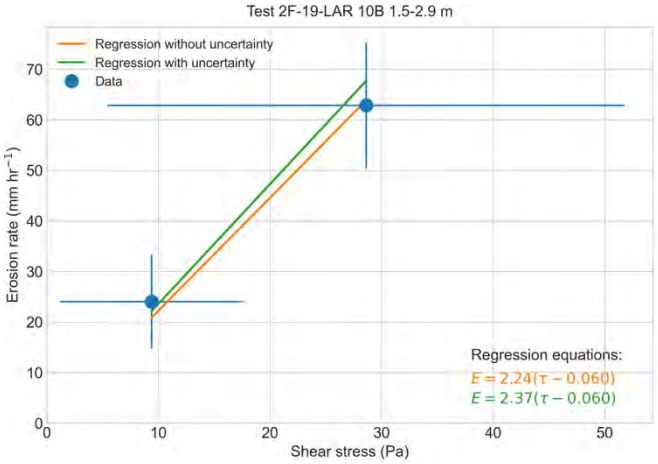
Test 2F-19-LAR 10B 1.5-2.9 m
Regression without uncertainty
Regression with uncertainty
Data
Erosion rate (mm hr^{-1})
Shear stress (Pa)
Regression equations:
$E = 2.24(\tau - 0.060)$
$E = 2.37(\tau - 0.060)$

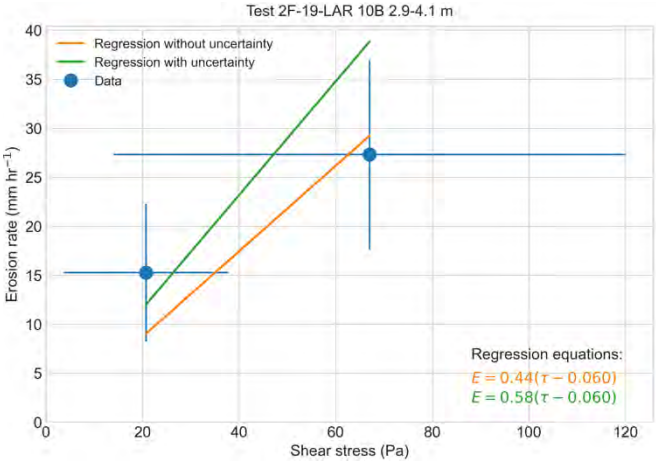
Test 2F-19-LAR 10B 2.9-4.1 m
Regression without uncertainty
Regression with uncertainty
Data
Erosion rate (mm hr^{-1})
Shear stress (Pa)
Regression equations:
$E = 0.44(\tau - 0.060)$
$E = 0.58(\tau - 0.060)$

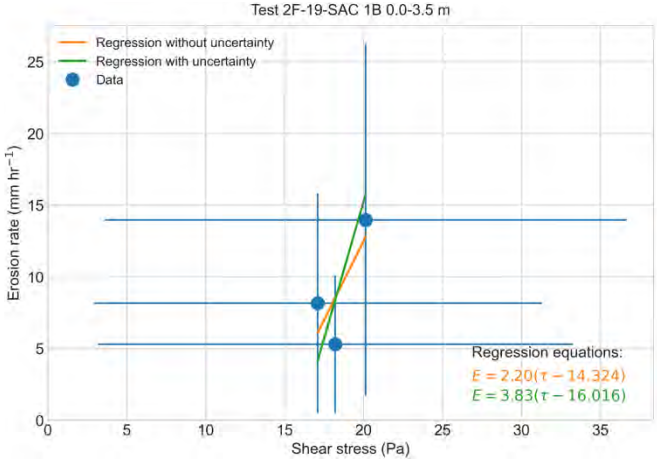
Test 2F-19-SAC 1B 0.0-3.5 m
Regression without uncertainty
Regression with uncertainty
Data
Erosion rate (mm hr^{-1})
Shear stress (Pa)
Regression equations:
$E = 2.20(\tau - 14.324)$
$E = 3.83(\tau - 16.016)$

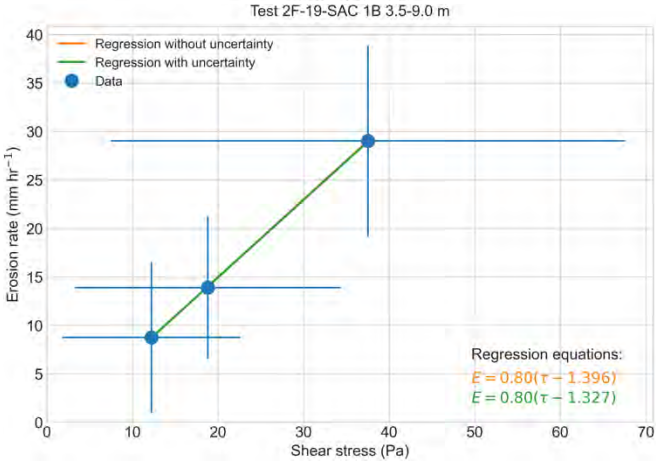
Test 2F-19-SAC 1B 3.5-9.0 m
Regression without uncertainty
Regression with uncertainty
Data
Erosion rate (mm hr^{-1})
Shear stress (Pa)
Regression equations:
$E = 0.80(\tau - 1.396)$
$E = 0.80(\tau - 1.327)$

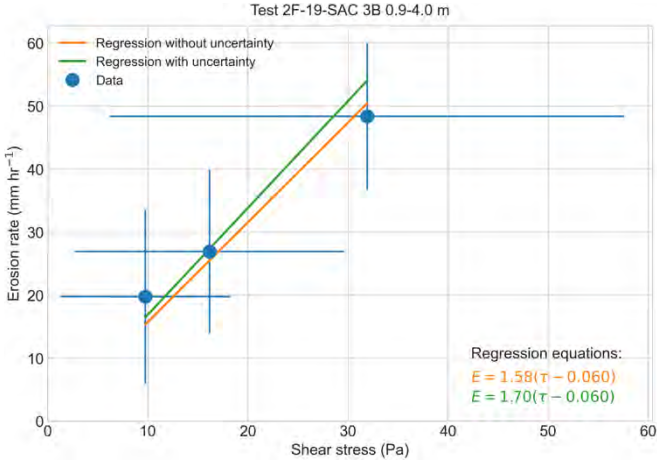
Test 2F-19-SAC 3B 0.9-4.0 m
Regression without uncertainty
Regression with uncertainty
Data
Erosion rate (mm hr^{-1})
Shear stress (Pa)
Regression equations:
$E = 1.58(\tau - 0.060)$
$E = 1.70(\tau - 0.060)$

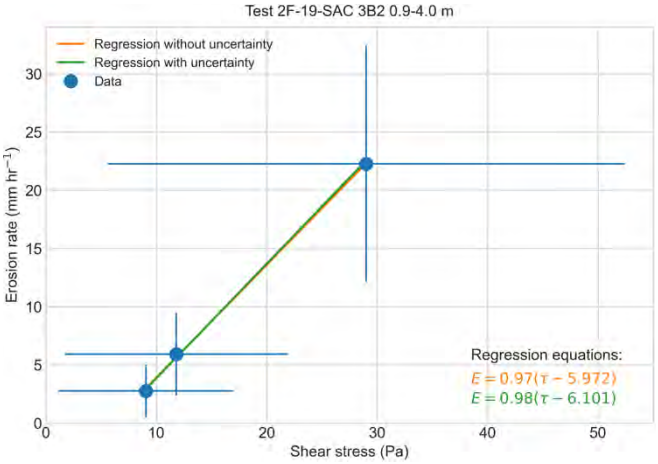
Test 2F-19-SAC 3B2 0.9-4.0 m
Regression without uncertainty
Regression with uncertainty
Data
Erosion rate (mm hr⁻¹)
Shear stress (Pa)
Regression equations:
$E = 0.97(\tau - 5.972)$
$E = 0.98(\tau - 6.101)$

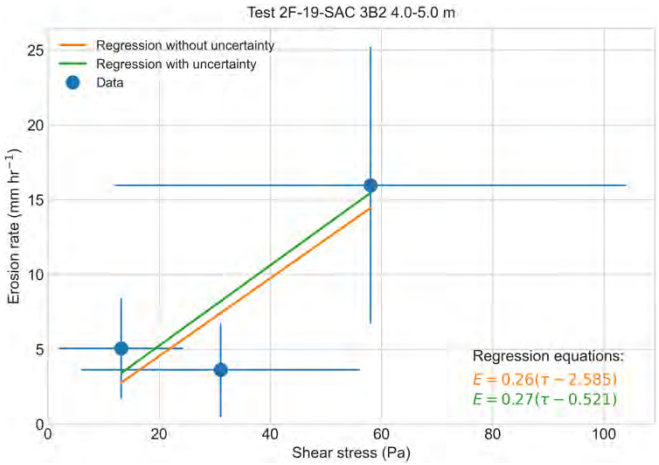
Test 2F-19-SAC 3B2 4.0-5.0 m
Regression without uncertainty
Regression with uncertainty
Data
Erosion rate (mm hr⁻¹)
Shear stress (Pa)
Regression equations:
$E = 0.26(\tau - 2.585)$
$E = 0.27(\tau - 0.521)$

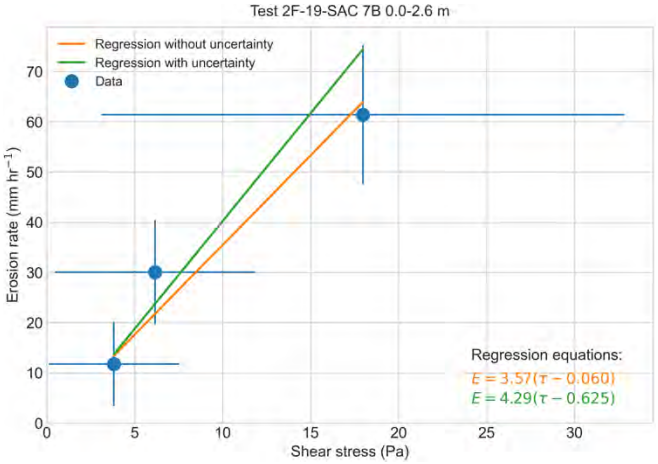
Test 2F-19-SAC 7B 0.0-2.6 m
Regression without uncertainty
Regression with uncertainty
Data
Erosion rate (mm hr⁻¹)
Shear stress (Pa)
Regression equations:
$E = 3.57(\tau - 0.060)$
$E = 4.29(\tau - 0.625)$

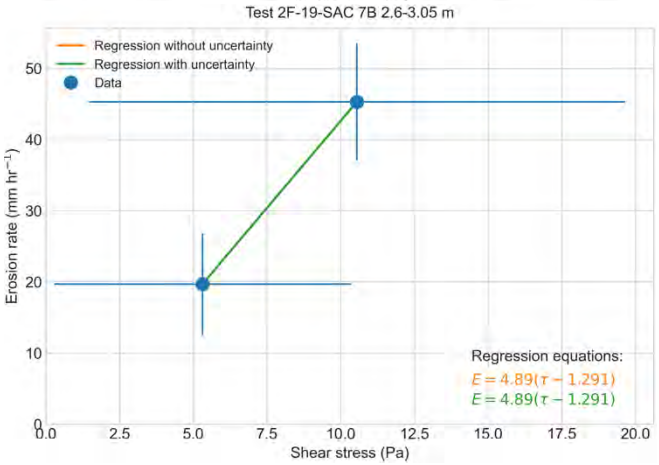
Test 2F-19-SAC 7B 2.6-3.05 m
Regression without uncertainty
Regression with uncertainty
Data
Erosion rate (mm hr⁻¹)
Shear stress (Pa)
Regression equations:
$E = 4.89(\tau - 1.291)$
$E = 4.89(\tau - 1.291)$

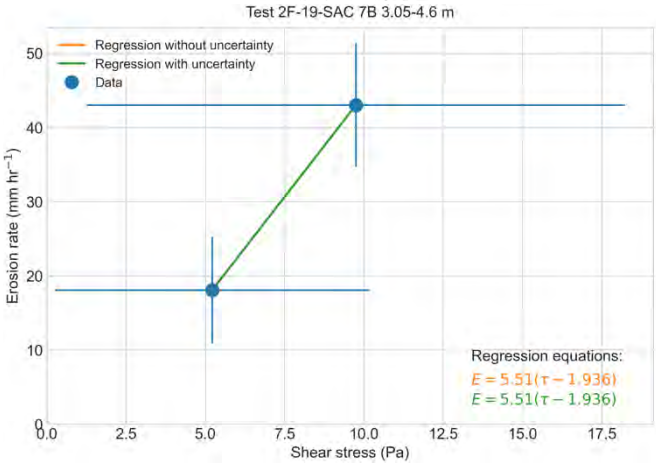
Test 2F-19-SAC 7B 3.05-4.6 m
Regression without uncertainty
Regression with uncertainty
Data
Erosion rate (mm hr⁻¹)
Shear stress (Pa)
Regression equations:
$E = 5.51(\tau - 1.936)$
$E = 5.51(\tau - 1.936)$

APPENDIX E

Table 11 presents averaged erosion rate and applied shear stress BET data over individual soil layers and flow sequence for each site. Values greater than zero were used to average erosion rates in an attempt to remove values that imply accretion. Negative values are likely caused by the accuracy of the caliper, the travel path of the caliper, and uneven erosion through the borehole. It is important to note that removal of negative values may bias the resulting erodibility parameters by providing weight to non-negative values. USCS classifications used for the BET are based on field methods and not laboratory classifications; consistent with TAMU reports and figures.

TABLE 11 – AVERAGED BET DATA BY SITE, SOIL LAYER, AND FLOW RUN. USCS SOIL TYPE IS BASED ON FIELD CLASSIFICATION.

Site	Flow run	Depth Range (m)	USCS class	Erosion Rate (mm hr^{-1})	Shear Stress (Pa)	Grain shear stress (Pa)
LAR2	1	0.8-1.4	SM	96.2	7.3	4.8
LAR2	1	1.4-2.0	ML	99.5	30.3	20.8
LAR2	1	2.0-2.6	SM	99.9	48.0	35.6
LAR2	1	2.6-3.0	ML	203.6	127.3	52.1
LAR2	2	0.8-1.4	SM	1.5	2.0	2.5
LAR2	2	1.4-2.0	ML	19.1	6.3	4.9
LAR2	2	2.0-2.6	SM	21.3	11.6	9.3
LAR2	2	2.6-3.0	ML	30.3	5.0	2.8
LAR2	3	0.8-1.4	SM	1.7	2.4	2.2
LAR2	3	1.4-2.0	ML	5.3	5.0	4.4
LAR2	3	2.0-2.6	SM	9.5	9.5	6.8
LAR2	3	2.6-3.0	ML	22.4	2.3	1.6
LAR3	1	0.0-1.2	CL	10.1	49.1	21.9
LAR3	1	1.2-1.4	SM	46.1	23.0	9.6
LAR3	1	1.4-1.6	CL	14.4	14.3	8.4
LAR3	1	1.6-5.5	SM	5.4	34.1	21.6
LAR3	2	0.0-1.2	CL	14.6	22.9	12.4
LAR3	2	1.2-1.4	SM	40.5	13.0	5.1
LAR3	2	1.4-1.6	CL	11.7	13.2	7.4
LAR3	2	1.6-5.5	SM	13.0	31.1	20.0
LAR3	3	0.0-1.2	CL	3.7	8.5	5.2
LAR3	3	1.2-1.4	SM	6.1	7.8	2.8
LAR3	3	1.4-1.6	CL	1.2	10.1	5.3
LAR3	3	1.6-5.5	SM	1.2	19.5	12.8
LAR5	1	0.0-1.5	SC	101.2	8.1	5.1
LAR5	1	1.5-2.1	SP-SC	15.3	17.3	16.4
LAR5	1	2.1-2.7	SM	15.4	21.1	14.6
LAR5	1	2.7-3.4	SP-SM	13.2	33.9	23.5
LAR5	1	3.4-4.0	SM	143.5	23.1	13.9
LAR5	2	0.0-1.5	SC	5.2	4.3	2.7
LAR5	2	1.5-2.1	SP-SC	4.1	10.7	10.5
LAR5	2	2.1-2.7	SM	4.5	14.9	9.7
LAR5	2	2.7-3.4	SP-SM	5.7	22.3	14.7

Site	Flow run	Depth Range (m)	USCS class	Erosion Rate (mm hr^{-1})	Shear Stress (Pa)	Grain shear stress (Pa)
LAR5	2	3.4-4.0	SM	9.8	7.4	4.1
LAR6	1	0.9-1.5	SM	39.1	5.8	3.1
LAR6	1	1.5-2.3	SM	8.9	7.8	3.3
LAR6	1	2.3-2.7	SM	13.5	20.8	7.3
LAR6	1	2.7-3.6	SP	6.0	53.8	34.2
LAR6	1	3.6-3.9	SP	13.0	60.4	26.3
LAR6	1	3.9-5.1	SP-SM	6.1	177.3	86.8
LAR6	2	0.9-1.5	SM	13.7	3.9	2.1
LAR6	2	1.5-2.3	SM	3.0	7.5	4.8
LAR6	2	2.3-2.7	SM	3.6	13.8	5.2
LAR6	2	2.7-3.6	SP	3.3	75.1	40.9
LAR6	2	3.6-3.9	SP	5.3	47.0	23.6
LAR6	2	3.9-5.1	SP-SM	1.9	159.9	104.9
LAR6	3	0.9-1.5	SM	41.1	21.4	11.6
LAR6	3	1.5-2.3	SM	89.9	22.2	16.4
LAR6	3	2.3-2.7	SM	60.9	100.2	38.0
LAR6	3	2.7-3.6	SP	93.1	146.0	81.6
LAR6	3	3.6-3.9	SP	19.1	196.4	123.0
LAR6	3	3.9-5.1	SP-SM	57.3	253.9	166.8
LAR6	4	0.9-1.5	SM	7.9	8.7	5.5
LAR6	4	1.5-2.3	SM	23.8	7.4	5.3
LAR6	4	2.3-2.7	SM	28.8	42.5	16.5
LAR6	4	2.7-3.6	SP	8.6	55.3	29.5
LAR6	4	3.6-3.9	SP	2.8	96.9	57.9
LAR6	4	3.9-5.1	SP-SM	11.0	78.1	45.2
LAR7	1	0.0-1.5	SP	22.6	6.4	3.8
LAR7	1	1.5-3.4	CL	14.1	8.0	5.6
LAR7	1	3.4-4.6	SC	16.6	11.4	6.9
LAR7	1	4.6-5.5	SP	29.4	9.7	3.8
LAR7	2	0.0-1.5	SP	37.0	15.7	11.0
LAR7	2	1.5-3.4	CL	0.6	23.9	17.1
LAR7	2	3.4-4.6	SC	1.9	38.8	23.8
LAR7	2	4.6-5.5	SP	0.9	29.3	12.2
LAR9	1	0.0-2.3	SM	16.2	1.1	0.5
LAR9	1	2.3-4.0	CL	7.0	9.4	7.4
LAR9	1	4.0-8.8	SM	6.6	1.8	0.9
LAR9	2	0.0-2.3	SM	22.2	2.9	1.8
LAR9	2	2.3-4.0	CL	10.3	16.0	13.8
LAR9	2	4.0-8.8	SM	26.1	3.3	1.8
LAR10	1	0.0-1.5	SM	23.9	198.3	114.7
LAR10	1	1.5-2.9	ML	62.8	53.9	28.6

Site	Flow run	Depth Range (m)	USCS class	Erosion Rate (mm hr^{-1})	Shear Stress (Pa)	Grain shear stress (Pa)
LAR10	1	2.9-4.1	CH	27.3	116.9	67.0
LAR10	2	0.0-1.5	SM	18.6	47.8	29.1
LAR10	2	1.5-2.9	ML	24.0	17.9	9.4
LAR10	2	2.9-4.1	CH	15.3	37.4	20.7
LAR12	1	0.0-1.5	SM	1.4	0.5	0.5
LAR12	1	1.5-4.3	SP	23.1	1.9	1.6
LAR12	1	4.3-4.8	SW	360.2	1.1	0.5
SAC1	1	0.0-3.5	SM	14.0	28.1	20.1
SAC1	1	3.5-9.0	CL	29.0	36.8	37.5
SAC1	2	0.0-3.5	SM	8.2	23.2	17.1
SAC1	2	3.5-9.0	CL	13.7	18.0	18.5
SAC1	3	0.0-3.5	SM	5.3	23.9	18.2
SAC1	3	3.5-9.0	CL	8.7	13.0	12.2
SAC3 (1)	1	0.0-0.9	ML	6.3	3.4	3.1
SAC3 (1)	1	0.9-4.0	SM	48.4	51.8	31.9
SAC3 (1)	2	0.0-0.9	ML	0.1	2.6	3.2
SAC3 (1)	2	0.9-4.0	SM	26.9	31.8	16.2
SAC3 (1)	3	0.0-0.9	ML	0.1	2.5	3.3
SAC3 (1)	3	0.9-4.0	SM	19.8	18.2	9.8
SAC3 (2)	1	0.0-0.9	ML	7.5	11.7	4.2
SAC3 (2)	1	0.9-4.0	SM	22.3	91.5	32.0
SAC3 (2)	1	4.0-5.0	SP-SM	16.0	243.1	77.4
SAC3 (2)	2	0.0-0.9	ML	5.2	5.5	2.2
SAC3 (2)	2	0.9-4.0	SM	5.9	48.7	18.0
SAC3 (2)	2	4.0-5.0	SP-SM	3.6	129.8	37.2
SAC3 (2)	3	0.0-0.9	ML	2.2	3.5	1.1
SAC3 (2)	3	0.9-4.0	SM	2.8	17.3	6.8
SAC3 (2)	3	4.0-5.0	SP-SM	5.1	38.8	13.2
SAC7	1	0.0-2.6	ML	61.4	25.6	18.0
SAC7	1	2.6-3.05	CL	49.6	45.2	40.0
SAC7	1	3.05-4.6	ML	53.3	43.4	34.7
SAC7	2	0.0-2.6	ML	30.1	8.3	6.2
SAC7	2	2.6-3.05	CL	45.3	13.3	10.5
SAC7	2	3.05-4.6	ML	43.0	12.1	9.7
SAC7	3	0.0-2.6	ML	11.8	4.9	3.8
SAC7	3	2.6-3.05	CL	19.7	6.5	5.3
SAC7	3	3.05-4.6	ML	18.1	6.4	5.2
SAC9	1	0-0.9	SM	24.7	10.8	8.9
SAC9	1	0.9-1.5	CL	44.1	7.0	6.6
SAC9	1	1.5-3.5	CL	29.0	6.9	7.3
SAC9	1	3.5-4.9	CH	21.8	39.3	40.7